Effect of nanoparticles and pre-shearing on the performance of water-soluble polymers flow in porous media

Mirzaie Yegane, M.

DOI
10.4233/uuid:e57ae88c-19eb-4bac-be3a-903fa68d319b

Publication date
2021

Document Version
Final published version

Citation (APA)
Mirzaie Yegane, M. (2021). *Effect of nanoparticles and pre-shearing on the performance of water-soluble polymers flow in porous media*. [Dissertation (TU Delft), Delft University of Technology]. https://doi.org/10.4233/uuid:e57ae88c-19eb-4bac-be3a-903fa68d319b

Effect of nanoparticles and pre-shearing on the performance of water-soluble polymers flow in porous media

Mohsen Mirzaie Yegane

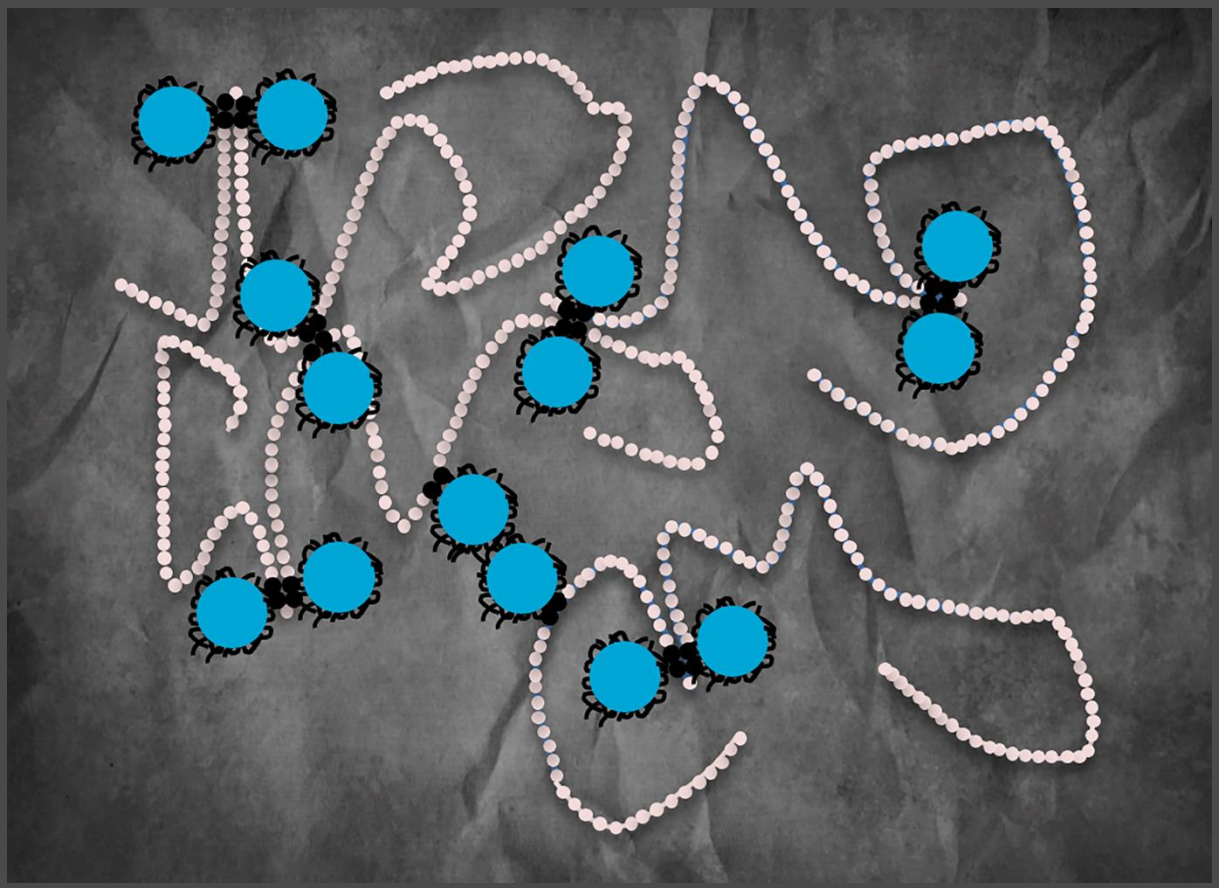

EFFECT OF NANOPARTICLES AND PRE-SHEARING ON THE PERFORMANCE OF WATER-SOLUBLE POLYMERS FLOW IN POROUS MEDIA

Effect of nanoparticles and pre-shearing on the performance of water-soluble polymers flow in porous media

Proefschrift

ter verkrijging van de graad van doctor

aan de Technische Universiteit Delft,

op gezag van de Rector Magnificus Prof.dr.ir. T.H.J.J. van der Hagen,

voorzitter van het College voor Promoties,

in het openbaar te verdedigen op

donderdag 27 mei 2021

om 12.30 uur

door

Mohsen MIRZAIE YEGANE

Master of Science in Petroleum Engineering,

Politecnico di Torino, Italië

geboren te Borojerd, Iran.

Dit proefschrift is goedgekeurd door de

promotor: Prof.dr. P.L.J. Zitha
promotor: Dr. P.E. Boukany

Samenstelling promotiecommissie:

Rector magnificus,	voorzitter
Prof.dr. P.L.J. Zitha,	Technische Universiteit Delft, promotor
Dr. P.E. Boukany,	Technische Universiteit Delft, promotor

Onafhankelijke leden:

Prof.dr. S.J. Picken	Technische Universiteit Delft
Prof.dr. R. Gharbi	Kuwait University/ Kuwait Oil Company
Prof.dr. Y. Feng	Sichuan University
Prof.dr. W.R. Rossen	Technische Universiteit Delft
Dr. J. Gebert	Technische Universiteit Delft

The work presented in this thesis was conducted in the Department of Geoscience and Engineering, Delft University of Technology, Delft, The Netherlands. This research was funded by TNO and Kuwait Oil Company.

Keywords: Water-soluble polymers, nanoparticles, pre-shearing, flow in porous media, enhanced oil recovery

Printed by: Ipskamp Printing

ISBN: 978-94-6366-420-2

An electronic version of this dissertation is available at

http://repository.tudelft.nl/

To my dear parents

Ahmadali Mirzaie Yegane and Shahnaz Noori Motlagh

In loving memory of my brother

Mahdi Mirzaie Yegane

Propositions

accompanying the dissertation

EFFECT OF NANOPARTICLES AND PRE-SHEARING ON THE PERFORMANCE OF WATER-SOLUBLE POLYMERS FLOW IN POROUS MEDIA

By

Mohsen MIRZAIE YEGANE

1. The addition of hydrophobically modified silica nanoparticles, above a critical concentration, to a solution containing a hydrophobically modified polyacrylamide in the semi-dilute regime significantly improves its viscosity at high salinity and temperature conditions (**Chapter 3**).
2. Ensuring good injectivity is the most important aspect when developing new polymer-based chemicals for enhanced oil recovery at high salinity and temperature conditions (**Chapters 2**, **4**, and **5**).
3. Pre-shearing a polymer solution, to induce high-stretching of the polymer chains and thus promote the breakup of the longest ones, improves its injectivity in porous media significantly without considerably reducing its viscosity (**Chapter 5**).
4. The injection of nanoparticles in porous media for enhanced oil recovery and other purposes without systematically studying their colloidal stability at reservoir conditions is senseless (**Chapters 2**, **3**, and **4**).
5. There is no such thing as failure in scientific research. One either succeeds or learns.
6. European countries are the leading nations in the energy transition to renewables but also the ones who benefit the most.
7. There should be a strong connection between PhD research and industrial applications. This should not, however, sacrifice the scientific mission of the PhD research.
8. The process of writing a movie script and a research paper is similar. It initiates with an idea and proceeds with the drawing of a clear structure, knowing the beginning, turning points, and the end. But what makes them both a great piece of work is the attention to detail.

9. “Good artists copy, great artists steal.” -Pablo Picasso. A similar attitude for scientists is dangerous.
10. ‘The Office’ and ‘Friends’ are the two funniest franchises in the history of television with the former being the funnier one.

These propositions are regarded as opposable and defendable, and have been approved as such by the promotors prof. dr. P.L.J. Zitha and dr. P.E. Boukany.

Summary

Polymer flooding is a commercially viable chemical enhanced oil recovery (cEOR) method. It includes the injection of water-soluble polymers into a reservoir to improve the drive water viscosity and consequently to increase the sweep and displacement efficiency of the water. Despite the success in both laboratory and field applications, there are still some challenges associated with the application of polymers for cEOR. The first challenge is that the implementation of conventional polymers used for cEOR at high salinity, hardness, and temperature reservoirs is difficult and costly because of the viscosity loss and polymer precipitation at these harsh conditions. The second challenge concerns the injectivity of the polymers. Long polymer chains tend to block the small pores which leads to a time-dependent injectivity decline. This thesis investigates the potential solutions to address these two challenges in order to improve the performance of water-soluble polymers.

Firstly, **Chapter 2** presents a critical review of the most recent research progress in the application of polymers for cEOR. The transport mechanisms of water-soluble polymers in porous media namely polymer rheology and polymer retention are discussed, and the areas which need further research are highlighted. This critical review is also focused on the limitations of conventional polymers at high salinity and temperature. It is discussed that the modification of polyacrylamides by the incorporation of small hydrophobic monomers, or salt- and temperature-tolerant monomers can improve the polymer performance at high salinity and temperature. Nonetheless, commercial implementation of these polymers seems to be challenging. The modified polyacrylamides have a lower molecular weight than the conventional polymers used for cEOR which implies they should be overdosed to meet the target viscosity, thus making them an economically unattractive choice.

Chapter 3 investigates an alternative approach to improve the viscosity and enhance the stability at high salinity and temperature. This approach consists of combining a hydrophobically modified polyacrylamide (HMPAM) and hydrophobically modified silica nanoparticles (NPs). Hydrophobic modification of the NPs ensures their colloidal stability at high salinity by providing sufficient steric stabilization, while also causing them to interact with HMPAM chains through hydrophobic–hydrophobic interactions. By performing rheological measurements, it is shown that the hybridization of HMPAM with NPs leads to a higher viscosity at high salinity and temperature. Such an increase is more

pronounced when the concentration of HMPAM is in the semi-dilute regime and the concentration of the NPs is higher than a critical threshold where NPs can bridge between the HMPAM chains, thus increasing the hydrodynamic radius which in turn increases the viscosity.

Chapter 4 investigates the porous media behaviour of the HMPAM and NPs at high salinity and temperature conditions. Core-flood experiments are performed by injection of either HMPAM solution, NPs suspension, or a HMPAM–NPs hybrid at superficial velocities of 1 and 10 ft/day to assess their retention and injectivity. It is shown that the injection of HMPAM and NPs in the same solution has the following benefits: (a) the HMPAM–NPs hybrid has a higher flow resistance as compared to the injection of HMPAM alone (b) the HMPAM–NPs hybrid prevents filtration of the NPs in the inlet while the injection of NPs alone results in significant filtration in the inlet and (c) the co-injection of HMPAM and NPs also decreases the retention of both HMPAM and NPs as compared to when they are injected individually. The results are discussed in light of the transport mechanisms of HMPAM and NPs. The results of both **Chapters 3** and **4** show the potential of the HMPAM–NPs hybrid as a mobility control agent for cEOR at high salinity and temperature.

Chapter 5 studies the effect of pre-shearing, by agitators and flow through contractions, on the flow enhancement of water-soluble polymers through porous media. Pre-shearing the polymer solutions is done under fast flow to induce high-stretching of the polymer chains and thus promote breaking of the high-end fragments of the molecular weight distribution (i.e. breaking the longest polymer chains which results in a decrease in relaxation time and shear-thinning level). The pre-sheared polymers are then forced through sand-packs to assess the flow enhancement. It is shown that the reduction in both the viscosity and the screen factor of the pre-sheared polymer solutions, as a function of energy input, is path independent regardless of the shearing device. The viscosity of the polymer solutions remains unchanged up to a critical Weissenberg number and starts to decrease only beyond that. Sand-pack experiments show that pre-shearing the polymer solution can considerably enhance its flow through porous media while its viscosity is not significantly affected. Our numerical simulation suggests that the main mechanism behind this is a reduction in the size of the polymer chains which results in a less significant mechanical entrapment. This strategy can be used to improve the injectivity of polymers in cEOR applications.

Samenvatting

Polymeer stroming [Engels: polymer flooding] is een methode om het rendement van oliewinning uit een reservoir te verhogen doormiddel van het injecteren van polymeren [Engels: chemical enhanced oil recovery (cEOR)]. Het is bewezen dat de methodiek commercieel haalbaar is. De methode omvat de injectie van in wateroplosbare polymeren in een reservoir om de viscositeit van het water te verhogen en, als gevolg hiervan, de veeg- en verplaatsingsefficiëntie van het water te verhogen. Ondanks het succes in zowel laboratorium- als veld-toepassingen, nog steeds zijn er enkele uitdagingen verbonden aan het gebruik van polymeren voor cEOR. De eerste uitdaging is de implementatie van conventionele polymeren die worden gebruikt voor cEOR bij een reservoir met een hoog zoutgehalte, hoge hardheid en hoge temperatuur. Dit is moeilijk en kostbaar vanwege het viscositeitsverlies en de polymeerprecipitatie onder deze zware omstandigheden. De tweede uitdaging betreft de injectiviteit van de polymeren. Lange polymeerketens verstoppen de kleine poriën, wat vervolgens leidt tot een tijdsafhankelijke afname van de injectiviteit. In dit proefschrift onderzoeken we de mogelijke oplossingen om deze twee uitdagingen aan te pakken.

In eerste instantie, in **Hoofdstuk 2**, presenteren we een kritisch overzicht van de meest recente voortgang dat is geboekt door onderzoekers met betrekking tot het gebruik van polymeren voor cEOR. We bespreken de transportmechanismen van in wateroplosbare polymeren in poreuze media, inclusief polymeerreologie en polymeerretentie, en kaarten aspecten aan die verder diepgaand onderzoek vereisen. Dit overzicht gaat ook over de beperkingen van conventionele polymeren bij een hoog zoutgehalte en hoge temperatuur. We bespreken de modificatie van polyacrylamiden door het opnemen van kleine hydrofobe monomeren, of zout- en temperatuur-tolerante monomeren. Deze monomeren kunnen de prestaties van polymeren verbeteren bij een hoog zoutgehalte en hoge temperatuur. Desalniettemin is de commerciële implementatie van deze gemodificeerde polymeren een uitdaging. De gemodificeerde polyacrylamiden hebben een lager molecuulmassa dan de conventionele polymeren die voor cEOR worden gebruikt. Dit betekent dat ze in een overdosis aanwezig moeten zijn om aan de beoogde viscositeit van het water te voldoen, waardoor ze een economisch onaantrekkelijke keuze zijn.

In **Hoofdstuk 3**, onderzoeken we een alternatieve benadering om de viscositeit en de stabiliteit bij een hoog zoutgehalte en een hoge temperatuur te verbeteren. Deze benadering omvat de combinatie van een hydrofoob gemodificeerd polyacrylamide

[Engels: hydrophobically modified polyacrylamide (HMPAM)] en hydrofobe gemodificeerde silica nanodeeltjes [Engels: nanoparticles (NPs)]. Hydrofobe modificatie van de NPs zorgt voor hun colloïdale stabiliteit bij een hoog zoutgehalte. Dit resulteert ook in hun wisselwerking met HMPAM-ketens door middel van hydrofobe-hydrofobe interacties. Door reologische metingen uit te voeren, laten we zien dat de hybridisatie van HMPAM met NPs leidt tot een hogere viscositeit bij een hoog zoutgehalte en hoge temperatuur. Deze toename in viscositeit is significanter wanneer de concentratie van HMPAM zich in het semi-verdunde regime bevindt en de concentratie van de NPs hoger is dan een kritische drempel. In deze toestand kunnen NPs een brug slaan tussen de HMPAM-ketens, waardoor de hydrodynamische straal toeneemt, wat op zijn beurt de viscositeit verhoogt.

In **Hoofdstuk 4**, onderzoeken we het gedrag van de HMPAM en NPs in poreuze media bij een hoog zoutgehalte en hoge temperatuur. We voeren stromingsexperimenten uit door injectie van HMPAM-oplossing, NPs-suspensie en HMPAM-NP hybride met oppervlakkige snelheden van 1 en 10 ft /dag om hun retentie en injectiviteit te beoordelen. We laten zien dat de injectie van HMPAM en NPs in dezelfde oplossing de volgende voordelen heeft: (a) de HMPAM-NPs hybride heeft een hogere stromingsweerstand in vergelijking met de injectie van alleen HMPAM, (b) de HMPAM-NPs hybride voorkomt filtratie van de NPs in de injectiepunt, terwijl de injectie van NPs alleen resulteert in aanzienlijke filtratie in het injectiepunt en (c) de gelijktijdige injectie van HMPAM en NPs vermindert ook de retentie van zowel HMPAM als NP's in vergelijking met wanneer ze afzonderlijk worden geïnjecteerd. De resultaten worden besproken om de transportmechanismen van HMPAM en NPs te interpreteren. De resultaten van beide hoofdstukken (3 en 4) laten het potentieel zien van de HMPAM-NPs hybride als een middel om de mobiliteit te controleren bij een hoog zoutgehalte en hoge temperatuur.

In **Hoofdstuk 5**, bestuderen we het effect van afschuiven, door drie verschillende afschuiven apparaten, op de stromingsverbetering van polymeren door poreuze media. Het afschuiven van de polymeren wordt gedaan om alle polymeerketens uit te rekken en de langste ketens te breken. Dit leidt tot het breken van de hoogwaardige fragmenten van de molecuulgewichtsverdeling. Met andere woorden, het resulteert in het breken van de langste polymeerketens, wat leidt tot een afname van de relaxatietijd en de mate van afschuifverdunning. De polymeren worden vervolgens in zandpakken geïnjecteerd om de stromingsverbetering te beoordelen. We laten zien dat de verlaging van zowel de viscositeit als de schermfactor van de polymeeroplossingen, als functie van de energie-

input, onafhankelijk is van afschuifapparaten. De viscositeit van de polymeeroplossingen blijft onveranderd tot een kritiek Weissenbergnummer en begint pas daarna af te nemen. Experimenten met zandpakken tonen aan dat afschuiven van de polymeeroplossing de doorstroming door poreuze media aanzienlijk kan verbeteren, terwijl de viscositeit niet significant wordt beïnvloed. Onze numerieke simulatie suggereert dat het belangrijkste mechanisme hierachter een vermindering van de grootte van de polymeerketens is, wat resulteert in een minder significante mechanische beknelling. Deze strategie kan worden gebruikt om de injectiviteit van polymeren in cEOR-toepassingen te verbeteren.

CONTENTS

1 INTRODUCTION

Life without energy is inconceivable. Throughout history, Homo sapiens have used energy in their daily life. Before the industrial revolution, their needs for energy were scanty. They relied on the sun for heat and when there was no sun, they burned wood, dried dung, and straw. They used the muscle of horses and the power of the wind for transportation and exploited animals to do things that they were not able to do with their own labour. After the industrial revolution, however, with the appearance of steam engines and electric motors, etc. the energy use, and demand significantly increased. This needed energy was predominantly generated from biomass and later on from coal. Coal had twice the calorific value of wood and was cheaper and easier to distribute. Nonetheless, there were great environmental concerns involved with coal. In the early 20th century, the appearance of crude oil as the most important source of energy changed the world forever. Oil was relatively cheap, and compared to coal had a higher calorific value and lower carbon footprint.

Since then, oil has become to be the backbone of contemporary life. The oil's products underpin our daily life, predominantly providing energy to the power industry, providing heat to our houses, and supplying fuel for means of transportation to carry goods, and people around the globe. Along with other technological advances, oil brought well-being and prosperity across the globe and led to unprecedented growth in world population in the 20th century (from ~1.5 billion in 1900 to ~6 billion in 2000). As can be seen in Figure 1.1, energy use increased by a factor of ~10 during the course of the 20th century. Even unprecedented events, such as the current global pandemic because of COVID-19, have had an only a marginal impact on energy consumption. A recent study has shown that as

the COVID-19 lockdowns are relaxed, energy consumption will start to recover quickly [1].

With the increasing world population, meeting the growing energy demand in a safe and environmentally responsible manner is a vital challenge. The oil industry, now more than ever, is facing public opposition predominantly with respect to its environmental impact. There is thus an increasing mandate to move towards energies with a lower CO_2 emission. Nonetheless, for the foreseeable future, oil will remain a part of the energy mix, particularly in developing countries. Figure 1.2 shows that the International Energy Agency's Sustainable Development scenario and the Shell Sky scenario – both aggressive decarbonisation forecasts – indicate a continuing, long-standing role for oil, even while demand levels decrease as compared to today's level. In contrast, the International Energy Agency's Stated Policies scenario indicates continued increase in oil demand.

In the author's opinion, while a quick transition to low carbon emissions is essential and inevitable, oil will remain an important primary energy source throughout the period of transition. Oil companies can have a major role during the transition period and they could invest part of their revenues in low carbon business models that minimise carbon utilisation while maintaining their profitability. They can thus expand the application of low carbon technologies such as carbon capture and storage (CCS), blue and green hydrogen, etc.

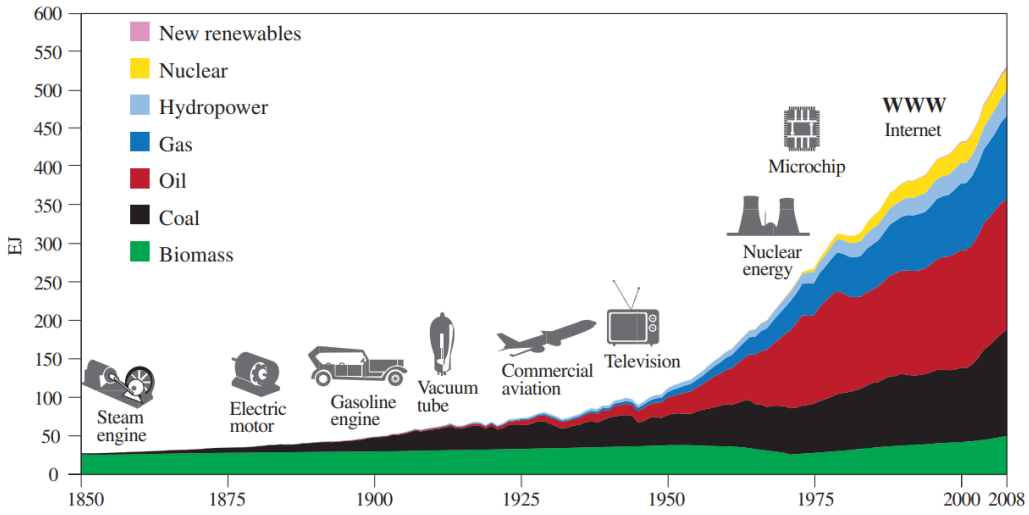

Figure 1.1: The world energy use throughout recent history [2]

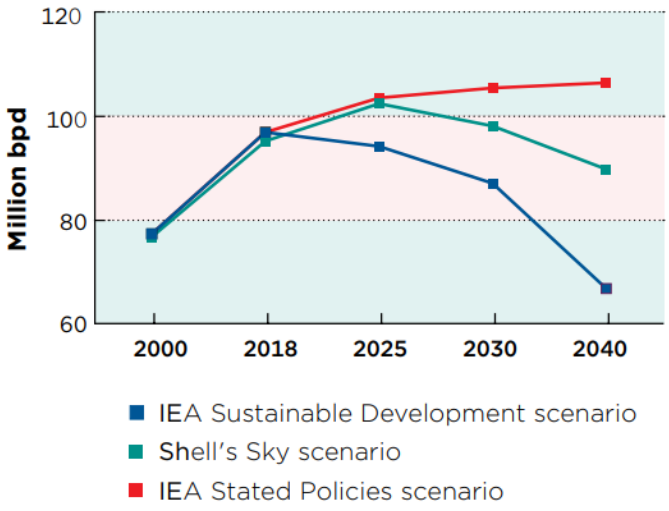

Figure 1.2: Long-term oil demand forecast based on different scenarios (bpd=barrel per day, IEA=international energy agency) [3]

Due to increased energy demand, it is imperative to maximize the recovery from existing oilfields, given that the discovery of new giant oilfields is becoming exceedingly difficult. The recovery factor from mature oilfields is only almost 30% [4,5], which means that a large proportion of the original oil in place (OOIP) is left behind in the subsurface. This necessitates the use of secondary and tertiary recovery techniques after the primary oil recovery. In primary oil recovery, the oil is produced due to natural flow, which is a result of the pressure difference between the oil-bearing reservoir and the well. However, over time and as a result of oil production, the reservoir pressure falls and a point is reached where there is insufficient underground pressure to bring the oil to the surface. Subsequently, secondary recovery techniques are employed. These techniques involve the supply of external energy into the reservoir by the injection of fluids, such as water and gas, or the use of an artificial gas lift to increase the reservoir pressure.

By the injection of water into the injection well, oil can be produced in the production well – this is commonly known as waterflooding. The efficiency of waterflooding is dependent on both the microscopic displacement efficiency and the volumetric sweep efficiency. The microscopic displacement efficiency refers to the ratio of the oil mobilised to the oil contacted by water. It is reported that microscopic displacement efficiencies can be as high as ~70% [5], only leaving behind oil droplets within the pore space that are trapped because of capillary forces. The volumetric sweep efficiency is the product of areal and vertical sweep efficiencies. The areal sweep efficiency refers to the fraction of the reservoir area contacted by water and it depends on several parameters: the relative flow properties of oil and water, the injection-production well patterns, the pressure

distribution between the injection and production wells, the injection rate, the total volume of injected water, and the directional permeability [6]. The vertical sweep efficiency is the fraction of the reservoir in a vertical plane that is contacted by water and depends mainly on the degree of vertical stratification existing in the reservoir. An illustration of areal and vertical sweep efficiencies is shown in Figure 1.3.

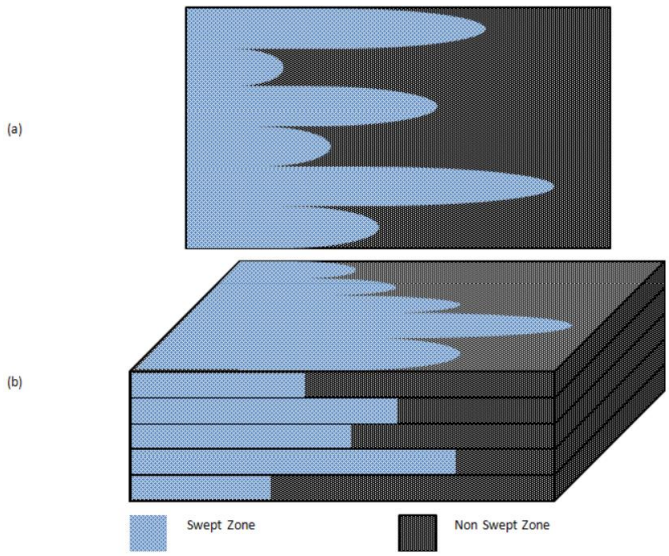

Figure 1.3: A representation of volumetric sweep efficiency: (a) areal sweep and (b) vertical sweep in a stratified reservoir [7]

The volumetric sweep efficiency is typically considerably lower than the microscopic displacement efficiency [5]. If the water moves more easily than the oil, tongues of water form at the interface, a phenomenon known as viscous fingering. This occurs at high capillary numbers where the viscous forces are superior to the capillary forces, and this can be a result of the water having a lower viscosity than the oil. The result of such a phenomenon is an early breakthrough of water followed by a long period of two-phase production. On average, the recovery factor after primary and secondary oil recovery is between 35% and 45% [8] denoting that a large proportion of oil still remains in the subsurface.

Polymer flooding is a tertiary oil recovery technique where a small amount of a water-soluble polymer is added to water (brine) to increase its viscosity. The presence of the polymer macromolecules in water reduces its mobility and consequently reduces the fractional flow of water. This in turn helps with the reduction of viscous fingering and increases the volumetric sweep efficiency (see Figure 1.4). Polymers can also provide in-depth diversion effects in heterogonous reservoirs. To achieve this, a crosslinking polymer is injected that propagates deep into the reservoir where it forms a gel [9]. This

can substantially reduce the permeability of thief zones and improve the vertical sweep efficiency. Throughout this thesis, the application of crosslinking polymers will not be discussed. The general screening criteria for a polymer flood based on the oilfield data is shown in Table 1.1.

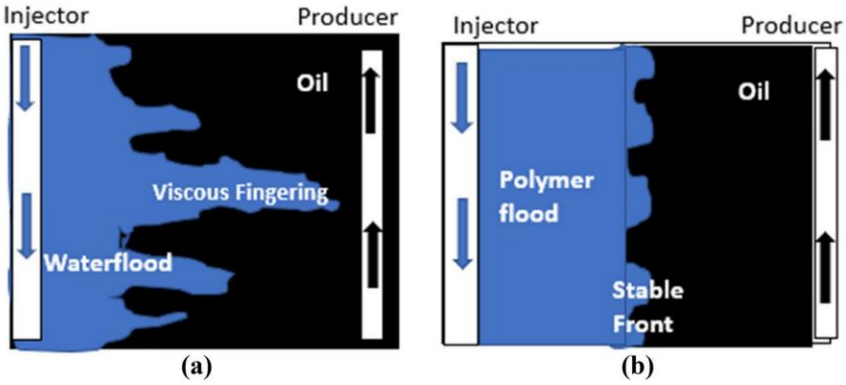

Figure 1.4: An illustration of (a) an unstable water flooding and (b) a stable polymer flooding displacement [10]

Table 1.1: Criteria guide for polymer flooding in the data set adopted from [11]. The values in the table represent the mean values of the data set

Oil gravity (°API)	Oil Viscosity (mPa s)	Porosity (%)	Oil saturation, start (%)	Oil saturation, end (%)	Average permeability (mD)	Depth (ft)	Temperature (°C)
31.2	12.21	18.15	55.85	46.57	384.88	4,004.21	47.8

The two most common polymers for polymer flooding applications are hydrolysed polyacrylamide (HPAM) and xanthan gum. HPAM, which is by far, the most frequently used polymer in field projects, has shown promising results and can improve oil recovery after water flooding. However, there are two main restrictions associated with HPAM: (a) the implementation of HPAM at elevated temperature and/or at high salinity has proved to be significantly more difficult and costly than anticipated because of the polymer degradation at these conditions and (b) HPAM macromolecules tend to block small pores, particularly in low permeability reservoirs, which leads to a time-dependent injectivity decline. In this thesis, these two challenges are addressed and potential solutions to improve the performance of water-soluble polymers are investigated. In the next sections, each of these two challenges is briefly discussed. Thereafter, the research objectives and the thesis organization are presented.

1.1 Polymer degradation at elevated temperatures and high salinities

HPAM increases the viscosity of water due to two reasons: (a) the high molecular weight of the HPAM (reaching 30×10^6 g/mol [12]) and (b) the degree of hydrolysis of HPAM (ranging from 15% to 35% [13]). Thanks to the hydrolysis, negative charges are induced along the polymer backbone as a result of the dissociation of the carboxylate groups. The electrostatic repulsion between these negative charges expands the polymer chain in water, which leads to an increase in viscosity compared to a neutral chain.

Salinity and hardness have been linked with two major problems that impact polymer performance: viscosity loss and polymer precipitation. For HPAM, the viscosity loss at high salinities has been attributed to the shielding effect of the charges [14]. As high molecular weight HPAM has a flexible structure, it responds strongly to the ionic strength of the aqueous solvent [10]. As a result, at high salinities, the negative charges along the HPAM backbone are screened. This results in a decrease in the electrostatic repulsion among the polymer chains and thus to a less substantial expansion of the polymer coils in the solvent. As can be seen in Figure 1.5a, the end result of this process is a relatively lower hydrodynamic volume of the polymer coils, which is equivalent to a reduction in viscosity. Another major issue for HPAM at high salinities is the high concentration of divalent cations such as Ca^{2+} and Mg^{2+}. In the presence of the divalent cations, polyion–metal complexes can be formed and the HPAM chains can be bridged by the cations. This bridging leads to polymer precipitation due to the complexing ability of the HPAM carboxylate groups (see Figure 1.5b) [15,16].

In many reservoirs, high salinity and hardness in are often accompanied by high temperatures. The viscosity loss and polymer precipitation of HPAM become more severe at high temperatures as further hydrolysis of the polymer backbone is promoted. This hydrolysis then causes additional interaction between the charged polymer backbone and ions in the solvent (see Figure 1.5c). Moreover, HPAM precipitation occurs more readily at temperatures that are higher than the cloud point of the solution [17]. The cloud point is referred to as a critical temperature above which the polymer starts to separate from the water solution. This makes the solution turbid due to the creation of polymer-rich emulsion droplets [18].

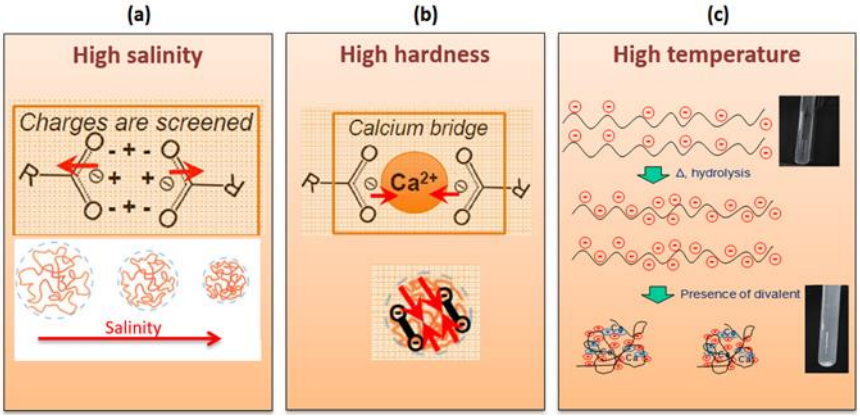

Figure 1.5: HPAM challenges in harsh conditions. (a) At high salinities, negative charges along the HPAM backbone are screened which results in a less substantial expansion of the polymer coils. (b) At high divalent concentrations, the HPAM chains are bridged by divalent cations which leads to polymer precipitation. (c) At high temperatures, the additional negative charges in the HPAM chain interact with the mono- and divalent cations. Also, above the cloud point, the solution becomes turbid and polymer separates from the water solution

1.2 Polymer injectivity challenges

Polymer injectivity is an indication of how easily a polymer solution can flow from the near-wellbore region into the reservoir or how fast it can propagate within the porous medium of the reservoir [19]. Mechanical entrapment is one important mechanism which can hinder the propagation of polymers through porous media. It occurs when larger polymer molecules become trapped in narrow pore throats [20]. This happens when polymer molecules are smaller than the inlet of the pore throats but larger than their outlet [21,22]. Once polymer molecules are trapped in the narrow pore throats, the size of the pores gradually becomes smaller, which increases the probability of trapping smaller polymer molecules. This will ultimately lead to pore-clogging and a time-dependent injectivity decline. Major sources of mechanical entrapment are the high-end fragments of the polymer molecular weight distribution and the highly-entangled polymer chains, formed as a result of hydrogen bonding as well as precipitation due to the presence of divalent ions, are [10].

Polymer injectivity is represented by the resistance factor (RF) and the residual resistance factor (RRF) [23]. The former is the ratio of the mobilities of the brine and the polymer solution and is related to pressure drop according to the following equation:

$$RF = \frac{\lambda_{b_0}}{\lambda_p} = \frac{\left(\frac{k}{\mu}\right)_{b_0}}{\left(\frac{k}{\mu}\right)_p} = \frac{\Delta P_p}{\Delta P_b^0} \tag{1.1}$$

where λ, μ, k and ΔP are the mobility, viscosity, permeability and pressure drop respectively and where the subscripts b_0 and p refer to the brine before the polymer injection and polymer solution respectively. In practice, RF shows an increase during the polymer injection, due to the viscosity increase and a reduction in permeability. RRF describes the permeability reduction after the polymer injection. It is the ratio of the brine mobility before the polymer injection (corresponding to subscript b_0) to the brine mobility after the polymer injection (corresponding to subscript b_1):

$$RRF = \frac{\lambda_{b_0}}{\lambda_{b_1}} = \frac{\left(\frac{k}{\mu}\right)_{b_0}}{\left(\frac{k}{\mu}\right)_{b_1}} = \frac{\Delta P_b^1}{\Delta P_b^0} \tag{1.2}$$

If the polymer injectivity is good, RF levels off to a plateau value after polymer breakthrough and RRF is close to 1, suggesting that there is no significant retention of polymer in porous media. However, if the polymer injectivity is poor, there will be a time-dependent increase in RF with the injection of several pore volumes of the polymer solution and RRF will be significantly higher than 1.

1.3 Research questions and objectives

This thesis addresses the knowledge gap and challenges outlined in the previous sections. The two main hypotheses of this work are as follows: (a) a hybrid of modified polyacrylamide and silica nanoparticles is capable of improving mobility control in high salinity and temperature reservoirs, and (b) controlled pre-shearing of water-soluble polymers can enhance their flow through porous media. More specifically, the sub-questions related to each hypothesis are stated below.

(a) First hypothesis: hybridization of polymer and nanoparticles for mobility control in high salinity and temperature conditions

Here, the first sub-question is: at what concentration of polymer and nanoparticles the viscosity improvement of the hybrid is expected? The hypothesis related to this sub-question is that the viscosity improvement is more noticeable when the concentration of polymer is in the semi-dilute regime and the concentration of nanoparticles is higher than a critical threshold. Therefore, the objective here is to investigate the rheological response of hybrid mixtures of hydrophobically modified polyacrylamide with hydrophobically modified silica nanoparticles at various concentrations as a strategy for achieving enhanced stability and improved viscosity at high salinity and temperature conditions.

The second sub-question is whether the hybrid of polymer and nanoparticles results in higher flow resistance in porous media compared to the polymer alone. The hypothesis concerning this sub-question is that hybrid shows larger flow resistance, consistent with its higher viscosity, compared to the simple polymer. Thus the objective here is to investigate the behaviour of the polymer–nanoparticles hybrid in porous media. The main goal is to investigate the rheology, retention and injectivity of the hybrid at typical salinities, pressures and temperatures encountered in oil reservoirs.

(b) Second hypothesis: pre-shearing for flow enhancement of polymers in porous media

Here, the first sub-question is: what is the rheological response of polymer chains to pre-shearing? The hypothesis related to this sub-question is that pre-shearing of the polymer under fast flow induces high-stretching of the polymer chains and thus promotes the break-up of the longest ones (i.e. the high-end fragments of molecular weight distribution). This results in flow enhancement of the polymer in porous media without a significant reduction in its viscosity. The objective here is to find a suitable range of strain rates (translated to volume specific energy input) at which the polymer flow performance in porous media is optimised.

The second sub-question is: what is the impact of pre-shearing on time-dependent injectivity decline? The hypothesis regarding this sub-question is that the reduction in the size of polymer chains after pre-shearing leads to smaller mechanical entrapment and a less pronounced increase in the flow resistance. Therefore, the objective here is to describe how the flow of un-sheared and pre-shared polymer solutions through porous media impact the mechanical entrapment and consequently flow resistance of water-soluble polymers.

1.4 Thesis organisation

This thesis consists of six chapters including this introduction and the conclusions. Chapter two through five address the research objectives introduced in the previous section. While there is a reasonable connection between chapters, they are a collection of papers and therefore can also be read independently.

Firstly, to fully understand the state-of-the-art for polymers and nanoparticles in cEOR applications, a critical review of the most recent research progress in this field is presented in **Chapter 2**. It lays the ground for the development of polymer–nanoparticles hybrid systems for elevated temperatures and high salinities. The important physical and chemical characteristics of polymers and nanoparticles and their transport mechanisms in

porous media are highlighted. Their use in enhanced oil recovery is also discussed and the effect of salinity and temperature on their performance is studied.

Chapter 3 examines the rheological response of the polymer–nanoparticles hybrid for achieving enhanced stability and high viscosity at high salinity (>20 wt% total dissolved solids), hardness (>1.5 wt% divalent cations), and temperature (>70 °C). Hydrophobically modified silica nanoparticles are added to a solution of hydrophobically modified polyacrylamide to facilitate the bridging between polymer chains. Silica nanoparticles are modified by a low molecular weight organic ligand to provide steric stabilization and ensure colloidal stability at high salinity. To describe the colloidal stability of nanoparticles, an extended DLVO theory is used. To study the improvement in the flow responses of the hybrids, viscosity measurements are performed at various concentrations of polymer and nanoparticles.

In **Chapter 4**, the performance of the polymer–nanoparticles hybrid in 3D porous media is assessed. This is done by performing core-flood experiments with sandstone core using, the polymer, the nanoparticle, or their hybrid, and injecting at both low and high flow rates. The retention and injectivity of the polymer and nanoparticles in the porous media are examined. Furthermore, their porous media flow characteristics are discussed in light of their bulk rheological properties.

Chapter 5 investigates the porous media flow enhancement of polymer solutions containing an acrylamide-based copolymer by controlled pre-shearing. The pre-shearing is achieved using two agitators and the pressure-driven flow through capillaries at various energy inputs. The porous media flow behaviour for polymer solutions that have been pre-sheared with different shearing devices is studied. This flow behaviour is then compared with the rheological response in both Ubbelohde and screen viscometers as well as in a rotational rheometer. Moreover, a numerical simulation based on a one-dimensional model is carried out aiming at studying the mechanisms of flow efficiency in porous media.

Finally, in **Chapter 6**, the conclusions based on the findings in this thesis are given with recommendations for future work.

2 WATER SOLUBLE-POLYMERS FOR EOR: A REVIEW

Polymer flooding is the most frequently used chemical enhanced oil recovery (cEOR) method in field applications which increases oil sweep and displacement efficiency. The commercial implementation of polymer flooding at elevated temperature and/or high salinity reservoirs is significantly more difficult and costly than in more conventional reservoirs. Hybrid mixtures of polymers and nanoparticles have emerged as a promising strategy for achieving enhanced stability and high viscosity at high salinity and temperature conditions. (**Chapter 3**). In this chapter, the characteristics of the components of such a hybrid (i.e. polymers and nanoparticles) are discussed. A critical review is presented which is about the most recent research progress in the application of polymers and nanoparticles, including their mechanisms of oil recovery improvement and their transport mechanisms in porous media. The focus is on recent advances that have been made to develop polymers that are suitable for high salinity and temperature conditions.

2.1 Introduction

Injection of water-soluble polymers improves the oil recovery over water flooding by viscosifying the drive water [8]. The concept of polymer injection was first established by Pye [24] and Sandiford [25] in 1964, when they observed that water mobility was reduced and oil recovery was improved, by the addition of small amounts of water-soluble polymers. These included the extended family of acrylamide polymers. Several pilots and field applications were then reported in the USA during the 70s and 80s [26-30]. Since the mid-90s polymer flooding has also been implemented in China with success [31-34]. The characteristics of water-soluble polymers, including the fundamental physical and chemical properties and the structure-property relationship, have been thoroughly discussed and reviewed in previous review articles [26,27,35-44]. These reviews also discuss full-scale polymer floods, the knowledge, and learning related to the logistics of

field execution, process development, and key concepts for successful implementation of the technology as well as any remaining challenges.

The two most common polymers used in field applications are hydrolyzed polyacrylamide (HPAM) and xanthan gum. HPAM, which is by far the most widely used polymer for cEOR, is a synthetic water-soluble polymer. The viscosifying power of HPAM is due to two reasons: (a) the high molecular weight (which can vary up to nearly 30×10^6 g/mol [12]) and (b) the degree of hydrolysis (ranging from 15% to 35% [13]). As a result of hydrolysis, the induced negative charges of the carboxylate groups along the polymer backbone expand the polymer chain in water which leads to an increase in viscosity in comparison with neutral polyacrylamide (PAM). However, at high salinities, electrostatic repulsions between the negatively charged groups along the chain are almost completely screened by mono- or divalent cations which leads to a reduction in viscosity [45]. This effect is worsened as temperature increases due to further hydrolysis of acrylamide monomers in the polymer backbone [46]. Even though the xanthan gum biopolymer is more resistant to high salinities and temperatures, it is very susceptible to bacterial degradation [47,48] and its solution contains some cellular debris that can cause pore-clogging [12]. Cost, availability, and the limited possibilities of modification for xanthan gum are the other reasons which make HPAM far more popular than xanthan gum for field applications.

Reservoirs with both high salinity and high temperature, which are potential targets for polymer flooding, remain untouched due to the scarcity of suitable polymers at these conditions. This shows that there is a need for polymers that can maintain their viscosity in the long term at high salinity and temperature conditions. Several approaches for synthesizing water-soluble polymers with improved rheological properties at high salinities and temperatures have been reported [49-53]. Many focus on the substitution of the acrylamide monomer by at least another monomer type which can enhance the stability of the polymer in harsh conditions [49-51,54] (this will be discussed in more detail in **Section 2.2.6**). Even though modified polyacrylamides have shown promising results at high temperatures and salinities, they are more expensive than HPAM and need to be overdosed to reach target viscosities since their molecular weight is low [43]. Therefore, the use of such modified polymers is often economically unattractive. An alternative approach to overcome the above issues consists of combining the polymer with nanoparticles (NPs) to form a hybrid system with enhanced stability and high viscosity at

elevated temperatures and high salinities (**Chapter 3**). NPs are abundant and relatively cheap and their combination with the state-of-the-art polymers used for cEOR can be economically appealing.

In order for one to develop a polymer–NPs hybrid system, a profound understanding of polymers, NPs, and their flow performance in porous media is required. With this aim in mind, the goal of this review is to elaborate and summarize the current status of water-soluble polymers and NPs for cEOR from their fundamental chemical and physical properties to innovations as well as limitations associated with them. The overview of this paper is given in Figure 2.1. The important characteristics of polymers and NPs are highlighted namely their oil recovery and transport mechanisms in porous media and insights for future developments of polymer–NPs hybrids for high salinity and temperature conditions are provided.

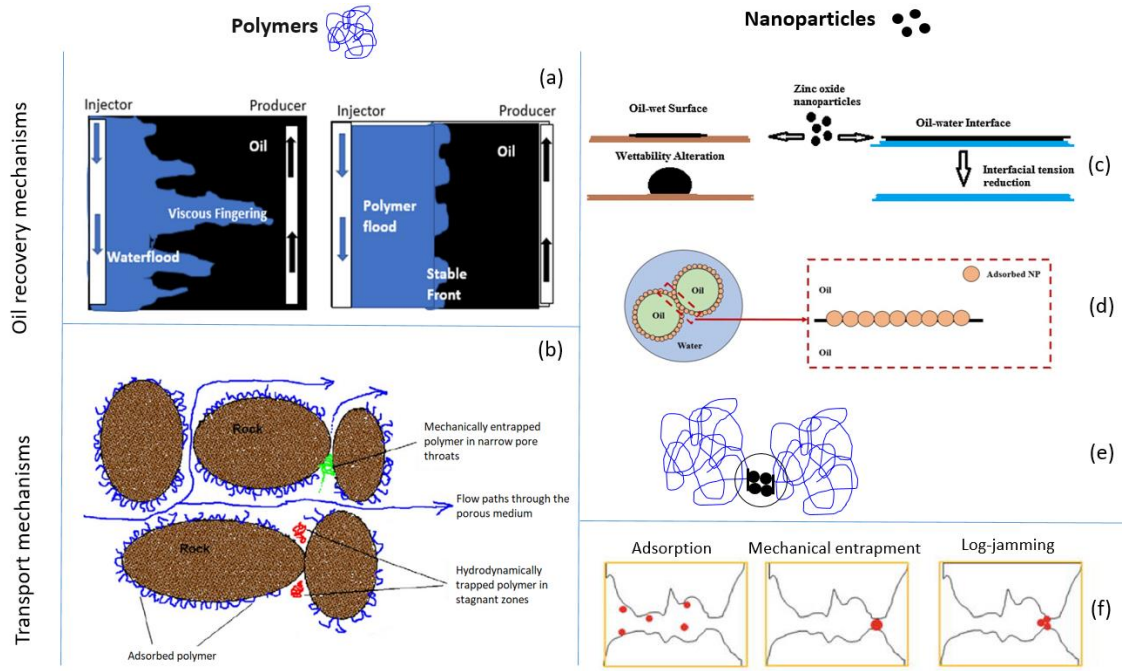

Figure 2.1: Oil recovery and transport mechanisms of polymers and nanoparticles, as will be discussed in this chapter. (a) The decrease in water mobility due to the presence of polymer macromolecules in water [10]. (b) Polymer retention mechanisms in porous media [10]. (c) Reduction in interfacial tension and wettability alteration by nanoparticles [55]. (d) Nanoparticles-stabilised emulsions [56]. (e) Increase in the viscosity of polymer solution because of bridging between polymer chains by nanoparticles. (f) Nanoparticles retention mechanisms in porous media

2.2 Polymers for enhanced oil recovery

2.2.1 Polymer flooding mechanisms

2.2.1.1 Mobility control

It is conventionally believed that oil recovery improvement in polymer flooding is attributed to the concept of the mobility ratio [8,10,57] which is defined by Equation 2.1:

$$M = \frac{\lambda_w}{\lambda_o} = \frac{k_{rw}^e \mu_o}{k_{ro}^e \mu_w} \tag{2.1}$$

where λ, k_r^e and μ are the mobility, endpoint relative permeability, and viscosity respectively, and where the subscripts o and w refer to oil and water respectively. Once the mobility ratio (M) is unfavourable (i.e. $M > 1$), there is a macroscopic sweep inefficiency that triggers an early breakthrough of water. The presence of polymer macromolecules in the water reduces the mobility of the displacing fluid and consequently reduces the fractional flow of water which in turn increases the volumetric sweep efficiency of the system. This is achieved through two mechanisms: (a) by increasing the drive water viscosity and (b) by the reduction in disproportionate permeability. The latter means that the water relative permeability is significantly reduced, while there is a minimum decrease in the oil relative permeability [58,59]. The disproportionate permeability reduction results from the formation of an adsorbed layer of polymer on the pore wall and the segregation of the oil and water flow pathways [60-65]. It should be pointed out that the importance of the disproportionate permeability reduction is more significant for water control than for polymer flooding.

2.2.1.2 Effect of polymer on residual oil saturation

Until recently it was believed that water-soluble polymers merely improved the macroscopic sweep efficiency with no impact on the microscopic displacement efficiency. However, an unexpected increase in the recovery factor from the Daqing oil field, of 13% of the original oil in place (OOIP), generated questions about whether this can be justified by only considering the macroscopic efficiency [66]. Recent studies have suggested that polymer flooding may also improve microscopic displacement efficiency [67,68]. This is accomplished by mobilizing and displacing the residual oil trapped by capillary forces and is attributed to the viscoelastic properties of the polymer solutions. The oil stripping, pulling effect, oil thread and/or column flow, and shear-thickening

behaviour of the polymers have been suggested as mechanisms to elucidate the reduction in residual oil saturation [69].

2.2.2 Polymer rheology in porous media

2.2.2.1 Shear-thickening behaviour

The flow in the microscopic structures of a porous medium is much more complex than the flow in the well-defined geometries of a classical rotational rheometer [10]. For increasing shear rates, the apparent viscosity of polymer solutions versus shear rate in porous media exhibits three main regions. At low shear rates, the polymer viscosity is independent of shear rate (Newtonian behaviour). Above a critical shear rate, the polymer viscosity decreases with increasing shear rate (shear-thinning or pseudo-plastic behaviour). Finally, above a second critical shear-rate, the polymer viscosity increases with shear rate (shear-thickening or dilatant behaviour) [70].

The shear-thickening behaviour of polymer solutions has been investigated by flow experiments in a capillary as a very simple model porous media [71,72]. During flow through capillaries, polymer solutions experience both shear stresses and extensional stresses, the latter being essentially confined to the entry and exit zones of the capillary. Figure 2.2 compares the shear viscosity, measured by a rheometer, and the apparent viscosities in capillaries with varying lengths for an HPAM solution [73]. Below the second critical shear rate, the apparent and shear viscosities are identical. However, above this shear rate, high-pressure drops are observed in the capillaries which results in the deviation of the apparent viscosity from the shear viscosity. The observed pressure drops can be expressed as a summation of three contributions: (1) entry pressure drop, (2) exit pressure drop, and (3) pressure drop due to friction of polymer solution with the wall over the length of the capillary. In capillaries with equal diameter, entry and exit pressure drops are nearly equal and are independent of the capillary length, while the frictional pressure drop increases with capillary length [74]. This results in an increase in apparent viscosity as the entry and exit effects become more significant as the length to radius ratio (l/r) decreases.

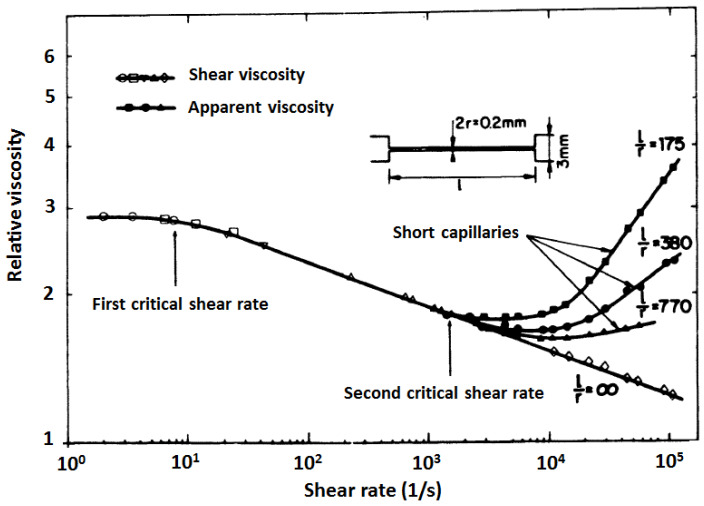

Figure 2.2: Comparison of shear and apparent viscosities in capillaries with different lengths. The experiments were performed at 30 ℃ with 0.034 wt% HPAM dissolved in a brine containing 2 wt% NaCl (1 wt% =10,000 ppm). The radius (r) of the capillary was 1 mm and the length (l) varied [73]

The exact mechanism of shear-thickening behaviour in porous media has been a subject of much research and debate among researchers [75-80]. Several studies have demonstrated that the presence of extensional flow (also referred to as elongational flow) leads to shear-thickening behaviour [45,81-84]. Nonetheless, there is no consensus about the mechanism responsible for the extensional flow of polymer solutions in porous media. There are two difficulties in describing polymer flow through porous media: (1) the topological complexity of the pore network and the geometric complexity of the pore space and (2) the complex behaviour of polymer molecules in extensional flows. The former was studied by using simplified geometries such as (converging-diverging) capillaries to isolate the effects of the extensional flow [81,83,84] and the latter was addressed in more recent studies using microfluidic devices that enabled simultaneous measurements of the apparent viscosity and the visualisation of the polymer deformations due to extensional flows [85]. Here the three main theories found in the literature, that justify the increase in the viscosity of polymer solutions at high flow rates, are presented: (a) the coil–stretch theory, (b) the transient network theory, and (c) the presence of elastic flow instabilities.

In the coil–stretch theory, as De Gennes [86] predicted, the randomly coiled polymers will become fully extended at a critical strain rate ($\dot{\varepsilon}_c$) larger than the rate of relaxation and the coil–stretch transition will occur. This is equivalent to a Weissenberg number Wi (defined as the product of strain rate and relaxation time) larger than 1. Later, a theoretical calculation based on the generalized Zimm model [87] and a numerical calculation by

Larson and Magda [88] have indicated that the onset of the coil– stretch transition takes place when $Wi > 0.5$. Notably, single molecule experiments (based on the DNA visualization) were combined with microfluidic devices to confirm the onset of the coil–stretch transition during flow at $Wi > 0.5$ [89-91].

In the transient network theory, the shear-thickening behaviour of polymer solution is related to the formation of transient networks of polymer chains. Such transient networks exist when entanglements among polymer chains become mechanically effective (i.e. both ends of a chain are incorporated in the network) at timescales shorter than the disentanglement time [92,93]. Shear-thickening effects were observed in (nearly) non-inertial flows for very dilute polymer solutions which would usually disfavour the transient network concept. However, if the polymer molecules are in the stretched state, the probability of forming locally transient networks will increase considerably.

The shear-thickening behaviour has also been recently ascribed to elastic flow instabilities at negligible inertial effect [94-96]. These instabilities are principally a result of inhomogeneous flow fields, which in turn depend on the rheology of the polymer solution and the geometry of flow fields. Kawale et al. [85] found that flowing an HPAM solution in the presence of salt through a model porous media leads to two elastic instabilities. The first elastic instability exists during an apparent shear-thinning regime at $Wi{\sim}80$. By increasing the flow rate at $Wi{\sim}626$ the second elastic instability is observed. The authors attributed the onset of shear-thickening to the second type of elastic instability.

2.2.2.2 Rheological models for polymer flow through porous media

Most of the studies that have looked at modelling polymer rheology in porous media [97-102] have been based on the analytical and numerical solutions of non-Newtonian fluids. Comprehensive reviews on this subject have been given by Savins [103] and Sochi [104]. According to Sochi [104], there is no general methodology yet that can deal with all cases of non-Newtonian flow in porous media. In the absence of a general approach, the continuum approach, capillary bundle models and pore-scale network modelling have received greater attention. These approaches are briefly described below.

Continuum approach: In this model, the porous media is considered as a continuum and its microscopic properties are translated into Darcy-scale parameters such as permeability. The Darcy and Blake-Kozeny-Carman equations are examples of

continuum models. For a non-Newtonian flow such as polymer solution, Darcy's law can be used to determine the polymer apparent viscosity (η_{app}) according to Equation 2.2:

$$\eta_{app} = \frac{k}{V_s}\frac{\Delta P}{L} \tag{2.2}$$

where k is the permeability, ΔP is the pressure drop across a porous medium with length L, and V_s is the superficial velocity in the porous medium. Darcy's law is valid only at a low Reynolds number where the flow is laminar. It also considers only the viscous term and ignores the inertial term. However, at high superficial velocities, inertial effects are no longer negligible. Modifications to Darcy's equation are available to include these non-linearities using the homogenization or volume averaging method [105,106].

A semi-empirical Blake-Kozeny-Carman model is a microscopic approach that is used in fluid dynamics to determine the pressure drop from the superficial velocity of a fluid flowing through a granular packed bed of solids. According to this model, the polymer apparent viscosity can be calculated according to Equation 2.3:

$$\eta_{app} = \frac{\phi^3}{(1-\phi)}\frac{L}{\Delta P}\frac{\psi^2 D^2}{150}\frac{1}{V_s} \tag{2.3}$$

where ϕ is the bed porosity, ψ is the sphericity of the particles in the packed bed and D is the diameter of the spherical particle [107].

Capillary bundle models: In this approach, it is assumed that the porous medium consists of parallel capillaries. For the simplest case where the capillaries are uniform and all have the same radius and length, the permeability is given by [108]:

$$k = \frac{\phi R^2}{8} \tag{2.4}$$

where R is the radius of each tube and ϕ is the porosity of the medium. This is a very simple approach to the porous medium. However, it works very well for the flow of (quasi) Newtonian fluids. Nonetheless, this simplicity ignores several characteristics of the porous medium such as heterogeneity, converging-diverging nature, and morphology of pore space (e.g. pore size distribution, the tortuous character of any flow path). These ignored characteristics can be very important in modelling the flow behaviour of the polymer solution in porous media. For instance, the tortuous character of the flow path causes the polymer molecules to be accelerated and decelerated, and the converging-diverging nature of pore space strongly affects the flow of viscoelastic polymer solutions

[104]. Capillary bundle models have been modified by considering a bundle of capillaries of varying cross-sections [109], to account for the tortuosity [110] and pore size distribution of porous media [111].

Pore-scale network modelling: The basis of the above two approaches is on providing an analytical solution for non-Newtonian fluid flow through porous media. However, the microscopic features of porous media are overlooked, as mentioned above. The modelling of viscoelastic behaviour on the pore-scale aims to take into account both macroscopic and microscopic features. Typically, in pore-scale network modelling, the porous media is considered as a connected network of capillaries [112]. To depict the flow through the network, a simplified form of the flow equations are used. To solve a system with multiple flow equations in order to determine the flow field, a numerical approach is typically exploited. Applying this methodology for a particular random network gives the macroscopic properties (e.g. the apparent viscosity) as a function of flow rate. Generally, the rheology of the polymer solution in the bulk phase and a pore space depiction of the porous media are used as input to the model. The pore-scale simulation begins with solving the flow equation for one single capillary as described in Equation 2.5:

$$Q = H\Delta P \tag{2.5}$$

where Q is the volumetric flow rate, ΔP is the pressure drop along the capillary and H is the flow conductance which is dependent on the viscosity and pressure drop. To find the apparent viscosity of the polymer solution, a set of flow equations is solved for a connected network of capillaries with the assumption that mass conservation is satisfied. The inlet and outlet pressures of the network are set as boundary conditions. In Equation 2.5, the viscosity is pressure-dependent and unknown. Therefore, first, an initial guess for the viscosity is considered. Thereafter, to start, the pressure field is solved iteratively and the viscosity is updated after each iteration cycle, up to the point where the convergence is achieved [113]. Even though pore-scale network modelling is capable of envisaging the general trend of polymer flow through porous media, it still cannot comprise all the complexities. The limitations of this approach include the difficulty in identifying the deformation history of the polymer in the pore throats, the compromise in the viscoelasticity of the polymer solution due to the idealization of the void space, and the adoption of the no-slip-at-wall condition [104].

2.2.3 Polymer retention in porous media

Polymer retention results from the interaction between polymer molecules in the solution and the porous media itself. It leads to the loss of polymer, and if this loss is significant, to a reduction in the viscosity of the polymer solution which in turn results in a decline in oil recovery. Therefore, polymer retention can have an enormous impact on the technical feasibility and economic viability of commercial polymer flooding projects.

2.2.3.1 Polymer retention mechanisms

There are three mechanisms for the retention of polymer in porous media: mechanical entrapment, hydrodynamic retention, and adsorption (see Figure 1b). Retention by mechanical entrapment occurs in porous media when larger polymer molecules become lodged in narrow pore throats [20]. This happens when polymer molecules are smaller than the inlet of the pore throats but larger than their outlet [21,22]. When polymer molecules become trapped in narrow pores, the pore size decreases which increases the probability of trapping the smaller polymer molecules. This self-amplifying process ultimately leads to pore-clogging.

Hydrodynamic retention is caused by an increase in the hydrodynamic forces acting upon the polymer molecules. Once equilibrium in polymer retention is reached, a sudden increase in flow rate will result in extra polymer loss in the porous media as some of the polymer molecules are trapped in stagnant flow regions by hydrodynamic drag forces. When the flow rate is reduced or flow is completely stopped, polymer molecules may diffuse back to the main flow channels and the newly-retained polymer molecules will be released; therefore this phenomenon is reversible [20,114,115].

Adsorption takes place when there is an attractive interaction between the polymer molecules and the rock surface. Polymer adsorption onto the rock is considered a physical phenomenon and is a result of the high affinity of the polymer due to van der Waals forces and hydrogen bonding [116-118]. The adsorbed flexible polymer chain exists as a series of trains, loops and tails. The trains are the polar groups along the polymer chain that are attached to the various polar points on the rock surface. The loops are those parts of the chain that exist between two trains that stretch out into the solution. The tails are at the end of the polymer chain and have merely one end fixed to the surface [57,119]. Even though some of the trains of the polymer chain might detach from the surface of the rock, other trains will remain in place. Once other trains detach, the formerly detached trains may reattach to the surface of the rock. Therefore, it is statistically very unlikely that a

polymer chain would release all the attachment points simultaneously. This was explained by Zitha et al. [120] using a mechanism comprised of the following stages: (a) chain stretching in the zones where the flow is strongly extensional, (b) a transport short enough for the stretched chains not to be relaxed, and (c) adsorption by the formation of bridges across the smallest pore restrictions. If the ends of the molecules attach to the rock, a plugging or increased resistance to flow can develop.

Among the above three mechanisms, hydrodynamic retention is probably the one that contributes the least and is often neglected [70]. The relative importance of mechanical entrapment and adsorption depends on the ratio between the hydrodynamic radius of the polymer coil (R_h) and the pore radius (R_p). For $R_p > 50R_h$, which is almost always the case for high-permeability sands [115], polymer adsorption is the dominant mechanism while for $R_p < 3R_h$, which is typical of low-permeability rocks, mechanical entrapment is dominant [20,22,115]. However, there are exceptions to this criterion. For instance, only 35.2% of the retention of an HPAM solution in a high-permeability silica pack (5.6 Darcy) was accounted for by adsorption and the remaining retention was attributed to mechanical entrapment and hydrodynamic retention. This discrepancy can be accounted for by the high heterogeneity of the tested silica pack [121].

2.2.3.2 Polymer depletion and inaccessible pore volume

If the size of the polymer chain is not negligible compared to the pore size, which is the case for low permeability rocks, the following consequences for polymer rheology may be expected: (a) in a non-adsorbent porous media, pore wall depletion excludes the polymer macromolecules from the slowest streamlines near the wall, thus giving a polymer velocity higher than the solvent velocity and (b) in an adsorbent porous media, the flow is modified due to adsorbed layer thickness [45].

The inaccessible pore volume (IPV) [20,122] accounts for the volume of the pores through which the large polymer molecules cannot flow. Several models and mechanisms have been proposed in the literature to explain the occurrence of IPV, including the relative size of pore throats, pore wall exclusion, and entropic effects [123-127]. As a result of the existence of IPV, polymer adsorption is reduced as there will be less contact between the polymer molecules and the rock surface.

2.2.3.3 Measurement of polymer retention in porous media

The measurement of polymer retention in the laboratory can be done in bulk or core-flood experiments. Bulk tests are usually referred to as static adsorption tests, which measures

the change in polymer concentration when it is mixed with a crushed rock sample. Polymer retention in core-flood experiments is referred to as dynamic adsorption (DA). A polymer solution together with a non-adsorbing tracer (commonly potassium iodide) is injected into the cores and the effluent is collected over time. Thereafter, the effluent is analysed to determine the variation in the tracer and polymer with time, and thus to find the level of adsorption (i.e. the comparison of the effluent concentration to the initial polymer concentration). The two most frequently used methods in the literature to measure dynamic adsorption are described below.

In the first method, which is known as the single injection method, the polymer and tracer are co-injected and their normalized concentrations (i.e. the effluent concentration divided by the initial concentration) are plotted as a function of pore volumes (PV) injected. The DA is then determined by calculating the area between the polymer and tracer curves and subtracting the IPV [122]. Alternatively, the DA can be calculated by reading the pore volumes of the injected tracer and polymer where their normalized concentration is 0.5 and subtracting the IPV [20]. The disadvantage of the single injection method is that the IPV must be known in order to obtain an accurate result.

The second method, known as the double injection or extended injectivity method, is proposed by several authors [128-130]. In this method, two injection steps are taken. An illustration of these two injection steps is shown in Figure 2.3.

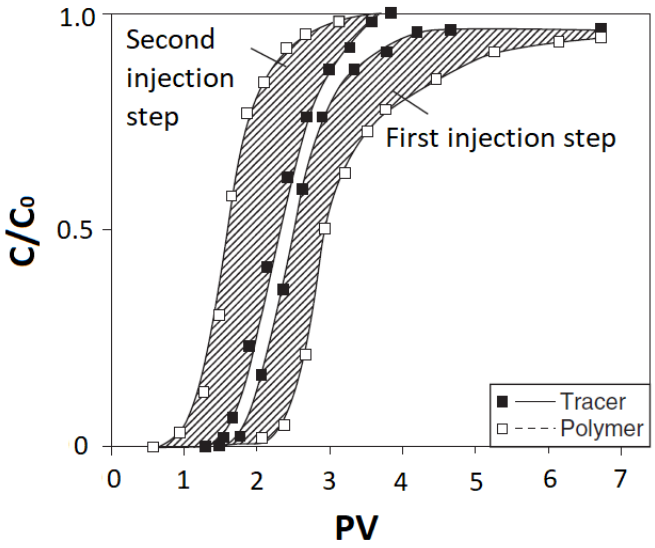

Figure 2.3: The tracer and polymer normalised concentration profiles in the effluent in the double injection method for polymer retention measurement in porous media. Taken from [129] with minor changes

In the first step, the polymer and tracer are co-injected. In this step, the tracer leads the polymer because of polymer adsorption which delays the polymer advancement through the porous medium. The assumption here is that the injection of many pore volumes of polymer solution leads to saturation of all the adsorption sites on the rock surface by the polymer molecules. In the second step, brine is first injected to displace all the mobile polymer and tracer, followed by the co-injection of polymer and tracer once again. In this step adsorption no longer plays a role. Since some of the pores are not accessible to the polymer molecules, but are to the tracer, the polymer leads the tracer. Consequently, the IPV is determined during the second step by calculating the difference between the areas of the tracer and polymer curves according to Equation 2.6:

$$\mathrm{IPV} = \Sigma\left[\left(\left(\frac{C}{C_0}\right)_p - \left(\frac{C}{C_0}\right)_t\right) \times \Delta\mathrm{PV}\right] \tag{2.6}$$

where C and C_0 are the effluent and initial polymer concentration respectively, ΔPV is pore volume increment for each effluent sample and where subscripts p and t refer to polymer and tracer respectively. It should be noted that this IPV, measured in the presence of adsorbed polymer, could be different from the IPV of the bare porous medium before any adsorption has taken place. The DA is then determined from the first injection step by Equation 2.7:

$$\mathrm{DA} = \frac{\Sigma\left[\left(\left(\left(\frac{C}{C_0}\right)_p - \left(\frac{C}{C_0}\right)_t\right) \times \Delta\mathrm{PV}\right) + \mathrm{IPV}\right] \times (C_0)_p \times \mathrm{PV}}{m} \tag{2.7}$$

where m is the rock mass.

2.2.3.4 Modelling of polymer retention in porous media

To model the polymer retention in porous media, simulators such as UTCHEM and Eclipse consider a Langmuir type isotherm. In this approach, polymer retention is modelled as a function of polymer concentration, salinity, and permeability according to Equation 2.8 [131]:

$$\widehat{C_4} = \min\left[\widetilde{C_4}, \frac{a_4\,(\widetilde{C_4} - \widehat{C_4})}{1 + b_4\,(\widetilde{C_4} - \widehat{C_4})}\right] \tag{2.8}$$

where $\widehat{C_4}$ and $\widetilde{C_4}$ are the polymer retention and concentration respectively. The minimum is taken to ensure that the polymer retention is smaller than the total polymer concentration. a_4 is defined as:

$$a_4 = (a_{41} + a_{42}C_{\mathrm{SEP}})\left(\frac{k_{ref}}{k}\right)^{0.5} \tag{2.9}$$

where C_{SEP} is the effective salinity described as follows:

$$C_{\mathrm{SEP}} = \frac{C_{51} + (\beta_{\mathrm{p}} - 1)C_{61}}{C_{11}} \tag{2.10}$$

where C_{51}, C_{61}, and C_{11} are the anion, divalent cation, and water concentrations in the aqueous phase and β_{p} is the covalent coefficient which is known from laboratory experiments. The value of a_4/b_4 characterizes the highest amount of adsorbed polymer and b_4 controls the curvature of the isotherm. The reference permeability (k_{ref}) is the permeability at which the input adsorption parameters are stated.

2.2.4 Factors influencing polymer performance in porous media

2.2.4.1 Polymer type

As discussed, high molecular weight synthetic polymers like HPAM exhibit shear-thickening behaviour in porous media due to their flexible coil conformation. However, such shear-thickening behaviour is absent for biopolymers like xanthan gum and scleroglucan due to their rigid rod-like conformation. They are likely to align in the flow field and remain shear-thinning instead of showing viscoelastic behaviour [132-134]. Biopolymers have also shown significantly lower retention in porous media compared to synthetic polymers [10,57]. For synthetic polyacrylamides, the degree of hydrolysis plays an important role in polymer retention, and as it increases the polymer retention in porous media decreases [135]. Lecourtier et al. [136] observed that the retention of a non-ionic polyacrylamide (PAM) solution with pH 7 onto a SiC surface was dramatically higher than that of HPAM with a degree of hydrolysis of 30%. This was because the negatively charged surface of SiC at pH 7 gives rise to a repulsion term once it interacts with the negative charges present in the HPAM chain. The retention of PAM and HMPM were comparable only at a salinity of 2.4 wt% (24,000 ppm), where the negative charges along HPAM are screened.

Modifying the polymers (as discussed in **Section 2.2.6**) can also influence polymer adsorption and retention. Szabo [137] showed that the adsorption of poly(2-acrylamido-2-methyl-1-propanesulfonic acid) commonly known as AMPS, is lower than HPAM.

Vermolen et al. [138] also reported that the incorporation of AMPS, as well as N-vinyl pyrrolidone (N-VP) into HPAM, can dramatically reduce its retention.

2.2.4.2 Polymer molecular weight

Higher molecular weight, i.e. longer polymer chains, implies higher viscosifying power and potentially higher resistance to flow in porous media. However, flow resistance, also referred to as injectivity decline, can be time-dependent [21,139] as higher molecular weight polymers are more sensitive to mechanical degradation. Mechanical degradation will be more likely to occur in extensional flow fields, but some degradation of polymer chains with very high molecular weight (or degree of polymerization) may also occur for pure shear flows [140]. Odell et al. [141] predicted that a mid-chain scission will occur, in the dilute regime, when there is a continuous increase of stress on the centre of the chain and after a critical strain rate known as the critical fracture ($\dot{\varepsilon}_f$). Since the relaxation time increases with chain length, Wi is larger for the longest chains than for the shortest chains. Hence, the higher molecular weight polymers are more prone to mid-chain scission than the lower molecular weight ones. It has been experimentally shown that mid-chain scission is induced by a transient extensional flow field [142,143] as well as ultrasonic cavitation [144,145].

The effect of molecular weight on polymer retention has also received attention. Dang et al. [146] reported a simulation study showing that the maximum adsorption of HPAM was obtained with the lowest molecular weight in good agreement with the experimental study of Yang et al. [147] in which adsorption of HPAM on sodium–montmorillonite decreased with increasing molecular weight. In some studies, however, with increasing molecular weight, the adsorption level first increased and then became constant [148,149].

2.2.4.3 Polymer concentration regimes

Depending on the target viscosity, polymer solutions may be used at different concentrations. Several authors have proposed that HPAM retention is dependent on the polymer concentration regime [22,122,150,151]. In the semi-dilute regime, polymer retention increases with increasing concentration. Szabo and Corp [22] suggested that the concentration dependence of HPAM adsorption in the semi-dilute regime is linear. In the dilute and concentrated regimes, on the other hand, polymer retention is basically concentration-independent [150]. This implies that a Langmuir isotherm can describe the concentration dependency of the polymer retention [152] (see **Section 2.2.3.4**). Furthermore, polymer chain scission is also concentration-dependent. In the dilute

regime, beyond the critical fracture, the mid-chain scission occurs and the polymer chain is broken almost precisely in half. Whereas in the semi-dilute regime, with increasing the polymer concentration, the chain scission does not occur in the centre of the chain and is increasingly randomized [153].

2.2.4.4 Porous media permeability

When the retained polymer molecules form an adsorption layer on the rock surface, the effective pore size is reduced, resulting in a decrease in the rock permeability or an increase in the residual resistance factor. This phenomenon typically becomes more severe when the rock permeability is smaller than 500 mD [154-157].

In such lower-permeable rocks (<500mD), the polymer retention also increases dramatically with decreasing permeability. Vela et al. [155] measured the polymer retention from the material balance of injected and produced fluids, and found that the retention of HPAM increases from ~12 μg/g in 137 mD sandstone to ~130 μg/g in 12 mD sandstone. In contrast, in higher permeability rocks, polymer retention is generally insensitive to permeability [65].

2.2.4.5 Residual oil saturation

In water-wet cores, the presence of residual oil in the core has little effect on the polymer retention [158], or even reduces it [22,129,159], as compared to oil-free, 100% brine saturated cores. However, in contradiction to these findings, Hughes et al. [129] observed that the retention of xanthan gum on 127 mD Berea sandstone increased in the presence of residual oil. The authors ascribed this phenomenon to the increase in polymer trapping caused by the reduction, due to the presence of the oil, of the core permeability.

The effect of residual oil on polymer retention may be different in oil-wet cores. Broseta et al. [158] described that the existence of residual oil (iso-octane) saturation in oil-wet cores significantly decreased the HPAM retention by a factor of 2–5.

2.2.4.6 Iron and clay content

The presence of iron and clay can strongly affect the surface properties of the core. The point of zero charge (PZC) for pure quartz is reported to be 1–3 [136,160,161]. Farooq et al. [162] reported that the PZCs of Bentheimer and Berea sandstone samples were approximately 3.0 and 8.2 respectively. In their experiments, the quartz fractions for Bentheimer and Berea sandstone samples were found to be approximately 98.0% and 82.5% respectively whereas the clay fractions were approximately 0.5% and 9.0%

respectively. Peksa et al. [163], whose Bentheimer sample had a quartz fraction of approximately 92%, measured a PZC of nearly 8. This unexpectedly high PZC was attributed to the presence of clay (~ 2.7 %) and iron particles (~ 0.2 %) distributed within the sample. Clay particles are well distributed in sandstone and become mobile in contact with fluids at pH higher than 8 [164,165]. The higher the pH, the more visible the effect is. In addition, the effect of the iron minerals, such as goethite and hematite, present in sandstone on the PZC was observed. Iron oxides represent a PZC in the range of 8.5–11 [166]. This suggests that even a small proportion of iron and clay content, if well distributed in the rock, can dramatically increase the PZC of the sandstones. Further work on the effect of iron and clay particles on the PZC of sandstone is needed. A PZC of 8 for sandstone leads to a positively charged rock surface at injected water pH of around 7, which results in increased interactions with negatively charged polymers such as HPAM or xanthan gum.

2.2.4.7 Salinity and hardness

Salinity and hardness have been associated with two major effects on polymer performance in the literature: viscosity loss and polymer precipitation. For synthetic polymers, namely HPAM, the viscosity loss at high salinities has been ascribed to shielding of the electric charges along the polymer chain [14]. Since high molecular weight HPAM has a flexible coil conformation, it responds strongly to the ionic strength of the aqueous solvent [10]. At high salinities, the negative charges along the HPAM backbone are screened leading to a reduction in electrostatic repulsion and a shrinking of the polymer coils in the solvent. The end result of this process is a relatively lower hydrodynamic radius of the polymer coils. The reduction of the hydrodynamic radius of the polymer coils results in viscosity loss.

In addition, a major challenge for the use of HPAM at high salinities is the presence of a high concentration of divalent cations such as Ca^{2+} and Mg^{2+}. In the presence of the divalent cations, polyion–metal complexes can be formed, which in turn leads to polymer precipitation due to the complexing ability of the carboxylate groups of HPAM [15,16].

Biopolymers, namely xanthan gum have shown less sensitivity to salinity and hardness compared to synthetic polymers. At high salinities, the structure of the xanthan gum backbone experiences a conformational alteration from a disordered conformation to an ordered and more rigid structure (coil-helix transition) [167-169]. As a result of the rigidity of the polymer chain, xanthan gum is less sensitive to the presence of ions in the solvent, as compared to HPAM.

2.2.4.8 Temperature

High salinity and hardness in oil reservoirs are often accompanied by high temperatures. Viscosity loss and polymer precipitation of HPAM become more severe at elevated temperatures, as the further hydrolysis of the polymer backbone is promoted. This causes additional interaction between the charged polymer backbone and ions in the solvent. Moradi-Araghi and Doe [17] suggested a temperature stability limit for HPAM based on the cloud point and rate of hydrolysis. They demonstrated a "safe" limit of approximately 75, 88, 96, and 204 ℃ for HPAM in brines containing 2,000, 500, 270, and 20 ppm hardness respectively. They suggest that even a small concentration of divalent cations at high temperatures can substantially hinder the use of HPAM.

A helix-coil transition occurs in the structure of xanthan gum at high temperatures which causes a reduction in the viscosity. However, compared to HPAM, xanthan gum is more resistant to high temperatures due to its more rigid backbone. Long-term stability experiments carried out using a commercial xanthan gum showed that the solution viscosity remained almost unchanged for about 2 years at 80 ℃ [170].

A common way of assessing the long-term stability (ageing) of polymers at combined high salinity, hardness, and temperature is to keep the samples in an oven for up to one year and monitor the viscosity loss or polymer precipitation over time. Alternatively, thermal gravimetric analysis (TGA) can be used to assess the polymer resistance to thermal degradation [171-173]. For long-term stability experiments, the polymer samples should be completely de-oxygenated (i.e. the experiments are performed at anaerobic conditions). This is needed to ensure that viscosity loss is only due to the effect of high salinity, hardness, and temperature, rather than the effect of a free radical attack caused by the presence of oxygen in the samples.

2.2.5 Polymer flooding in practice

Several authors have proposed criteria for polymer flooding projects based on the effects of the parameters discussed in the preceding sections. There is a consensus about the fact that, prior to any field applications, laboratory experiments should be carried out to assess the feasibility of a polymer flooding project and estimate the probability of success [174,175]. Specific criteria in laboratory experiments to enhance the chances of success of a polymer flooding project include the following: (a) meeting the target viscosity at reservoir conditions, (b) good filterability to ensure good injectivity, (c) suitable solubility

in brine, and (d) maintaining stability and viscosity under the influence of degrading factors such as shearing, heating, salinity and hardness [174].

Table 2.1 shows the range of parameters for polymer flooding in laboratory experiments compared to real field applications. Table 2.2 gives a summary of these parameters in different field projects that have been performed recently.

A summary of the range of parameters in the laboratory experiments, as shown in Table 2.1, is as follows. HPAM, xanthan gum, and associative polymers have been extensively used in laboratory experiments. There is a wide range in both the molecular weight (1–25 × 10^6 g/mol) and the concentration (from 30 up to 10,000 ppm) of these polymers in the performed experiments. The salinity of the water, in which the polymers are dissolved, is as high as 186,000 ppm. The experiments are performed at temperatures of up to 120 ℃. Moreover, in laboratory experiments, the behaviour of the polymers is studied in various types of model porous media including sandstone and carbonate cores, sand-packs and microfluidics. The permeabilities of these porous media range from very low (<10 mD) to very high (>13,000 mD) and the porosity ranged from 10 to 47%.

As can be seen in Table 2.1, in field applications, HPAM is the most commonly used polymer by far and only one project used an associative polymer (SZ36-1, China). As for the polymer molecular weight and concentration, the selected range for field applications is more limited than the laboratory experiments. The main motivation behind this is to avoid the injectivity problems, which can be a result of the high concentration and molecular weight of the injected polymer solution. The range of polymer molecular weights used is strongly dependent on reservoir permeability. High molecular weight polymers (>17×10^6 g/mol) have been used in reservoirs with an average to high permeability (> 400 mD).

In contrast to the laboratory experiments, polymer injection has rarely been used in carbonate reservoirs in field applications and its use is mainly limited to sandstone reservoirs. The salinity of the injected water in the majority of field applications is lower than 50,000 ppm. It should be noted that for the Dalia/Camelia field in Angola, the formation water salinity was 117,000 ppm but the injected water salinity was 24,900 [176,177]. To our knowledge, the only field application with a very high salinity in the injected water is the Bockstedt field in Germany in which schizophyllan was used but despite good injectivity, considerable biological degradation was observed even in presence of biocide [178,179].

The lack of successful projects in harsh conditions inspires the need for polymers that are stable at high salinity, especially in situations where there are high temperatures, which can worsen the degradation effects. In the following section, the recent developments in polymers for high salinity and temperature conditions are discussed.

Table 2.1: Range of parameters for polymer flooding in laboratory vs. field applications [36,174,175]

Parameter	Laboratory experiments	Field applications
Polymer type	HPAM Xanthan gum Associative polymer	HPAM Xanthan gum Associative polymer (1 project)
Polymer molecular weight (g/mol)	1–25 × 10^6	12–25 × 10^6
Polymer concentration (ppm)	30–10,000	300–4,000
Permeability (mD)	2.5–13,000	>50
Porosity (%)	10–47	4–37
Oil viscosity (mPa s)	1.7–5,500	<5,000
Lithology	Sandstone cores Carbonate cores Sand-packs Micromodels	Majority in sandstone reservoirs Very few in carbonate reservoirs
Water salinity (ppm)	250–186,000	Majority <50,000
Temperature (℃)	20–120	<99

Table 2.2: Range of parameters in recent polymer flooding field applications (1 MDa =10^6 g/mol, NR = not reported)

Country	Field	Formation water salinity (ppm)	Temperature (°C)	Oil viscosity (cp)	Polymer type	Polymer concentration (ppm)	Polymer viscosity (cp)	Ref.
Canada	East Bodo/Lloydminster	29,000	NR	417–2,000	HPAM (F3630/F3830)	1,500	50–60	[180]
	Pelican Lake	6,853	23	1000–3000	HPAM (13.6 MDa)	600–3,000	13–50	[181]
China	SZ36-1	6,071	65	70	Associative polymer	600–2,400	98	[182]
	Daqing	6,000	45	44,113	HPAM	1,000–2,500	40–300	[183,184]
	Shengtuo	21,000	80	10–40	HPAM	1,800	30–50	[174]
	Bohai Bai	2,873–20,000	50–70	30–450	HPAM	1,200–2,500	98	[185]
	Gudao	8,207	65	50–150	HPAM	2,000	350	[174]
	ShuangHe	5,060	72	7.8	HPAM	1,090	93	[186]
Brazil	Buracica	41,000	60	44,013	HPAM (Flopam)	500	10	[187]
	Carmopolis	17,091	50	10.5	HPAM (Flopam)	500	40	[188]
Oman	Marmul	3,000	46	80–90	HPAM (Nalco Q41F)	1,000	15	[189,190]
Suriname	Tambaredjo	5,000	38	325–2,209	HPAM (3630S)	1,000–2,500	45–140	[191]
India	Mangala	5,400	62	44,805	HPAM	2,000–2,500	20	[192,193]
Germany	Bockstedt	186,000	54	47,423	Schizophyllan	300	25	[178,179]
Angola	Dalia/Camelia	117,700	45–56	44,136	HPAM (18–20 MDa)	900	3	[176,177]

2.2.6 Polymers for high salinity and temperature

The synthesis of modified polymers, with higher temperature and/or salt tolerance, has been reported by several authors. These modified polymers are listed in Table 2.3. They were typically obtained by hydrophobically modifying conventional polymers or by the incorporation of salt- and temperature tolerant monomers such as 2-acrylamido-2-methyl-1-propanesulfonic acid (AMPS) and n-vinyl pyrrolidone (N-VP) to the HPAM backbone.

Table 2.3: Polymers stable at high salinity and/or high temperature (TDS=total dissolved solids, DC=divalent cations)

	Polymer	Salinity (ppm)	Temperature (°C)	Ref.
No.1	Hydrophobically modified polyacrylamide with methylene	100,000	25	[194]
No.2	Hydrophobically modified polyacrylic acid with alkyl acrylate	40,000	25	[195]
No.3	Hydrophobically modified polyacrylic acid with 2-(N-ethylperfluorooctanesulfoamido) ethyl acrylate (FA) or 2-(N-ethylperfluorooctanesulfoamido) ethyl methacrylate (FMA)	19,000	25	[196]
No.4	Hydrophobically modified polyacrylamide with *N*-phenethylacrylamide	90,000	25	[197]
No.5	Terpolymers of acrylamide (AM) with sodium 3-acrylamido-3-methylbutanoate (Na-AMB) and 2-acrylamido-2methylpropanedimethylammonium chloride (AMPDAC)	30,000	30–60	[198]
No.6	Hydrophobically modified polyacrylic acid with 3-pentadecylcyclohexylamine (3-PDCA)	0	30–60	[199]
No.7	Hydrophobically modified polyacrylamide 3-(2-acrylamido-2-methylpropanedimethylammonio)-l-propanesulphonate (AMPDAPS)	0	25–60	[200]

No.8	Poly(propylene oxide) methacrylate	0	25–70	[201]
No.9	Thermoviscosifying polymers (TVP) mainly based on thermosensitive poly(*N*-isopropylacrylamide) (PNIPAM) and polyethylene (PEO)	33,000 (TDS), 900 (DC)	90	[202]
No.10	Copolymer of hydrolysed polyacrylamide (HPAM) and 2-acrylamido-2-methylpropane sulfonic acid (AMPS)	50,000	80	[203]
No.11	Incorporation of Acrylamido-Ter-Butyl-Sulfonate (ATBS) and/or N-vinyl pyrrolidone (N-VP) into hydrolysed polyacrylamide (HPAM)	500–100,000	85–140	[204]
No.12	Synergy of hydrolysed polyacrylamide (HPAM) or and 2-acrylamido-2-methylpropane sulfonic acid (AMPS) with surfactant	172,000	95	[205]
No.13	Incorporation of sodium 2-acrylamido-2-methylpropane sulfonic acid (Na-AMPS) and/or N-vinyl pyrrolidone (N-VP) and/or sodium 3-acrylamid 3-methyl butyrate (N-AMB) and/or N-vinyl amide (N-VAM) into hydrolysed polyacrylamide (HPAM)	34,600–180,000 (TDS)	90–120	[206]
No.14	Incorporation of Acrylamido-Ter-Butyl-Sulfonate (ATBS) and/or N-vinyl pyrrolidone (N-VP) into hydrolysed polyacrylamide (HPAM)	13,000 (TDS), 7,000 (DC)	85	[207]
No.15	Copolymer of 2-acrylamido-2-methylpropane sulfonic acid (AMPS) and hydrolysed polyacrylamide (HPAM)	170,000 (TDS), 17,000 (DC)	100	[52]
No.16	Incorporation of sodium 2-acrylamido-2-methylpropane sulfonic acid (Na-AMPS) and/or N-vinyl pyrrolidone (N-VP) into hydrolysed polyacrylamide (HPAM)	43,700–179,800 (TDS), 2,100–17,700 (DC)	120	[138]

In literature, the experiments that investigate the effectiveness of modified polymers at high salinity and temperature conditions fall into the following three categories: (a) the viscosity of the modified polymer is compared with the viscosity of a conventional polymer such as HPAM, both dissolved in brine [171,208] (b) the viscosity of the modified polymer dissolved in brine is compared with its viscosity in de-ionised (DI) water [134,209,210] and (c) the viscosity of the modified polymer is measured in brine with different compositions and ionic strengths [134,171,209,211]. Such experiments are often performed at various temperatures and consider both short- and long-term temperature effects on the performance of the modified polymers. In the following sections, a summary of these investigations is given, and the mechanisms for the enhanced performance of polymers at high salinity and temperature are discussed.

2.2.6.1 Hydrophobically modified polyacrylamides

Hydrophobically modified polyacrylamides differ from the conventional polyacrylamides used for cEOR, as they have small hydrophobic units in the polymer chain. Several hydrophobic monomers, for example, acrylate or alkyl groups with different topologies and number of carbons, have been used as the hydrophobic units of these polymers [212-214]. The fraction of hydrophobic units should be minimized to ensure the solubility of the polymer in water. However, even a small hydrophobic fraction can significantly change polymer properties.

Hydrophobically modified polyacrylamides are synthesized using different techniques such as micellar [215-217], homogeneous, and heterogeneous polymerisation [215]. The hydrophobic units may be distributed in various ways through the polymer, such as randomly or block-like [51,54,213,215,218-220], and they can be coupled at one or both ends [221-226]. The distribution of the hydrophobic groups as a result of micellar copolymerization is block-like while solution copolymerization results in a random distribution. This will be discussed in more detail in **Chapter 3**.

a) General properties

Hydrophobic–hydrophobic interactions among the polymer chains result in either intra- or inter-molecular associations or their combination. An illustration of the concept of intra- or inter-molecular associations for a hydrophobically modified polyacrylamide is shown in Figure 2.4.

The dominance of either association type depends on the polymer concentration and has a strong impact on the viscosity of the polymer solution. In the dilute regime, HMPAM forms more intra-molecular associations than intermolecular ones, twisting the macromolecular chains and reducing the hydrodynamic radius, and thus reducing the viscosity. At concentrations higher than the critical association concentration (CAC), inter-molecular associations become more dominant which abruptly increases the hydrodynamic radius of the polyacrylamides [227-231].

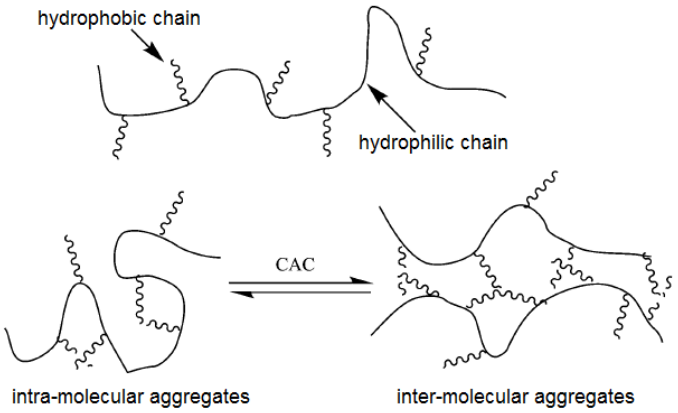

Figure 2.4: Intra- and inter-molecular associations in a hydrophobically modified polyacrylamide [231]

b) Effect of salinity

Several authors have reported that the addition of salt can enhance the viscosity of hydrophobically modified polyacrylamides [213,232,233]. The reason for this appears to be that, by screening the electric charges along the chains with the salts, the electrostatic interactions are suppressed. As a result, the hydrophobic associations are less likely to be disrupted by electrostatic interactions, and this results in a higher solution polarity. The higher polarity leads, in turn, to the reinforcement of the hydrophobic associations which allow the formation of aggregates and a stronger network through inter-molecular hydrophobic associations [196]. Therefore, an increase in the viscosity of the solution is expected in the presence of salt (see polymers 1, 2, 3, 4 in Table 2.3).

However, upon a further increase in salinity, the hydrophobic aggregates become more compact. These condensed aggregates then associate to form larger aggregates, which results in the phase separation of the polymer and a reduction in the viscosity [213,234]. For instance, Al Sabagh et al. [235] reported a rheological study of three HMPAMs [236] at 30 ℃. The authors found that first, the viscosity increases with increasing NaCl concentration up to 2.9 wt% (salt-thickening) and then above this value, the viscosity decreases as the NaCl concentration increases (salt-thinning) (see Figure 2.5a). Rather

similar behaviour was observed for $CaCl_2$ concentration. However, the transition from salt thickening to salt thinning behaviour occurs at a much lower concentration for $CaCl_2$ (0.2 wt%) (see Figure 2.5b). Zhong et al. [237] suggested that salt thickening behaviour can occur at two ranges of salinities (2–3 wt% and 5–9 wt%) but at salinities higher than 9 wt%, the viscosity decreased.

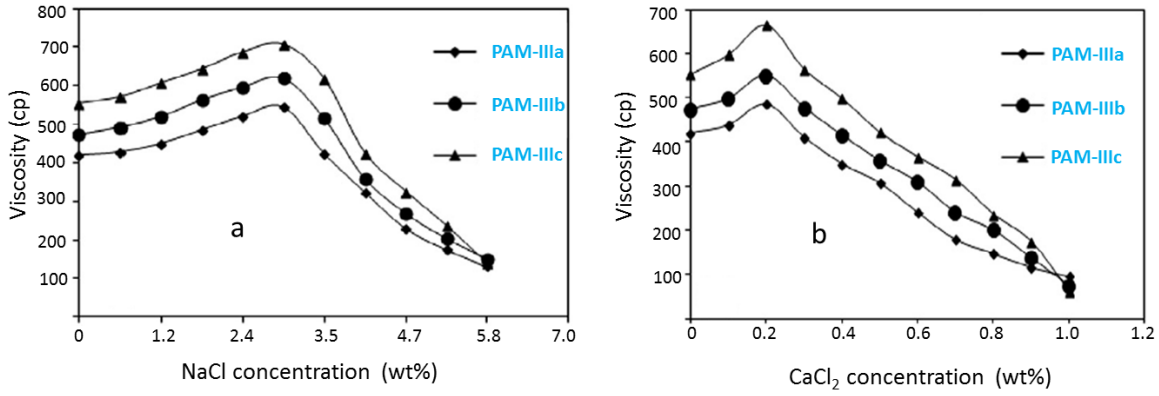

Figure 2.5: Effects of NaCl and $CaCl_2$ Concentration on the viscosity of hydrophobically modified polyacrylamides at 30 °C [235]

More recently, Mirzaie Yegane et a. [238] showed that the viscosity of HMPAM in a brine containing 20 wt% NaCl and 1.5 wt% Ca^{2+} has a viscosity some 55% higher than its viscosity in DI water regardless of HMPAM concentration. This exceptional viscosity increase at high salinity was attributed to the excellent solubility of the HMPAM in both brine and DI water, as well as the increase in solvent viscosity which was measured to be 0.9 ± 0.1 and 1.4 ± 0.1 mPa s for DI water and brine respectively. It is our understanding that the solubility of the hydrophobic group plays a key role in maintaining the viscosity with increasing salinity and hardness. Therefore, it is recommended to estimate the solubility limit of the hydrophobic comonomers prior to polymerization to decide on (a) the type of hydrophobic group and (b) the fraction of hydrophobic units to be incorporated into the polymer backbone.

c) Effect of temperature

For both compositional and structural reasons, the behaviour of the HMPAMs is significantly affected by temperature. An increase in temperature improves the solvent quality of the hydrophilic segments of the HMPAM. This will tend to increase the hydrodynamic radius of the chains. At the same time, the solvent quality for the hydrophobic segments will deteriorate. Therefore, the hydrophobic units will have an

increased tendency to form stable networks. Both effects could lead to an increase in viscosity as temperature increases.

The increase in the viscosity of the HMPAMs with increasing temperature is also explained by the concept of so-called thermo-thickening copolymers (also known as thermo-associative and thermo-stimulated copolymers) [239-241]. This concept is based on the switch properties of polymers characterized by a lower critical solution temperature (LCST). These polymers have a highly water-soluble macromolecular backbone, with some LCST side chains or blocks (see Figure 2.6). With increasing temperature, these thermo-sensitive moieties can undergo reversible micro-phase segregation. Above the CAC, this change results in an increase in the solution viscosity through inter-molecular associations. It is noteworthy that the thermo-thickening behaviour of the polymer solution is more evident at low salinities and shear rates [242].

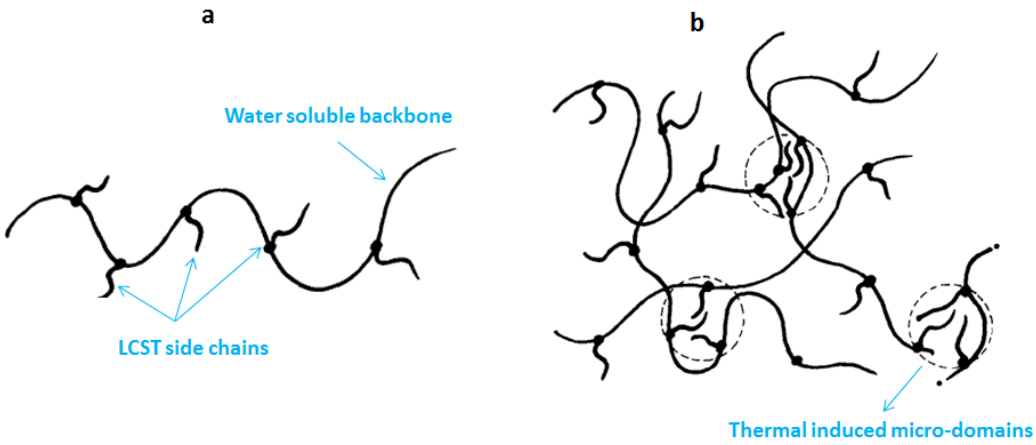

Figure 2.6: Thermo-thickening concept in aqueous solutions: (a) copolymer structure; (b) association mechanism (*T*>LCST) [241]

The viscosities of solutions of polymers 5 or 6 in Table 2.3 are not significantly dependent on the temperature, when in the range of 30–60 ℃ [198,199]. The intrinsic viscosity of a solution containing polymer 7**,** rose from 6.5 to 8.5 dl/g as temperature increased from 25 to 60 ℃ [200]. Thermo-thickening behaviour at low ionic strength and shear rate was observed with polymer 8 [201]. This was ascribed to the increase in the concentration of poly(propylene oxide) (PPO) in the hydrophobic micro-domains. This resulted in an increase in chain mobility at fairly high temperatures. With further increase in the temperature, the viscosity of the hydrophobically modified polymers is expected to decrease. This is ascribed to the loss in the network connectivity because of changes in the hydrophobic micro-domains.

Even though hydrophobically modified polymers can enhance the solution viscosity at moderately high salinity and temperature, their application at higher salinity (>5 wt% TDS) and higher temperature (>80 ℃) is challenging. This becomes more difficult, in particular, when high salinity and high temperature coexist in a reservoir where the polymer solution viscosity will potentially be strongly reduced.

2.2.6.2 Salt- and temperature-tolerant modified polyacrylamides

Several researchers have attempted to synthesize modified polyacrylamides with both salt- and temperature-tolerant comonomers, in order to enlarge the envelope of polymer flooding at high salinity and temperature conditions. The synthesis attempts were based on the modification of polyacrylamide by the incorporation of one or more of the monomers that can enhance the stability of the polymer in such conditions (see polymer 9 through 16 in Table 2.3). For instance, the incorporation of AMPS or Acrylamido-Ter-Butyl-Sulfonate (ATBS) to polyacrylamide increases the tolerance to high salinity and hardness [52,203,204]. The incorporation of N-VP to polyacrylamide, on the other hand, seems to protect the polyacrylamide units against hydrolysis. Stahl et al. [243] studied a wide range of synthetic and biopolymers at an elevated temperature and moderately high salinity (121 ℃ and 3.3 wt% TDS). They found that the incorporation of N-VP in acrylamide prevents precipitation of the polymer at this temperature. They also observed that N-VP limits the level of acrylamide hydrolysis, and argued that this gives the copolymer its enhanced stability in high salinity and hardness brines. Vermolen et al. [138] studied the effect of HPAM modification with AMPS and/or N-VP monomers, with aim of maintaining the viscosity at elevated temperature (120 ℃) and high salinity (20 wt% TDS) in both the absence and presence of divalent ions (up to 1.8 wt%). They found that, in the absence of divalent ions (no hardness), HPAM is stable for more than 180 days. Unfortunately, the incorporation of 20–25 mol% AMPS to HPAM did not enhance the resistance against the presence of divalent ions at high temperatures. However, a terpolymer including acrylamide, 20–25 mol% AMPS, and 35%–50 mol% N-VP monomers did stabilize the polymer in such harsh conditions.

2.3 Nanoparticles for chemical enhanced oil recovery

The application of nanoparticles (NPs) in the oil and gas industry, and particularly in cEOR, gained much attention in the last decade as illustrated by the establishment of various dedicated research centres [244]. Nanoparticles, or ultrafine particles, are defined

as a particle of matter ranging in size from 1 to 100 nm [245]. The small size of the NPs results in many interesting characteristics such as high specific surface area, high surface energy, and active chemical responses which provide a platform to easily modify their surface. The aim of using NPs for cEOR is to improve on the existing conventional methods, by co-injection of NPs with other chemical agents such as polymers and surfactants. The NPs can penetrate into small pore spaces that are not accessible to conventional chemical agents. Moreover, because of the ease of surface modification of NPs, they can easily be tailored to adjust the rock and fluid properties including wettability, interfacial tension (IFT), and mobility ratio in order to improve the oil recovery.

Silica NPs have been the most frequently studied for cEOR due to their potential to change the rock wettability and reduce the IFT [246], and also to enhance the viscosity of the base-fluid [247]. The surface properties of silica NPs can be changed from hydrophobic to hydrophilic by silanisation with hydrophilic hydroxyl groups, hydrophobic sulphonic acid, or hydrophilic polyethylene glycol [248]. Moreover, silica NPs have shown good thermal stability [249]. However, their main downside is their tendency to aggregate to larger particles which can lead to injectivity problems [248]

Several reviews on the fundamental properties of NPs and their application for EOR have been reported [250-258]. In this section, the focus is on the mechanisms through which NPs can improve oil recovery and their transport mechanisms in porous media.

2.3.1 Nanoparticles enhanced oil recovery (nEOR) mechanisms

This section presents a brief survey of the current status of the research on nanoparticles enhanced oil recovery (nEOR). The key nEOR mechanisms will be examined. The discussion will be restricted to mechanisms relevant to nEOR as an extension of more conventional cEOR.

2.3.1.1 Stabilising emulsions

Oil/water emulsions can be used as the mobility control agent for oil recovery improvement [259,260]. The fundamental principles and applications of emulsions in the petroleum industry have been described in detail by Schramm [261]. Traditionally, emulsions are stabilised by using surfactants. However, the benefits of emulsions stabilized using colloidal particles, referred to as Pickering emulsions, were recognized as well. Nevertheless, the application of Pickering emulsions in EOR has been limited

because the relatively large colloidal particles are easily trapped in narrow pores, leading to clogging of the porous media. NPs proved to be an excellent alternative for the following main reasons [262]: (a) since NPs are at least two orders of magnitude smaller than colloidal particles, they can flow through the narrowest pores without being subject to retention, (b) they can endure the high temperature in the subsurface for prolonged times, and (c) they may have added functionalities, for instance, super-paramagnetism, which helps to control their transport by application of magnetic field, or reaction catalysis, which facilitates the in-situ reduction of the oil viscosity. Zhang et al. [263] studied the phase behaviour of NPs-induced suspensions. They investigated the effect of 5 nm and 10 nm silica NPs, which were coated with short-chain polyethylene oxide (PEO) and a silane end group, on the stability of emulsions. They found that NPs can create stable toluene-in-water and oil-in-water emulsions. Nonetheless, an increase in NPs concentration and salinity had an unfavourable effect on the stability of the emulsions. Pei et al. [264] investigated the recovery improvement, for a medium-heavy oil (350 mPa s at 50 ℃), by an emulsion that was stabilized with a hybrid of NPs–surfactant hybrid. Through phase behaviour and rheological analysis, they found that the addition of NPs leads to improved stability of the emulsion, and its viscosity was significantly increased. This improved the oil recovery by up to 40% of OOIP, which was a substantial recovery improvement as compared to the surfactant-stabilized emulsion. Using microfluidic devices (2D micro-flow models), they also observed that NPs can dramatically improve the sweep efficiency by thickening the emulsion. Kim et al. [265] investigated the effect of an NPs–surfactant hybrid on the stability of an oil-in-brine emulsion (8% NaCl and 2% $CaCl_2$). They noticed that strong and stable emulsions were successfully produced for the combinations of either cationic or non-ionic surfactant with NPs, whereas applying NPs or surfactants individually did not lead to a stable emulsion.

2.3.1.2 IFT reduction

The IFT between the aqueous and oleic phases is reduced by surface-active agents such as surfactants. The co-presence of NPs and surfactant in the aqueous phase can reduce the IFT value further [266]. This is due to the presence of NPs in the interfacial layers. When the concentration of NPs is above a critical threshold, they become attached to the liquid interface and, as a result of the adsorption process, decrease the IFT. Consequently, the IFT of the aqueous phase is defined by a mixed layer consisting of the attached NPs and adsorbed surfactant in the liquid interface [267]. Using an aqueous solution of anionic

surfactant with the addition of light non-ferrous metal NPs, Suleimanov et al. [268] observed that the IFT on an oil boundary was reduced by 70–90%, as compared to the case where only surfactant in aqueous solution was used. This led to an increase in the oil recovery of 35% after primary water flooding in a homogeneous porous media, whereas the surfactant alone increased the recovery by only 17%. Hendraningrat et al. [269] studied the application of hydrophilic silica NPs for oil recovery improvement in Berea sandstones with various permeability (9–400 mD). They observed that a dispersion of NPs can reduce the IFT between the aqueous and oleic phases, as well as making the solid surface more water-wet, which can lead to an increase of about 4–5% in the oil recovery as compared to water flooding. Nonetheless, they argued that a decrease in the IFT with increasing NPs concentration at low permeability cores does not guarantee improved oil recovery because the aggregation of NPs tend to clog the narrow pores.

Zargartalebi et al. [270] investigated the properties of a surfactant (sodium dodecyl sulfate) upon the addition of either hydrophilic or hydrophobically modified fumed silica NPs (AEROSIL 300 and AEROSIL R816 respectively). at very low surfactant concentrations, the inclusion of NPs, no matter whether hydrophilic or hydrophobically modified, had the following effect: below a certain crossover surfactant concentration, the NPs augmented surfactant exhibits systematically lower IFT values. However, above the crossover concentration, the benefit of the NPs was lost. Below the crossover concentration, the surfactant efficiency was considerably improved as surfactant concentration increased up to about the critical micelle concentration (CMC), after which the IFT started to increase. Moreover, increasing the concentration of hydrophobically modified NPs from 1,000 to 2,000 ppm did not lead to an additional decrease in the IFT (see Figure 2.7b).

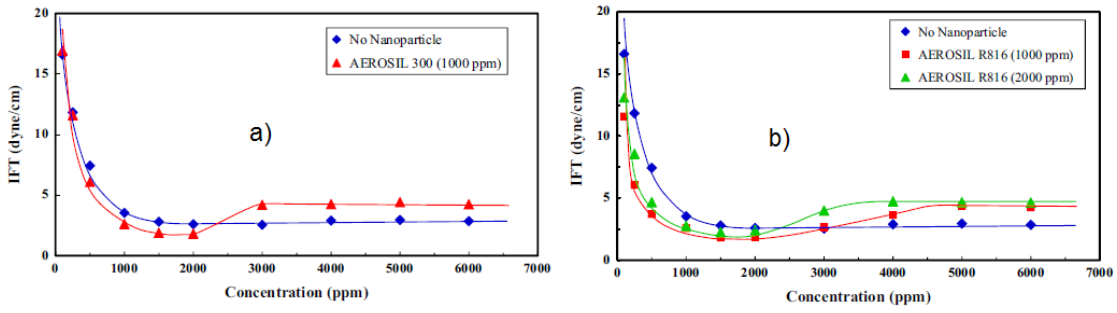

Figure 2.7: The interfacial tension between aqueous and oleic phase as a function of surfactant concentration in combination with a) 1,000 ppm hydrophilic silica NPs (AEROSIL 300) and b) 1,000 and 2,000 ppm hydrophobically modified silica NPs [270]

2.3.1.3 Wettability alteration

Surface-active agents change the wettability of the rock surface to a condition where oil recovery can be improved. For instance, the hydrophobic tail of anionic surfactants can interact with the adsorbed crude oil components on the surface of an oil-wet rock and form a monolayer. This monolayer of adsorbed surfactants with hydrophilic head groups covers the rock surface and alters the wettability of the surface to more water-wet. However, the change in the wettability of the rock surface by NPs has a more complicated mechanism. Once NPs are confined in the thin aqueous film between an oil drop and a solid substrate immersed in the aqueous phase, they are likely to organize themselves in well-ordered layers (Figure 2.8). The existence of ordered, solid-like structures is due to the fact that the ordering causes an increase in the entropy of the NPs dispersion by permitting greater degrees of freedom for the NPs in the bulk liquid. Such ordered microstructures near the contact line result in high disjoining pressures which leads to a wedge-like spreading of the aqueous phase containing the NPs and as a result to two contact lines. Thanks to this wedge-like spreading of the aqueous phase, the NPs can interact with the rock surface and alter the wettability from an oil-wet surface to a more water-wet state (see an illustration of this concept in Figure 2.8a). The disjoining pressure has an oscillatory exponential decay with increasing film thickness (see Figure 2.8b) and both the period of oscillation and decay factor equal the effective diameter of the NPs [271].

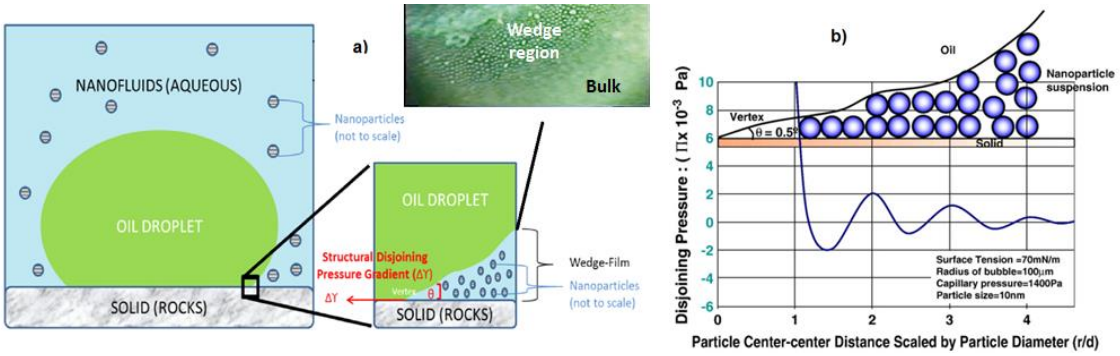

Figure 2.8: An illustration of the concept of wettability alteration by NPs. (a) Wedge-like spreading of the aqueous phase containing NPs. (b) The oscillatory exponential decay of disjoining pressure (from [271-273])

Several researchers have assessed the contact angle of oil-wet surfaces before and after treatment with NPs, and have observed that NPs are able to decrease the contact angle of different surfaces [274-277]. Ju and Fan [276] conducted adsorption experiments of lipophobic and hydrophilic polysilicon NPs (LHPN) on a sandstone surface to detect the wettability change of the surface. They also carried out a transmission electron

microscopy (TEM) to observe the NPs attached to pore walls. The alteration in the contact angle proved that the sandstone surface wettability can be changed from oil-wet to water-wet by the adsorption of the LHPN. Karimi et al. [275] assessed the wettability alteration of oil-wet carbonates by zirconium NPs and performed contact angle measurement and imbibition tests. The zirconium NPs reduced the water contact angle significantly i.e. they reversed the wettability of the carbonate. The spontaneous imbibition tests recovered 60% of the OOIP while the recovery by DI water was less than 5% of the OOIP. The authors, however, speculated that this significantly high oil recovery could not be attributed only to the alteration of wettability.

2.3.1.4 Viscosity enhancement

The presence of NPs in a dispersion can increase the shear viscosity of the base-fluid [278-281]. Several experimental [282-286] and theoretical [286-289] studies have investigated the mechanisms of this viscosity enhancement. There is a consensus that the aggregation of NPs into particles of larger size increases the viscosity. This was attributed to the fact that aggregates result in an apparent volume fraction of NPs higher than the real one [290]. In addition, the short-range local interactions within the equilibrium microstructure (e.g. collisions caused by Brownian motion) can have an important role in increasing viscosity. These interactions within the microstructure of the nanofluids and the resultant increase in viscosity are discussed in terms of an enhancement in thermal conductivity [282].

The viscosity of hard spheres in a dilute system is described by Einstein's equation as follows [291]:

$$\eta_D = \eta_B(1 + 2.5\varphi) \tag{2.11}$$

where η_D is the viscosity of the dispersion, η_B is the viscosity of the base-fluid and φ is the volume fraction of the solids in the dispersion. The viscosity of the dispersion increases with increasing NPs volume fraction. Even when the NPs volume fraction is small and their aggregation is insignificant, η_D can differ significantly from the prediction of Einstein's equation, which is usually valid for φ<2% [292]. Balasubramanian et al. [292] used equilibrium molecular dynamics simulations to describe the rise in the water viscosity around the suspended silica NPs. They recognized the contribution of the NPs surface area to the rheological behaviour of the dispersion and presented an empirical model that takes this into account. Their model perfectly matched the shear viscosity predictions with the experimental measurements. Jamshidi et al. [293] observed that by increasing the silica NPs volume faction in water, the viscosity of the base-fluid also

increases. The increase in the viscosity did not follow Einstein's equation and they presented new correlations for predicting the dispersion viscosity. The data they presented showed that increasing the temperature decreases the viscosity of the dispersion. Zhao et al. [247] investigated the thickening ability of silica NPs on the wormlike micelles. They prepared an NPs-enhanced wormlike micellar system by adding silica NPs at different concentration to 50 mM cetyltrimethyl ammonium bromide (CTAB) and 60 mM sodium salicylate (NaSal). As shown in Figure 2.9, the rheological results showed that as the concentration of NPs first increased, the zero-shear viscosity increased, regardless of temperature. However, at some critical concentration (i.e. 0.1 wt%), the zero-shear viscosity reached a maximum, and at higher concentrations the viscosity only decreased.

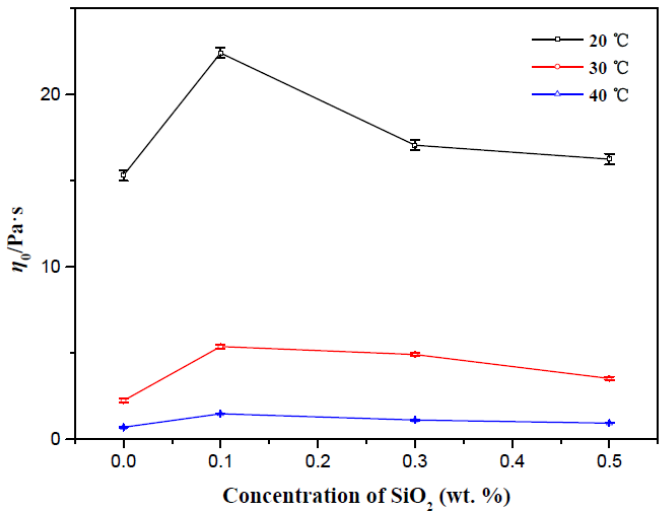

Figure 2.9: Zero-shear viscosity of silica NPs-enhanced wormlike micellar system at various NPs concentrations at 20, 30, and 40 ℃ [247]

NPs have also been used in combination with polymers to enhance the viscosity of polymer solutions and improve oil recovery by providing better mobility control. Maghzi et al. [294] showed that the addition of 0.1 wt% silica nanoparticles to a solution of 0.1 wt% polyacrylamide can increase the oil recovery by 10%. Cao et al. [295] also showed that combination of 0.25 wt% copolymer of acrylamide and AMPS and 0.1 wt% silica nanoparticles leads to 16.3% oil recovery, while the copolymer alone recovered only 6% of the OOIP. The effect of hybridization of NPs and polymers, particularly at high salinity and temperature will be discussed in detail in **Chapters 3** and **4**.

2.3.2 Transport of nanoparticles in porous media

To improve the oil recovery, the NPs should propagate deep into the porous media and thus facilitate the oil displacement. Based on the observation of several researchers, this

can be challenging [296-300]. As NPs propagate through porous media, various mechanisms can lead to their retention [301]. As illustrated in Figure 2.10a and 2.10b, the main mechanisms for the retention of NPs in porous media are adsorption on the pore walls, mechanical entrapment, and log-jamming [302].

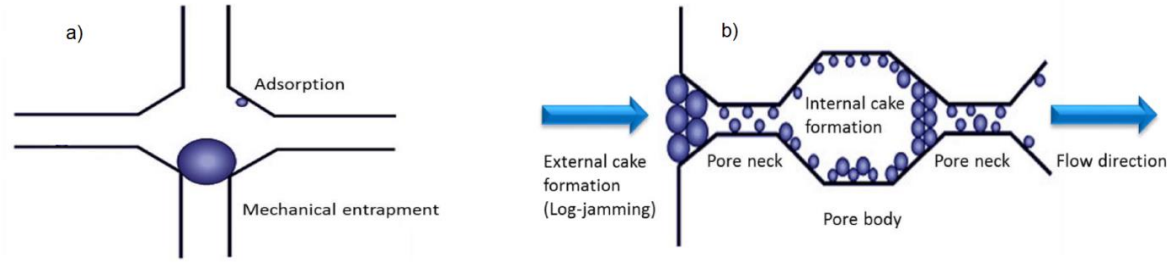

Figure 2.10: Particle retention mechanisms; (a) adsorption and mechanical entrapment, (b) Log-jamming [303]

2.3.2.1 Adsorption of NPs on pore walls

Adsorption onto solid surfaces may hinder the NPs transport. As the size of NPs is in the range 1–100 nm, they are considered as Brownian particles, and five forces then dominate the interactions between the NPs and the pore walls: the London-van der Waals attractive force, the repulsive force due to the overlap of the double electrical layers of the NPs and the rock surfaces, the Born Repulsion (significant at a distance of less than 5 Å), the hydrodynamic drag force (which depends on the interstitial velocity of the permeating liquid) and the Lewis acid-base interaction [257]. An overall attractive interaction between the NPs and the pore walls results in the adsorption of NPs onto the pore walls. On the other hand, if the overall interaction is repulsive, the desorption of NPs from the pore walls occurs. Zhang et al. [304] suggested that both reversible and irreversible adsorption of NPs occurs during their propagation in porous media. They showed that finite capacities exist, for both reversible and irreversible adsorption, which depend on the operating conditions (e.g. concentration, volumetric flow rate etc.) and the porous medium characteristics (e.g. clay content, NPs type etc.).

2.3.2.2 Mechanical entrapment

Mechanical entrapment occurs if the size of the NPs is larger than the pore throat size, which leads to clogging of the pores (Figure 2.10a). This is crucial in low permeability rocks, where the pores are of a narrow size. Sometimes the particle size is smaller than the pore throat size but mechanical entrapment can still occur because of aggregation of NPs and the formation of bigger particles that do not pass through pores. The tendency of nanoparticles to aggregate, particularly at high salinities, is one of the main reasons

that limits the use of NPs in field applications [248]. For non-aggregated particles, the size, shape, and aspect ratio play an important role in whether they can pass through a pore medium. For instance, NPs with a high aspect ratio (e.g. platelet and needle-like NPs) are more likely to clog the pores.

2.3.2.3 Log-Jamming

Log-jamming causes the clogging of the pore throats that are larger than the NPs. It can be advantageous for improving oil recovery. When a dispersion of NPs flows from a pore body to a pore throat, the constant differential pressure will result in an increase in the velocity of the fluid at the pore throat. The water molecules in the base-fluid flow faster than the NPs, and this leads to an accumulation of NPs at the entrance of the pore throats [302] (see Figure 2.10b). The blocked pore throat causes a pressure drop build-up across the adjacent pores, and this pushes the oil, which is trapped in the pore throats, out. When the oil is freed, the neighbouring pressure falls off and as a result of the flow reversal, the NPs begin flowing with the water. This is regarded as temporary log-jamming. Log-jamming is primarily influenced by flow rate, NPs concentration, and the pore size distribution.

2.4 Key observations

In this review, a critical overview of the state-of-the-art research on polymers and nanoparticles for cEOR was presented. Polymers can improve oil recovery by increasing the viscosity of the aqueous phase, thus reducing the mobility ratio. Another proposed mechanism is that, due to their viscoelastic properties, polymers can displace the residual oil trapped by capillary forces. However, only a few studies have investigated this phenomenon and the exact mechanism behind it is not entirely clear. The shear-thickening behaviour of flexible polymers in porous media is one of the most debated subjects in this field. It has previously been explained by the coil–stretch transition and transient network theories and more recently attributed to flow instabilities at negligible inertial effect. The performance of polymers in porous media (i.e. polymer rheology and retention) is dependent on many parameters, including polymer type, polymer molecular weight and concentration, porous media permeability, residual oil saturation, iron and clay content of the rock, salinity, and temperature. The employment of conventional polymers at high salinity and temperature reservoirs is a challenge and there is limited success in field applications. The modification of polyacrylamide with monomers such as AMPS and N-

VP has shown promising results at high temperature and salinity; however, these polymers are more expensive than conventional polymers used for cEOR such as HPAM. Moreover, they need to be overdosed to reach target viscosities since their molecular weight is low.

Nanoparticles have recently emerged as potential agents for cEOR. They have been used for emulsion stabilisation, interfacial tension reduction, wettability alteration, and viscosity enhancement. Notwithstanding their success in the laboratory, their application in field projects has been limited as they show some challenges. Nanoparticles tend to aggregate because of strong van der Waals interactions at harsh reservoir conditions, and this results in pore-clogging and injectivity problems. Therefore for the successful implementation of nanoparticles in field applications, their tendency to aggregate should be mitigated.

3 RHEOLOGY OF POLYMER–NANOPARTICLES HYBRIDS AT HIGH SALINITY AND TEMPERATURE

Chapter 2 discussed that water-soluble polymers are susceptible to degradation at combined high salinity and elevated temperature conditions which limits their overall performance. In this chapter, a novel polymer-based chemical for harsh conditions is introduced. Hybrid mixtures of hydrophobically modified polyacrylamide (HMPAM) with hydrophobically modified silica nanoparticles (NPs) emerged as a promising strategy for achieving enhanced stability and high viscosity in brines having a high total dissolved solids (TDS) content and high hardness at elevated temperatures (> 20 wt% TDS, including > 1.5 wt% divalent cations at T > 70 °C). The rheological response of the hybrids at various concentrations of HMPAM and NPs was examined to investigate the synergic effects. Hybridization of HMPAM with NPs led to a higher viscosity at high salinity and elevated temperature. The viscosity improvement was more pronounced when the concentration of HMPAM was in the semi-dilute regime and the concentration of NPs was higher than a critical threshold where the viscosity increased roughly by a factor of 1.5. Here, the mechanisms of improved viscosity behaviour are presented. The rheological data suggest the role of NPs in the bridging between HMPAM molecules, which in turn increases the hydrodynamic radius and consequently the viscosity of the hybrids. The porous media flow characteristics of the HMPAM–NPs hybrids will be discussed in **Chapter 4**.

3.1 Introduction

The stability of colloidal systems at high electrolyte concentration is critical for optimum performance of various industrial products and processes, including water-based coatings or paints [305-307], environmental applications [308-310] and chemical enhanced oil

recovery (cEOR) [311-313]. In paints, for instance, once the salt concentration in the rust layer at the steel-paint interface exceeds a threshold, premature deterioration of the paint coating is observed [314].

As a basic cEOR method, polymer injection increases oil recovery over water flooding by viscosifying the aqueous drive water [8]. Partially hydrolysed polyacrylamide (HPAM) is the most commonly utilised polymer for cEOR [8,10,70,315]. HPAM is characterized by the presence of negatively charged carboxylic groups along the polymer backbone [316]. Electrostatic repulsion among the carboxylic groups results in the expansion of the coiled HPAM chains, thus increasing the solution viscosity, compared to non-ionic polyacrylamide (PAM) [10]. At high ionic strength, however, electrostatic repulsions between the negatively charged groups are almost completely screened by mono- and divalent cations. Therefore, the excluded volume and consequently the molecular size of the polymer chains are reduced [45]. For this reason, HPAM viscosity decreases as salinity increases. At sufficiently high concentrations of divalent cations, complexation of the metal ion by the carboxylate groups occurs leading to polymer precipitation [15,16]. These effects are exacerbated as temperature increases due to further hydrolysis of acrylamide monomers in the polymer backbone [46].

Several approaches for synthesising water-soluble polymers with improved rheological properties at high salinities up to 20 wt% total dissolved solids (TDS) and temperatures up to 120 °C have been reported [49-53]. Many focus on the substitution of the acrylamide monomer by at least another monomer type which can enhance the stability of the polymer at such harsh conditions [49-51,54]. For instance, the incorporation of 2-acrylamido-2-methylpropane sulfonic acid (AMPS) [52,138] and N-vinyl-2-pyrrolidone (N-VP) [53,138] co-monomers increases tolerance to high salinity particularly to the presence of divalent cations and against thermal hydrolysis respectively. Even though modified polyacrylamides have shown promising results at high temperatures and salinities, they are more expensive than HPAM and need to be overdosed to reach target viscosities since their molecular weight is low [317]. Therefore, the use of such polymers is economically unattractive.

3.2 A novel approach

Despite the above-described research efforts, developing polymeric or polymer-based materials to improve water viscosity at elevated temperature and high salinity, especially

in presence of divalent cations remains an unresolved issue. Because a significant amount of oil remains in place after primary water flooding in high salinity and temperature reservoirs, this brings up the necessity of a new chemical system that can survive in these harsh conditions and increase the sweep efficiency of the flooding.

An alternative approach is to use a hybrid of polymer–NPs to form a hybrid system that is stable at high salinity and temperature. This novel approach is based on the idea that the rheological properties of polymer solution at such harsh conditions can be controlled by polymer–NPs interactions. Several studies have shown that hybrid networks based on reversible associations, can be obtained by the inclusion of silica NPs into the macromolecular architecture of associative polymers [318-322]. Moreover, the associative polymers also show LCST properties, as discussed in **Section 2.2.6.1**, temperature and salting-out may be used to modify the viscoelastic properties of the hybrid network [318]. Bhardwaj et al. [323] observed improved thermo-resistance and high thermal stability behaviour for nano-size silica–polyacrylamide composites. Maghzi et al. [294] showed that the viscosity of a hybrid of polyacrylamide–silica was higher than the viscosity of the polyacrylamide solution for salinities ranging from 1.4 wt% to 8.4 wt% TDS. Hu et al. [324] observed that the introduction of silica NPs considerably enhanced the viscosity of HPAM at salinities up to 8 wt% NaCl and temperatures up to 80 ℃. Cao et al. [295] reported that the salt-tolerance and heat-resistance properties of a copolymer of acrylamide and AMPS solution were improved at salinities up to 8 wt% NaCl and 0.12 wt% $CaCl_2$ at 70 ℃ upon addition of amino-functionalized silica NPs. The interaction between silica NPs and polymer was mainly attributed to hydrogen bonds between the functional groups on polymer molecule including hydroxyl, amide, and carboxylate groups and the silanol groups on the surface of silica NPs [295,323-325].

However, the above approaches suffer from some drawbacks: (a) no polymer–NPs hybrid was studied for salinities higher than 8.4 wt%, (b) the colloidal stability at high salinity conditions, and (c) the role of polymer concentration on the rheological response of hybrids was not investigated. To address these limitations, it is proposed that enhanced stability and increased viscosity can be achieved at extreme salinities (>20 wt% TDS, including >1.5 wt% divalent cations) and elevated temperatures (T > 70 ℃) by the hybridization of hydrophobically modified polyacrylamide with hydrophobically modified silica NPs [238].

In the experiments presented in this chapter, hydrophobically modified silica NPs were added to a solution of hydrophobically modified polyacrylamide (HMPAM) to facilitate the bridging between polymer chains. Silica NPs were modified by gamma-glycidoxypropyltrimethoxysilane (GPTMS), a low molecular weight organic ligand to provide steric stabilization and ensure the colloidal stability at high salinity [326]. By modification, the surface becomes more hydrophobic than the original bare silica but still has sufficient polarity to allow a good dispersion in water. To describe the colloidal stability of NPs in this work, an extended DLVO (xDLVO) [298,327,328] theory has been used in different ionic strengths and with or without surface modification of NPs. In order to study the improvement of flow responses of the hybrids, viscosity measurements were performed at various concentrations of HMPAM and NPs.

The results showed that the addition of NPs increases the viscosity of HMPAM solutions. The increase was more pronounced once the concentration of HMPAM was in the semi-dilute regime and the concentration of NPs was larger than a critical threshold. The results suggest that in the semi-dilute regime, where polymer chains are in closer proximity to each other, NPs-induced bridging between HMPAM chains can occur which in turn enlarge the hydrodynamic radius of the hybrids and consequently increase their viscosity.

3.3 Experiments

3.3.1 Materials

GPTMS-modified silica NPs which are available under the commercial name Levasil CC301 were supplied by AkzoNobel in suspension (ρ = 1.2 g cm^{-3}) containing 28.1 wt% silica with an average particle diameter of 7 nm as reported by the manufacturer. Bare silica NPs were supplied by Sigma-Aldrich in powder form with a particle diameter of 10–20 nm obtained from BET. Acrylamide and t-butyl acrylamide monomers were purchased from Sigma-Aldrich. HMPAM (98 mol% acrylamide and 2 mol% t-butyl acrylamide) and PAM (100 mol% acrylamide) were synthesised using free radical polymerization [53]. Their average molecular weights were estimated using the methodology used by Wu et al [329] which is based on viscosity measurements and found to be approximately 2.1 × 10^6 and 2.7 × 10^6 g mol^{-1} for HMPAM and PAM respectively (see **Appendix A**). Sodium chloride (NaCl) and calcium chloride dihydrate ($CaCl_2.2H_2O$) used for brine preparation were purchased from Sigma-Aldrich as well. All materials were used as received without further purification.

3.3.2 Preparation of modified silica NPs, polymers and hybrids

3.3.2.1 GPTMS-modified silica NPs

Detail of typical modification conditions and characteristics of GPTMS-modified silica NPs are described elsewhere [326,330,331]. Here, only the important aspects are highlighted. GPTMS is a silane epoxy functional group ($RSi(OMe)_3$) which is not stable in aqueous solutions**.** It undergoes a hydrolysis reaction according to the following chemical reaction:

$$RSi(OMe)_3 + 3H_2O \rightarrow RSi(OH)_3 + 3MeOH \tag{3.1}$$

Pre-hydrolysed silane is continuously added to the colloidal silica at 60 °C, at a rate of nearly 1.4 molecules GPTMS per nm^2 silica surface per hour while being agitated. The pre-hydrolysed silane reacts with silanol groups on the surface of silica NPs, according to the following condensation reaction:

$$\begin{aligned} &Y{-}R{-}Si(OH)_3 + (HO)_X{-}\text{silica particle} \\ &\rightarrow Y{-}R(OH)_{3\text{-}X}{-}\text{silica particle} + xH_2O \end{aligned} \tag{3.2}$$

An aqueous silica sol contains 4.6 silanol groups per nm^2 silica surface [326]. Since each silane reacts with three silanol groups and there exists 1.4 molecules GPTMS per nm^2, only 0.4 silanol groups per nm^2 remain on the surface, which shifts the surface from hydrophilic to hydrophobic [332]. During silylation, GPTMS covalently binds to the surface of silica and the epoxy ring opens and converts to a diol as indicated in Scheme 3.1a. The silylation of silica surface also substantially decreases the total of charged surface groups and specific surface area. The schematic of a GPTMS-modified silica nanoparticle is shown in Scheme 3.1b.

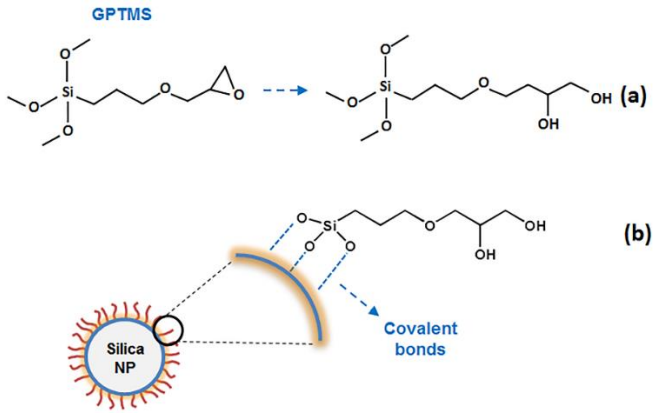

Scheme 3.1: (a) Ring-opening of GPTMS during silylation reaction. (b) The schematic of attachment of GPTMS to a silica nanoparticle surface by covalent bonds

3.3.2.2 Polymers

Polymerization reactions of acrylamide monomers to synthesize PAM and acrylamide and t-butyl acrylamide monomers to synthesize HMPAM were performed in a double-walled glass sealed reactor with magnetic stirring coupled through the lid towards an internal propeller stirrer. The reactor was filled with a pre-set amount of monomers and de-ionised (DI) water. Thereafter, a water-cooled condenser was placed on the lid and the temperature was raised to 40 °C using an external thermostat connected to the lid. Subsequently, an inlet tube was lowered into the liquid phase, purging the water-monomer phase with nitrogen under stirring to remove any oxygen present. After 30 minutes of purging, the nitrogen tube was lifted into the headspace. Shortly after, 10 mL of DI water containing 0.05 mole potassium persulfate as the initiator was introduced through a septum to commence the polymerization. Viscosity was built up within 5–10 minutes; however, polymerization was allowed to run for two hours to complete the process. The original concentration of the solution of monomers was 5 wt%. The feed molar ratio of acrylamide to t-butyl acrylamide monomers in HMPAM was 98 to 2.

3.3.2.3 Hybrid samples

Hybrid samples were prepared by adding the required amounts of HMPAM and modified NPs in brine with a salinity of 20 wt% TDS including 1.5 wt% Ca^{2+}, hereafter referred to as Brine2015. Polymer solutions and NPs dispersions were diluted from their original concentration to the desired concentration in Brine2015 as the dispersant medium and stirred overnight and for 2 hours respectively until they became completely homogenous and transparent. In order to achieve a hybrid at desired concentration of polymer (C_p) and NPs (C_{np}), the required mass of NPs dispersion with a concentration of $2C_{np}$ was added to the equal mass of polymer solution with a concentration of $2C_p$. The hybrid sample was then homogenized by stirring for nearly 2 hours. In order to ensure the homogeneity and stability of the hybrid sample, it was stored for one week, in the absence of degrading factors such as light and heat, before viscosity measurements were made.

3.3.3 Characterization of NPs and HMPAM

3.3.3.1 Zeta potential

The zeta potential of the NPs in DI water was identified using a Malvern Zetasizer Nano ZS at room temperature. The NPs concentration was adjusted to provide a count rate of *ca*. 500 kcPs on this instrument. Samples were run in triplicate in the auto mode and the

average was recorded. There was a 30–60 second pause between each run, so the sample is able to relax. For GPTMS-modified silica NPs the zeta potential was measured to be -29 ± 5 mV.

3.3.3.2 Transmission electron microscopy (TEM)

TEM imaging on the NPs was performed using a JEOL JEM 1400 TEM with a 120 kV beam. For preparing the samples, a 10 µL droplet of the NPs dispersion was brought into contact with the carbon grid. The sample droplet was slid off the grid after approximately 5 seconds of contact. The grid was then dried in ambient conditions for 5 minutes before inserting it into the TEM machine.

3.3.3.3 Determination of ligand grafting density

The number of moles of bound ligands per unit surface area (i.e. the grafting density σ) was experimentally derived from total organic carbon (TOC) analysis [333]. TOC analysis was performed using a DC-190 Dohrmann high temperature TOC Apparatus. A 100 µL sample was placed in the combustion tube. Catalytic oxidation of the sample in a furnace produced a gaseous mixture of CO_2 and H_2O. The CO_2 and steam were moved into the internal circulation reactor using a carbon-free carrier. Then, it passed through a condenser, a liquid gas separator and the moisture trap. The permeation dryer removed the H_2O. After that, the dried CO_2 passed through the non-dispersive infrared detector (NDIR) in order to measure the total carbon content. The grafting density from the TOC analysis was determined using Equation 3.3 [333]:

$$\sigma = \frac{\frac{[C]}{[Np]}\rho_c \frac{4}{3}\pi R_c^3}{MW_l 4\pi R_c^2} \tag{3.3}$$

where [NP] represents the concentration of NPs, [C] is the organic carbon concentration obtained from TOC analysis, ρ_c and R_c are the density and radius of a nanoparticle respectively and MW_l is the molecular weight of GPTMS.

3.3.3.4 NMR elucidations

The prepared stock polymer solutions were freeze-dried by Christ Alpha 1-4 LD plus apparatus. The solutions were frozen quickly with liquid nitrogen in a glass flask, which was then attached to the freeze-dryer and left there overnight without further cooling. Thereafter, the obtained polymer powders were dissolved in D_2O. Before the test, air bubbles were removed by centrifuging the sample at 10,000 revolutions per minute (rpm) for 20 minutes. All spectra were recorded on a wide-bore 500 MHz Bruker NMR. ^1H

NMR spectra were acquired at 500 MHz to determine the hydrophobic content of HMPAM. As a reference, a similar analysis was performed on PAM.

3.3.3.5 Rheological measurements

The viscosity of the polymer solutions, NPs dispersions and hybrid samples were measured by an Anton Paar rheometer (MCR-302) in Couette geometry. To investigate any shape memory effects, all measurements were done four times by repeating the sequence (a) from low to high shear rates and (b) then from high to low shear rates. It turned out that the four different series of viscosity data per sample were identical within the experimental error (< 5%). Hence, the average values of the viscosity of the four series were considered.

In order to study the shear-thinning behaviour of the polymer solutions, the Carreau–Yasuda model [334] as shown in Equation 3.4 was used:

$$\eta - \eta_\infty = (\eta_0 - \eta_\infty)[1 + (\dot{\gamma}\lambda)^a]^{\frac{n-1}{a}} \tag{3.4}$$

where η is the polymer viscosity, η_∞ denotes the viscosity of second Newtonian plateau which is assumed to be equal to the viscosity of the solvent, η_0 is the zero shear rate viscosity of the polymer, $\dot{\gamma}$ is the shear rate and λ is a time constant known as relaxation time which is an inverse of a critical shear rate at which the transition from Newtonian to shear-thinning regimes occurs. The parameter *n* is the power-law slope obtained from the shear-thinning part and the parameter *a* controls the width of transition from Newtonian to shear-thinning. For oscillatory tests, the amplitude sweep was attempted at a constant frequency to realize the linear viscoelastic regime after which the frequency dependence of the hybrids was analysed within this viscoelastic regime.

3.3.4 Colloidal stability of dispersed NPs

3.3.4.1 Inter-particle interactions

Dispersed NPs are subject to Brownian motion which induces frequent inter-particle collisions. The balance between inter-particle interactions determines whether the dispersion of NPs is stable. Inter-particle interactions between coated NPs have been successfully described by the xDLVO theory [328,335]. According to this theory, the total interaction between two functionalized spherical NPs (V_t) with radius *R*, at separation distance *h* is specified by the sum of van der Waals (V_{vdw}), electrostatic (V_{ele}), and steric (V_{str}) potentials:

$$V_t(x) = V_{vdw}(x) + V_{ele}(x) + V_{str}(x) \tag{3.5}$$

where x is the normalised separation distance equal to h/R.

The van der Waals potential is [336]:

$$\frac{V_{vdw}(x)}{k_B T} = -\left(\frac{\left(\sqrt{A_p} - \sqrt{A_m}\right)^2}{6k_B T}\right)\left[\frac{2}{x(\mathrm{x}+4)} + \frac{2}{(\mathrm{x}+2)^2} + ln\left(\frac{x(\mathrm{x}+4)}{(\mathrm{x}+2)^2}\right)\right] \tag{3.6}$$

where A_p and A_m are Hamaker constants for particle and medium respectively [337], k_B is the Boltzmann constant and T is the absolute temperature. The electrostatic potential is given by [338]:

$$\frac{V_{ele}(x)}{k_B T} = \frac{2\pi\varepsilon_0\varepsilon_r\psi_0^2 R}{k_B T}\ln(1 + e^{-\kappa R x}) \tag{3.7}$$

where ε_0 is the vacuum permittivity, ε_r is the medium relative permittivity, ψ_0 is the surface potential and κ^{-1} is Debye length. The latter is calculated as follows:

$$\kappa^{-1} = \left(\frac{\varepsilon_0\varepsilon_r k_B T}{2N_A e^2 I}\right)^{0.5} \tag{3.8}$$

where e is the electronic charge, N_A is the Avogadro number, and I is the medium ionic strength [339]. Surface potential is approximated by knowing the zeta potential (ζ) using Equation 3.9:

$$\psi_0 = \zeta\left(1 + \frac{1}{\kappa R}\right)\exp(1) \tag{3.9}$$

The steric potential (V_{str}) for the grafted ligand is calculated by summing the osmotic (V_{osm}) and elastic potentials (V_{ela}) [339]. These are short-range repulsive interactions that tend to kinetically stabilize the NPs dispersion. The osmotic potential can be expressed as [340]:

$$\frac{V_{osm}(x)}{k_B T} = \frac{4\pi R L N_A}{\nu_1}\phi_l^2\left(\frac{1}{2} - \chi\right)\left(1 - \frac{\mathrm{x}}{2\alpha}\right) \qquad \alpha \le x \le 2\alpha$$

$$\frac{V_{osm}(x)}{k_B T} = \frac{4\pi R L^2 N_A}{\nu_1}\phi_l^2\left(\frac{1}{2} - \chi\right)\left[\frac{\mathrm{x}}{2\alpha} - \frac{1}{4} - ln\left(\frac{\mathrm{x}}{\alpha}\right)\right] \qquad x < \alpha \tag{3.10}$$

where L is the particle coating thickness, α is equal to L/R, ν_1 is the solvent molar volume, ϕ_l is the ligand volume fraction (see **Appendix A**) and χ is the Flory–Huggins interaction parameter which is a function of solvent quality [339]. When the particle separation distance is shorter than the thickness of particle coating (i.e. $x < \alpha$) entropic effects arise from the compression of the ligand resulting in elastic repulsion between particles given by [341]:

$$\frac{V_{ela}(x)}{k_B T} = \left(\frac{2\pi R N_A}{MW_l}\phi_l L^2 \rho_l\right)\left[\frac{\mathrm{x}}{\alpha} ln\left(\frac{\mathrm{x}}{\alpha}\left(\frac{3-\frac{\mathrm{x}}{\alpha}}{2}\right)^2\right) - 6ln\left(\frac{3-\frac{\mathrm{x}}{\alpha}}{2}\right) + 3\left(1-\frac{\mathrm{x}}{\alpha}\right)\right] \quad (3.11)$$

where ρ_l is the bulk density of the pure ligand. Dispersions of NPs stay kinetically stable if the potential barrier (V_{max}) is larger than $\sim 16/k_B T$ [342,343].

3.4 Results and discussion

3.4.1 Stability of hydrophobically modified silica NPs

Dispersions of GPTMS modified silica NPs in Brine2015 were found to be stable for over three months (Figure A.1, **Appendix A**). In order to characterize the morphology of GPTMS-modified NPs (i.e. shape and size), TEM was performed for modified NPs dispersed either in DI water or in Brine2015. In order to study the impact of GPTMS modification on the prevention of aggregation of silica NPs, TEM was also performed on bare silica NPs with an approximately identical particle diameter (10–20 nm as reported by the supplier). Figure 3.1 shows the TEM images of dilute dispersions of hydrophobically modified and bare silica NPs in DI water and in Brine2015. Stable dispersions were obtained for both types of NPs in DI water. However, the dispersion of modified NPs was completely transparent while the dispersion of bare NPs showed some turbidity (Figure A.2, **Appendix A**). Figure 3.1a shows that for the bare silica NPs in DI water, NPs formed aggregates even though the dispersion showed no phase separation. In contrast, for the GPTMS-modified NPs dispersed in DI water the TEM image (Figure 3.1b) shows the presence of individual NPs and small clusters of NPs with a narrow cluster size distribution (see Figure A.5, **Appendix A**) suggesting a slight tendency of NPs to form large aggregates.

When bare NPs were dispersed in Brine2015 most of them adhered to one another and large aggregates were formed (see Figure 3.1c). This is in agreement with the flocculation

of small silica NPs into particulate networks, resulting in sedimentation as also reported by others [344,345]. Figure 3.1d shows that for GPTMS-modified silica NPs in Brine2015, even though a few slightly larger agglomerates were formed, a majority of the NPs remained separated from each other. This shows that grafting low molecular weight ligands to the surface of NPs can prevent their aggregation in media with high ionic strength [333,346]. The sample pictures of a suspension of bare and modified silica NPs in DI water and Brine2015 at a concentration of 0.05 wt% are shown in Figure A.2, **Appendix A**.

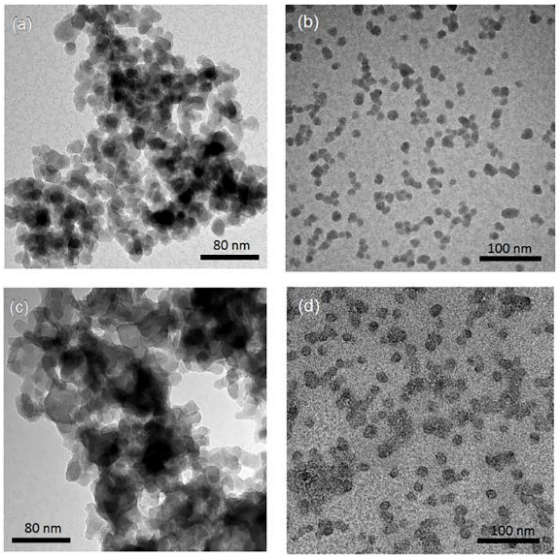

Figure 3.1: TEM images of dried samples (a) bare NPs in DI water (b) GPTMS-modified NPs in DI water (c) bare NPs in 20 wt% TDS brine (Brine2015) and (d) GPTMS-modified NPs in Brine2015

Table 3.1: Functionalised NP parameters at 298.15 K used in xDLVO theory calculations

Parameter	NPs functionality
Hamaker constant for water (J)	3.7×10^{-20}
Hamaker constant for silica (J)	6.3×10^{-20}
Particle diameter (nm)	7
Bulk density of ligand (g cm^{-3})	1
Ligand molecular weight (g mol^{-1})	236
Ligand grafting density (µmol m^{-2})	2.6
Ligand length (nm)	0.95
ζ potential (mV)	-29
Flory–Huggins interaction parameter	0.49

To determine the relative contributions of the surface forces to NPs interactions, the van der Waals, electrostatic and steric potentials were estimated using the xDLVO theory (see inter-particle interaction section). This provides a semi-quantitative description of stability of NPs and the calculations highlight the importance of the grafted ligand for NPs stabilization at high salinity. For this purpose, three scenarios were considered: (a) bare silica NPs dispersed in a medium with low ionic strength (I=10 mM, equivalent to 0.06 wt% NaCl), (b) bare silica NPs in a high ionic strength medium (I=3834 mM representing the ionic strength of Brine2015) and (c) GPTMS modified NPs in a medium with similar high ionic strength. Table 3.1 summarises the parameters which were used for the calculations. All three scenarios were considered at room temperature. The ligand grafting density from TOC analysis according to Equation 3.3 was calculated to be 2.6 ± 0.1 μmol m^{-2}. The thickness of the particle coating (L) was regarded as the length of a GPTMS molecule which is 0.95 nm [346]. Even though it is reported in the literature that GPTMS is relatively well solvated in high salinities water [326,346], the Flory–Huggins interaction parameter was taken as 0.49 to give a conservatively low estimate of V_{osm}.

The calculated interaction potentials are shown in Figure 3.2. As Figure 3.2a suggests, for bare silica NPs dispersed in a low ionic strength medium, V_{ele} decreased exponentially with increasing h, approaching zero at large h. V_{vdw}, which indicates an inverse power law with h, did not decay to zero. V_{vdw} is dominant over V_{ele} in very short particle separation distances, which results in a deep minimum in the V_t profile. However, for larger h values (i.e. h > 0.1 nm), the electrostatic double layer repulsion becomes dominant and a potential barrier of larger than $55/k_BT$ is obtained ($V_{max} > 55/k_BT$). This implies that the colloidal stability is ensured. When bare silica NPs were dispersed in Brine2015 (Figure 3.2b), V_{vdw} did not change, as it is independent of aqueous phase salinity. However, as can be inferred from Equation 3.8, the Debye length diminishes with increasing ionic strength, resulting in significant reduction in V_{ele}. This is also evident in V_t and the potential barrier becomes smaller than $16/k_BT$ ($V_{max} < 16/k_BT$) implying that the colloidal stability is not achieved. The fact that the potential barrier did not completely disappear was due to the high ζ potential and small size of the NPs. The latter makes the van der Waals attracting potential smaller.

When two GPTMS-modified silica NPs approach each other to a separation distance h smaller than $2L$ ($h < 2L$) the ligand molecules interact with each other, which leads to an increase in the local segment density of ligand molecules in the interaction zone. This

results in strongly repulsive interaction due mainly to two effects: (a) to rise in osmotic potential in the interaction zone according to Equation 3.10 and (b) decrease in configurational entropy of the ligand molecules in the overlap region due to decrease in volume available for ligand molecules, as is shown in Equation 3.11. Figure 3.2c indicates that the contribution of V_{osm} and V_{ela} significantly increases the potential barrier to more than $50/k_BT$ ($V_{max} > 50/k_BT$) which ensures the colloidal stability of GPTMS-modified silica NPs at such high salinity. Note that these calculations are based on some inherent assumptions in xDLVO theory [347] and were used to semi-quantitatively show the effect of NPs surface modification by GPTMS on the colloidal stability of the system.

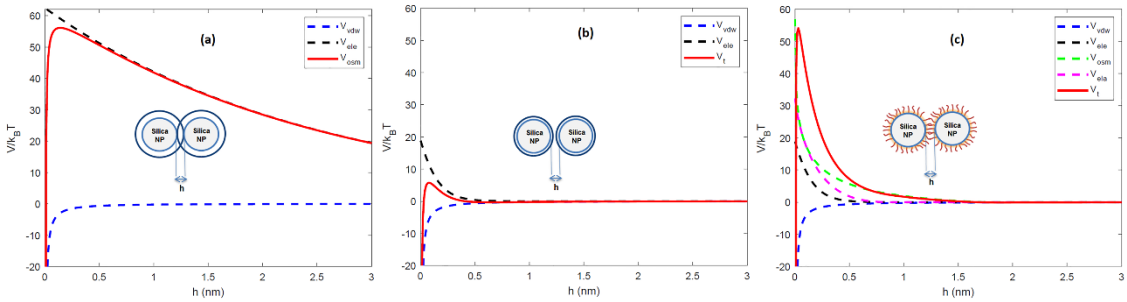

Figure 3.2: Inter-particle interaction potential (V) as a function of particle separation distance (h) calculated by xDLVO theory for (a) un-modified NPs in a medium with low ionic strength (I=10 mM) (b) un-modified NPs in a medium with high ionic strength (I=3834 mM) and (c) GPTMS-modified NPs in same high ionic strength medium

3.4.2 Hydrophobic content of HMPAM

The result of ^{1}H NMR spectra is shown in Figure 3.3. For PAM, as can be seen in Figure 3.3a, peaks a and b correspond to aliphatic CH_2 and aliphatic CH respectively in polyacrylamide. Moreover, some other peaks appear in the range of 5.65–6.25 ppm. These peaks are attributed to vinylic CH and CH_2 in acrylamide monomer which means some of the monomers were not polymerized [348]. The yield of polymerization was estimated to be 92.5 ± 0.5 %. For HMPAM, as can be seen in Figure 3.3b, compared with PAM two additional peaks were detected. Peak c corresponds to the proton in the methyl group ($-CH_3)_3$) of HMPAM. Another peak (c') was observed next to peak c. This small peak is attributed to the methyl groups in t-butyl acrylamide monomer which were not polymerized (see the ^{1}H NMR spectrum of t-butyl acrylamide in Figure A.8, **Appendix A**). Also here, the peaks in the range of 5.65–6.25 ppm correspond to vinylic CH and CH_2 in acrylamide and t-butyl acrylamide monomers which were not polymerized. As compared to PAM, the integrating areas of these peaks appear to be larger. This indicates that the yield of the polymerization is smaller and it was estimated to be 81.0 ± 0.5 %.

The hydrophobic content of HMPAM was estimated according to the following equation:

$$\frac{S_c}{S_a + S_b} = \frac{9z}{3y + 3z} \tag{3.12}$$

where S_a, S_b, and S_c are the integrating areas of peaks a, b and c respectively, and y and z are the non-hydrophobic and hydrophobic content of HMPAM respectively (y+z=100). This leads to a hydrophobic content of 1.80 ± 0.50 mol% which is slightly smaller than the hydrophobic content in the original feed.

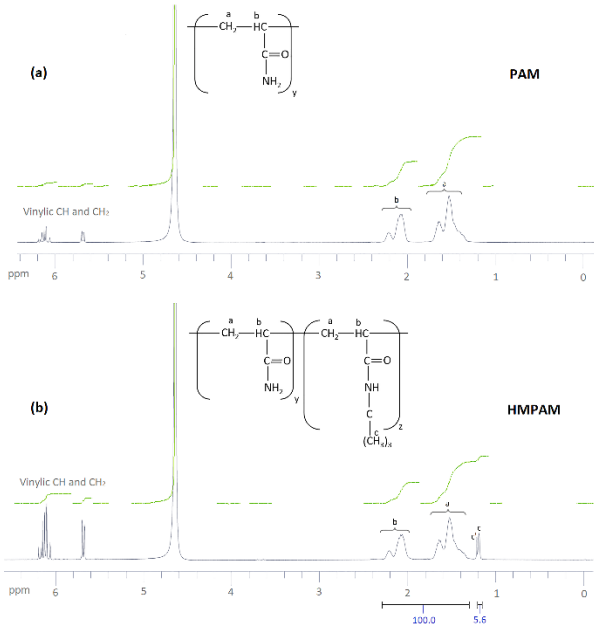

Figure 3.3: ^{1}H NMR spectra of (a) PAM and (b) HMPAM. Peaks a and b correspond to aliphatic CH_2 and aliphatic CH respectively in PAM and HMPAM. Peak c corresponds to the proton in the t-butyl group of t-butyl acrylamide in HMPAM. Peak c' corresponds to t-butyl group in t-butyl acrylamide monomers which were not polymerized

3.4.3 Rheology of HMPAM solutions

Figure 3.4 shows the viscosities of HMPAM solution in DI water and Brine2015 at 25 °C and in Brine2015 at 70 °C as a function of shear rate at different concentrations. The Carreau–Yasuda model (Equation 3.4) was used to fit the experimental rheology data. The list of fitting parameters is tabulated in Tables A.1–A.3, **Appendix A**. From Figure 3.4a, it can be observed that HMPAM solutions in DI water showed a Newtonian behaviour at low to intermediate shear rates which was followed by a shear-thinning behaviour at higher shear rates. The extension of the Newtonian and shear-thinning regimes depends on the concentration of HMPAM. The shear-thinning effect was more pronounced for high concentrations of HMPAM solution. This is explained by the deformation of polymer chains in the shear direction, which allows for easier flow of the molecules, resulting in the reduction of the viscosity with an increase in shear rates [349].

However, it was found that at concentrations lower than 0.1 wt%, HMPAM solution only exhibits a Newtonian behaviour over the range of tested shear rates. This suggests that, in this case, the structural characteristics of the polymer chains no longer affect the viscosity. The shear rate dependency of HMPAM solution increased with an increase in polymer concentration. This is ascribed to an increase of associations among polymer chains leading to the higher viscosity and extending the shear-thinning region [350]. Such shear rate dependency was more pronounced at concentrations larger than the overlap concentration (C_p^*), which was calculated to be approximately 0.49 ± 0.01 wt% for HMPAM in DI water (see Figure A.7a, **Appendix A**). From Table A.1 in **Appendix A**, it can be seen that relaxation time increases as concentration rises. This means that at higher concentrations, when HMPAM molecule is deformed by shear forces, it requires a longer time to relax to its original conformation.

HMPAM showed an excellent solubility in Brine2015 over the range of tested concentrations, up to 0.5 wt%, which led to complete transparent solutions. Since HMPAM is a non-ionic polymer, it did not strongly respond to the presence of cations in the solvent. Figure 3.4b shows that, irrespective of concentration, the viscosity of HMPAM solutions increased in Brine2015 throughout all the tested shear rates as compared to HMPAM solutions in DI water. As HMPAM showed an excellent solubility both in DI water and Brine2015, this is mainly attributed to an increase in solvent viscosity which was measured to be 0.9 ± 0.1 and 1.4 ± 0.1 mPa s for DI water and Brine2015 respectively. This implies that the increase in viscosity is approximately 55% which is close to the observed increase in the viscosity for HMPAM at various concentrations.

The overlap concentration of HMPAM dissolved in Brine2015 was found to be approximately 0.30 ± 0.01 wt% (see Figure A.7b, **Appendix A**). This infers that an association among HMPAM chains occurs at lower concentrations in Brine2015 than in DI water. As can be seen in Figure 3.4b and Table A.2, **Appendix A**, it was also found that at a given concentration, the shear-thinning behaviour was more pronounced and the relaxation time was longer in Brine2015 when compared with HMPAM in DI water. Figure 3.4c shows that increasing the temperature from 25 °C to 70 °C reduced the viscosities of HMPAM solution in Brine2015 and made the shear dependency of concentration less pronounced. Such a reduction in the viscosity was by a factor of 2.3 for HMPAM solutions with concentrations of 0.05 and 0.1 wt%, which is comparable

with the reduction in viscosity of Brine2015. At higher concentrations, this factor increased up to 3.3 for 0.5 wt% HMPAM.

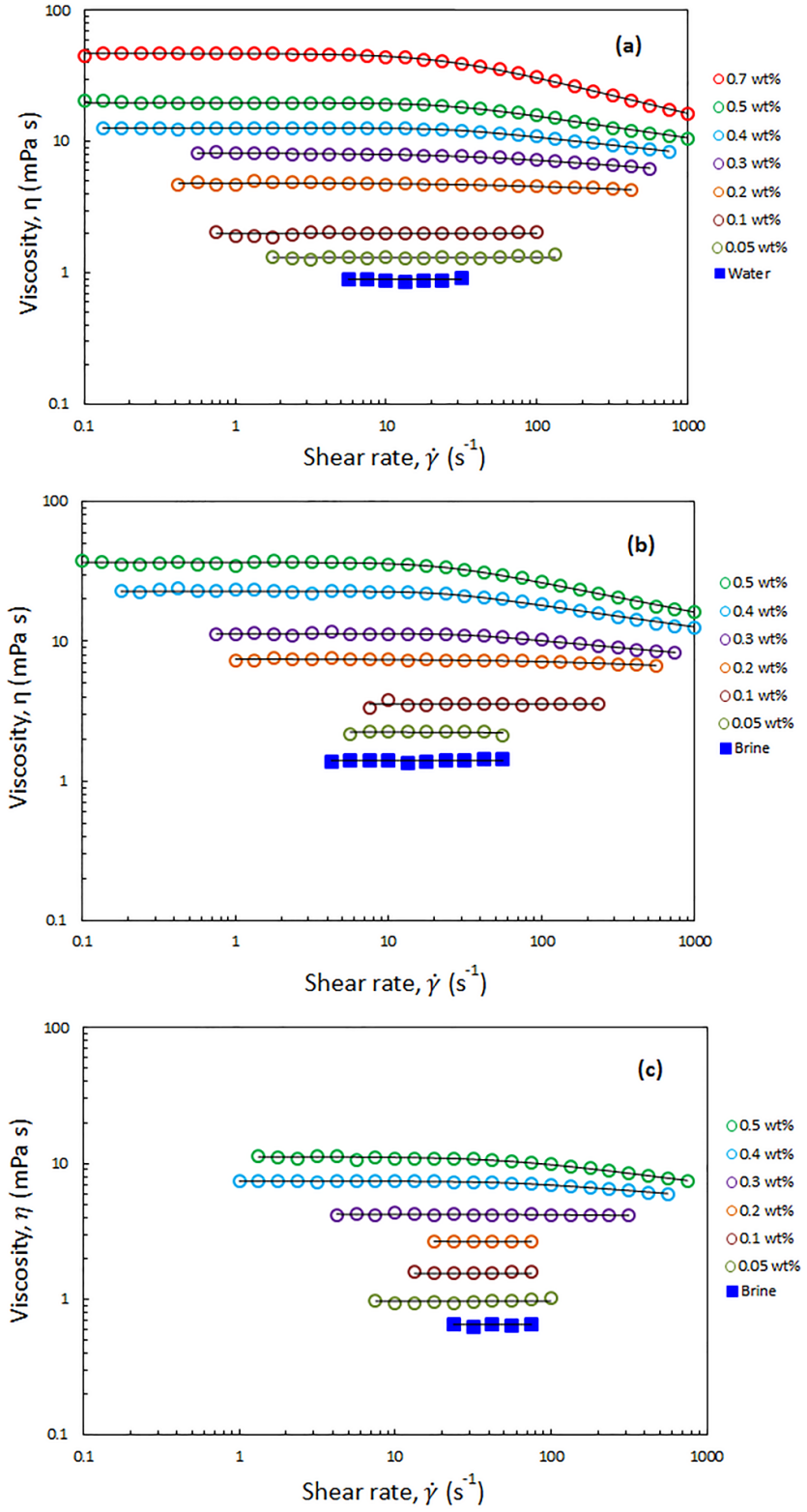

Figure 3.4: Steady state shear viscosity of HMPAM at different concentrations in (a) DI water at 25 °C (b) Brine2015 at 25 °C and (c) Brine2015 at 70 °C. The solid line is acquired by fitting the experimental data into Carreau–Yasuda model. The fitting parameters are presented in Table A.1–A.3, Appendix A

3.4.4 Rheology of HMPAM–NPs hybrids at high salinity and temperature

The rheological response of the hybrids of HMPAM and GPTMS-modified NPs at high salinity and the elevated temperature was investigated at various HMPAM and NPs concentrations. All the samples were prepared in Brine2015 and the viscosity measurements were performed at 70 °C. The concentration of HMPAM was selected as 0.05, 0.1 and 0.2 wt% in the dilute regime, 0.3 wt% in the boundary of transition from dilute to semi-dilute and 0.5 and 0.6 wt% in the semi-dilute regime. The concentration of NPs also varied from 0.5 to 4 wt%. Figure 4.4 shows the results of such viscosity measurements. All the reported viscosities are at shear rate of 7.5 s^{-1} which is within the typical range of practical shear rate values in various industrial processes [351]. The inserted values on the horizontal axis of the plot in Figure 3.5 correspond to the viscosities of HMPAM solutions without NPs. The viscosity of Brine2015 at 70 ^{o}C (corresponding to the origin of the graph) was 0.6 ± 0.1 mPa s. Once up to 0.3 wt% of HMPAM was added to Brine2015, the viscosity increased to 4.2 ± 0.1 mPa s. An additional increase of the concentration to 0.5 and 0.6 wt% significantly increased the viscosity to 11.2 ± 0.1 and 19.5 ± 0.1 mPa s respectively as the association among chains was achieved. The values along the vertical axis of the plot in Figure 3.5 represent the viscosity of NPs dispersion in the absence of HMPAM. The increase in NPs concentration from 0.5 to 4 wt% increased the viscosity from 0.6 ± 0.1 to 1.0 ± 0.1 mPa s. The viscosity of HMPAM–NPs hybrids is discussed at different polymer concentration regimes. In the dilute regime (C_p = 0.05,0.1 and 0.2 wt%), the addition of NPs to HMPAM solution did not have a substantial impact on the viscosity of the hybrids. For instance, the addition of 4 wt% NPs to 0.2 wt% HMPAM only increased the viscosity another 1.0 ± 0.1 mPa s. Once the HMPAM concentration was close to the overlap concentration (C_p^* = 0.3 wt%), as the NPs concentration increased, a more substantial increase in viscosity was perceived (incremental viscosity of 1.8 ± 0.1 mPa s with the addition of 4 wt% NPs). Furthermore, in the semi-dilute regime (C_p = 0.5 and 0.6 wt%) the most significant synergic effect was witnessed. Addition of 4 wt% NPs to 0.5 and 0.6 wt% HMPAM solution increased the viscosity another 6.4 ± 0.1 and 9.4 ± 0.1 mPa s respectively. In this polymer concentration regime, there appears to be a critical NPs concentration ($C_{np,c}$) present, above which the increase in the viscosity of the hybrid is more pronounced.

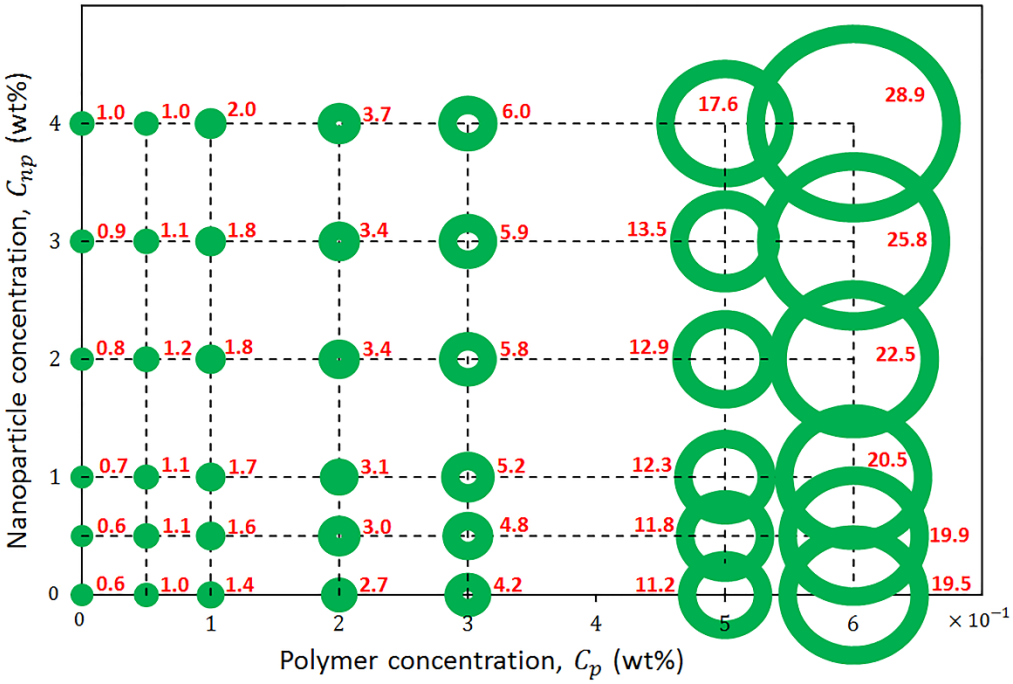

Figure 3.5: Viscosities of HMPAM–NPs hybrids at shear rate of 7.5 s-1 at different concentrations. The materials were dispersed in Brine2015 and the measurements were done at 70 °C. The magnitude of viscosity in terms of mPa s is shown next to or inside the circle. The viscosities scale with the radius of the circles

In order to provide a better assessment of the effect of $C_{np,c}$ on the viscosity of the HMPAM–NPs hybrid when HMPAM is in the semi-dilute concentration regime, Figure 3.6 was plotted. The viscosity measurement was also attempted for the hybrid of 0.5 wt% HMPAM and 3.5 wt% NPs (this was not represented in Figure 3.5 for better readability of the graph). As can be seen in Figure 3.6, regardless of concentration, the viscosity of the dispersion of NPs remained low, suggesting that the viscosity enhancement of HMPAM–NPs hybrid cannot be considered as a superposition of viscosity of HMPAM solution and NPs dispersion. On the other hand, the increase in NPs concentration increased the viscosity of the hybrids containing 0.5 and 0.6 wt% HMPAM in two different regimes: for the hybrids containing 0.5 wt% HMPAM, with the addition of up to 3 wt% NPs, the viscosity of hybrid grew linearly with a relatively small growth rate; however, from 3 wt% to 4 wt% a second more significant linear increase in viscosity was observed. This suggests that in order to have a considerable increase in the viscosity of the hybrid, the NPs concentration should be above a certain critical threshold ($C_{np,c}$) to bridge between HMPAM chains using hydrophobic–hydrophobic interactions. $C_{np,c}$ for the hybrids containing 0.5 wt% HMPAM was 3.0 ± 0.1 wt%. For the hybrid containing 0.6 wt% HMPAM, however, it was found that $C_{np,c}$ is lower (1.5 ± 0.1 wt%). This can be explained by the fact that with an increase in the HMPAM concentration in the semi-

dilute regime, the polymer chains come in closer proximity to each other and a smaller amount of NPs is needed to enable the bridging between HMPAM molecules.

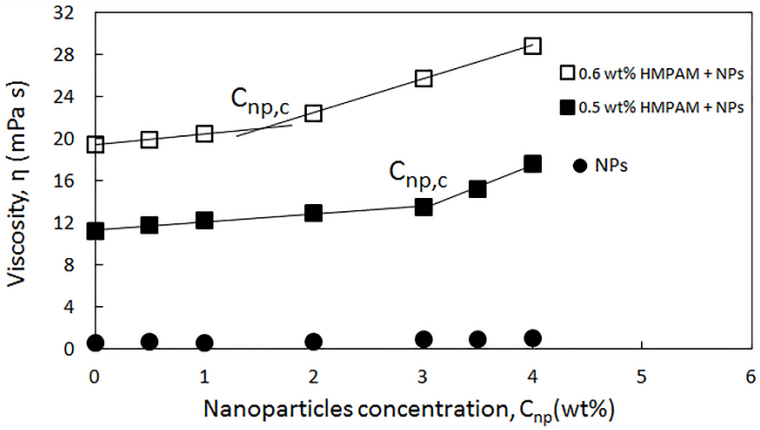

Figure 3.6: Viscosities of 0.5 and 0.6 wt% HMPAM in combination with NPs at different concentrations ranging from 0 to 4 wt% at shear rate of 7.5 s^{-1}

To investigate the influence of hydrophobic–hydrophobic interactions on the NPs-induced bridging between HMPAM molecules, the shear rate dependency of two combinations were studied (a) the hybrid of 0.5 wt% HMPAM and 4 wt% NPs and (b) the hybrid of 0.5 wt% PAM and 4 wt% NPs. As mentioned earlier, unlike HMPAM, PAM does not contain the hydrophobic group of t-butyl acrylamide and it was selected to examine whether there is a similar synergic effect between PAM and NPs or not. As can be seen in Figure 3.7, the viscosity of the hybrid of HMPAM and NPs is considerably higher than the viscosity of HMPAM, whereas a synergic effect was not observed for the hybrid of PAM and NPs and the viscosity of this hybrid was only slightly higher than the viscosity of PAM. This finding suggests that NPs can facilitate the bridging between HMPAM molecules only using hydrophobic–hydrophobic interactions, with the end result of creating larger molecules, whereas such an effect was not observed for the hybrid of NPs and PAM. Therefore, it can be inferred that as expected there is no effective interaction between PAM and hydrophobically modified silica NPs.

Moreover, to investigate the rheological properties of the hybrids, where shear-thinning occurs, the shear rate dependency of the hybrids was studied. As can be seen in Figure 3.7, the hybrid of HMPAM and NPs showed a shear-thinning behaviour both in low shear rates (< 10 s^{-1}) and high shear rates (> 100 s^{-1}). The power-law slope of the second shear-thinning is close to the power-law slope of the shear-thinning observed for HMPAM at high shear rates, whereas at low shear rates a shear-thinning for HMPAM was not detected. The presence of two shear-thinning regimes for HMPAM–NPs hybrid is

hypothesized as follows. HMPAM chains are bridged by NPs through two types of interactions between HMPAM chains and NPs; weak interactions and strong interactions. When the hybrid is exposed to a shear-flow field, first at low shear rates, the weak interactions are continuously broken which results in the first shear-thinning regime. In intermediate shear rates, only strong interactions play a role in NPs-induced bridging between HMPAM chains which are not yet broken. As a result, a Newtonian regime is observed for the HMPAM–NPs hybrid at intermediate shear rates. At high shear rates, however, strong interactions are also broken which leads to the second shear-thinning regime. It should be noted that the hybrid of PAM–NPs did not show a shear-thinning behaviour at low shear rates which is again an indication of a lack of effective interactions between PAM and NPs.

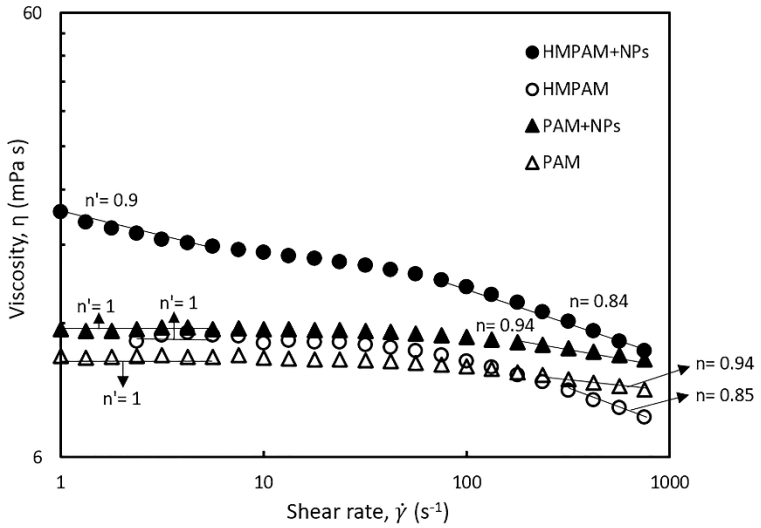

Figure 3.7: Viscosities of polymer–NPs in Brine2015 at 70 °C as a function of shear rate. Open and filled circles represent viscosity of 0.5 wt% HMPAM and hybrid of 0.5 wt% HMPAM and 4 wt% NPs respectively. Open and filled triangles represent viscosity of 0.5 wt% PAM and hybrid of 0.5 wt% PAM and 4 wt% NPs respectively. n and n' represents the power-law slope at low and high shear rates respectively

The shear-thinning behaviour was also investigated in different HMPAM concentration regimes. The selected hybrids contained constant NPs concentration of 4 wt% and the concentration of HMPAM varied from 0.2 to 0.6 wt% (i.e. from dilute to the semi-dilute regime). As can be seen in Figure 3.8, at low shear rates, for the hybrids with HMPAM in the dilute regime, there was no shear-thinning regime, whereas for the hybrids with HMPAM in the semi-dilute regime we observed a shear-thinning behaviour and the power-law slope was around 0.9 (0.9 and 0.89 for 0.5 and 0.6 wt% HMPAM respectively). At high shear rates, for the hybrids with HMPAM in the dilute regime, the power-law slope was close to unity (1 and 0.96 for 0.2 and 0.3 wt% respectively), whereas

when HMPAM was in the semi-dilute regime, the power-law slope was around 0.8 (0.84 and 0.81 for 0.5 and 0.6 wt% respectively). This increase in the power-law slope of the hybrids from dilute to semi-dilute regime is attributed to bridging between different HMPAM chains by NPs in the semi-dilute regime. In a shear-flow field, these bridges are broken and a more shear-thinning behaviour is expected. The formation of such bridges in the dilute regime is not expected as the HMPAM chains are not in close proximity of each other.

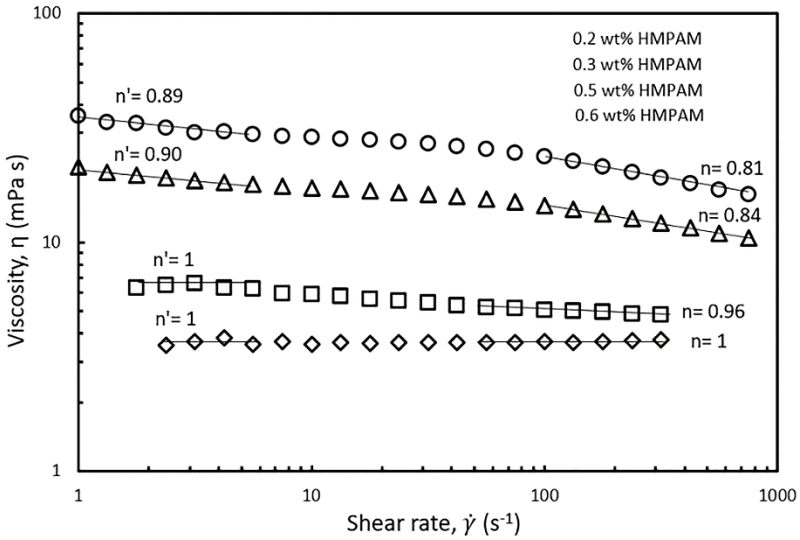

Figure 3.8: Shear rate dependency of HMPAM–NPs hybrids in Brine2015 at 70 °C. The concentration of NP was kept constant at 4 wt% and the concentration of HMPAM varied from 0.2 to 0.6 wt%. Power-law slope decreased with increasing HMPAM concentration. n and n' represents the power-law slope at low and high shear rates respectively

3.4.5 Dynamic rheological behaviour of the hybrids at different NPs concentration

In order to shed light on the viscoelastic response of HMPAM–NPs hybrids, the dynamic viscoelasticity was examined. For this purpose two oscillatory tests were performed: i) the amplitude sweep test to measure the storage modulus (G') and loss modulus (G'') as a function of strain (ε) and ii) the frequency sweep test to assess the frequency dependence of the storage and loss moduli. The hybrids for which this analysis was performed contained constant NPs concentration of 4 wt% and the concentration of HMPAM varied from 0.2 to 0.6 wt% (i.e. from the dilute to semi-dilute regime). This was to investigate the viscoelastic response of the hybrids in the different HMPAM concentration regimes.

As can be seen in Figure 3.9a and 3.9b, for the amplitude sweep test performed on the hybrids, the loss modulus is larger than the storage modulus over the range of strains up to 1000% regardless of HMPAM concentration, implying that even for HMPAM in the

semi-dilute regime the rheological response of the hybrids is controlled by the viscous component. The loss modulus was almost constant for the hybrids with 0.2 and 0.3 wt% HMPAM (i.e. when the polymer is in the dilute regime) but it slightly decreased for hybrids containing 0.5 and 0.6 wt% HMPAM (i.e. when the polymer is in the semi-dilute regime) at high strains. The storage modulus of these hybrids, however, showed a sharper decrease at high strains (note that accurate values of storage modulus were not measured for the hybrid with 0.2 wt% HMPAM at low and high strains due to the limitations of the rheometer). The stronger decrease of the storage modulus for these hybrids as compared to hybrids with HMPAM in the dilute regime is an indication of a more effective interaction between HMPAM and NPs.

Figure 3.9c shows that for all the tested frequencies, from 1 to 100 rad/s, all the hybrids exhibited predominantly viscous behaviour over elastic behaviour irrespective of HMPAM concentration. It can be seen that with the increase in HMPAM concentration, *G'* and *G"* became stronger. The slope of *G'* over the slope of *G"* in a log-log plot was calculated for these four hybrids. It was found that for the hybrids containing 0.2 and 0.3 wt% HMPAM (i.e. dilute regime) the slope ratio was 2.0 ± 0.1 and 1.9 ± 0.1 Pa s/rad respectively indicating the hybrids behave like a liquid. Nonetheless, for the hybrids containing 0.5 and 0.6 wt% HMPAM (i.e. semi-dilute regime) the slope ratio was 1.7 ± 0.1 and 1.6 ± 0.1 Pa s/rad respectively. This decrease in slope ratio with increasing HMPAM concentration indicates that in the semi-dilute regime some degree of bridging between HMPAM chains induced by NPs occurs.

In Figure 3.10, the viscosity and storage and loss moduli of the hybrids are plotted within the linear viscoelastic regime. This regime was obtained from the amplitude sweep test at a constant angular frequency of 20 rad/s in different HMPAM concentration regimes from dilute to semi-dilute. As can be observed for all three parameters the slope of the data points obtained in the semi-dilute regime became larger than their slope in the dilute regime. It can be concluded that the addition of 4 wt% NPs to HMPAM has a stronger viscoelastic effect when HMPAM is in the semi-dilute concentration regime.

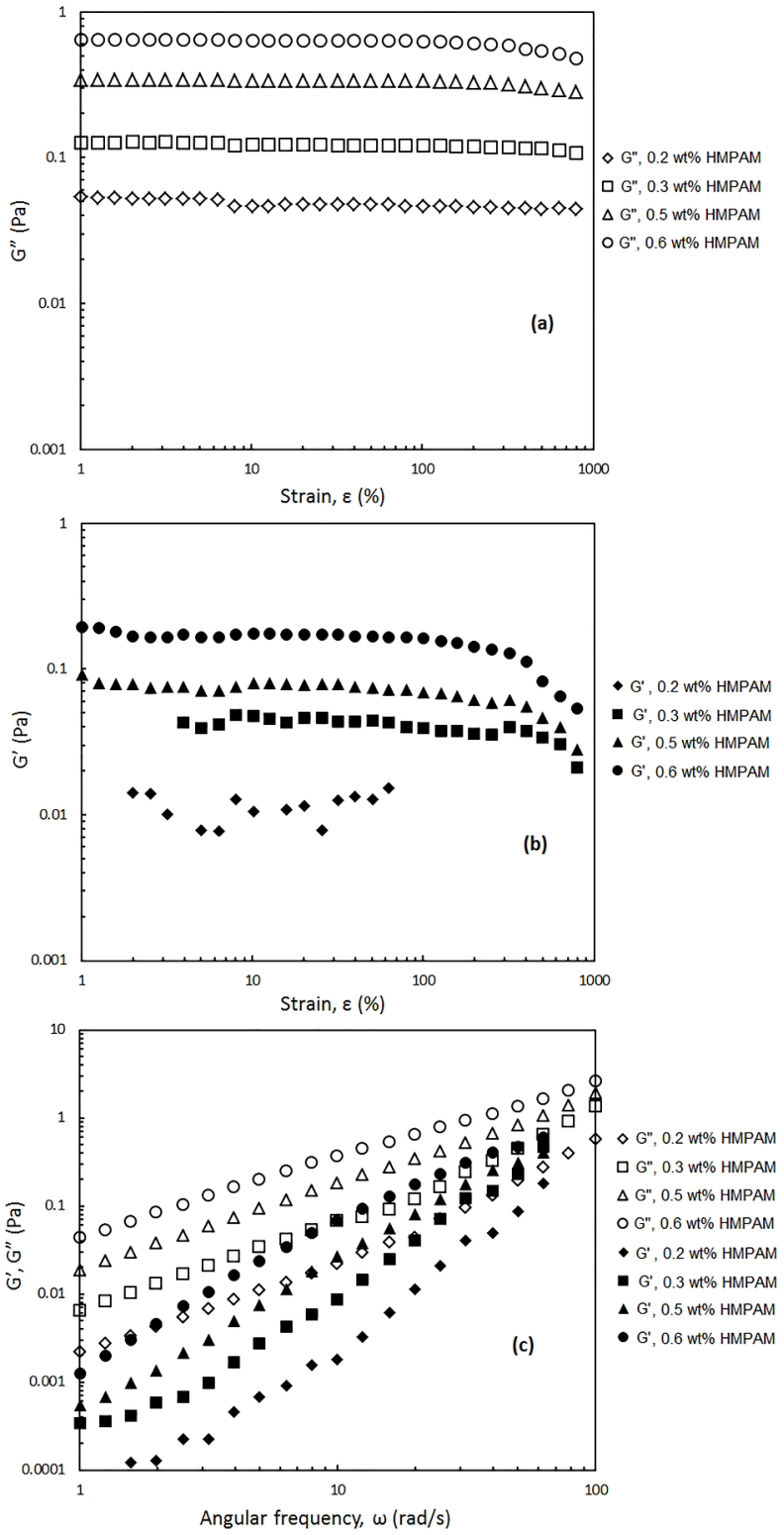

Figure 3.9: Amplitude and frequency sweep tests. (a) Loss modulus *G*" as a function of strain *ε* at constant angular frequency ω=20 rad/s. (b) Storage modulus *G*' as a function of ε at constant ω=20 rad/s. (c) *G*' and *G*" as a function of ω at constant ε within the linear viscoelastic regime (*ε* was selected in the range of 50–75% depending on the test). Filled and open symbols represent *G*' and *G*" respectively. The concentration of NPs was kept constant at 4 wt%. The concentration of HMPAM varied: diamonds, squares, triangles, and circles represents HMPAM concentration of 0.2, 0.3, 0.5, and 0.6 wt% respectively

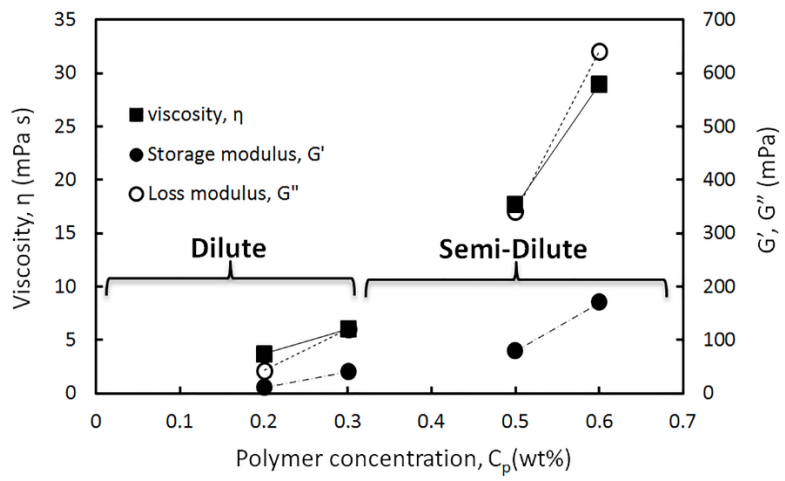

Figure 3.10: Comparison of the viscosity and storage and loss moduli of the hybrids at constant NPs concentration of 4 wt% and varying HMPAM concentration from 0.2 to 0.6 wt%. *G*' and *G*" were obtained from amplitude sweep test and constant angular frequency of 20 rad/s

To illustrate various interactions in HMPAM–NPs hybrids, the molecular scenario as indicated in Figure 3.11 was drawn. The distribution of hydrophobic groups on HMPAM is random and HMPAM chains have a radius of gyration of approximately 80 ± 5 nm (see Equation A.4 in **Appendix A**), while the size of silica NPs is approximately 7 nm. The contour length of HMPAM was estimated to be 9.9 ± 1.9 µm which is much larger than the estimated persistence length of 2.2 ± 0.6 nm (see Equation A.5 in **Appendix A**). Therefore, our long-chain polymer behaves like a random coil. As indicated in Figure 3.11a, for HMPAM chains in the semi-dilute regime in absence of NPs, two types of interactions are possible: (a) intra-chain hydrophobic association within an HMPAM chain (orange circles) and (b) inter-chain hydrophobic association between HMPAM chains (red circles). Figure 3.11b represents the interaction of hydrophobic groups on HMPAM and hydrophobically modified silica NPs and how silica NPs can play as bridging sites between the HMPAM chains. As discussed before, based on the viscosity results, bridging between HMPAM chains occurs only when the concentration of NPs is above $C_{np,c}$. At concentrations lower than $C_{np,c}$, hydrophobic groups present in the HMPAM are anchored onto hydrophobically modified NPs and there are no free NPs in the dispersant. Nonetheless, beyond the $C_{np,c}$, free NPs come to be available and a further increase in C_{np} will result in bridging between different HMPAM chains by NPs (black circle). The existence of the $C_{np,c}$ is in agreement with observations of Hu et al. [324] and Zhu et al. [325] who argued that interaction between polymer and silica NPs occurs by hydrogen bonding. It should be noted that the reason why the synergic effect between HMPAM and NPs is more significant when $C_p > C_p^*$, is because the inter-chain

association between some HMPAM chains has occurred previously and the chains are in closer proximity to each other. Consequently, the probability of bridging between HMPAM chains by NPs becomes higher compared to the dilute regime where HMPAM chains are distant from each other. As a result of bridging between HMPAM chains, the movement of HMPAM chains is limited and the hydrodynamic radius of the hybrid increases which eventually results in an increase in the viscosity.

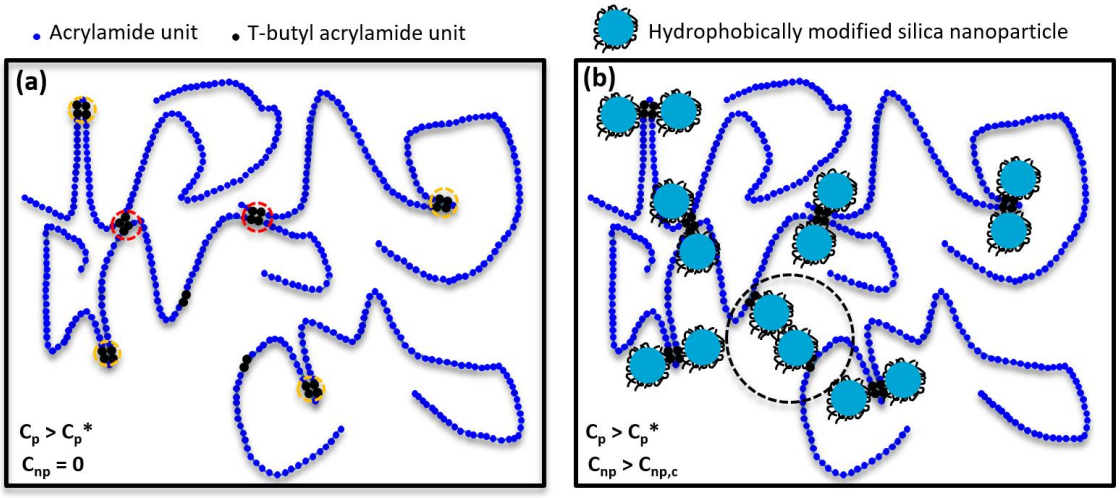

Figure 3.11: Schematic of various interactions in HMPAM–NPs hybrids. (a) Intra-chain (orange circles) and inter-chain (red circles) hydrophobic associations in HMPAM chains in the semi-dilute regime in absence of NPs. (b) Bridging of HMPAM chains by NPs (black circle) in the semi-dilute regime when the concentration of NPs is larger than $C_{np,c}$

It should be noted that regardless of the concentration of HMPAM and NPs, all the developed hybrids were transparent and no phase separation was observed (see Figure A.3, **Appendix A**). This demonstrates an important aspect of HMPAM–NPs hybrid as an alternative for conventional cEOR polymers at harsh conditions as enhanced stability is achieved.

3.4.6 Conclusions

An innovative hybrid system using a combination of a hydrophobically modified polyacrylamide (HMPAM) and hydrophobically modified silica nanoparticles (NPs) was investigated. This system exhibited enhanced stability in high total dissolved solids (TDS) content and high hardness brines and improved the rheological properties of HMPAM at elevated temperatures. The silica NPs that had been modified by grafting an organic ligand (gamma-glycidoxypropyltrimethoxysilane) onto their surface showed good colloidal stability against aggregation at high salinity, due to the increased potential barrier as compared to bare silica NPs. Viscosity measurements at different HMPAM and

NPs concentrations showed that the improved rheological behaviour was more pronounced when the concentration of HMPAM was more than the overlap concentration (C_p^*~0.3 wt%). This occurred because in the semi-dilute regime HMPAM chains are in closer proximity and they can be bridged by NPs which in turn increases the hydrodynamic radius of the hybrid. Results also showed that for a given concentration of HMPAM in the semi-dilute regime, there was a critical concentration of NPs above which the bridging between HMPAM chains by NPs occurred and increased the viscosity more substantially. Dynamic rheological tests indicated that the hybrids were viscous dominated and storage and loss moduli had a stronger increase with HMPAM concentration in the semi-dilute regime compared to the dilute regime due to NPs-induced bridging between HMPAM chains. The results of this study provide insights into the interaction of polymer molecules and NPs in hybrid systems with the end result of enhancing the stability and improving the rheological properties, thus opening a pathway for developing other polymer-based systems for use in harsh conditions.

4 FLOW OF MODIFIED POLYACRYLAMIDE–SILICA NANOPARTICLES IN POROUS MEDIA

This chapter is devoted to the behaviour of HMPAM–NPs hybrids in porous media. The primary goal of the study was to investigate their rheology, retention, and injectivity at the typical salinity, pressure, and temperatures encountered in oil reservoirs. Core-flood experiments were therefore performed using the HMPAM, NPs, and their hybrids, in Bentheimer core samples at both low and high flow superficial velocities of 1 and 10 ft/ day (equivalent to 0.3048 and 3.0480 m/day). The apparent viscosity of the HMPAM–NPs hybrid in porous media was found to be the same as the shear viscosity in bulk. The injection of a dispersion of NPs resulted in a significant increase in the pressure drop over the core. This could be attributed to the external and internal filtration of nanoparticle aggregates. Intriguingly, the co-injection of HMPAM and NPs resulted in a much milder increase of the pressure drop. This supports the proposed concept in **Chapter 3**, where bridging among the HMPAM chains is caused by NP-mediated hydrophobic–hydrophobic interactions. This prevents the aggregation of NPs with one another and facilitates their transport through porous media with the HMPAM. Moreover, the injection of the HMPAM–NPs hybrid reduced the retention of both the HMPAM and the NPs as compared to when they were injected individually. This can be explained by the availability of fewer adsorption sites on the surface of the rock for HMPAM and NPs when both of them are present in the same solution. These results show the potential of the HMPAM–NPs hybrid as a mobility control agent for chemical enhanced oil recovery at high salinity and temperature.

4.1 Introduction

In **Chapter 2**, it was shown that there is a need for a polymeric system with improved viscosity and enhanced stability at elevated temperature and high salinity particularly in presence of divalent cations. Despite the efforts to develop modified polymers suitable for such harsh conditions (**Section 2.2.6**), there is very limited data in the literature on their behaviour in porous media.

In **Chapter 3**, a novel approach was presented that includes the hybridization of hydrophobically modified polyacrylamide (HMPAM) with hydrophobically modified silica nanoparticles (NPs) to achieve enhanced stability and high viscosity at extreme salinities and elevated temperatures (>20 wt% TDS, including >1.5 wt% divalent cations, and T > 70 ℃). It was shown that the hybridization of HMPAM with NPs leads to a higher viscosity at high salinity and temperature. This was due to the fact that the NPs bridge between the HMPAM chains, and increase the hydrodynamic radius, which in turn increases the viscosity.

In this chapter, the behaviour of HMPAM–NPs hybrids in porous media is investigated. The main objective of the study is to examine their rheology, injectivity, and retention at typical salinity, pressure and temperatures encountered in oil reservoirs. The assessment of injectivity is based on an estimation of the resistance factor and residual resistance factor for the flow of HMPAM and NPs through porous media. This was discussed in detail in **Section 1.2**. The injectivity assessment was done at both low and high superficial velocities of 1 and 10 ft/day (equivalent to 0.3048 and 3.0480 m/day). The former is within the typical range of practical superficial velocities in oil reservoirs far from the wellbore and the latter is a typical superficial velocity encountered in the near-wellbore region [351]. The assessment of retention is based on the single injection method as discussed in **Section 2.2.3.3**. This was done at a low superficial velocity of 1 ft/day. In a series of core-flood experiments, first the HMPAM and NPs were individually injected into the Bentheimer core samples and their flow characteristics were studied. Next, the impact of the hybridization of the HMPAM and NPs on the transport mechanisms in porous media was investigated by observing the dependencies between core-flood experiments and the rheological experiments performed in bulk.

4.2 Experimental section

4.2.1 Chemicals

Silica NPs, available under the commercial name Levasil CC301, were supplied by AkzoNobel in suspension (ρ = 1.2 g cm^{-3}) containing 28.1 wt% silica with an average particle diameter of 7 nm as reported by the manufacturer. The surface of the NPs was modified by gamma-glycidoxypropyltrimethoxysilane (GPTMS), a low molecular weight organic ligand to provide steric stabilization and ensure colloidal stability at high salinity [238]. Acrylamide and t-butyl acrylamide monomers were purchased from Sigma-Aldrich. HMPAM (98 mol% acrylamide and 2 mol% t-butyl acrylamide) was synthesised using free radical polymerization [238]. Its average molecular weight was estimated using the methodology used by Wu et al. [329] which is based on viscosity measurements, and found to be approximately 2.1×10^6 g mol^{-1} (see Figure A.6 in **Appendix A**). The sodium chloride (NaCl) and calcium chloride dihydrate ($CaCl_2.2H_2O$) used for brine preparation and the potassium iodide (KI), used as the tracer, were also purchased from Sigma-Aldrich. All materials were used as received without further purification.

4.2.2 Solution preparation

The HMPAM and NPs were diluted from their original concentration to the desired concentration in Brine2015 (20 wt% TDS including 1.5 wt% Ca^{2+}) as the dispersant medium. The mixtures were stirred either overnight or for 2 hours respectively, until they became completely homogenous and transparent. The density and viscosity of Brine2015 at 25 ℃ were 1.2 ± 0.01 g/cm^3 and 1.4 ± 0.01 mPa s respectively. The hybrid samples of HMPAM–NPs were prepared in Brine2015 using the procedure explained in **Section 3.3.2.3**. Before the core-flood experiments, the solution of polymer and/or NPs was stirred until the creation of a vortex, and then 0.1 wt% of the tracer (KI) was added to it. All the solutions were degassed to remove any dissolved oxygen.

4.2.3 Porous medium

The core-flood experiments were performed using Bentheimer sandstone of the Early Cretaceous age from the south-western part of the Lower Saxony Basin. The properties of the Bentheimer core samples used in the experiments are listed in Table 4.1 , and it can be seen that they consist mostly of quartz. The porosity of the core samples was measured by the standard gas expansion method.

To prepare the sandstone for the core-floods, cores were first cut and then dried in an oven for up to 48 hours at 60 ± 1 ℃. Subsequently, the cores were cast in an epoxy resin to prevent the bypassing of the flow alongside the core. The resin penetrated approximately 1.0 mm inside the core. Thereafter, the cores were machined to an effective diameter of 3.8 ± 0.1 cm and a length of 38.0 ± 0.1 cm. The machined samples were placed in an oven for 15 hours at 40 ± 1 ℃ to dry. The absolute permeability of each core to Brine2015 was then estimated using Darcy's law.

Table 4.1: Properties of the Bentheimer core samples used for core-flood experiments

Components	Quartz	Kaolinite	
	99.3 ± 0.1%	0.7 ± 0.1%	
Porosity (%)	24.4 ± 0.2		
Length (cm)	38.0 ± 0.1		
Diameter (cm)	3.8 ± 0.1		
Initial Permeability (mD)	Exp. 1	Exp. 2	Exp. 3
	2640 ± 20	2560 ± 20	2680 ± 20

4.2.4 Experimental set-up

The core-flood experimental setup is shown in Figure 4.1. A core sample was positioned in a core holder (poly-ether-ether-ketone). The core holder was oriented vertically to mitigate the effect of gravity. Fluids were injected into the core using a Quizix pump, which was operated at a constant flow rate. The pump had a flow rate accuracy of ± 2%. Six differential pressure transducers (KEMA03 ATEX 1561) with ± 300 mbar range and ± 1 mbar accuracy were employed to measure the pressure drop in different sections of the core. The length of each section was either 6 or 6.5 cm. The pressure drop along the whole core length was measured using a seventh differential pressure transducer. The pressure drops were recorded as a function of time by a National Instruments™ data acquisition system. A back-pressure (BP) regulator connected to a nitrogen cylinder (100 ± 1 bar) was utilised for applying the desired back-pressure of 25 ± 1 bar.

The effluent samples were collected using a GE Frac 920 fraction collector. Since the experiments needed to be conducted at high temperature, the core holder was kept in an oven, where the temperature was fixed at 70.0 ± 0.1 ℃, and the injected fluid flowed

through a coiled tube to ensure the solutions were heated up to the desired temperature before entering the core. The confining pressure was also taken from the injection line and it was inserted into the middle of the core to ensure the core does not break.

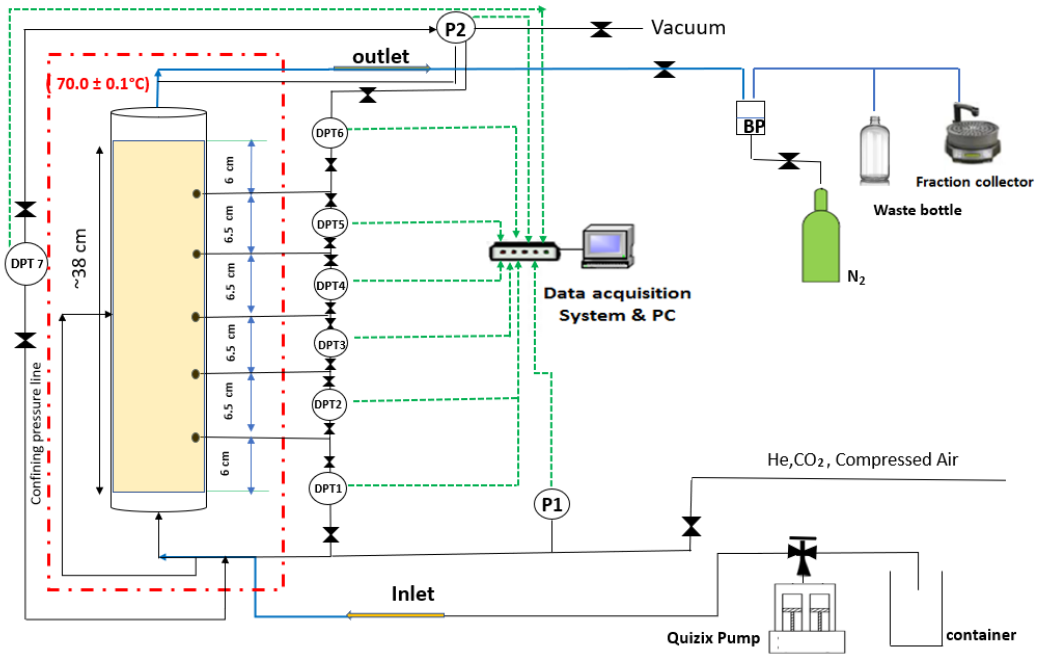

Figure 4.1: The schematic of the experimental setup used to perform the core-flood experiments

4.2.5 Experimental Procedure

Prior to the core-flood experiments, the viscosities of the polymer solutions, NPs suspension, and the hybrid samples were measured by the methodology explained in **Chapter 3** (see **Section 3.3.3.5**).

For the core-flood experiments, the procedure for setting up a new core was as follows. After ensuring that there were no leaks, the system was flushed with carbon dioxide (CO_2) for 30 minutes at a pressure of 5 ± 0.5 bar for the removal of air in the set-up. Thereafter, the setup was vacuumed to remove any remaining gas. Brine2015 was then injected for 10.00 ± 0.05 pore volumes (PV) at a flow rate of 1.00 ± 0.02 mL/min to saturate the core. The permeability test was performed using the injection of Brine2015 at various flow rates. All the solutions were filtered with a 5-micron syringe filter before injection into the core.

Three core-flood experiments were performed: the first experiment with 0.05 wt% HMPAM (Exp. 1), the second experiment with 0.5 wt% NPs (Exp. 2), and the third one with a combination of both (Exp. 3). The experiments were performed at two different flow rates: (a) low flow rate of 0.25 mL/min, equivalent to 1 ft/d and (b) high flow rate

of 2.5 mL/min equivalent to 10 ft/d. Table 4.2 describes all the steps in the procedure used in the core-flood experiments. Note that the letter a or b after the experiment number refers to the injection flow rate as described above.

Table 4.2: The procedure of the performed core-flood experiments

<table>
<tr><th>Step</th><th colspan="3">Description</th><th>Back-pressure</th><th>Flow rate (mL/min)</th><th>PV injected</th></tr>
<tr><td>1</td><td colspan="3">CO_2 flushing</td><td>-</td><td>-</td><td>-</td></tr>
<tr><td>2</td><td colspan="3">Vacuuming</td><td>-</td><td>-</td><td>-</td></tr>
<tr><td>3</td><td colspan="3">Brine2015 saturation</td><td>25</td><td>1.00</td><td>>10</td></tr>
<tr><td>4</td><td colspan="3">Permeability test</td><td>25</td><td>1.00–5.00</td><td>>10</td></tr>
<tr><td rowspan="6">5</td><td rowspan="6">Low flow rate</td><td colspan="2">Brine2015 injection</td><td rowspan="6">25</td><td rowspan="6">0.25</td><td>~3</td></tr>
<tr><td>Exp. 1a</td><td>0.05 wt% HMPAM injection</td><td rowspan="3">~10</td></tr>
<tr><td>Exp. 2a</td><td>0.5 wt% NPs injection</td></tr>
<tr><td>Exp. 3a</td><td>0.05 wt% HMPAM + 0.5 wt% NPs injection</td></tr>
<tr><td colspan="2">Brine2015 injection</td><td>~7</td></tr>
<tr><td rowspan="6">6</td><td rowspan="6">High flow rate</td><td colspan="2">Brine2015 injection</td><td rowspan="6">25</td><td rowspan="6">2.50</td><td>~3</td></tr>
<tr><td>Exp. 1b</td><td>0.05 wt% HMPAM injection</td><td rowspan="3">~10</td></tr>
<tr><td>Exp. 2b</td><td>0.5 wt% NPs injection</td></tr>
<tr><td>Exp. 3b</td><td>0.05 wt% HMPAM + 0.5 wt% NPs injection</td></tr>
<tr><td colspan="2">Brine 2015 injection</td><td>~7</td></tr>
</table>

a) Injection at a low flow rate

Injection at a low flow rate was carried out to assess the retention of materials and their propagation through porous media at a superficial velocity common in oil reservoirs (1 ft/day). After ensuring that the core is saturated with Brine2015, the flow rate was set to 0.25 mL/min. Then, as described in Table 4.2 (Step 5), Brine2015 was injected for ~3 PV followed by ~10 PV injection of HMPAM and/or NPs. Thereafter, Brine 2015 injection was resumed and continued for ~7 PV.

To assess the retention of the materials, the effluent samples were collected every 20 min. The effluent samples were examined for total organic carbon (TOC), using a DC-190 Dohrmann high-temperature TOC apparatus to determine the concentration of polymer. The samples with NPs were sent to Analytische Laboratorien GmbH for measurement of the concentration of silica nanoparticles by atomic absorption spectroscopy (AAS). The concentration of the potassium iodide tracer was measured using a UV-VIS Spectrophotometer UV Mini 1240 (Shimadzu).

b) Injection at a high flow rate

Injection at a high flow rate was carried out to assess the injectivity of the materials at a superficial velocity common in the near-wellbore region (10 ft/day). High flow rate injection of HMPAM and/or NPs was done immediately after the low flow rate injection, in the same core sample. After a steady-state pressure drop was achieved for the Brine2015 injection at a flow rate of 0.25 mL/min (Step 5), the flow rate was switched from 0.25 to 2.5 mL/min, and a similar procedure to that applied for the low flow rate was followed (i.e. ~3 PV Brine2015 injection followed by ~10 PV injection of HMPAM and/or NPs followed by ~10 PV Brine2015 injection, Table 4.2, Step 6).

4.3 Results and discussion

In **Section 3.4.3**, an extensive study on the rheological response of HMPAM and/or NPs at various concentrations was performed. In this chapter, the focus is on the porous media response at low concentrations of HMPAM and NPs. The experiments were performed with the following materials: 0.05 wt% HMPAM, 0.5 wt% NPs and their combination. They were dissolved/dispersed in Brine2015. All the experiments were carried out at 70 °C.

Figure 4.2 shows the solutions' viscosities as a function of shear rate. The measured viscosities are compared at a shear rate of 7.5 s^{-1}, which is within the typical range of practical shear rate values in a Bentheimer core at a superficial velocity of 1 ft/day (0.3048 m/day) [352]. The viscosity of Brine2015 was 0.65 ± 0.02 mPa s. The viscosities of the HMPAM, NPs and the HMPAM–NPs hybrid were 1.00 ± 0.02, 0.69 ± 0.02, and 1.10 ± 0.02 mPa s respectively. According to the Blake–Kozeny or Cannella equation [353], the effective shear rate in porous media scales linearly with the superficial velocity. Therefore, at a superficial velocity of 10 ft/day (3.048 m/day), the effective shear rate is expected to be approximately 75 s^{-1}. As the hybrid of HMPAM–NPs, and also the

HMPAM and the NPs, showed Newtonian behaviour in the range of shear rates of 7.5–75 s^{-1}, the viscosities at shear rates of 75 s^{-1} and 7.5 s^{-1} were equal.

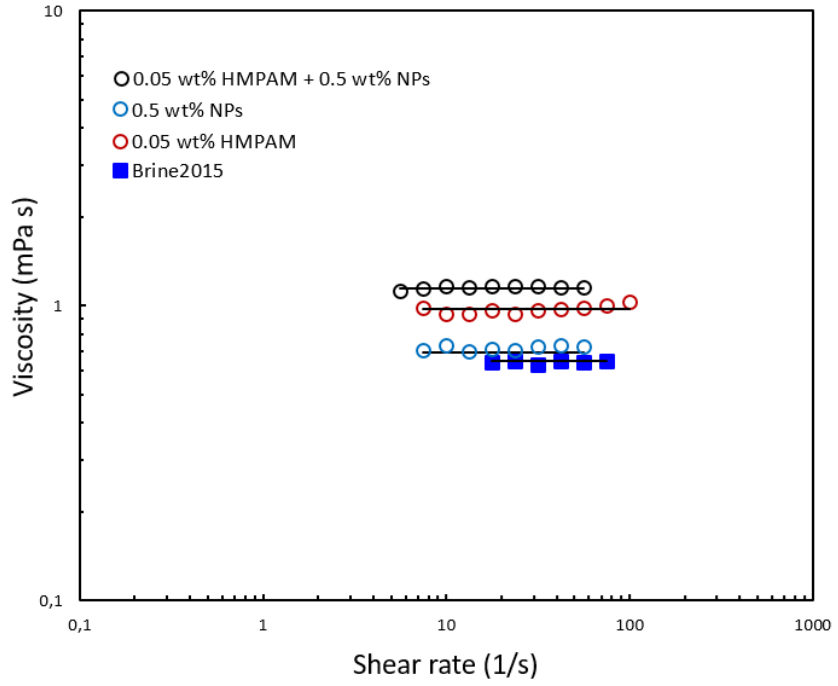

Figure 4.2: Viscosity as a function of shear rate for 0.05 wt% HMPAM, 0.5 wt% NPs and their combination. The viscosity of Brine2015 is given as a reference. The solid lines represent the Carreau–Yasuda model fit to the experimental data

In the following sections, the porous media flow behaviour of HMPAM and NPs, when injected individually, is discussed and compared to when the HMPAM–NPs hybrid is injected. The results of the experiments will be discussed in terms of: (a) the pressure drop observed along the core at low and high flow rates (superficial velocities of 1 and 10 ft/day) and (b) the concentration of the injected solution/suspension and effluents. The former is used to assess the injectivity and propagation of materials and the latter is used to assess the retention of materials in porous media.

4.3.1 The flow of HMPAM through porous media

a) Pressure drops

Figure 4.3 shows the pressure drop profiles obtained in Exp. 1a during the flow of both the Brine2015 and the HMPAM solutions through the porous medium at a flow rate of 0.25 mL/min. During the injection of Brine2015 in the first step, a steady-state pressure drop was observed. Upon injection of the HMPAM solution, the pressure drop started to increase. This indicates the entrance of the HMPAM molecules into the core. After the

injection of approximately 2.1 ± 0.1 PV of the HMPAM solution, the rate of pressure drop growth significantly decreased. This suggests the breakthrough of the HMPAM at the core outlet. A very slight and gradual increase in the pressure drop beyond the HMPAM breakthrough shows the presence of an insignificant mechanical entrapment of HMPAM within the porous medium. After the HMPAM injection was complete, Brine2015 was injected again which led to a gradual decrease and then stabilization in the pressure drop. The plateau value in the secondary Brine2015 injection (3.5 ± 0.1 mbar) was slightly higher than the one observed in the primary Brine2015 injection (3.2 ± 0.1 mbar) (i.e. the Brine2015 injection before injection of the HMPAM solution). This is a clear indication of the irreversible retention of polymer in the core.

Considering the pressure drop profiles for each section in Figure 4.3, during the flow of the HMPAM through the core sample, it can be seen that the pressure drop profiles at the beginning of each section had a horizontal part, which represents the pressure drop due to the Brine2015 injection. This horizontal part was very short in the first section, as this section feels the polymer pressure drop almost immediately after the polymer solution moves through the inlet lines and the core holder cap. As the polymer travels from one section to the next, the total ΔP monotonically increases and persists up to a point where breakthrough occurs. However, the rate of increase may be slightly different from one section to another depending on the absolute permeability and amount of polymer retention inside each section. The behaviour of the pressure drop for the sixth section was identical to the total pressure drop i.e. a very slight and gradual increase in pressure drop. This suggests the presence of mechanical entrapment of HMPAM chains. It should be noted that minor fluctuation in pressure drop profile along the core may be a result of the long injection period of the experiments. This required the experiments to run over days and nights which yields inevitable temperature differentiation.

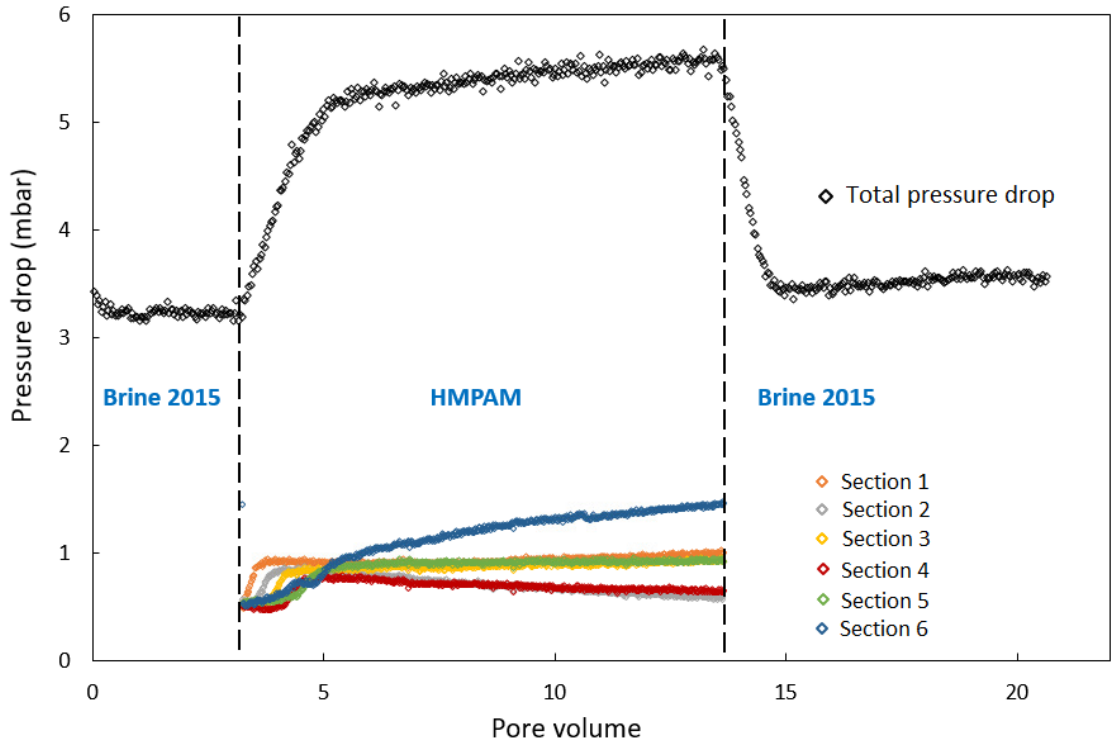

Figure 4.3: Pressure drop profile during low flow rate injection of HMPAM (Exp. 1a). The experiment was performed at a flow rate of 0.25 mL/min (equivalent to a superficial velocity of 1 ft/day) with the following sequence: injecting Brine2015 for 3.0 ± 0.1 PV, then injection of HMPAM solution for 10.1 ± 0.1 PV and resuming Brine2015 injection for 7.3 ± 0.1 PV to finish

Upon completion of the HMPAM injection at a low flow rate, the core was flushed with at least 10 PV of Brine2015. Exp. 1b was performed at a constant flow rate of 2.50 mL/min equivalent to a superficial velocity of 10 ft/d. During the primary Brine2015 injection a steady-state pressure drop was observed (Figure 4.4.). For the HMPAM injection, the pressure drop first increased continuously with the number of pore volumes injected. After the injection of 1.30 ± 0.1 PV, the pressure drop reached a steady-state value suggesting HMPAM breakthrough at the outlet. The stabilised pressure drop values after the breakthrough point indicate only trivial mechanical entrapment within the core in Exp. 1b. The fact that the total pressure drop levels off to a plateau is an indication of the very good injectivity of HMPAM. As can be seen in Figure 4.4, a similar trend was observed in all six sections of the core. There are obvious differences in plateau values of pressure drops of each section which is due to different permeabilities in each section. It is also noted that the pressure drop in the first section is higher than in the rest of the sections. This can be explained by the fact that because of the high flow rate of HMPAM injection there was not sufficient time for the solution to heat up to 70 ℃ in the inlet. As

a result, the viscosity is slightly higher which leads to a higher pressure drop compared to the rest of the sections.

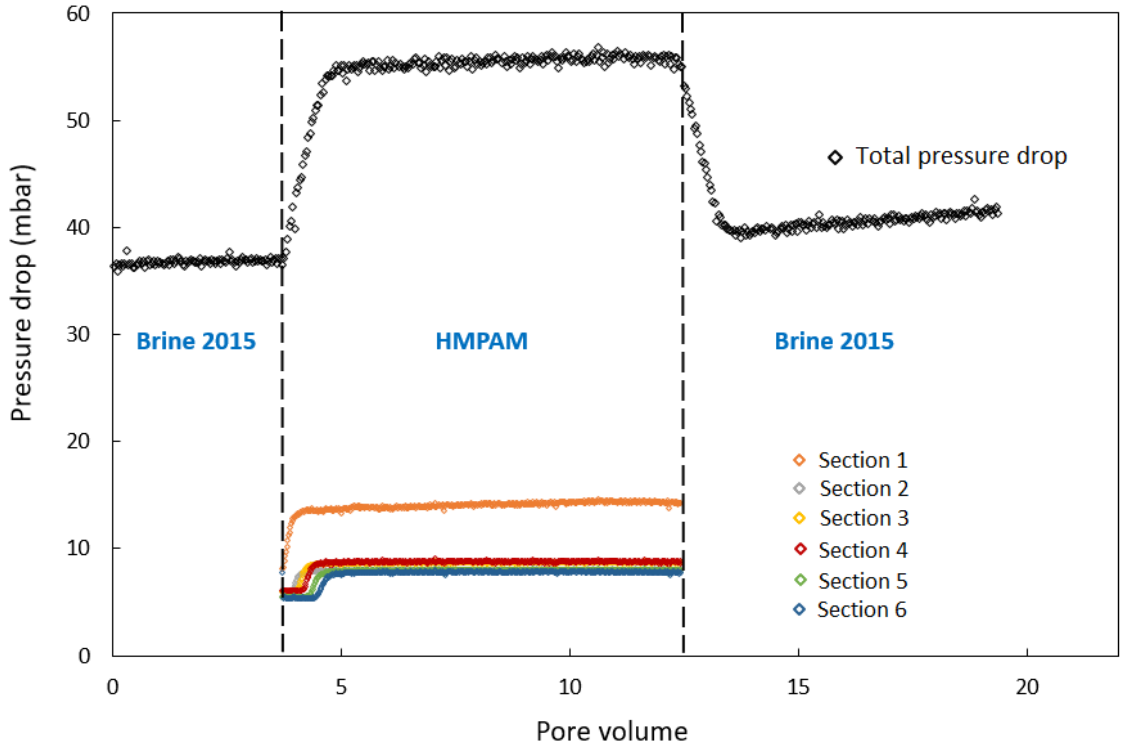

Figure 4.4: Pressure drop profiles for the injection of HMPAM at a high flow rate (Exp. 1b). The experiment was carried out at a flow rate of 2.5 mL/min (equivalent to a superficial velocity of 10 ft/day) with the following sequence: injecting Brine2015 for 3.7 ± 0.1 PV, then injection of HMPAM solution for 8.7 ± 0.1 PV and finishing with Brine2015 injection for 6.9 ± 0.1 PV

Based on the pressure drop profiles measured at both low and high flow rates, as shown in Figures 4.3 and 4.4, values for RF and RRF were estimated. Table 4.3 indicates the observed pressure drop values and the estimated RF and RRF at the end of the injection process. The increase in pressure drop during the HMPAM injection is a result of energy dissipation arising from (a) the interactions between the HMPAM molecules, which manifests as the higher HMPAM viscosity than Brine 2015, and (b) the interaction between the HMPAM molecules and the rock surface, which leads to the irreversible reduction in the rock permeability. As mentioned in **Section 1.2**, RF includes both these effects, while the permeability reduction alone is described by RRF. Therefore, the following equation relates RF to RRF:

$$RF = \frac{\eta_p}{\eta_b} \times RRF \tag{4.1}$$

where η_p and η_b are the polymer and brine viscosities respectively. For the low flow rate injection experiment (Exp. 1a), this equation is in excellent agreement with our

experimental data based on the measured pressure drops (see Table 4.3) and viscosities (see Figure 4.2). The estimated RF value suggests that the mobility of Brine2015 is reduced by 1.7 ± 0.1 times by the HMPAM, which can be beneficial for improving sweep efficiency. The estimated RRF shows that the permeability of the core to Brine2015 is reduced only 1.10 ± 0.1 times. This suggests that the permeability of the porous medium was affected only marginally by the injection of HMPAM solution. Since the high flow rate injection experiment (Exp. 1b) was carried out in the same core used for Exp. 1a, most of the adsorption sites on the rock surface were already occupied with the polymer molecules, and the estimated RF and RRF did not follow Equation 4.1. For Exp. 1b RF was higher than RF for Exp. 1a. RRFs in Exp. 1a and Exp. 1b were comparable.

Table 4.3: The observed pressure drops, and the estimated *RF* and *RRF* for the injection of the primary and secondary Brine2015 and HMPAM at low and high flow rates (Exp. 1a and 1b). Superscript 0 is for the primary injection and 1 is for the secondary injection

Q (mL/min)	ΔP_b^0 (mbar)	ΔP_p (mbar)	ΔP_b^1 (mbar)	RF (-)	RRF (-)
0.25	3.2 ± 0.1	5.6 ± 0.1	3.5 ± 0.1	1.7 ± 0.1	1.10 ± 0.1
2.5	36.9 ± 0.1	55.6 ± 0.1	41.3 ± 0.1	1.5 ± 0.1	1.10 ± 0.1

b) Concentration of the injected HMPAM solution and effluents

The retention of the HMPAM was obtained using the single injection method, as explained in **Section 2.2.3.3**. The normalised concentration (i.e. the ratio of the effluent concentration to the concentration of the injected solution) was plotted as a function of the pore volumes injected. The polymer retention was estimated using Equation 2.7 by reading the pore volumes of the injected tracer and polymer where the normalized concentration is 0.5. The IPV (see Section 2.2.3.2) can be neglected in this study due to the much smaller size of the polymers and nanoparticles as compared to pore throats size (the radius of gyration of the polymer is ~80 nm and nanoparticle radius is 7 nm while more than 85% of pore throats in Bentheimer sandstone have a size larger than 10 μm and only 5% of them are smaller than 5 μm [163]).

As shown in Figure 4.5, the tracer and HMPAM pass through the 0.50 ± 0.05 normalised concentrations at 1.10 ± 0.05 and 2.10 ± 0.05 PV respectively. The retardation of the HMPAM (*R*) is a measure of its retention. Table 4.4 shows the parameters used to calculate the retention of the polymer. The HMPAM retention was estimated to be 63.0

± 0.5 µg HMPAM/g rock. After approximately 3.50 ± 0.05 PV, the normalized concentration of HMPAM levels off to about one.

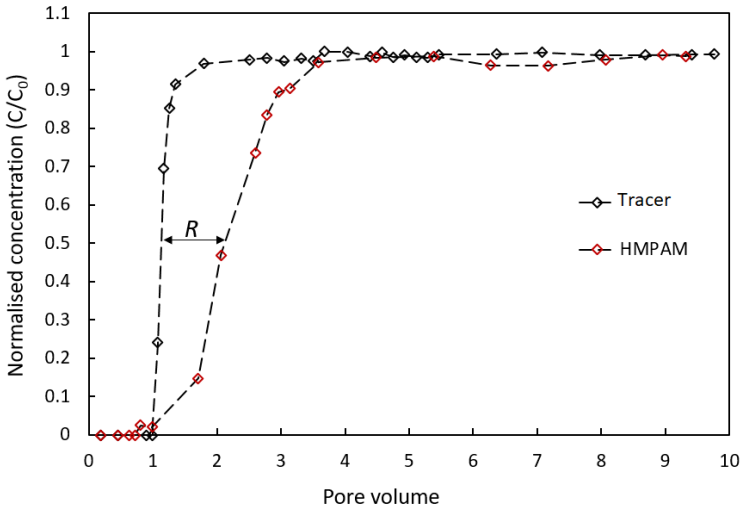

Figure 4.5: Normalised concentrations of tracer and HMPAM as a function of injected pore volumes. The experiment was done at a low flow rate of 0.25 mL/min (equivalent to 1 ft/d)

Table 4.4: Parameters used to calculate the HMPAM retention

ΔPV @ 0.5 $\frac{C}{C_0}$	1.0
Pore volume (mL)	108
Polymer concentration (wt%)	0.05
Mass of sandstone grains (g)	858.8
Adsorbed amount (µg/g rock)	63.0

4.3.2 The flow of NPs through porous media

a) Pressure drops

Exp. 2a was performed at a low flow rate of 0.25 mL/min to investigate the propagation of NPs through porous media. Figure 4.6 shows the pressure drop profiles obtained from this experiment. The steady-state value of the pressure drop for the primary Brine2015 injection was constant at 3.4 ± 0.1 mbar. Then, during the first 9.0 ± 0.1 PV of NPs injection, the pressure drop rose gradually from 3.4 ± 0.1 to 6.3 ± 0.1 mbar. However, the increase in pressure drop was much more dramatic in the final pore volume of injection of NPs, when the value rose to 20.6 ± 0.1 mbar. To interpret this phenomenon, a sample of NPs suspension used in the experiment, as well as the inlet of the core sample, were examined directly after the experiment. Upon careful visual inspection, the dispersion of

NPs was found to be completely transparent and showed no signs of NPs aggregation and sedimentation. A white layer of NPs, however, was observed at the core inlet of the sandstone core. As can be seen in Figure 4.6, the pressure drop in the first section of the core behaves similarly to the total pressure drop, and it also increased significantly in the first section. This indicates a filtration of the NPs at the inlet of the core, which eventually leads to the formation of a filter cake. Upon injection of the secondary Brine2015, the cake of NPs was gradually washed out which resulted in a decrease in the pressure drop.

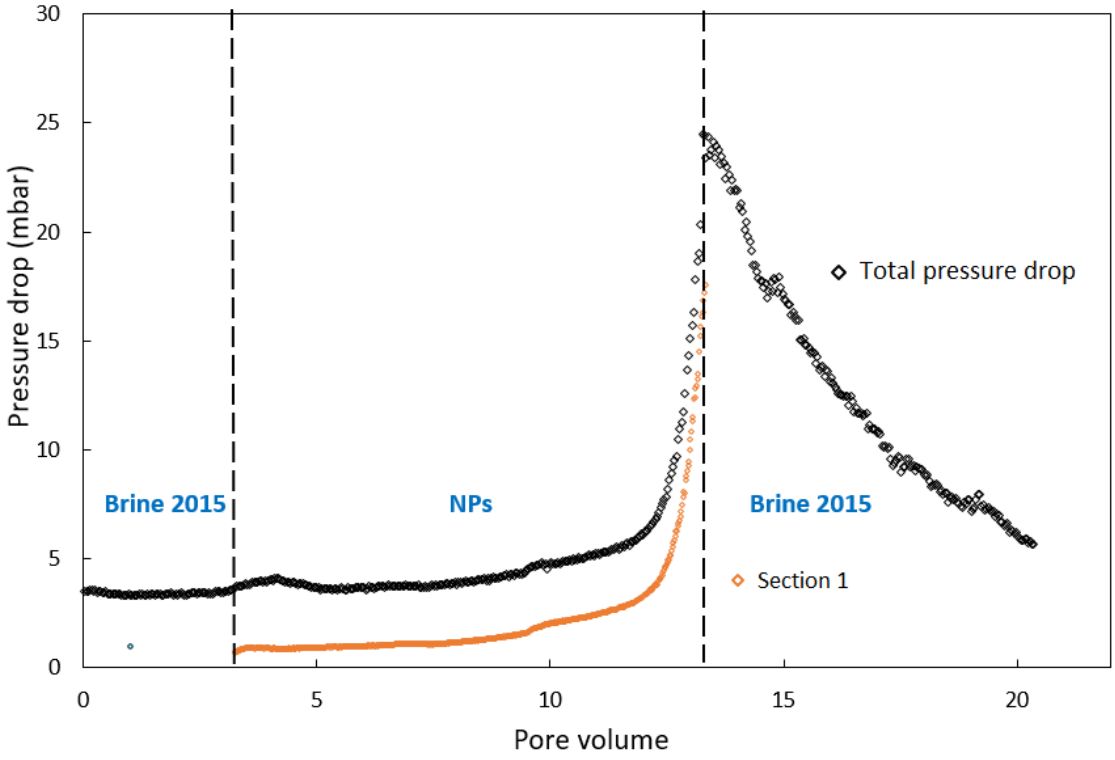

Figure 4.6: Pressure drop profiles of the NPs suspension injection at a low flow rate (Exp. 2a). The experiment was carried out at a flow rate of 0.25 mL/min (equivalent to a superficial velocity of 1 ft/day) with the following sequence: injecting Brine2015 for 3.1 ± 0.1 PV, then injection of NPs dispersion for 10.1 ± 0.1 PV and finishing with Brine2015 injection for 6.2 ± 0.1 PV

Figure 4.7 shows the pressure drop obtained during the high flow rate injection of the NPs suspension (Exp. 2b). The experiment was done at a flow rate of 2.5 mL/min (equivalent to a superficial velocity of 10 ft/day) using the same Bentheimer core as used for Exp. 2a. The pressure drops over the core length and the first section (near the inlet) increased slightly during the NP injection while they remained practically constant for all other sections. The small increase in the pressure drop is most likely due to the filtration of NP aggregates near the core inlet. A remarkable feature of Exp. 2b is that the measured increase in pressure drop and, correspondingly, the retention of NPs, is much smaller than that obtained at the low flow rate (0.25 mL/min) in Exp. 2a. This hints at a strong

competition between the attractive forces responsible for the retention of NPs and the hydrodynamic drag which tends to prevent such retention. Finally, during the injection of secondary Brine2015, the filtered NPs in the inlet were washed out. As a result, the pressure drop first decreased and then levelled off to a plateau value.

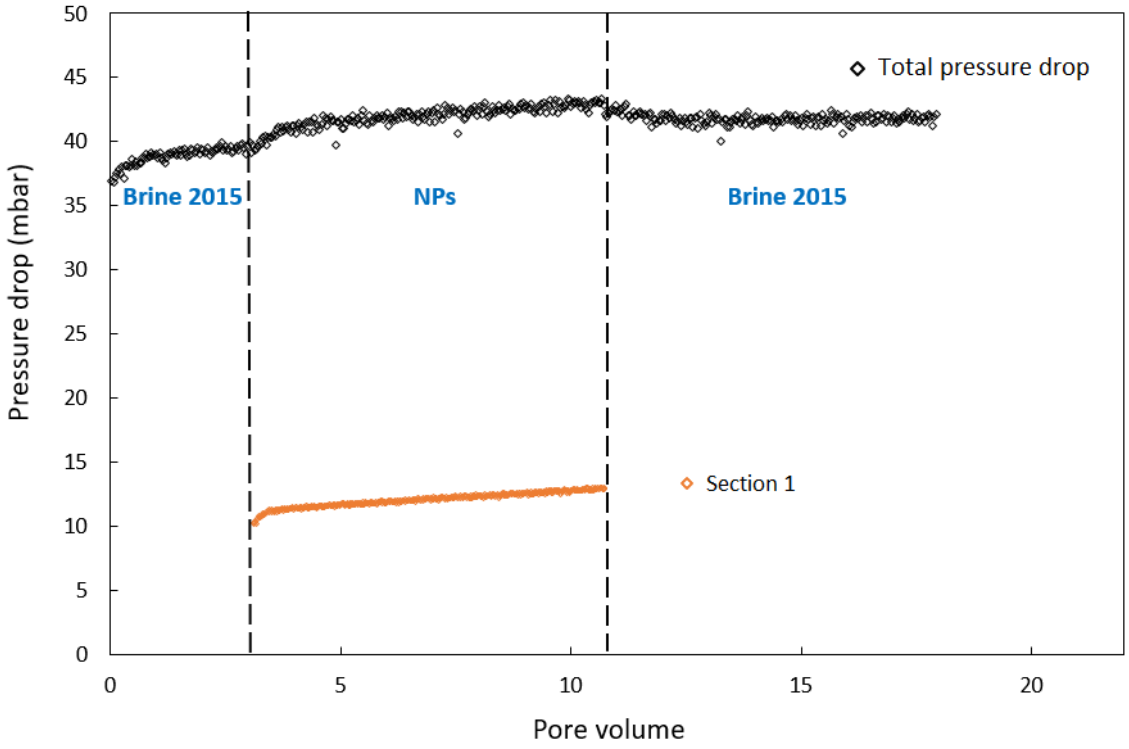

Figure 4.7: Pressure drop profiles during the high flow rate injection of the NPs suspension (Exp. 2b). The experiment was carried out at a flow rate of 2.5 mL/min (equivalent to a superficial velocity of 10 ft/day) with the following sequence: injecting Brine2015 for 2.7 ± 0.1 PV, then injection of NPs suspension for 8.2 ± 0.1 PV and ending with Brine2015 injection for 6.9 ± 0.1 PV

Table 4.5 shows the measured pressure drop values and estimated RF and RRF at the end of the injection of the NPs suspension at the high flow rate (2.5 mL/min). These factors were not investigated for the low flow rate as the pressure drop across the core was increasing rapidly at the end of the injection period. It can be observed that the end-pressure drop values for the injection of NPs suspension and secondary brine were close. This is probably can be due to the small viscosity difference between the NPs suspension and Brine2015 (0.69 ± 0.02 vs. 0.65 ± 0.02 mPa s respectively) and the small reduction in the permeability of the core sample which is also visible from a RRF value close to 1.

Table 4.5: The observed pressure drops and estimated values of *RF* and *RRF* for injection of Brine2015 and NPs suspension in Exp. 2b

Q (mL/min)	ΔP_b^0 (mbar)	ΔP_p (mbar)	ΔP_b^1 (mbar)	RF (-)	RRF (-)
0.25	39.50 ± 0.10	42.90 ± 0.10	41.3 ± 0.10	1.08 ± 0.10	1.06 ± 0.10

b) Concentration of the injected suspension and effluents

As can be seen from Figure 4.8, the tracer passes through the 0.50 ± 0.05 normalised concentration at 1.10 ± 0.05 PV, whereas this happens for the NPs at 1.75 ± 0.05 PV, due to the retardation in the propagation of NPs (*R*'). Between 2–5 PV, the normalised concentration of NPs fluctuated, which means that the NPs concentration at the outlet is not constant. This can be because of temporary log-jamming of the NPs in some pores. After 7 PV, the normalised concentration of NPs stabilized but did not approach the unity because of ongoing NPs filtration at the inlet of the core. A similar methodology used to determine the HMPAM retention was also used to estimate the NPs retention (Equation 2.7). Table 4.6 shows the parameters used for the calculation of the NPs retention in the porous medium. The NPs retention was estimated to be 409.0 ± 0.5 µg NPs/g rock.

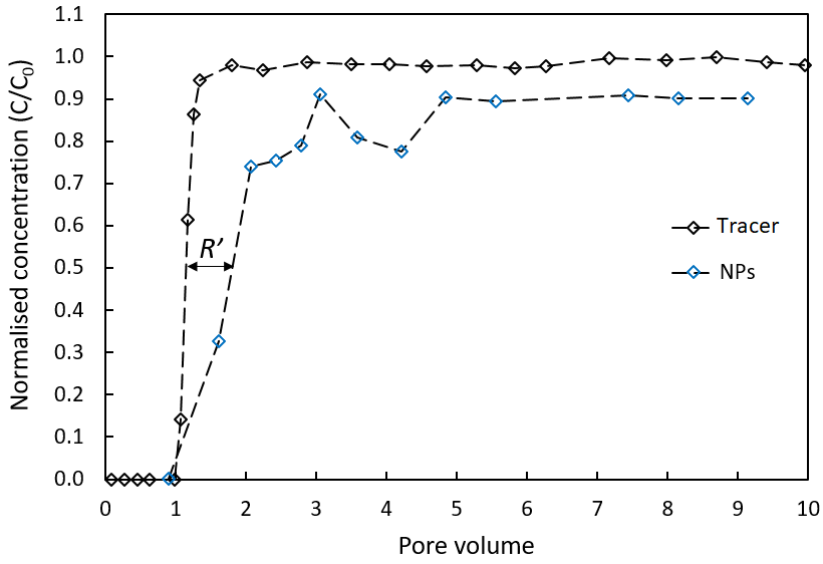

Figure 4.8: Normalised concentrations of tracer and NPs as a function of the injected pore volumes. The experiment was carried out at a low flow rate of 0.25 mL/min (equivalent to 1 ft/d)

Table 4.6: Parameters used to calculate the NPs retention

ΔPV @ 0.5 $\frac{C}{C_0}$	0.65
Pore volume (mL)	108
NPs concentration (wt%)	0.5
Mass of sandstone grains (g)	858.8
Adsorbed amount (µg/g rock)	409.0

4.3.3 The flow of the HMPAM–NPs hybrid through porous media

a) Pressure drops

Exp. 3a was the low flow rate injection of the HMPAM–NPs hybrid. As can be seen in Figure 4.9, the steady-state pressure drop for the primary Brine2015 injection was 3.5 ± 0.1 mbar. During the HMPAM–NPs hybrid injection, the pressure drop increased from the time of the entry of the hybrid into the core up to its breakthrough at the core outlet, at approximately 2.0 ± 0.1 PV. Beyond this injected volume, the pressure drop reached a steady-state value, if the small increase due to mechanical entrapment within the core is discounted. Resuming the Brine2015 injection led to a gradual decrease in the pressure drop, before a stabilization at a plateau value only slightly larger than that for the primary Brine2015 injection. This suggests that the permeability of the core is not significantly affected by flowing the HMPAM–NPs hybrid through the porous medium.

As can be seen in Figure 4.9, the pressure drop profiles in the six different sections of the core suggest a smooth propagation of the HMPAM–NPs hybrid from the injection line through the core to the outlet. Similar to the HMPAM, the pressure drop for each section had a horizontal part which shows the presence of the Brine2015 in that section. In the first section, however, such a horizontal part was very short. As soon as the HMPAM–NPs hybrid entered the core the pressure drop rose in the first section. As the HMPAM–NPs hybrid propagated from one section to another, the pressure drop monotonically increased and levelled off to a plateau value after the breakthrough. It should be noted that there seems to be an interference between the signals of the differential pressure transducers in the fourth and fifth sections. Moreover, the minor fluctuations in the pressure drop profiles can be attributed to the long-running time of the experiment and possible variations in the temperature.

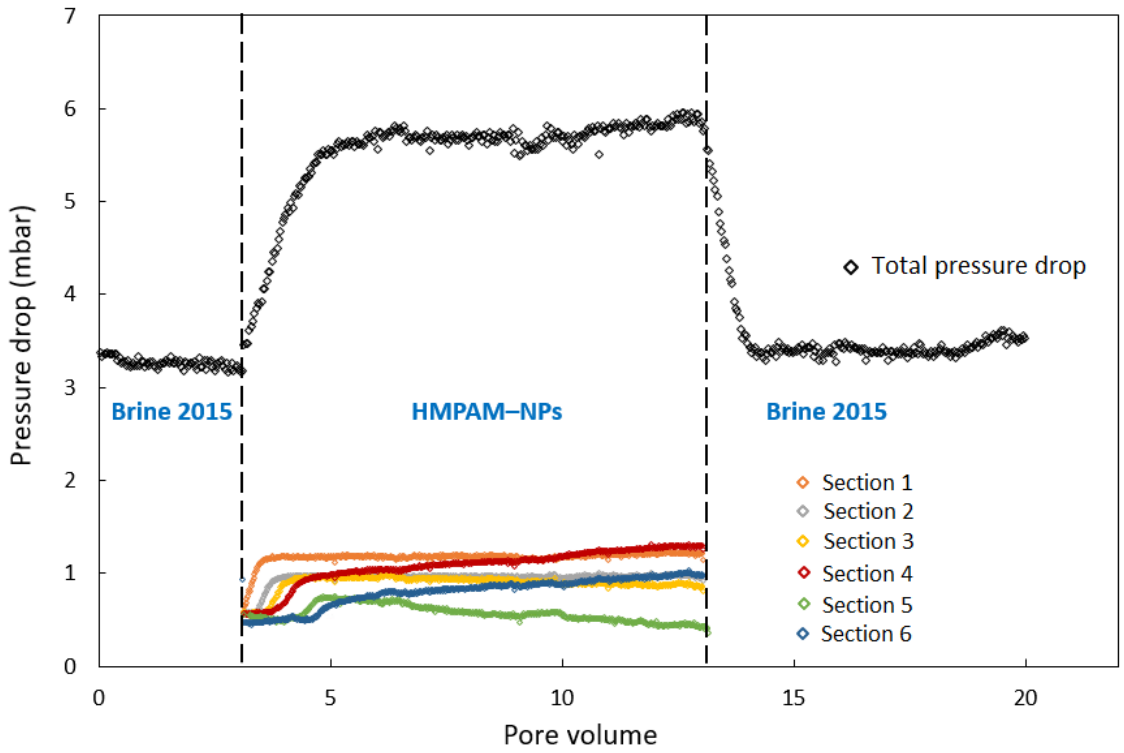

Figure 4.9: Pressure drop profiles during the low flow rate injection of the HMPAM–NPs hybrid (Exp. 3a). The experiment was carried out at a flow rate of 0.25 mL/min (equivalent to a superficial velocity of 1 ft/day). The injection sequence was as follows: primary Brine2015 for 3.0 ± 0.1 PV, HMPAM–NPs hybrid for 9.9 ± 0.1 PV, then the secondary Brine2015 for 7.0 ± 0.1 PV

Upon completion of the low flow rate injection of HMPAM–NPs hybrid, the core was flushed with Brine2015 for at least 10 PV after which the high flow rate injection of the hybrid began (Exp. 3b). Figure 4.10 shows the pressure drop profiles along the full core length and each section as a function of the injected HMPAM–NPs pore volumes. During the primary Brine2015 injection, a steady-state pressure drop value of 37.9 ± 0.1 mbar was observed. During the HMPAM–NPs hybrid injection, the pressure drop first increased continuously with the pore volumes injected. Then, after an injection of 1.5 ± 0.1 PV of the hybrid, the pressure drop reached a steady-state value. This shows that there is an insignificant amount of mechanical entrapment within the core, in addition to a very good injectivity of the HMPAM–NPs hybrid. Similarly, the propagation of the HMPAM–NPs hybrid in each section also experienced a trivial mechanical entrapment. The small differences between the pressure drops for sections 2 through 6 are probably due to small differences in their permeabilities. The higher pressure drop in the first section is due to the higher viscosity of the HMPAM–NPs hybrid as a result of the lower temperature, as explained in **Section 4.3.1**. The secondary injection of Brine2015, resulted in a gradual decrease of the pressure drop, before levelling off to a plateau value only slightly larger

than that for the primary Brine2015 injection. This suggested there was an insignificant reduction in the permeability of the core sample.

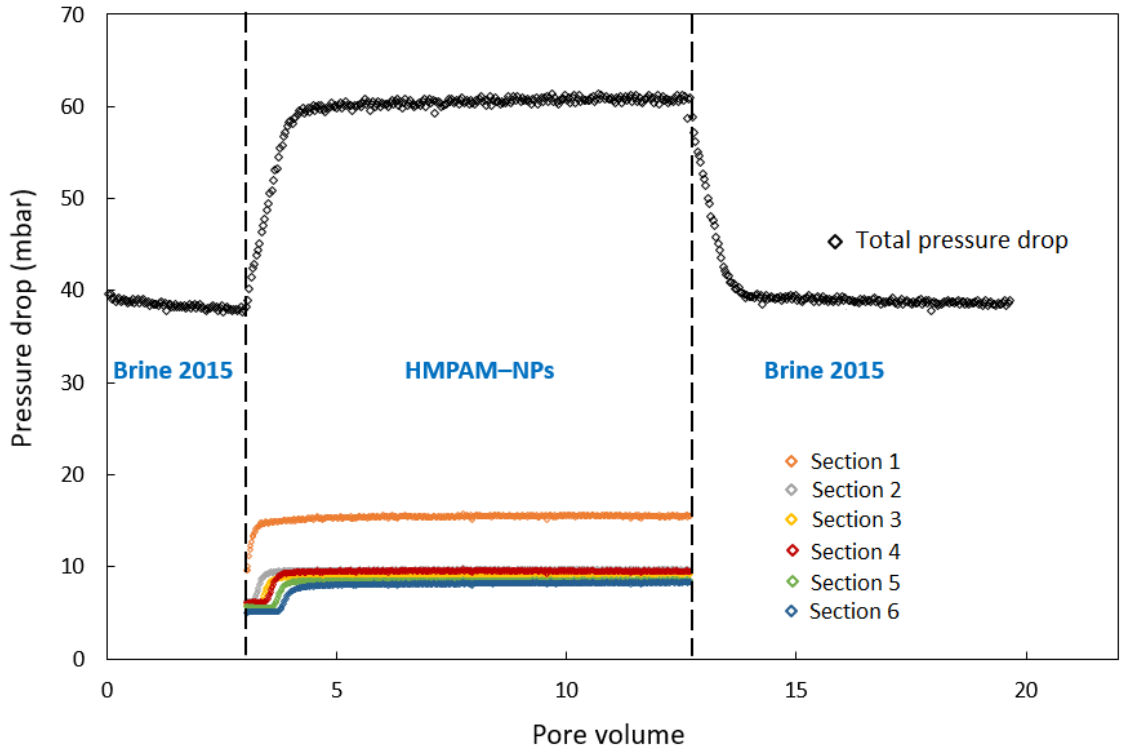

Figure 4.10: Pressure drop profiles during the high flow rate injection of the HMPAM–NPs hybrid (Exp. 3b). The experiment was performed at a flow rate of 2.5 mL/min (equivalent to a superficial velocity of 10 ft/day) with the following sequence: injecting Brine2015 for 2.8 ± 0.1 PV, then injection of HMPAM–NPs hybrid for 9.8 ± 0.1 PV and finally resuming Brine2015 injection for 7.2 ± 0.1 PV

Table 4.7 shows the measured end-pressure drops and estimated RF and RRF values during the flow of the HMPAM–NPs hybrid both at low and high flow rates (Exp. 3a and 3b respectively). For Exp. 3a, RF and RRF were estimated to be 1.8 ± 0.1 and 1.1 ± 0.1 respectively. The estimated RF value suggests that the mobility of the Brine2015 is reduced by 1.8 ± 0.1 times by the presence of the hybrid, which can be advantageous for providing mobility control. The estimated RRF shows that the permeability of the core with Brine2015 is reduced only 1.10 ± 0.1 times. Considering that the viscosities of the HMPAM–NPs hybrid and Brine2015 were 1.10 ± 0.02 and 0.65 ± 0.02 respectively, the model described by Equation 4.1 is in excellent agreement with the estimated RF and RRF based on the measured pressure drops in the experiments. This behaviour of the HMPAM–NPs hybrid is similar to what was observed for the flow of the HMPAM in porous media. The only difference is that the estimated RF for the HMPAM–NPs hybrid is higher than that for HMPAM. This is due to the higher viscosity of the HMPAM–NPs hybrid as compared to the HMPAM. For Exp. 3b, RF and RRF were estimated to be 1.60

± 0.10 and 1.05 ± 0.10 respectively (see Table 4.7). Considering that the core used for Exp. 3b was already used for Exp. 3a, most of the adsorption sites on the rock surface were already occupied with HMPAM and NPs and an RRF close to 1 was expected. The estimated RF for Exp. 3b approximately equal to the viscosity ratio of HMPAM–NPs the Brine2015.

Table 4.7: The observed pressure drops, and the estimated *RF* and *RRF*, for the injection of the primary and secondary Brine2015 and the HMPAM–NPs hybrid at low and high flow rates (Exp. 3a and 3b)

Q (mL/min)	ΔP_b^0 (mbar)	ΔP_p (mbar)	ΔP_b^1 (mbar)	RF (-)	RRF (-)
0.25	3.2 ± 0.1	5.9 ± 0.1	3.5 ± 0.1	1.8 ± 0.1	1.1 ± 0.10
2.5	37.9 ± 0.1	60.8 ± 0.1	38.6 ± 0.1	1.60 ± 0.10	1.05 ± 0.05

b) Concentration of injected dispersion and effluents

The retention of both HMPAM and NPs was investigated during the flow of the HMPAM–NPs hybrid in porous media using the single injection method. Equation 2.7 was used to estimate the retention of the HMPAM and NPs. The IPV was neglected due to fact that the HMPAM and NPs have much smaller size than the pore throats in the Bentheimer core sample (see **Section 4.3.1**) As shown in Figure 4.11, the tracer reached the 0.50 ± 0.05 normalised concentration at 1.10 ± 0.05 PV. In contrast, the HMPAM and NPs passed through the 0.50 ± 0.05 normalised concentration at 2.05 ± 0.05 and 1.7 ± 0.05 PV respectively. The retardation of the HMPAM (*R*) and NPs (*R*'), as compared to the tracer results, gives the difference between the motion of the HMPAM–NPs hybrid and the average motion of the fluid. This retardation decreases the average velocity of the HMPAM–NPs hybrid, to such an extent that these components travel slower than the solvent (and tracer). Table 4.8 shows the parameters used to calculate the retention. The HMPAM and NPs retention were estimated to be 59.8 ± 0.1 µg HMPAM/g rock and 377.6 ± 0.1 µg NPs/g rock respectively. The retention of both HMPAM and NPs through the flow of the HMPAM–NPs hybrid in the porous medium is lower than their retention when they were injected individually. Note also that the normalised concentrations of HMPAM and NPs do not reach unity over 9.9 ± 0.1 PV of the HMPAM–NPs hybrid injection. This is due to the combined effects of filtration, dispersion [159], and the mass transfer between the stagnant and flowing HMPAM–NPs hybrid [10]. Some effect of filtration at the core inlet was also noticed after the end of the experiment.

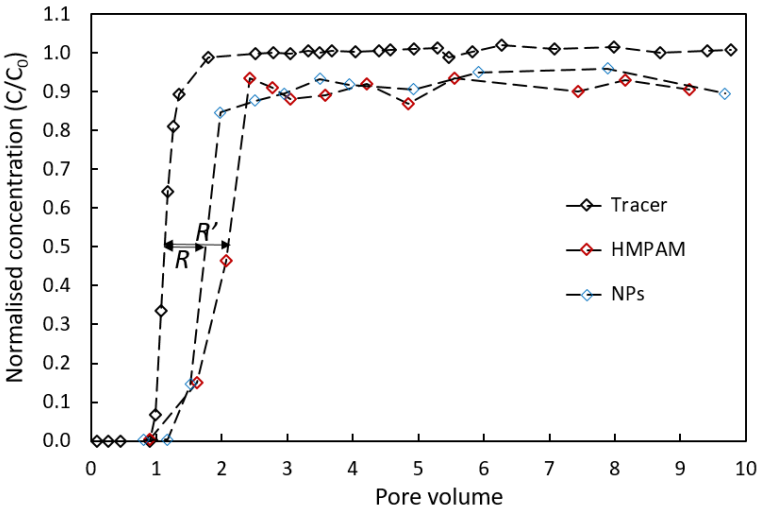

Figure 4.11: Normalised concentrations of the tracer, HMPAM and NPs as a function of injected pore volumes of the HMPAM–NPs hybrid. The experiment was carried out at a low flow rate of 0.25 mL/min (equivalent to 1 ft/d)

Table 4.8: Parameters used to estimate HMPAM and NPs retention during the flow of the HMPAM – NPs hybrid in porous media

ΔPV for HMPAM @ 0.5 $\frac{C}{C_0}$	0.95
ΔPV for NPs @ 0.5 $\frac{C}{C_0}$	0.60
Pore volume (mL)	108
HMPAM concentration (wt%)	0.05
NPs concentration (wt%)	0.5
Mass of sandstone grains (g)	858.8
Adsorbed amount of HMPAM (µg/g rock)	59.8
Adsorbed amount of NPs (µg/g rock)	377.6

4.4 Discussion

The purpose of this chapter was to study the porous media behaviour of a hybrid of hydrophobically modified polyacrylamide and hydrophobically modified silica nanoparticles. This hybrid was being considered as a potential mobility control agent at high salinity and temperature conditions. The proposed mechanism to improve mobility control was to add the NPs to the HMPAM solution to improve its viscosity by increasing the hydrodynamic radius (this was discussed in detail in **Chapter 3)**. The flow characteristics of the HMPAM–NPs hybrid were investigated by (a) performing rheological experiments in a rotational rheometer, (b) observing the pressure drop profiles

in a core-flood and (c) measuring the concentration of the injected solution/suspension and effluents in the core-flood.

In our experiments, the addition of 0.5 wt% NPs to a 0.05 wt% HMPAM solution improved the viscosity by 10%. The flow of the HMPAM solution alone through a porous media showed classic polymer behaviour. When the polymer molecules entered the core, the pressure drop first increased monotonically, and then levelled off to a plateau value. The addition of NPs to the HMPAM solution resulted in a pressure drop response similar to that of HMPAM. However, the plateau value for the HMPAM–NPs hybrid was higher. This was due to the larger flow resistance of the hybrid, consistent with its higher viscosity, as compared to the HMPAM solution.

Moreover, from the concentration profiles (Figure 4.11) is evident that during the flow of the HMPAM–NPs hybrid, the HMPAM and NPs propagate through porous media together. This supports the proposed mechanism that due to hydrophobic–hydrophobic interactions between the HMPAM and NPs, they are transported through the porous medium in unison. As a result, there was no significant retardation between the HMPAM and NPs during their flow in the porous medium. The effect of these hydrophobic–hydrophobic interactions was also advantageous for preventing significant filtration of the NPs. The injection of a NPs suspension at a low flow rate led to a significant increase in the pressure drop due to both external and internal filtration of nanoparticle aggregates (Figure 4.6). However, co-injecting the HMPAM and NPs under similar conditions, prevented the formation of large aggregates and thus no significant filtration was observed (Figure 4.9). As mentioned previously, the co-injection of HMPAM and NPs resulted in their lower retention as compared to when they were injected individually. Rock surfaces have a finite capacity for the adsorption of polymers and NPs [304], so when HMPAM and NPs are co-injected, there are fewer adsorption sites available as compared to when they are injected individually.

4.5 Conclusions

A systematic experimental study was conducted to investigate the porous media flow characteristics of a hybrid of hydrophobically modified polyacrylamide (HMPAM) and hydrophobically modified silica nanoparticles (NPs) at high salinity and high temperature conditions. A series of core-flood experiments was performed at two different superficial velocities of 1 and 10 ft/day to assess the retention and injectivity of the materials. By

comparing the rheological parameters and porous media flow behaviour of the materials, the following conclusions are driven:

- The viscosity of the HMPAM–NPs hybrid was higher than the viscosity of the HMPAM solution.
- The injection of the HMPAM–NPs hybrid into a porous medium led to a higher RF, as compared to that of the HMPAM solution injection, while their RRFs were comparable. Moreover, due to the hydrophobic–hydrophobic interactions between the HMPAM and NPs, they were transported through the porous media in unison.
- Hybridization of the HMPAM and NPs prevented significant external and internal filtration of nanoparticle aggregates and no substantial increase of the pressure drop in the inlet was observed.
- The HMPAM–NPs hybrid showed excellent injectivity, both at low and high superficial velocities. This ensures an easy flow from the near-wellbore region into the reservoir and within the porous medium of the reservoir.
- The Retention of the HMPAM and NPs decreased when they were co-injected. This is due to the availability of fewer adsorption sites on the surface of the rock for HMPAM and NPs when both of them are present in the same solution.
- In comparison with the HMPAM, the higher viscosity and lower retention of HMPAM–NPs hybrid, as well as its excellent injectivity, highlight the potential of the hybrid as a mobility control agent for chemical enhanced oil recovery at high salinity and temperature.

5 FLOW ENHANCEMENT OF WATER-SOLUBLE POLYMERS THROUGH POROUS MEDIA

In **Chapters 3** and **4** a polymer-based chemical for enhanced oil recovery at high salinity and temperature was introduced and its rheological response and porous media flow behaviour was investigated. In this chapter, the focus is on improving the injectivity of water-soluble polymers in porous media. The role of pre-shearing on the flow properties of polymer solutions is investigated. The polymer solutions contained an acrylamide-based copolymer obtained from an emulsified polymer emulsion inverted by a surfactant. The polymer solutions were pre-sheared using three possible methods: (1) a Buddeberg disperser (2) an Ultra-Turrax disperser or (3) a pressure-driven flow through a capillary. Shearing the polymer solution was done under a fast flow to induce high-stretching of the polymer chains, and thus promote the break-up of the longest ones (i.e. bring about a decrease in relaxation time and shear-thinning level). The un-sheared and pre-sheared polymer solutions were forced through sand-packs to compare the corresponding flow resistances. It was observed that the reduction in the viscosity and screen factor of the pre-sheared polymer solutions is path independent, regardless of the shearing device. A critical Weissenberg number (Wi_c~13) was found above which the viscosity of the polymer solutions started to decrease. The resistance factor for the polymer solutions pre-sheared with Ultra-Turrax at an energy input of 31.3 MJ/m^3 and 290.7 MJ/m^3 was nearly 3 and 7 times lower, respectively, than for the un-sheared polymer solution, while the viscosity only decreased by 27% and 48% respectively. The sand-pack experiments were successfully interpreted using a numerical model, taking into account time-dependent retention. The model showed that the flow of the pre-sheared polymer solutions through the sand-packs was mainly enhanced due to the breaking of the longest polymer chains, which results in smaller mechanical entrapment. This pre-shearing of the water-soluble polymers can be used in multiple industrial applications including chemical enhanced oil recovery and optimization of polymer processing.

5.1 Introduction

Long polymer chains can break due to strong flow-induced chain scission. This process can be undesirable in many practical applications including turbulent drag reduction of dilute solutions of high molecular weight polymers [354] or polymer/DNA characterization methods such as high shear rheology in microfluidics [355-357] and gel permeation chromatography (GPC). However, if done in a controlled manner, chain scission can be desirable in other applications. Examples include drug delivery [358,359], lithography [360,361] and chemical enhanced oil recovery (cEOR) [45].

In cEOR applications, polymers are added with the aim of viscosifying the water. Controlled chain scission of polymers (often referred to as controlled pre-shearing) has been used to improve their flow efficiency in porous media i.e. to reduce the flow resistance [8,10,70]. Polymers used in cEOR typically have a large size and are polydisperse, i.e. have a broad molecular weight distribution (MWD) [10]. Long polymer chains offer more flow resistance and tend to block the smallest pores in porous media, which leads to a time-dependent injectivity decline [20-22]. The premise of the controlled pre-shearing is to (a) stretch all the polymer chains and (b) break the longest polymer chains into smaller size chains by strong flow-induced chain scission [362], as will be discussed in more detail below. The latter includes the homolytic scission of valence bonds, which connects the atoms to form the macromolecule [363].

Pre-shearing of polymer solutions in dilute and semi-dilute regimes was investigated by several authors, building upon the work of De Gennes [86] which predicted that random polymers coiled in dilute solutions will be fully extended due to a coil–stretch transition at a critical strain rate ($\dot{\varepsilon}_c$). This strain rate is larger than the rate of relaxation ($\frac{1}{\lambda}$, where λ is the longest relaxation time of the polymer chain). This is equivalent to a Weissenberg number (Wi), defined as the product of strain rate and relaxation time, larger than 1. Theoretical calculation based on the generalized Zimm model [87] and numerical calculation by Larson and Magda [88] indicated that the onset of the coil–stretch transition takes place when $Wi > 0.5$. Later, single molecule experiments (based on DNA visualization) were combined with microfluidic devices to confirm the onset of the coil-stretch transition during flow at $Wi > 0.5$ [89-91]. Odell et al. [141] established that the mid-chain scission occurs due to a continuous increase in stress on the centre of the chain, when the strain rate is larger than a critical strain rate known as a critical fracture ($\dot{\varepsilon}_f$). Since the relaxation time increases with chain length [364], for a polydisperse polymer,

the Wi for the longest chains is larger than for the shortest chains. Hence, the longer chains are more prone to mid-chain scission than the smaller ones. This implies that first, at a certain critical strain rate ($\dot{\varepsilon_{fl}}$), the longer polymer chains are broken and consequently, at a higher critical strain rate ($\dot{\varepsilon_{fs}}$), the shorter chains are broken. It was experimentally shown that mid-chain scission can be induced by an extensional flow field [142,143] as well as by ultrasonic cavitation [144,145]. In contrast, pre-shearing a polymer solution in the semi-dilute regime is concentration dependent [365]. Unlike the dilute regime for which the mid-chain scission occurs, in the semi-dilute regime, the chain scission is increasingly randomized at higher concentrations [153].

Several studies have investigated the rheological properties of sheared polymer solutions [141,153], and their flow behaviour in contractions [365,366]. They found that shearing water-soluble polymers, such as hydrolyzed polyacrylamide (HPAM) and polyethylene oxide (PEO), improved their flow efficiency in contractions. However, the behaviour of pre-sheared polymer solutions in porous media remains poorly understood, which demands a detailed study that links the rheology of pre-sheared water-soluble polymers to their porous media flow characteristics.

In this chapter, the porous media flow enhancement of polymer solutions by controlled pre-shearing is investigated. The polymer solutions contained an acrylamide-based copolymer obtained from an emulsified polymer emulsion that had been inverted by a surfactant. The pre-shearing was achieved using either an agitator (a Buddeberg disperser or an Ultra-Turrax disperser) or pressure-driven flow through capillaries. The process of pre-shearing was performed at various shearing intensities, equivalent to different strain rates. To ensure the reduction of the porous media flow resistance while maintaining the viscosity, the applied strain rates were higher than $\dot{\varepsilon_c}$ and $\dot{\varepsilon_{fl}}$ but smaller than $\dot{\varepsilon_{fs}}$. A detailed rheological analysis was carried out to examine the effect of the pre-shearing on the polymer solutions for each shearing device. The viscosity, screen factor, and imposed energy input by pre-shearing were determined, which allows the dependencies and correlations between the rheological parameters to be studies. Based on the rheological experiments, sand-pack flow experiments were performed. The porous media flow behaviour for differently pre-sheared polymer solutions was studied by observing interdependence between these tests and the rheological experiments. Moreover, a numerical simulation based on a one-dimensional model was carried out, aimed at studying the mechanisms of flow efficiency in porous media.

5.2 Experimental section

5.2.1 Materials

The polymer solution used to conduct the experiments, designated as PS-A, contained essentially an acrylamide-based copolymer. PS-A was obtained from an active emulsion polymer (designated as EP-A) which was inverted by an active inverter surfactant (designated as IS-A). PS-A contained 0.4 wt% EP-A and 0.24 wt% IS-A (1 wt% ~ 10,000 ppm). The molecular weight of the polymer was estimated at around 2.5×10^6 g/mol (see Section 4 in **Appendix B**). The solvent was synthetic seawater SSW-A having total dissolved solids (TDS) of approximately 5 wt%. The exact composition of SSW-A is given in Table 5.1. Details of a typical inverse polymerization used to synthesize acrylamide-based polymers is described elsewhere [367,368]. Here, only the important aspects are highlighted and the focus is on the role of pre-shearing on the flow response of polymer solutions. PS-A was prepared by first adding IS-A to SSW-A, followed by the addition of EP-A under continuous mixing with a magnetic stirrer set to 600 revolutions per minute (rpm) at room temperature. The polymer system was fully inverted by a few minutes of gentle stirring. To make sure that all the polymer chains were released, the solution was stirred for an additional 45 min. During the stirring with the magnetic stirrer, no viscosity loss occurred, as confirmed by measuring the viscosity at different stirring times. The polymer solution resulting from this process is referred to as the un-sheared polymer solution. The critical overlap concentration of the polymer was found to be 0.40 ± 0.01 wt% (see Figure B.3, **Appendix B**). This indicates that the selected concentration of polymer in PS-A is close to the overlap concentration.

Table 5.1: The synthetic Seawater SSW-A composition with ~ 5 wt% TDS (1 wt% ~ 10,000 ppm)

Component	Na^+	K^+	Mg^{2+}	Ca^{2+}	Sr^{2+}	Cl^-	$SO4^{2-}$	$HCO3^-$	TDS
Concentration (ppm)	15,121	511	1,928	649	3	27,771	3,700	153	49,836

5.2.2 Polymer pre-shearing

Polymer solutions obtained as described above were pre-sheared using three different shearing devices. Two agitators were used, namely, a Buddeberg DS5 disperser (hereafter referred to as Buddeberg), and an Ultra-Turrax S25 N-18G disperser (hereafter referred to as Ultra-Turrax) to shear the polymer solution at various intensities The polymer

solution was sheared by Buddeberg by using a toothed circular disk stirrer, and by Ultra-Turrax by forcing the solution through the gaps of the rotating rotor in the shear gap between the rotor and stator. In the third shearing method, the polymer solution was forced through a capillary die. The capillary die was made up of a steel cylinder, having 300 mL volume, together with an attached capillary tube. The inner diameter of the capillary was 1 mm and the length varied from 3, 10 to 20 cm. At the top of the cylinder, pressures between 1 to 20 bar were applied using compressed air. 250 mL of the inverted polymer solution was filled in the cylinder and forced through the capillary at a constant pressure drop. At the capillary exit, the extruded polymer solution was collected in a beaker positioned on a weighing scale to estimate the volumetric flow.

A summary of the pre-shearing techniques is given in Table 5.2, showing the polymer solutions at the different shearing intensities for the Buddeberg and Ultra-Turrax or the different applied pressures for the capillary. These shearing intensities were then translated to volume specific energy input and Weissenberg number (see Sections 2 and 3 in **Appendix B** for details of strain rate calculations). As mentioned, pre-shearing the polymer solution promotes stretching of the polymer chains (equivalent to increasing Wi, see Figure 5.1a) and breaking of the longest ones. In literature, the latter is attributed to the breaking of the high molecular weight fragments of MWD into lower molecular weight fragments, resulting in a narrower MWD (see Figure 5.1b) [362,369].

Table 5.2: The shearing intensities or applied pressures for each shearing device

Shearing device	Shearing intensity (rotational speed or pressure drop)	Shearing duration or length of the capillary
Buddeberg	500, 750, 1000, 1250, 1500 and 1750 rpm	30 and 60 min
Ultra-Turrax	5,000, 10,000, and 20,000 rpm	1, 3.25, 5, 7.75, and 10 min
Capillary	1, 2, 3, 4, 5, 10, and 20 bar	3, 10 and 20 cm

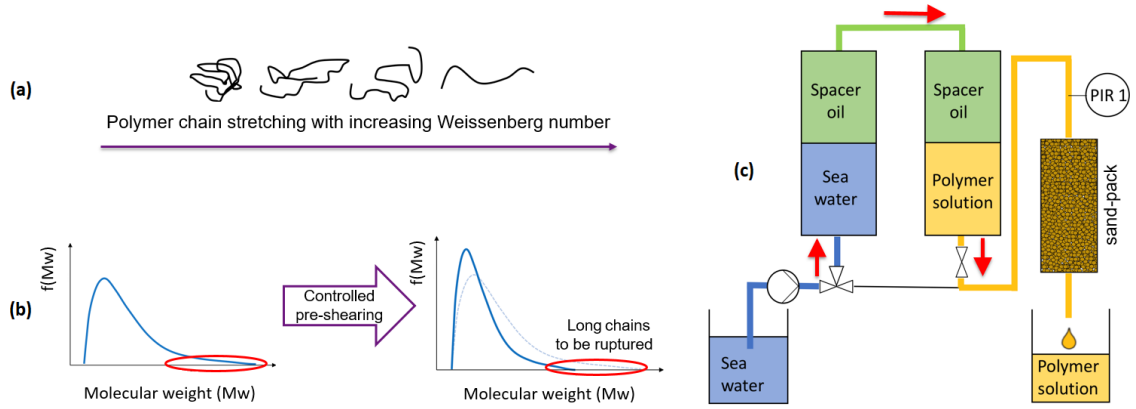

Figure 5.1: a) Stretching a polymer chain by increasing the Weissenberg number (*Wi*). At Weissenberg numbers higher than 1 the polymer is fully extended due to the coil–stretch transition. (b) Breaking the high-end fragments of the polymer MWD by controlled pre-shearing. The red ellipse highlights the longest chains which have a higher potential to be ruptured. In the molecular weight distribution on the right-hand side, the dashed line represents the original MWD and the solid line represents the MWD for the pre-sheared polymer. (c) Schematic of the flow of the pre-sheared polymer solution through a sand-pack. SSW-A is either directly forced into the sand-pack or is pumped into the first equalizing tank where the spacer oil stays on top. Thereafter, the spacer oil moves to the second equalizing tank and pushes the polymer solution into the sand-pack

5.2.3 Rheological measurements

To study the role of the pre-shearing devices on the flow properties of the polymer solutions, a rheological analysis of the polymer solutions (before and after pre-shearing) was performed. The viscosity of the polymer solutions (η) was determined by an Ubbelohde viscometer (type number 501 13 Ic). The screen factor (SF), which is a measure of the extensional viscosity from stretched to the coiled state, was determined in a screen viscometer [370]. The screen factor is defined as the ratio of the time that a certain volume of the polymer solution needs to pass through five 100-mesh screens to the flow time for the same volume of the solvent through the screens [70]. SF measurement has typically been employed to determine whether mechanical degradation of a polymer solution has occurred during a process [10]. The viscosity of the un-sheared polymer solution (η_0) was found to be 12.5 ± 0.6 mPa s and its screen factor (SF_0) was 19.0 ± 0.9.

The viscosity of the polymer solutions as a function of shear rate was measured using a commercial rheometer (MCR-302, Anton Paar GmbH) in a Couette cell (cup ID = 28.92 mm, bob OD = 26.66 mm, gap = 1.18 mm). To study the shear-thinning behaviour of the polymer solutions, the Carreau–Yasuda model [334] as shown below was used:

$$\eta - \eta_\infty = (\eta_i - \eta_\infty)[1 + (\dot{\gamma}\lambda)^a]^{\frac{n-1}{a}} \quad (5.1)$$

where η is the shear dependent polymer viscosity, η_∞ is assumed to be the solvent viscosity, η_i is the zero shear rate viscosity, $\dot{\gamma}$ is the shear rate and λ is the relaxation time which is the inverse of a critical shear rate where the transition from Newtonian to shear-thinning occurs. Here, the parameter n is the power-law exponent. It is obtained from the shear-thinning part of the viscosity response curve and gives information about the width of the transition region from Newtonian to shear-thinning.

The dynamic viscoelasticity of the polymer solutions was examined to elucidate their viscoelastic response. The amplitude sweep was performed and the storage and loss moduli were measured as a function of strain. All the rheological measurements in this study were performed at 30 ℃.

5.2.4 Sand-Pack flow experiments

A sand-pack was used as the model porous medium: 20.0 ± 0.1 g of quartz sand (99% pure quartz with trace quantities of iron oxide) having grain sizes smaller than 125 µm was packed in a cylindrical cell with inner diameter and length of 1.52 and 7.50 cm respectively. A 30 µm square mesh filter and a coarser filter were mounted at the bottom of the sand cell. The pore volume (PV) and porosity of the sand-pack were calculated to be 6.5 ± 0.1 cm^3 and 46 ± 1% respectively. Before the flow test, the air was evacuated from the sand-pack cell, and the cell then flushed with SSW-A for 10 min.

Figure 5.1c shows the schematic of the sand-pack flow set-up. A pressure sensor type A-10 from WIKA with a measurement range of 0 to 4 bar and an accuracy of 0.5% was installed on top of the sand-pack cell. SSW-A was pumped either directly into the sand-pack or into an equalizing tank initially filled with a spacer-oil. The spacer oil then displaces the polymer solution in the polymer tank. This causes the polymer solution to flow to the sand-pack cell without a need to be directly pumped. By doing this, it is ensured that any mechanical degradation of the polymer solution caused by pumping is minimised.

5.2.5 Sand-pack flow experimental procedure

The procedure for the sand-pack flow tests is shown in Table 5.3. The sand-pack was flushed with SSW-A for 30 min at 3 mL/min, which is equivalent to 14.0 ± 0.5 pore volumes (PV), to ensure 100% saturation of the sand-pack with SSW-A. After that, the permeability test was performed and the permeability of the sand-pack cell was determined to be 1,000 ± 20 mD. Next, the flow rate was switched to 0.5 mL/min and the

injection continued for another 30 min (equivalent to 2.0 ± 0.5 PV) followed by the polymer injection. The polymer solution was injected for 30.0 ± 0.5 PV. The resistance factor RF (defined as the ratio of the pressure drop for polymer solution to the pressure drop for the primary SSW-A) was recorded for the whole injection cycle to assess the flow resistance of the polymer solutions (see Section 1 in **Appendix B** for more details on RF).

Table 5.3: Overview of sand-pack flow experimental procedure

Sequence	Injected fluid	Injection rate (mL/min)	Injection time (min)	Number of injected pore volumes
1	Synthetic seawater SSW-A	3	30	~14
2	Synthetic seawater SSW-A	0.5	30	~2
3	Polymer solution PS-A	0.5	Overnight	~30

5.2.6 Numerical simulation of sand-pack flow

The polymer flow efficiency in the sand-packs was also investigated by solving numerically the one-dimensional model for polymer flow in porous media introduced by Yerramilli et al. [371]. The model accounts for the time-dependent polymer retention in addition to advection, dispersion, filtration, and static adsorption. A custom-made MATLAB code was used to solve the equations. The details and equations used in the model can be found in the above reference. Figure B.6 in **Appendix B** represents the workflow used for the simulation. Here, only the key features of the model are presented.

5.2.6.1 Polymer response to pre-shearing

The effect of pre-shearing the polymer chains was modelled using the conceptual model introduced by Sorbie and Roberts [369] which is based on a discrete multi-component representation of the polymer MWD. The model assumes that during pre-shearing, the MWD changes, as the higher components degrade into lower molecular weight fragments. Therefore, the average molecular weight ($\overline{Mw}$) of the polymers shifts to the left (i.e. lower molecular weight) while the amount of polymers corresponded to the average molecular weight ($\bar{C}$) shifts upward (i.e., increase in the amount). Sorbie and Roberts [369] proposed the following equations to model the change in MWD because of pre-shearing:

$$\overline{[\eta]} = A(\overline{Mw})^b \tag{5.2}$$

$$\bar{\eta} = \eta_s \overline{[\eta]} \bar{C} \tag{5.3}$$

where $\bar{\eta}$ and $\overline{[\eta]}$ are the average polymer viscosity and intrinsic viscosity respectively, and b and A are equal to 0.87 and 2.6 × 10^{-7}, respectively, gives $\overline{[\eta]}$ in ppm^{-1} and $\bar{C}$ in ppm [369]. For the un-sheared polymer solution, $\overline{Mw}$ used in the model was obtained using the methodology explained in Section 4 in **Appendix B** and $\overline{[\eta]}$ and $\bar{C}$ could then be calculated using Equations 5.2 and 5.3 respectively. For the pre-sheared polymer solutions, the average polymer viscosity is already known from the experiments and $\overline{Mw}$ and $\bar{C}$ are used as the matching parameters according to Equations 5.2 and 5.3, to obtain the same value of viscosity. The change in $\overline{Mw}$ and $\bar{C}$ is based on the trend explained above (i.e. decrease in $\overline{Mw}$ and an increase in $\bar{C}$ with increasing energy input). As a result, for each shearing condition the relevant values of $\overline{Mw}$ and $\overline{[\eta]}$ are input into the model.

5.2.6.2 Polymer viscosity model

The dependence of the polymer viscosity on concentration was modelled using the modified Flory–Huggins equation described by Equation 5.4 [371]:

$$\eta_i = \eta_s \left[1 + \left(a_1 c_p + a_1 c_p^2 + a_1 c_p^3\right) S_s\right]^m \tag{5.4}$$

where a_1, a_2 and a_3 are the polymer viscosity fitting parameters, which vary with the salinity of the solvent (S_s), and m is the slope of a log-log plot of (η_i- η_s)/ η_s versus S_s for a given energy input. Considering the viscosity values found from the experiments, the matching parameters for each shearing condition are obtained, and these can be seen in Table B.2 in **Appendix B**.

5.2.6.3 Time-dependent reduction of the pore throat radius

To capture the time-dependent pressure behaviour observed for the un-sheared model, a simple model is proposed where the pore throat radius decreases with time. Physically this is equivalent to the formation of an impermeable polymer adsorption layer on the pore walls with a thickness that grows over time. The growth rate of the polymer layer thickness depends on the characteristic size of the polymer molecules in the solution and thus also on the molecular weight. The model considers that the pore throat radius reduces with the injection of many pore volumes of the polymer solutions. In this simple model, the polymer retention, as a result of adsorption and mechanical entrapment, increases continuously rather than levelling off to an equilibrium value.

5.3 Results and discussion

5.3.1 Rheological response of pre-sheared polymer chains

To understand the impact of pre-shearing on the polymer performance, the viscosity and screen factor were measured for polymer solutions sheared by Buddeberg, Ultra-Turrax, or the capillary die with different shearing intensities (see Table 5.2 for details of the shearing conditions for each device). The viscosities were measured with an Ubbelohde viscometer and were converted to the zero shear rate viscosity using the correlation explained in Section 7 of **Appendix B**. Figures 5.2a-b show the viscosity and screen factor of Buddeberg sheared PS-A as a function of rotational speed. It was observed that shearing the PS-A for both 30 min and 60 min leads to comparable viscosities and screen factors. This suggests that doubling the shearing time, at these long time scales, had no significant impact on the viscosity reduction. Shearing the polymer solution at a rotational speed of 500 rpm hardly influenced the screen factor suggesting that the applied strain rate is too small to break the polymer chains. However, from this rotational speed upwards, the screen factor continuously decreased. It was found that at 1,750 rpm, the screen factor was reduced by 36%. Furthermore, the viscosity was not substantially affected by the shearing irrespective of the rotational speed and it decreased only by 7% after 30 min at 1,750 rpm. The significant difference between the change in the screen factor and the change in the viscosity indicates that Buddeberg ruptures the high-end fragments of MWD without significantly rupturing the shorter chains.

Figures 5.2c-d show that for Ultra-Turrax sheared PS-A at a rotational speed of 5,000 rpm, the screen factor dropped by 29% whereas the viscosity decreased only by 11%. This is identical to what was observed for Buddeberg (i.e. rupturing the high-end fragments of MWD only). However, increasing the rotational speed to 10,000, and 20,000 rpm had a much more significant effect on the viscosity and screen factor; the viscosity decreased by 35% and 50% respectively and screen factor dropped by 51% and 71% respectively. It can thus be inferred that shearing the polymer solution at rotational speeds larger than 5,000 rpm results in a strain rate higher than $\dot{\varepsilon_{fs}}$, which decreases the viscosity more significantly. Moreover, for each rotational speed, the screen factors asymptotically tend to a final value meaning that after some point the shearing time no longer affects the screen factor. This is consistent with the experimental observations for Buddeberg, where shearing the polymer solution for an additional 30 min had little effect on the screen factor.

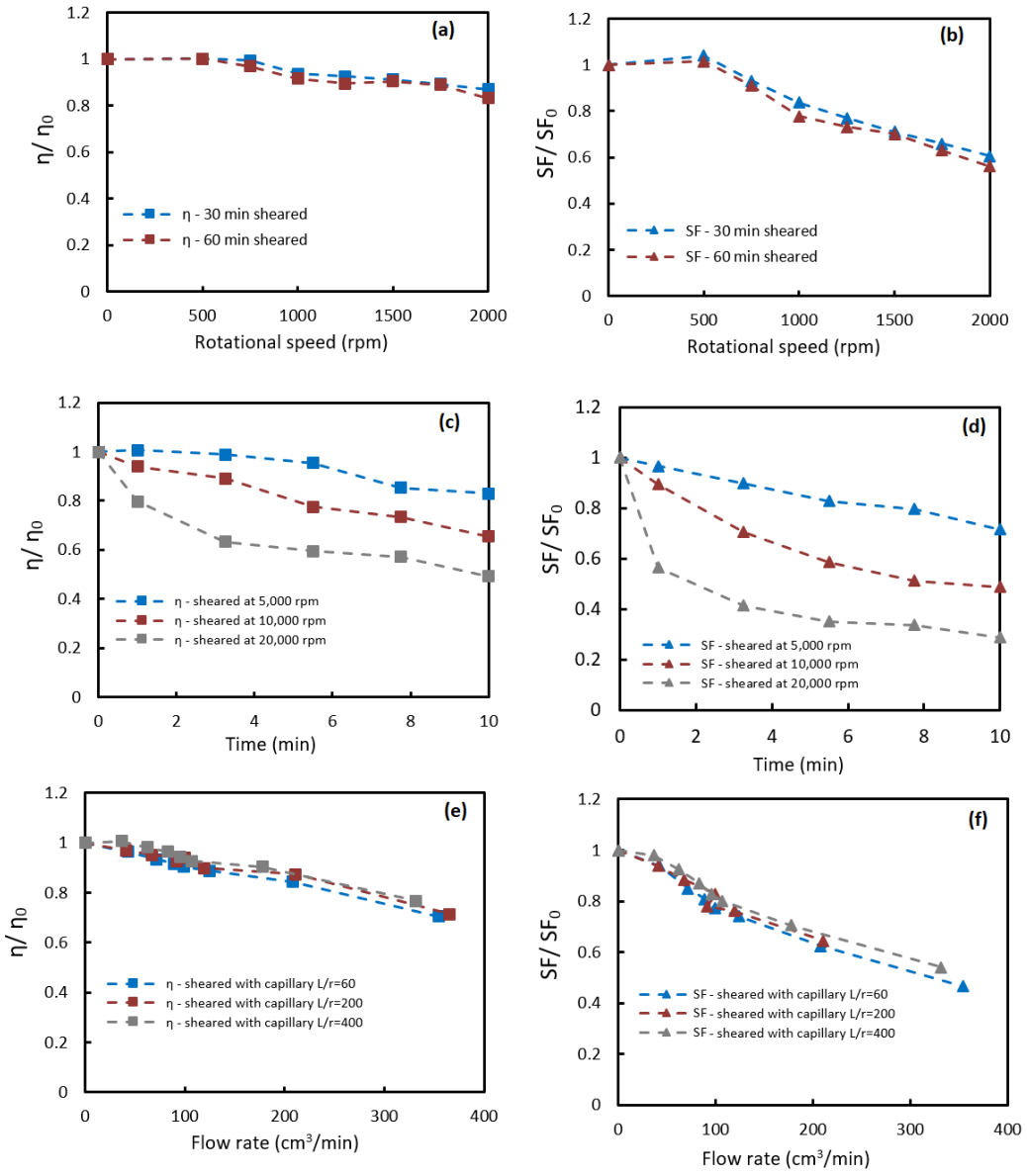

Figure 5.2: Impact of the pre-shearing on the viscosity and screen factor of the polymer solutions. For Buddeberg: (a) the normalized viscosity and (b) the normalized screen factor as a function of rotational speed after 30 and 60 min of shearing. For Ultra-Turrax: (c) the normalized viscosity and (d) the normalized screen factor as a function of shearing time at a rotational speed of 5,000, 10,000, and 20,000 rpm. For the capillaries: (e) the normalized viscosity and (f) the normalized screen factor as a function of flow rate for *L*/r ratios of 60, 200 and 400

For the capillary sheared polymer solutions, the viscosity and screen factor were measured for capillaries with different lengths at various pressure drops (see Table 5.2). The total pressure drop across a capillary die is a summation of three contributions: entry pressure drop, end pressure drop, and the pressure drop due to the friction of the polymer solution with the wall over the length of the capillary. The entry and end pressure drops are nearly equal for the different lengths while the frictional pressure drop increases with the capillary length. Therefore, for a certain pressure drop, the degradation is higher in shorter capillaries. To investigate the change in viscosity and screen factor as a function

of flow rate in capillaries, the pressure drops were translated to equivalent flow rates using the Poiseuille equation. As can be seen in Figures 5.2e-f, the viscosity and screen factor decreased with increasing flow rate. This decrease was more pronounced in the shortest capillary (L/r =60) where the observed viscosity and screen factor losses were 30% and 52% respectively.

The deformation and breaking of the polymer chains is dependent on the type of flow and the chemistry of the polymer [372]. The nature of the flow field created by these shearing devices is complex and differs from one device to another. Using shearing devices with a region of strong extensional flow such as Buddeberg and Ultra-Turrax, the chains may be completely stretched before breaking in their centre [365]. In the flow through the capillaries, however, a large proportion of the chains experience the extensional flow field and rupture before they are fully stretched (this has been reported for polyacrylamide in the turbulent flow and dilute regime [366,373] which is identical to the condition of our experiments). Moreover, the residence time for flow in the capillary die was shorter than for the flow in Buddeberg and Ultra-Turrax.

To gain a more detailed insight on how the polymer chains are deformed as a result of pre-shearing, the normalized viscosity is plotted as a function of Wi (see Figure 5.3). Note that the viscosity data reported in Figure 5.3 for the polymer solution pre-sheared by Ultra-Turrax, are for samples sheared for 7.75 min at rotational speeds of 5,000, 10,000, or 20,000 rpm. The relaxation time used for the calculation of Wi is obtained from the Carreau–Yasuda model (see Figure 5.5).

The minimum calculated Wi, for the polymer chains sheared by three shearing devices, was 6 ± 1. This suggests that a coil–stretch transition has occurred even at the lowest rotational speed of the agitators and the lowest flow rate of the capillary. The viscosity of the polymer solutions remained un-changed up to a critical Weissenberg number (Wi_c~13). Then beyond this value, it decreased according to a logarithmic function of Wi. The data in Figure 5.3 indicates that the polymer pre-shearing is path independent, i.e. the viscosity decreases in the same way regardless of the shearing device used for pre-shearing. Moreover, it can be inferred that the rate of viscosity reduction becomes slower at higher Wi (> 60 ± 1). This suggests that once a certain stress is applied to the polymer, the longer polymer chains (higher-end fragments of MWD) are ruptured first. To rupture the smaller polymer chains (lower-end fragments of MWD), a higher Wi is needed. This is in good agreement with the observation of Odell et al. [141,374] where the critical strain

rate to rupture the polymer chains scales with $1/Mw^2$. The Mw for the pre-shared polymer solutions was measured and plotted as a function of Wi (see Figure B.4, **Appendix B**). The fact that Mw decreases only at Weissenberg numbers higher than Wi_c indicates the rupture of the longest chains at high strain rates. The effect of shearing time on the reduction of the molecular weight for polymer solutions sheared with Ultra-Turrax was investigated (see Figure B.5, **Appendix B**). It was found that for a certain strain rate there is a critical Mw below which there is no reduction in viscosity. This means that the reduction of Mw as a function of shearing time evolves towards a plateau value corresponding to the critical Mw (Mw_c). Below Mw_c, polymer chains can no longer be broken irrespective of the duration of pre-shearing. The value of Wi_c obtained from our study is in good agreement with that obtained by Garrepally et al. [366] who found Wi_c for sheared polymers in the range of 11 to 22 depending on the Mw.

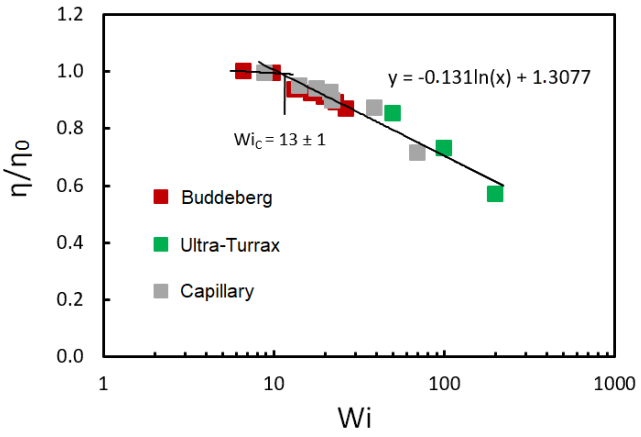

Figure 5.3: The normalized viscosity versus Weissenberg number. Red, green, and grey data points represent the Buddeberg, Ultra-Turrax, and capillary respectively

An important remark should be made concerning the calculation of the Weissenberg number. Wi can be used for both shear flow and extensional flow [375]. For the former, the Weissenberg number is defined as $Wi = \dot{\gamma}\lambda$ and for the latter, it is defined as $Wi = \dot{\varepsilon}\lambda$. The geometries used in this study combine shear and extensional flows. For these types of flow, it is generally accepted that a one-to-one relationship between strain rate and shear rate exists [376-378]; however, the exact form of such relationship may differ from one geometry to another. The Weissenberg number was calculated using $Wi = \dot{\varepsilon}\lambda$ for the capillary die. The Weissenberg numbers for Buddeberg and Ultra-Turrax, however, were calculated using $Wi = \dot{\gamma}\lambda$ as the available analytical expressions only allowed us to convert the rotational speed of these shearing devices to shear rate.

5.3.2 Effect of stored energy

The impact of pre-shearing on the performance of the polymer solution was further examined by calculating the energy input into the polymer chains. The calculation was based on the shearing intensity, and was used to reconcile the differences between flow types in the shearing devices. In this approach, the friction and consequent chain stretching and rupturing are not attributed to the strain experienced by the polymer. They are rather related to the total accumulated strain, corresponding to the total energy stored [365]. Degradation results from the energy accumulation during the stretching process which is correlated with the energy dissipated by the shearing devices [372,379].

The superimposed volume specific energy input by the agitators can be determined by turbine-power correlations, which is expressed by a power number (N_p) versus Reynolds number for agitators (R_e). For this, the power input (P_N) can be determined as follows [380]:

$$P_N = N_p \cdot \rho \cdot n_r^3 \cdot d_i^5 \tag{5.5}$$

where ρ is the fluid density, n_r the rotational speed, and d_i is the diameter of the agitator. The value of N_p is found from the power number-Reynolds number relationship, which is known for many agitators, and R_e is calculated by Equation 5.6 [381]:

$$R_e = \frac{\rho \cdot n_r \cdot d_i^2}{\eta} \tag{5.6}$$

The imposed volume specific energy input (E_v) on the polymer solution can then be determined using Equation 5.7:

$$E_v = \frac{P_N \cdot t}{V} \tag{5.7}$$

where t is the stirring time, and V is the stirred volume. A more detailed explanation of the calculation of the volume specific energy input is given in Section 2 of **Appendix B**.

As shown in Figures 5.4a-b, two master curves could be established between the viscosity/ screen factor and the volume specific energy input independent of the shearing device. Both the viscosity and the screen factor decrease as the energy input increases. The viscosity decreases as a power-law function and the screen factor decreases as a logarithmic function of energy input.

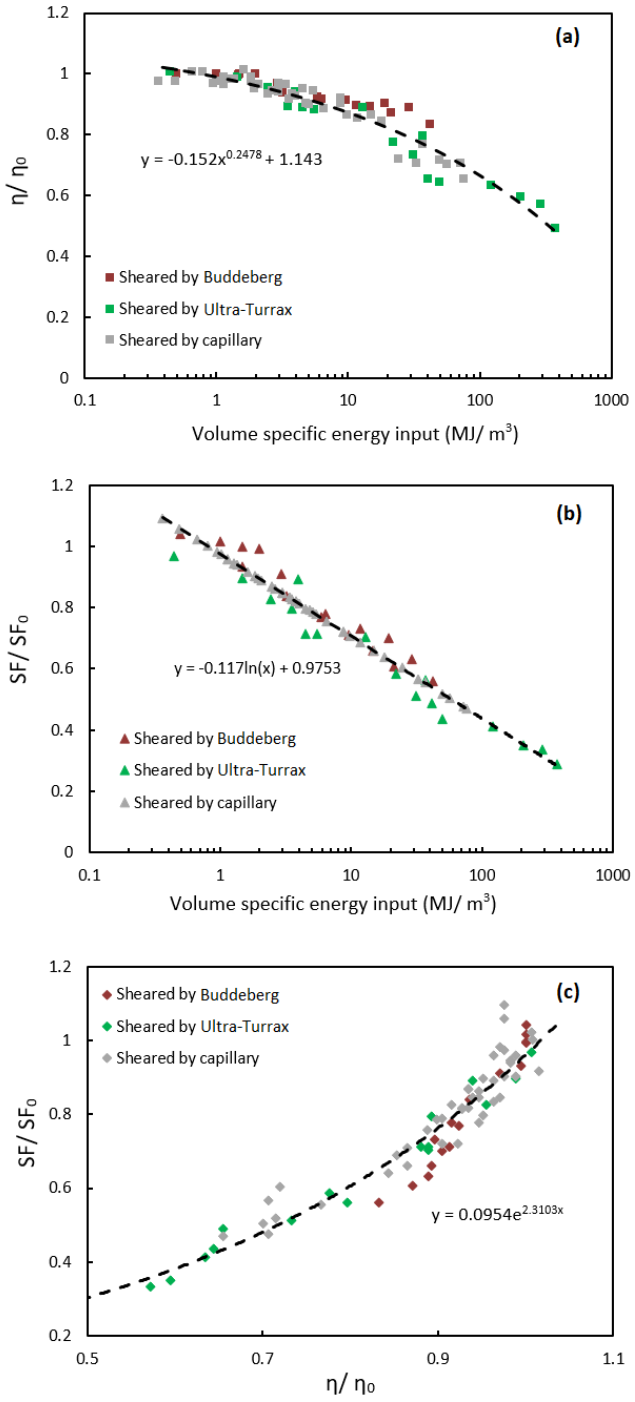

Figure 5.4: The change in viscosity and screen factor versus shearing intensity (based on the energy input) from the experimental series. (a) The normalized viscosity and (b) the normalized screen factor as a function of energy input and (c) the normalized screen factor as a function of the normalized viscosity. Red, green, and grey data points represent Buddeberg, Ultra-Turrax, and capillary respectively. The data presented here corresponds to the data given in Figure 5.2

As shown in Figure 5.4c, another master curve was established between the screen factor and the viscosity of the pre-sheared polymer solutions independent of the shearing device. The screen factor increased as an exponential function of the viscosity. At the beginning of the pre-shearing process, only the screen factor decreased sharply while the reduction

in viscosity was samller. Later, both the screen factor and viscosity decreased significantly. This supports the hypothesis that by shearing the polymer solution, first the long polymer chains are ruptured (which mainly causes a reduction in the screen factor) but after a critical strain rate, the shorter polymer chains are ruptured as well (which causes reduction in both the screen factor and viscosity).

The shear viscosity measurements were performed for the PS-A with no pre-shearing and the pre-sheared PS-A, using the Buddeberg, Ultra-Turrax, and capillary at different energy inputs as indicated in Figure 5.5a. The Carreau–Yasuda model (Equation 5.3) was used to fit the experimental data. The list of fitting parameters is tabulated in Table B.1 (see **Appendix B**). The data shows that regardless of the shearing conditions, the PS-A exhibits a Newtonian behaviour at low to intermediate shear rates, followed by a shear-thinning behaviour at higher shear rates. The extension of Newtonian and shear-thinning regimes depends on the energy input. The shear rate dependency of the PS-A decreased with increasing the energy input. On the other hand, from Table B.1, it can be seen that the relaxation time decreases with increasing energy input. This means that at a higher energy input, the polymer solutions contain shorter polymer chains, and these chains are more stretched. Consequently, when a polymer molecule is deformed by the shear forces, it requires a shorter time to relax to its original conformation.

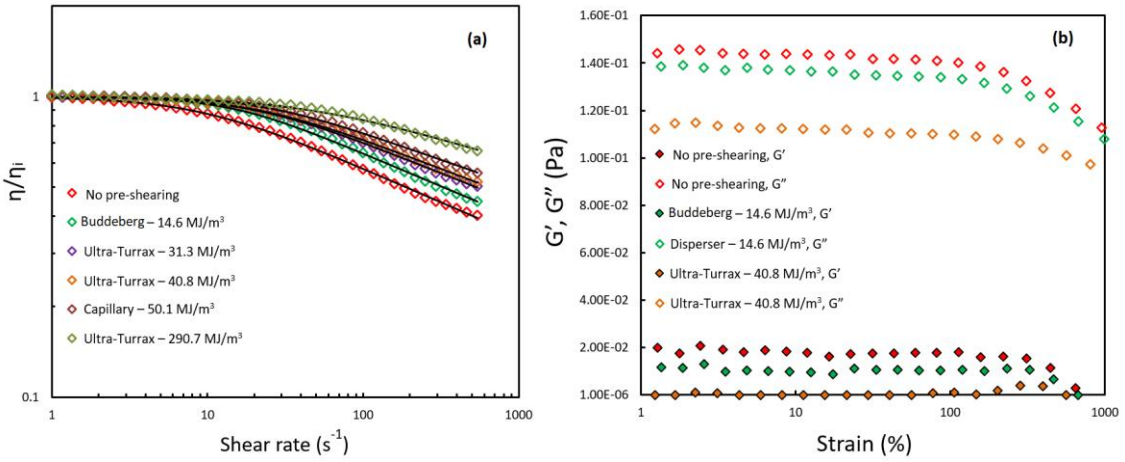

Figure 5.5: (a) The normalized steady-state shear viscosity of un-sheared and pre-sheared polymer solutions. The solid lines are acquired by fitting the experimental data with the Carreau–Yasuda model. The fitting parameters are presented in Table B.1 (see Appendix B). (b) The storage modulus (G') and loss modulus (G'') as a function of strain at a constant angular frequency ω=6.28 rad/s

Amplitude sweep tests were conducted to measure the storage modulus (G') and loss modulus (G'') as a function of strain (ε) at a constant angular frequency (ω) of 6.28 rad/s. This test was attempted with the PS-A with no pre- shearing and also with the PS-A

sheared with Buddeberg and Ultra-Turrax at volume specific energy inputs of 14.6 and 40.8 MJ/m^3 respectively. As can be seen in Figure 5.5b, for the PS-A with no pre-shearing the loss modulus was larger than the storage modulus over the whole range of strains, up to 1000%. This implies that even in the absence of pre-shearing the rheological response of the polymer solution is controlled by the viscous component and there is no significant entanglement among the polymer chains. With increase in the energy input imposed by the Buddeberg and Ultra-Turrax, both G' and G'' decrease, and the response was still completely viscous dominant. This is another indication of the stretching of the polymer chains and the breaking of the longest ones by pre-shearing.

5.3.3 Effect of pre-shearing on porous media flow

Based on the results of the rheology of the pre-sheared polymer chains, the following polymer solutions were selected for the sand-pack flow experiments: the PS-A with no pre-shearing and Ultra-Turrax sheared PS-A with an energy input of either 31.3 MJ/m^3 or 290.7 MJ/m^3. Here, the focus is only on the polymer solutions pre-sheared by the Ultra-Turrax, with different energy inputs, as the flow field is similar. This enables the investigation of the effect of energy input on the flow enhancement of the pre-sheared polymer solutions in porous media. The summary of the sand-pack flow experiments performed is given in Table 5.4. The results will be discussed and interpreted in terms of the resistance factor RF of the polymer solution. As a point of reference, the RF will be compared at 30.0 ± 0.5 PV for all the experiments. Thereafter, the results of the numerical simulation will be presented, to aid in the understanding of the behaviour of the polymer flow through the sand-packs.

Table 5.4: Summary of performed sand-pack flow experiments

	Volume specific energy input (MJ/m^3)	Viscosity (mPa s)	Screen factor	Resistance factor at 30 PV
No pre-shearing	0	25.7	18.4	84.5
Ultra-Turrax	31.3	18.7	10.3	29.0
Ultra-Turrax	290.7	13.3	6.4	13.0

In Figure 5.6a, the RFs of the un-sheared and pre-shared polymer solutions are plotted as a function of the number of pore volumes (PV) forced through the sand-pack. When the un-sheared PS-A was forced through the sand pack, a significant increase in the RF was immediately observed, and after only 3.5 ± 0.5 PV injection of PS-A, the resistance factor

rose to 30.0 ± 0.5. Thereafter, the rate of increase became slower and after 30.0 ± 0.5 PV, the RF reached 84.5 ± 0.5.

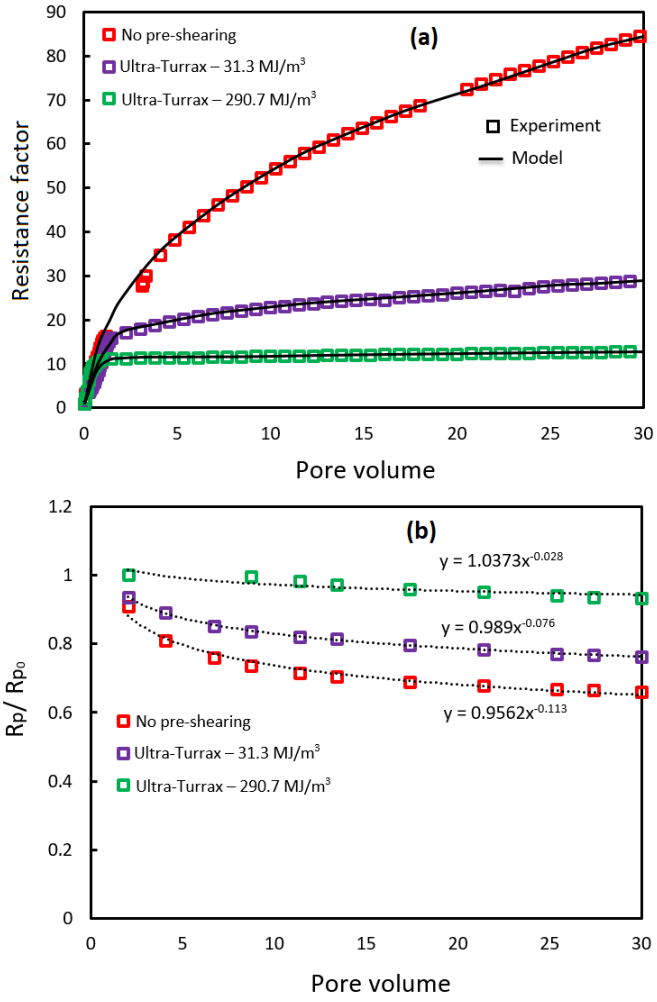

Figure 5.6: The sand-pack flow experimental and numerical modelling results. (a) Resistance factor (*RF*) as a function of pore volume for the flow of un-sheared and Ultra-Turrax sheared polymer solutions at different energy input through the sand-pack and (b) reduction in the radius of pore throat (R_p) as a function of pore volume

Pre-shearing the PS-A with the Ultra-Turrax significantly enhanced the flow through the sand-pack. However, when the Ultra-Turrax sheared PS-A with energy input of 31.3 MJ/m^3 was forced through the sand-pack for 30.0 ± 0.5 PV, the RF rose to 29.0 ± 0.5. This represents a 66% decrease in the RF compared to un-shared PS-A while the viscosity decreased by 27% only . When the energy input of the Ultra-Turrax was significantly increased to 290.7 MJ/m^3, RF at 30.0 ± 0.5 PV dropped by an additional 19% whereas the viscosity dropped by an additional 21%. The reduction in the RF of the pre-sheared polymer solutions is consistent with the reduction in the SF formerly observed in the screen factor experiments.

These results are in agreement with the study of Dupas et al. [382] who found that the moderate mechanical degradation of HPAM prior to injection improves its injectivity in sand-packs. The authors also found that at high injection velocities, the apparent rheo-thickening for the degraded HPAM solution was less pronounced as compared to the native HPAM solution. This was attributed to the reduction of the extensional viscosity at high degradation rates (through the rupture of longer chains) while the shear viscosity decreased only slightly.

A summary of the parameters used in the numerical simulation to match the sand-pack flow experiments for each pre-shearing condition is given in Table B.2 in **Appendix B**. Figure 5.6a shows that the model was able to perfectly match the sand-pack flow experiments. A significant increase in the RF of the un-sheared PS-A at the beginning of the flow through the sand-pack is due to the combined effect of adsorption and mechanical entrapment, which leads to drastic polymer retention. Whether mechanical entrapment or adsorption is dominant depends on the permeability of the porous medium. Comparing the hydrodynamic radius of the polymer coil (R_h) and the pore throat radius (R_p), the adsorption may be the dominant mechanism for polymer retentions in high-permeability sands ($R_p > 50R_h$) [115], while the mechanical entrapment dominates in low-permeability rocks ($R_p < 3R_h$) [20,22,115]. Hence, the adsorption here is more dominant as the permeability of the sand-pack is relatively high. Nevertheless, after all the adsorption sites in the sand-pack are occupied with the polymer molecules, the mechanical entrapment becomes the dominant factor for polymer retention. Our model considers a time-dependent reduction in pore throat radius meaning that the pore throat becomes smaller due to the flow of many pore volumes of PS-A through the sand-pack and the consequent mechanical entrapment. As can be seen in Figure 5.6b, upon flowing the PS-A through the sand-pack, the radius of the pore throat becomes smaller and smaller. After 30.0 ± 0.5 PV, a 34% reduction in the radius of the pore throat is observed. This is consistent with a significant reduction in the size of polymer chains.

The flow of 30.0 ± 0.5 PV of the Ultra-Turrax sheared PS-A (energy input of 31.3 MJ/m^3) through the sand-pack leads to a reduction of pore throat radius by 24%. This suggests that the longest polymer chains have been broken after pre-shearing, which makes the mechanical entrapment and continuous increase in RF less pronounced. The flow of 30.0 ± 0.5 PV of Ultra-Turrax sheared PS-A (energy input of 290.7 MJ/m^3) results in a

decrease in the pore throat radius of only 7%, which leads to a very gentle increase in the RF. This suggests that the size of polymer chains has significantly reduced.

Even though the pre-shearing PS-A with the high energy input of 290.7 MJ/m^3 leads to the best porous media flow enhancement, it should be noted that it also decreases the original viscosity by 48%. This lower viscosity results in a reduction in the ability of the polymer solution to improve the sweep efficiency and consequently to enhance the oil recovery. Moreover, the significant energy applied to break the polymer chains is costly. Pre-shearing the polymer solution with the energy input of 31.3 MJ/m^3, however, results in only a 27% reduction of viscosity while the applied energy is 90% reduced compared to the 290.7 MJ/m^3 case. Therefore, the trade-off between the flow enhancement, the viscosity reduction, and the cost of energy generation should always be considered when choosing the optimum level of energy input for pre-shearing the polymer solutions.

5.4 Conclusions

The effect of controlled pre-shearing on the flow of a polymer solution containing an inverse emulsion polymer dissolved in synthetic seawater was investigated. Three shearing devices were considered, namely a Buddeberg disperser, an Ultra-Turrax disperser, and pressure-driven flow through a capillary die. By comparing the flow properties of polymer solutions pre-sheared at different intensities, the following conclusions are driven:

- A critical Weissenberg number was found (Wi_c~13) above which the viscosity of the polymer solution started to decrease. The rate of viscosity reduction at large Wi became slower. Polymer pre-shearing was found to be path independent, regardless of the shearing device.
- Plotting the viscosity and screen factor of the pre-sheared polymer solution as a function of the energy dissipated by the shearing devices resulted in the establishment of master curves. By increasing the energy input, initially, only the screen factor decreased sharply, while the reduction in viscosity was more gradual. Later, both the screen factor and viscosity decreased significantly. These master curves for the polymer system were proven to be independent of the shearing device.

- Pre-shearing the polymer solution enhanced its flow efficiency in porous media. The Ultra-Turrax sheared polymer solution with an energy input of either 31.3 or 290.7 MJ/m3 showed a 66% and 85% drop in resistance factor respectively, while the viscosity was reduced by 27% and 48% respectively.
- A numerical model for polymer flow in porous media that accounted for time-dependent retention was built. The model predictions were found to be in good agreement with the reported experiments. The model assumed that the main mechanism for flow efficiency enhancement is a reduction in the size of polymer chains after pre-shearing which in turn leads to smaller mechanical entrapment and a less pronounced increase in resistance factor.
- The pre-shearing techniques can be applied to other polymers typically used for cEOR such as hydrolyzed polyacrylamide (HPAM). The shear degradation of HPAM (i.e. the decrease in viscosity in shear flow fields) has also been reported in several studies [79,383-386].
- Further studies are needed to determine the precise relationship between the shear and extensional flows as a result of pre-shearing. Moreover, direct measurements of MWD can better illustrate the concept of flow enhancement of water-soluble polymers in porous media. Our study could be extended by investigating the effect of porous media permeability on the effectiveness of pre-shearing for flow enhancement, particularly in low permeability cores where polymer injectivity is a serious challenge.

6 GENERAL CONCLUSIONS AND OUTLOOK

The implementation of conventional water-soluble polymers for chemical enhanced oil recovery (cEOR) at high salinity and temperature and their time-dependent injectivity decline are two common challenges in field applications. This thesis was focused on the investigation of a hybrid of hydrophobically modified polyacrylamide and hydrophobically modified silica nanoparticles for cEOR at high salinity, hardness, and temperature including characterizing each component of the hybrid, their rheological response, and behaviour in porous media. In the subsequent part of this thesis, the flow enhancement and injectivity improvement of an inverted emulsified polymer emulsion in porous media by pre-shearing through contractions and agitators were investigated. This chapter gives the general conclusions of the thesis followed by the outlook for future research.

6.1 General conclusions

A critical review of the most recent advances on polymers and nanoparticles for cEOR was given and the areas which need further researches were highlighted. The challenges for the application of conventional polymers for cEOR at high salinity and temperature conditions were discussed in some detail. A notable finding from the literature is that modified polyacrylamides by incorporation of small hydrophobic or salt- and temperature-tolerant monomers exhibit much higher stability at elevated temperature and high salinity. Nonetheless, few studies concerning their behaviour in porous media have been reported in the literature. Moreover, the molecular weight of the modified polyacrylamides, with salt- and temperature-tolerant monomers, is on the low side. For this reason, they need to be overdosed to meet the viscosities required for oil recovery, which has obvious economic disadvantages. This thesis addressed the limitations of the currently available polymer materials by proposing a novel approach for enhancing water viscosity. The new approach is based on the hybridization of polymers and nanoparticles to achieve stable hybrids with superior and tuneable rheological properties.

Concerning the four research questions presented in **Section 1.3**, the conclusions are given below.

6.1.1 The rheological response of hybrids at various concentrations

The proposed hybrid consists of a hydrophobically modified polyacrylamide (HMPAM) and hydrophobically modified silica nanoparticles (NPs). A detailed investigation of this hybrid at various concentrations was undertaken to characterize its physical-chemical properties and underlying mechanics concept. The NPs were hydrophobically modified by grafting a low molecular weight organic ligand (gamma-glycidoxypropyltrimethoxysilane) onto their surface. The modified polymer and NPs became more hydrophobic than the original polymer and NPs but still had sufficient polarity to allow a good dispersion in water. An xDLVO analysis showed that such modification led to an increased potential barrier compared to the bare nanoparticles due to provided steric stabilization which ensured the colloidal stability at high salinity. Hybridization of HMPAM with NPs resulted in a higher viscosity at high salinity and temperature. The viscosity improvement was more pronounced for HMPAM in the semi-dilute regime. Apparently, the HMPAM chains in the semi-dilute regime overlap, and therefore they can be bridged by NPs more easily. For a given HMPAM concentration, in the semi-dilute regime, there was a critical concentration of NPs above which the bridging of HMPAM chains by NPs happened more easily resulting in a significant increase in viscosity.

6.1.2 The effect of nanoparticles on the flow performance of polymers in porous media

The porous media flow behaviour of HMPAM, NPs, and HMPAM–NPs hybrid was investigated by performing a series of core-flood experiments at low and high superficial velocities. The hybrid showed larger flow resistance, consistent with its higher viscosity, compared to the simple polymer. Injection of NPs suspension at low superficial velocity led to a substantial increase in the pressure drop due to external and internal filtration of nanoparticle aggregates. However, co-injection of HMPAM and NPs under similar conditions prevented such filtration. This supports the proposed mechanism where hydrophobic–hydrophobic interactions between HMPAM and NPs prevent the aggregation of NPs as polymer and nanoparticles are transported through porous media in unison. Co-injection of HMPAM and NPs also reduced the retention of both HMPAM

and NPs compared to when they were injected individually. This can be explained by the availability of fewer adsorption sites on the surface of the rock for HMPAM or NPs when both of them are present in the same solution. The results show the potential of HMPAM–NPs hybrid as a mobility control agent for chemical enhanced oil recovery at high salinity and temperature.

6.1.3 The rheological response of the pre-sheared polymer chains

To understand the impact of pre-shearing on the rheological response of the polymer chains, the viscosity and screen factor were measured for polymer solutions sheared by two agitators and a capillary die with different shearing intensities. The polymer solution contained essentially an acrylamide-based copolymer obtained from an emulsified polymer emulsion inverted by a surfactant. Pre-shearing the polymer solution was done under fast flow to induce high-stretching of the polymer chains and thus promote the break-up of the longest ones (i.e. decrease in relaxation time and shear-thinning level). Beyond a certain critical Weissenberg number, independent of the shearing device, the viscosity of the polymer solution decreased. Plotting the viscosity and screen factor of pre-sheared polymer solution as a function of the energy dissipated by the shearing devices resulted in establishing master curves. These master curves for the polymer system were proven to be independent of the shearing device. By increasing the energy input, first, only the screen factor decreased sharply while the reduction in viscosity was not as much. Later, both the screen factor and viscosity decreased significantly.

6.1.4 The effect of pre-shearing on the flow performance of polymers in porous media

To understand the impact of pre-shearing on the flow performance of polymers in porous media, the un-sheared and pre-sheared polymer solutions at different energy inputs were forced through sand-packs to compare their corresponding flow resistances. Moreover, the sand-pack experiments were interpreted using a numerical model which takes into account the time-dependent retention of polymers. The porous media experiments in sand-packs proved that pre-shearing the polymer improves its injectivity considerably without a significant reduction in viscosity. The injectivity improvement was in excellent agreement with the proposed idea that pre-shearing breaks the longer chains thus reducing the effects of mechanical entrapment of polymer molecules.

6.2 Outlook

This thesis presented a novel polymer-based chemical for cEOR at high salinity and elevated temperature and a novel method for improving the injectivity of polymers. Some aspects of these novel approaches may require further research. Some of the research opportunities are outlined below.

Further investigation of the long-term stability of the HMPAM–NPs hybrid is recommended (**Chapter 3**). Complementary experiments such as the study of the colloidal stability and change in the hybrids viscosity over time are recommended to investigate the effectiveness of the hybrids at high temperatures in the long-term. The organic ligand can ensure the colloidal stability of NPs at high salinity; however, at high temperatures, in the long-term, the epoxy functional groups of the organic ligand can react/open up which increases the likelihood of NPs aggregation in presence of salt. Therefore, further research on the development of organic ligands suitable for high temperatures in the long-term will be helpful.

Flow resistance as a result of the HMPAM–NPs hybrid flow through porous media at the attempted concentrations proved to follow its bulk rheological behaviour (**Chapter 4**). Performing core-flood experiments at various HMPAM and NPs concentrations is recommended to investigate whether this observation is also valid at other concentrations. It would be particularly interesting to investigate if the good injectivity observed for the HMPAM–NPs hybrid also occurs at higher concentrations of NPs where the probability of NPs aggregation becomes higher.

Pre-shearing the polymer solutions clearly improved their injectivity through a porous medium with relatively high permeability (**Chapter 5**). An extension of our study can be to investigate the impact of porous media permeability on the effectiveness of the pre-shearing for flow enhancement of water-soluble polymers. In particular, performing the experiments at low permeable rocks, for which the propagation of long-chain polymers seems to be a challenge, is an interesting follow-up for this research.

7 APPENDICES

7.1 Appendix A: Rheology of HMPAM–NPs hybrid

1. Calculation of the volume fraction of the ligand

The volume fraction of a ligand (ϕ_l) in the shell is determined by the following equation [387]:

$$\phi_l = \frac{3\Gamma_{max}R^2}{\rho_l[(L+R)^3 - R^3]} \quad \text{(A.1)}$$

where ρ_l is the bulk density of a pure ligand, Γ_{max} is the grafting density of the ligand in units of ligand mass per nanoparticle surface area, R is the radius of the nanoparticle and L is the thickness of particle coating by the ligand. Γ_{max} is derived from the following equation:

$$\Gamma_{max} = \frac{\sigma MW_l}{N_A} \quad \text{(A.2)}$$

where σ, as calculated by Equation 3.3, is the grafting density of the ligand in units of molecules per nanoparticle surface area, MW_l is the molecular weight of the ligand and N_A is the Avogadro's number.

2. Stability of NPs and hybrids

Figure A.1 shows the samples of GPTMS modified NPs dispersed in Brine2015 in different concentrations from 0.05 to 4.0 wt% over the course of three months. As can be seen, all the samples were colloidally stable and no sedimentation was observed.

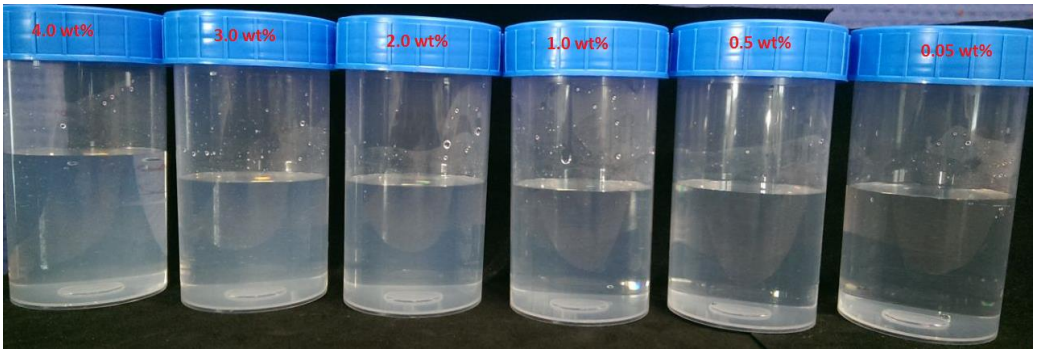

Figure A.1: Samples of GPTMS modified silica NPs at different concentrations dispersed in Brine2015; from right to left: 0.05, 0.5, 1.0, 2.0, 3.0 and 4 wt%

Figure A.2 shows the samples of bare and GPTMS modified NPs dispersed in DI water and Brine 2015 at a concentration of 0.05 wt% after three months. Both bare and GPTMS modified NPs were stable in DI water but bare NPs showed some turbidity while the dispersion of GPTMS modified NPs was transparent. On the other hand, the dispersion of bare NPs in Brine2015 resulted in sedimentation whereas the dispersion of GPTMS modified NPs in Brine2015 was stable.

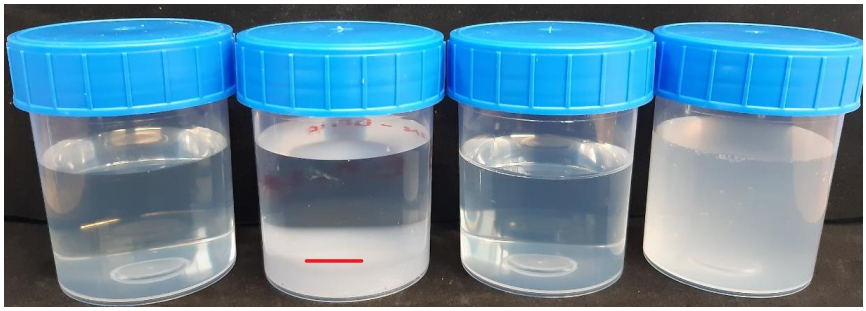

Figure A.2: Different samples of silica NPs. From right to left: bare silica NPs in DI water, GPTMS modified NPs in DI water, bare NPs in Brine2015 and GPTMS modified NPs in Brine2015. The dispersion of bare NPs in Brine2015 resulted in sedimentation

Figure A.3 shows hybrid samples of HMPAM and GPTMS modified NPs in Brine2015 at a constant NPs concentration of 4 wt%. The concentration of HMPAM varied from 0.05 to 0.6 wt%. As can be seen, all the hybrids were stable after three months and no sedimentation was observed.

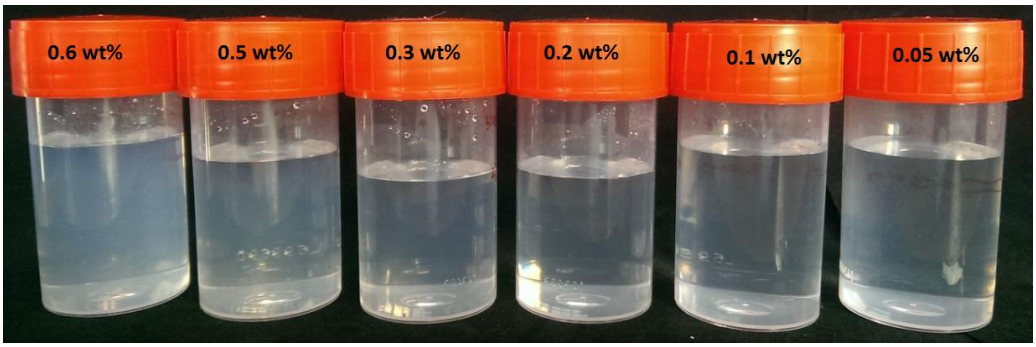

Figure A.3: Hybrid samples of HMPAM and GPTMS modified silica NPs in Brine2015. The concentration of NPs was 4 wt% for all the samples and the concentration of HMPAM varied. From right to left, concentration of HMPAM was 0.05, 0.1, 0.2, 0.3, 0.5 and 0.6 wt%

3. TEM of nanoparticles

In order to disperse the bare silica NPs in DI water and Brine2015, the solutions were sonicated in a water bath for 30 min. After the sonication, a visually homogenous dispersion of NPs was observed in DI water. In the Brine2015, some nanoparticle aggregates were still visible. Particle size distribution (PSD) analyses on the bare silica NPs dispersed in DI water and brine confirm larger agglomerations of the particles in brine compared to water (Figure A.4).

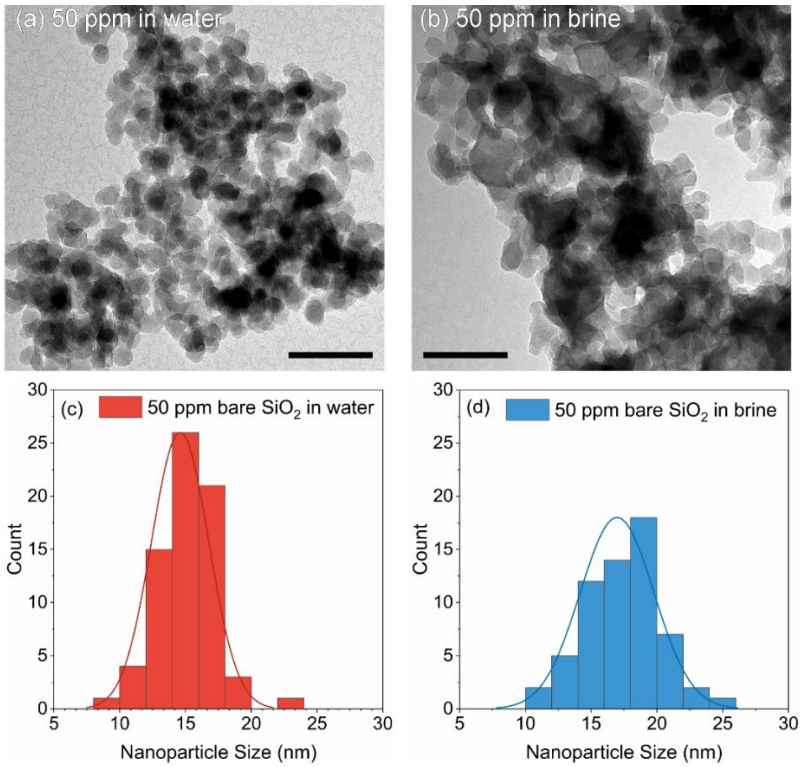

Figure A.4: 50 ppm dispersion of silica NPs in (a, c) DI water TEM and PSD analysis, (b, d) Brine2015 TEM and PSD analysis (scale bar: 80 nm). The solid line is the normal distribution of data

The TEM analysis of the GPTMS modified NPs in DI water shows the presence of individual and small clusters of NPs with a narrow cluster size distribution which has an average size of 22 nm (Figure A.5a and A.5c). For the NPs dispersed in Brine2015, larger agglomerates are formed resulting in clusters with a wider distribution averaging at about 42 nm (Figure A.5b and A.5d).

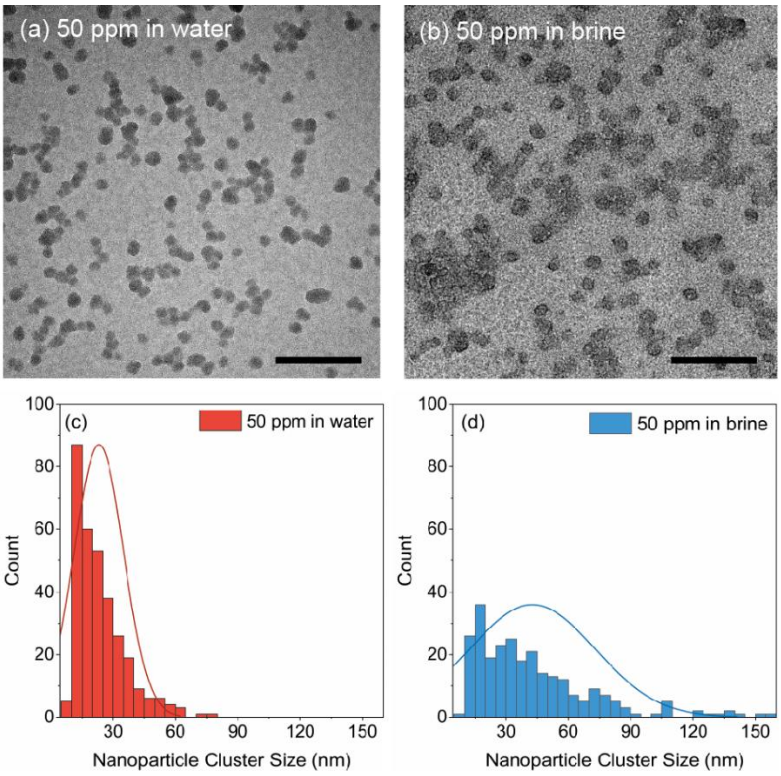

Figure A.5: 50 ppm dispersion of GPTMS modified silica NPs in (a, c) DI water TEM and PSD analysis, (b, d) Brine2015 TEM, and PSD analysis (scale bar: 100 nm). The solid line is the normal distribution of data

4. Carreau–Yasuda model for the shear-thinning response of polymer solutions

The viscosity of polymer solutions as a function of shear rate was fitted in Carreau–Yasuda model. The results were shown in Figure 3.3. In Table A.1 the fitting parameters are shown for HMPAM solutions in DI water at 25 °C. The DI water viscosity was considered 0.9 mPa s (i.e. η_∞=0.9 mPa s). Table A.2 shows the fitting parameter for HMPAM solutions in Brine2015 at 25 °C with solvent viscosity of 1.4 mPa s (i.e. η_∞=1.4 mPa s). In Table A.3 fitting parameters of HMPAM solutions in Brine2015 at 70 °C is shown (η_∞=0.65mPa s).

Table A.1: Fitting parameters for HMPAM solution in DI water at 25 °C (η_∞=0.9 mPa s)

Polymer conc. (wt%)	η_o (mPa s)	λ (s)	n	a
0.70	46.9	0.042	0.71	1.49
0.50	19.8	0.038	0.82	1.90
0.40	12.7	0.035	0.86	2.47
0.30	8.2	0.033	0.90	1.11
0.20	4.8	0.025	0.94	1.00
0.15	3.7	0.013	0.96	0.73
0.10	2.0	0.004	0.98	2.65

Table A.2: Fitting parameters for HMPAM solution in Brine2015 at 25 °C (η_∞=1.4 mPa s)

Polymer conc. (wt%)	η_o (mPa s)	λ (s)	n	a
0.50	36.7	0.045	0.77	1.98
0.40	22.8	0.043	0.83	2.62
0.30	16.1	0.032	0.87	3.00
0.20	7.4	0.025	0.93	0.83
0.10	3.5	0.0025	0.95	2.51
0.05	2.4	0.002	0.97	2.45

Table A.3: Fitting parameters for HMPAM solution in Brine2015 at 70 °C (η_∞=0.65 mPa s)

Polymer conc. (wt%)	η_o (mPa s)	λ (s)	n	a
0.50	11.2	0.019	0.84	1.45
0.40	7.4	0.017	0.90	2.00
0.30	4.2	0.009	0.98	1.31
0.20	2.7	0.003	0.99	1.50
0.10	1.4	0.0025	0.99	2.51
0.05	1.0	0.002	0.99	2.45

5. Molecular weight estimation of HMPAM and PAM

The free-radical based polymerization techniques employed to synthesize the polyacrylamide derivatives is anticipated to yield high molecular weight polymers (> 10^6 g mol^{-1}). Measuring molecular weights of these polymers via standard size exclusion chromatography proved to be challenging. Therefore, the molecular weights were estimated based on viscosity measurements. Wu et al. [329] reported the Mark-Houwink parameters for PAM homopolymers relating the intrinsic viscosity ($[\eta]$), which is directly related to the coil dimension of polymers in solution, to their molecular weight.

The intrinsic viscosity can be determined by measuring the solution viscosity (η) with respect to the solvent viscosity (η_0) in the dilute regime (no overlap between polymer coils) and extrapolation to zero polymer concentration as described by Equation A.3. η_{sp} represents the specific viscosity here.

$$[\eta] = \lim_{c\to 0}\left(\frac{\eta - \eta_0}{\eta_0}\right)/c = \lim_{c\to 0}\frac{\eta_{sp}}{c} \tag{A.3}$$

As the fraction of hydrophobic comonomers in HMPAM is only small, we assumed that this equation for polyacrylamide homopolymers holds for the hydrophobically modified polyacrylamide derivatives as well. Following the protocol from Wu et al. [329], η was measured in an aqueous 0.2 M Na_2SO_4 solution for HMPAM and PAM in a concentration

window ranging from 0–0.4 g/dL. A rolling ball micro-viscometer was used for the viscosity measurements, as this instrument is able to measure viscosities at significantly higher accuracy than a conventional rheometer. These measurements yielded a fairly linear relationship between η and the polymer concentration for both PAM (Figure A.6a) and HMPAM (Figure A.6c). This indicates that the measurements were performed in the dilute regime, ensuring that the intrinsic viscosities and hence molecular weights of single polymer chains were measured. Plotting the data according to Equation A.3 and perform the extrapolation yields intrinsic viscosities of 6.8 and 5.6 dL/g for PAM (Figure A.6b) and HMPAM (Figure A.6d) respectively. Based on these values, molecular weights of $2.7 \pm 0.1 \times 10^6$ and $2.1 \pm 0.03 \times 10^6$ g mol^{-1} were obtained for PAM and HMPAM, respectively. The molecular weights of both polymers are approximately the same, indicating that incorporating hydrophobic co-monomers in the PAM polymers is not significantly altering the polymerization kinetics and achievable monomer conversions.

We must note that the molecular weights reported here are merely estimates. Wu et al. [329] reported that the Mark-Houwink parameters depend on the degree of hydrolysis of the incorporated acrylamide monomers. At higher hydrolysis degrees the polymers behave more like polyelectrolytes. The introduction of charged moieties increases the coil volume of the polymers and hence the value for [η]. As the measured intrinsic viscosities were converted to molecular weights using parameters for polyacrylamide polymers with no hydrolysis, the reported molecular weights might be overestimated. As we did not attempt to measure the degree of hydrolysis for PAM or HMPAM, the reported values can be treated as an upper bound to the true molecular weight. Besides the unknown degree of hydrolysis, the relation reported by Wu et al. [329] was only verified for polymers of molecular weights up to $1.5 \cdot 10^6$ g·mol^{-1}. Small deviations of this relation when increasing the molecular weight a factor of 2–3 could be present.

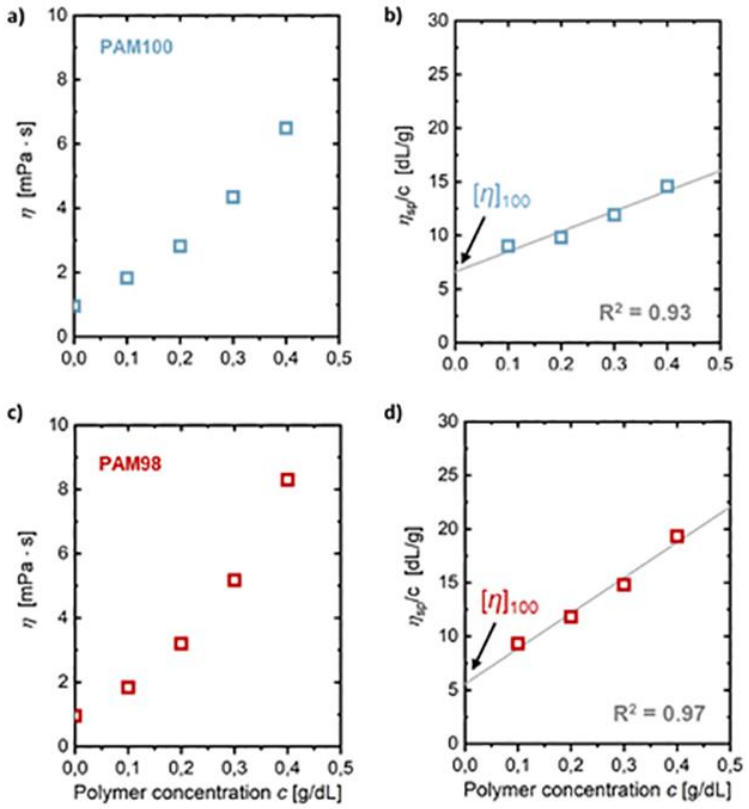

Figure A.6: Solution viscosity (η) versus polymer concentration for (a) PAM and (c) HMPAM. The plot of the specific viscosity ($\eta_{sp} = (\eta - \eta_0)/\eta_0$, with η_0 = viscosity of the pure solvent) divided by the polymer concentration versus the polymer concentration for (b) PAM and (d) HMPAM. Extrapolation to zero polymer concentration yields the intrinsic viscosities ($[\eta]$) of the polymers. Measurements were performed in 0.2 M Na_2SO_4 at 25 °C

6. Estimation of overlap concentration and radius of gyration

As can be seen in Figure A.7, the overlap concentration of HMPAM in DI water and Brine2015 was found to be 0.49 ± 0.01 wt% and 0.30 ± 0.01 wt% respectively. The radius of gyration (R_G) of HMPAM was estimated from the following equation [388]:

$$R_G = \left(\frac{[\eta]MW}{\Phi}\right)^{1/3} \quad \text{(A.4)}$$

where $[\eta]$ is the intrinsic viscosity, MW is the molecular weight of polymer and Φ is a universal constant (4.2×10^{24} mol^{-1}). R_G in DI water and Brine2015 was found to be 70 ± 5 and 80 ± 5 nm respectively.

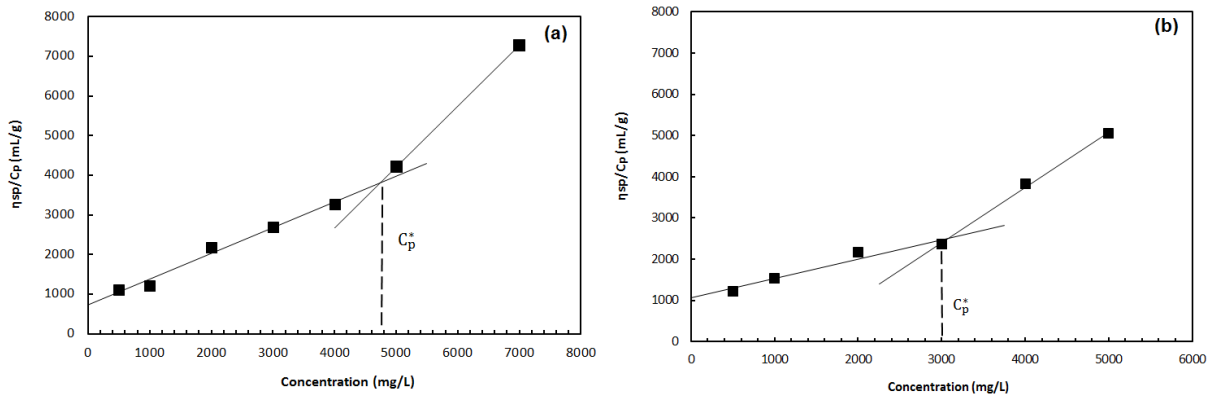

Figure A.7: Determination of C_p^* for HMPAM (a) in DI water and (b) in Brine2015

7. Estimation of HMPAM persistence length

To calculate the persistence length of HMPAM chains, we estimated the intrinsic viscosity (see Figure A.7) from which the radius of gyration (R_G) was estimated (see Equation A.4). For a non-branched wormlike chain, the persistence length can be estimated from R_G based on the following equation [389]:

$$< R_G^2 > = \frac{LL_t}{3} - L_t^2 + \frac{2L_t^3}{L} - \frac{2L_t^4}{L^2}(1 - e^{-\frac{L}{L_t}}) \quad \text{(A.5)}$$

where L_t is the persistence length and L is the contour length ($L = \frac{Mb}{m}$, with M and m being the polymer and monomer molecular weight and b is the contour length per monomer). Since both acrylamide and t-butyl acrylamide have the same "acrylamido" backbone, thus the same carbon-carbon bond length, the whole chain can be assumed as a connection of acrylamide. Therefore, for the sake of calculation, we assumed HMPAM as a pure polyacrylamide. The HMPAM contour length per monomer was considered to be within the range of 0.27–0.40 nm [390]. As a result, the HMPAM contour length and persistence length was estimated to be 9.9 ± 1.9 µm and 2.2 ± 0.6 nm respectively. Since the contour length is much larger than the persistence length, therefore, our long-chain polymer behaves like a random coil. Considering that the distribution of hydrophobic groups on HMPAM is random, three types of interactions are possible in an HMPAM–NPs hybrid: (a) intra-chain hydrophobic association within an HMPAM chain (b) inter-chain hydrophobic association between HMPAM chains, and (c) hydrophobic–hydrophobic interaction between t-butyl acrylamide units on HMPAM and hydrophobically modified silica NPs. Here, beyond $C_{np,c}$, NPs facilitate the bridging between different HMPAM chains.

8. ^{1}H NMR for t-butyl acrylamide

Figure A.8 shows ^{1}H NMR spectrum for t-butyl acrylamide in D_2O. Peak c' corresponds to the methyl groups in t-butyl acrylamide.

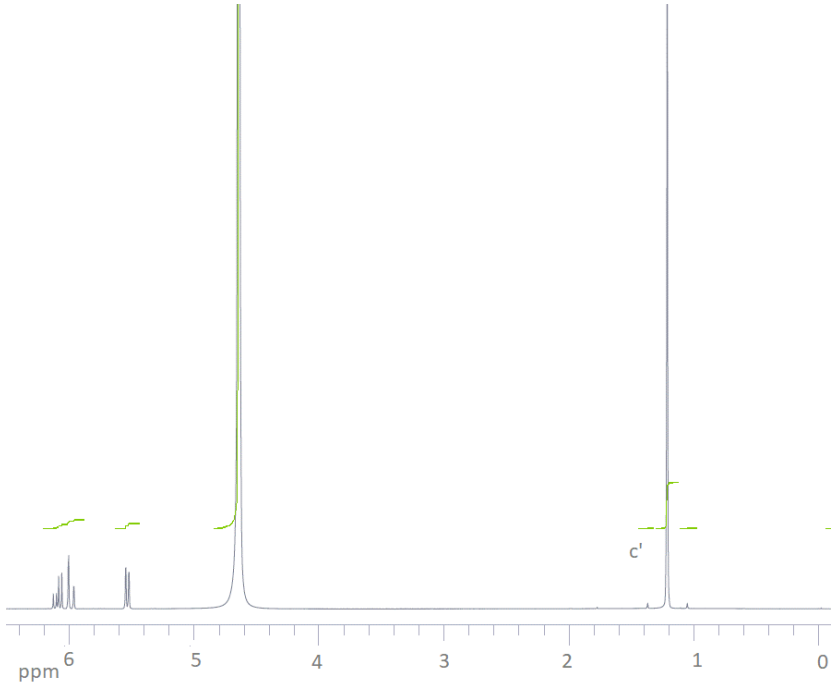

Figure A.8: ^{1}H NMR spectrum for t-butyl acrylamide

7.2 Appendix B: Polymer pre-shearing

1. Polymer injectivity

Mechanical entrapment is one important mechanism that can hinder the propagation of polymers through porous media. It will ultimately lead to pore-clogging and a time-dependent injectivity decline. The high-end fragments of the polymer molecular weight distribution and the highly-entangled polymer chains, formed as a result of hydrogen bonding along with precipitation due to the presence of divalent ions, are major sources of mechanical entrapment [10].

Polymer injectivity is described by the resistance factor RF [23] which is the ratio of the mobility of brine and polymer solution. RF is related to pressure drop according to the following equation:

$$RF = \frac{\lambda_{b_0}}{\lambda_{\mathrm{p}}} = \frac{\left(\frac{k}{\mu}\right)_{b_0}}{\left(\frac{k}{\mu}\right)_{\mathrm{p}}} = \frac{\Delta P_p}{\Delta \mathrm{P}_b^0} \tag{B.1}$$

where λ, μ, k and ΔP are the mobility, viscosity, permeability and pressure drop respectively and where the subscripts b_0 and p refer to brine before the polymer injection and polymer solution respectively. In practice, RF indicates an increase during the polymer injection, due to the viscosity increase and a reduction in permeability.

With the injectivity gradient IG, RF profile is examined over the injection of several pore volumes PV. IG is calculated by the ratio of RF at a certain pore volume $(x)PV$ to an RF at an earlier pore volume $(x-1)PV$:

$$RG_{(x)PV} = \frac{RF_{(x)PV}}{RF_{(x-1)PV}} \tag{B.2}$$

In the hypothetical case of lack of polymer retention, IG is 1 meaning that there is no increase in RF.

2. Calculation of shear rate and energy input

In an early work, Metzner and Otto [391] suggested that the average shear rate $\dot{\gamma}$ in a mixing tank is proportionate to the rotational speed of the impellers, described as below:

$$\dot{\gamma} = K_s N \tag{B.3}$$

where K_S is a non-dimensional constant, which depends on the geometry of the impeller, and N is the shaft rotational speed. This notion was broadly recognised and used in non-Newtonian fluid mixing studies [392-397]. The value of K_S has been reported in the range of 3–13 depending on the impeller geometry and whether the impeller generates radial or axial flow patterns.

It has been reported that for a rotational system creating a Couette geometry, the shear rate as a function of rotational speed can be calculated as follows [398]:

$$\dot{\gamma} = \frac{4\pi N}{m} \tag{B.4}$$

where m is the slop plot of torque as a function of rotational speed in a log-log plot. Therefore, to estimate m, the torque of the agitators at different rotational speed should be calculated. To do so, turbine power correlations are used.

Rushton, Costrich & Everitt [399] proposed using turbine-power correlations, which were also taken on by other researchers [400,401]. These turbine-power correlations are empirical geometry dependent. First, the power input P_N, has to be determined:

$$P_N = N_p . \rho \cdot N^3 \cdot d_i^5 \tag{B.5}$$

where N_p is the power number, ρ the fluid density and d_i the diameter of the agitator. N_p is found from the power number-Reynolds number relationship which is known for many agitators. R_e is calculated by Equation B.6 in the following way:

$$R_e = \frac{\rho \cdot N \cdot d_i^2}{\mu} \tag{B.6}$$

Torque T can also be calculated according to the following equation [402]:

$$T = \frac{P_N}{2\pi N} \tag{B.7}$$

The existing turbine-power correlation for disperser (Buddeberg disperser) and disk stirrer is shown in Figure B.1. The Ultra-Turrax geometry is comparable to the disk stirrer, but it offers a higher energy input because of the rotor and stator components. Thus, the curve for the disk stirrer was shifted by matching the rheological data of the polymer solution sheared by Ultra-Turrax to the Buddeberg-sheared solutions to provide a realistic

N_p. The calculated value of m for Buddeberg and Ultra-Turrax was 1.7 and 2.2 respectively.

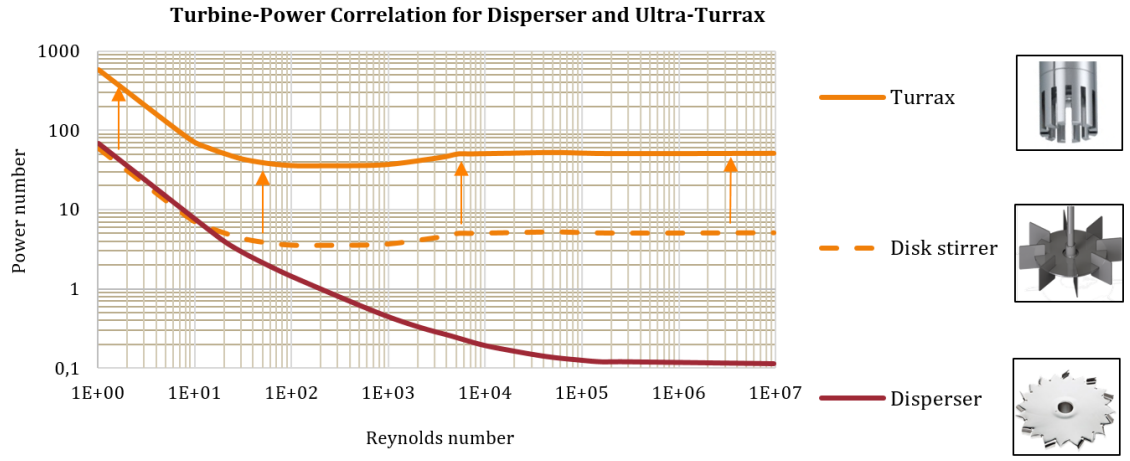

Figure B.1: Turbine-power correlation for Buddeberg disperser and Ultra-Turrax adapted from [399-401]

This also enables us to quantify the energy input applied to shear the polymer solution. The applied volume specific energy input E_v, is then estimated using Equation B.8 as follows:

$$E_v = \frac{P_N \cdot t}{V} \tag{B.8}$$

3. Calculation of strain rate in capillary

The strain rate in a capillary is calculated based on the following equation [403,404]:

$$\dot{\varepsilon} = \frac{Q}{\pi R_0^2 L}(\exp(\varepsilon_h) - 1) \tag{B.9}$$

where Q is the flow rate, R_0 is the outlet radius and ε_h is the Hencky strain found from the following equation:

$$\varepsilon_h = Ln(R_i^2/R_0^2) \tag{B.10}$$

where R_i is the inlet radius of the capillary.

4. Molecular weight estimation of polymer

The procedure used to estimate the average molecular weight of un-sheared and pre-sheard polymer solutions is described in this section. First, the polymer was extracted from the solution (see Figure B.2). For this, 50 mL of the polymer solution was added to a beaker containing 300 mL ethanol which was on a magnetic stirrer (Figure B.2a). After stirring the solution for a few hours, the polymer precipitated in the beaker (Figure B.2b).

A suction filter connected to a vacuum pump filtered the precipitated polymer. After that, ethanol was added to the extracted polymer in the suction filter and the vacuum pump was turned on to separate the remnants from the polymer. This was done three times. The extracted polymer was then placed in an oven to dry for 24 hours (Figure B.2c). Next, the extracted polymer was dissolved in de-ionised water at the original concentration of 0.5 wt% (Figure B.2d) which was then diluted to the desired concentrations. The intrinsic viscosity was determined by measuring the solution viscosity with respect to the solvent viscosity in the dilute regime and extrapolation to zero polymer concentration. The Mark-Houwink constants ($\eta_{int} = K \cdot {M_w}^a$), K and a, are chosen to be 6.31×10^{-3} and 0.8 respectively, which corresponds to water as solvent and polyacrylamide as polymer [405].

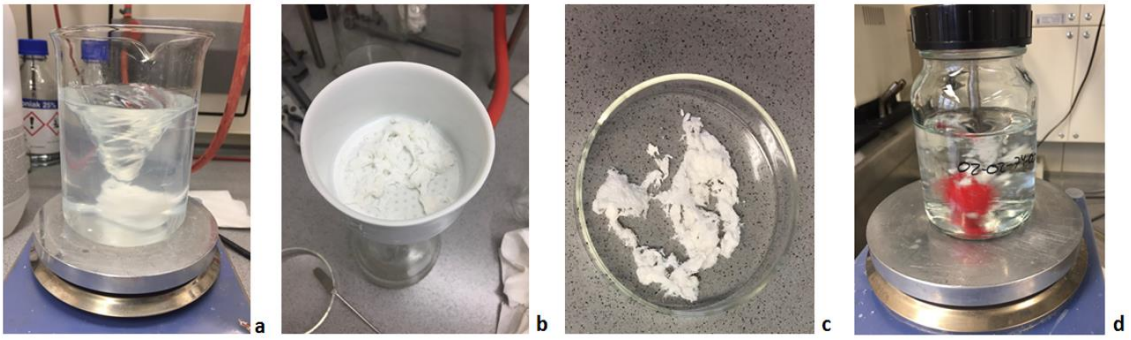

Figure B.2: Separation in ethanol (a]), washing separated polymer with suction filter (b), dried polymer (c), dissolved in distilled water (d)

As can be seen in Figure B.3, the overlap concentration of un-sheared polymer solution in synthetic seawater was found to be 0.40 ± 0.01 wt% (1 mg/L = 10^{-4} wt%). The intrinsic viscosity was also found to be 865 ± 5 mL/g which leads to a molecular weight of approximately 2.5×10^6 g/mol.

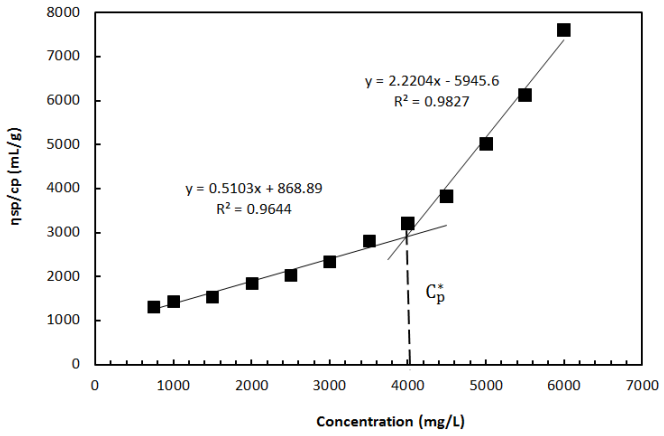

Figure B.3: Determination of C_p^* for un-sheared polymer solution in synthetic seawater

Results of estimated molecular weight as a function of Weissenberg number for three shearing devices and molecular weight as a function of shearing time for Ultra-Turrax at a rotational speed of 1750 rpm are shown in Figure B.4 and B.5 respectively.

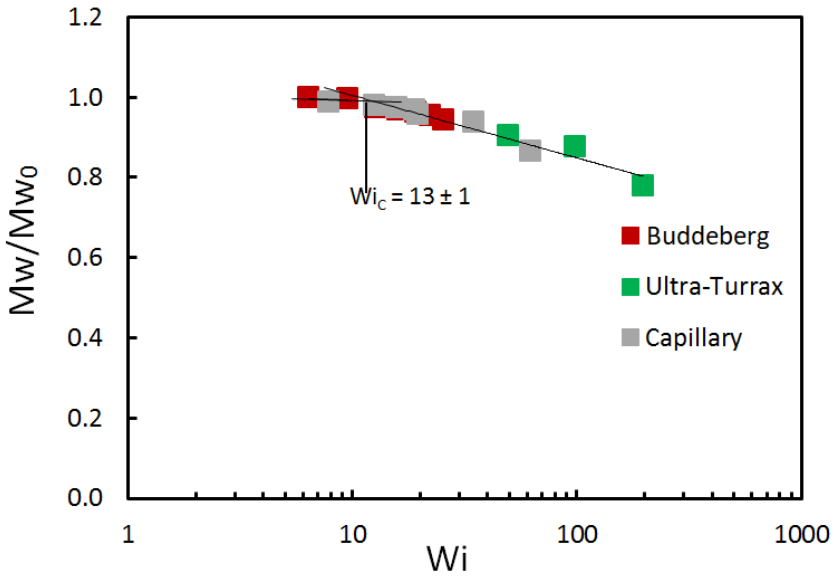

Figure B.4: Molecular weight versus Weissenberg number. Mw_0 represents the molecular weight of the un-sheared polymer

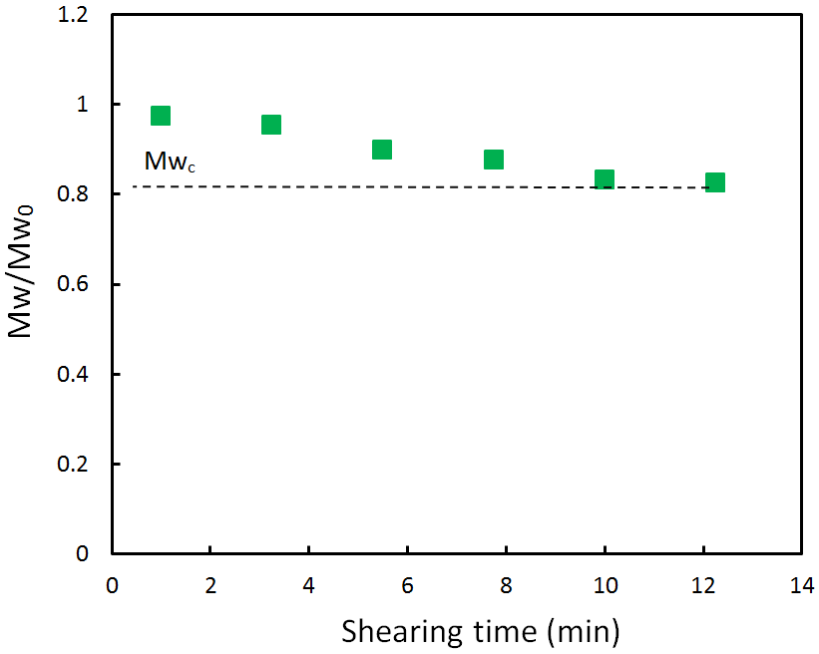

Figure B.5: The molecular weight as a function of shearing time for polymer solution sheared with Ultra-Turrax at a rotational speed of 1750 rpm. Mw_0 represents the molecular weight of the un-sheared polymer

5. Carreau–Yasuda model for polymer viscosity

The viscosity of polymer solutions as a function of shear rate was fitted in Carreau–Yasuda model. The results were shown in Figure 5.5a. In Table B.1 the fitting parameters

are shown for polymer solution with no pre-shearing and pre-sheared with Buddeberg, Ultra-Turrax, and a capillary at different volume specific energy input. The viscosity of synesthetic seawater in which polymer solution was dissolved, was considered 0.9 mPa s (i.e. η_∞=0.9 mPa s).

Table B.1: Fitting parameters for polymer solutions in synthetic seawater (η_∞=0.9 mPa s)

	η_o (mPa s)	λ (s)	n	a
No pre-shearing	25.6	0.103	0.75	1.27
Buddeberg –14.6 MJ/m^3	21.5	0.067	0.76	1.67
Ultra-Turrax–31.3 MJ/m^3	18.8	0.048	0.77	1.41
Ultra-Turrax–40.8 MJ/m^3	18.1	0.045	0.78	1.34
Capillary–50.1 MJ/m^3	16.9	0.041	0.80	1.56
Ultra-Turrax–290.7 MJ/m^3	13.2	0.02	0.82	1.04

6. Numerical simulation parameters to match the sand-pack flow experiments

A one-dimensional model based on the work of Yerramilli et al. [371] was carried out to solve the time-dependent mass conservation for polymer flow in porous media. Table B.2 in Appendix B gives a summary of parameters and Figure B.6 represents the workflow used for the simulation.

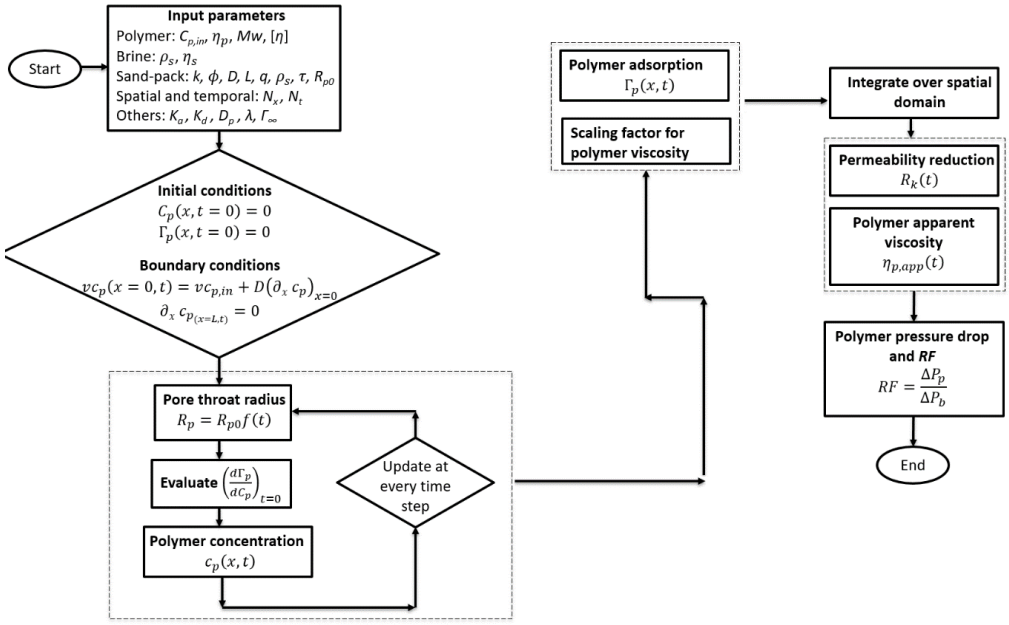

Figure B.6: Workflow for modelling the polymer flow through sand-packs

Table B.2: The summary of parameters used to match the sand-pack flow experiments

Polymer	An inverted emulsified polymer emulsion containing polymer solution containing essentially an acrylamide-based copolymer			
Conditions	0.4 wt% polymer and 0.24 wt% active inverter surfactant, Salinity S_s=50 g/L, T= 30 °C			
Sand-pack properties	K= 1000 mD, ϕ = 0.46, D= 1.58 cm, L= 7.5 cm			
Spatial and temporal parameters	Number of grids N_x=500, Number of time steps, N_t=500			
Sand-pack flow test	Unit	No pre-shearing	Ultra-Turrax–31.3 MJ/m^3	Ultra-Turrax–290.7 MJ/m^3
Polymer molecular weight, Mw	g/mol	2.5×10^6	1.95×10^6	1.35×10^6
Polymer intrinsic viscosity, [η]	cm^3/g	865	704	512
Equilibrium rate constant, K_e	cm^3/g	972.9	972.9	972.9
Maximum adsorption capacity, Γ_∞	g/cm^2	4.6×10^{-7}	4.6×10^{-7}	4.6×10^{-7}
Parameters for viscosity model (modified Flory-Huggins equation)	-	a_1 = 92.6, a_2 = 104545.2, a_3= 1905109.8, b= -0.58	a_1 = 85.2, a_2 = 99845.2, a_3= 1205109.8, b= -0.56	a_1 = 79, a_2 = 89955.2, a_3= 857109.8, b= -0.53

7. Zero-shear rate viscosity estimation from Ubbelohde viscometer data

The viscosity measurement with the Ubbelohde viscometer is easy to perform, quick, and independent of the total volume of the solution [406]. Considering the fact that viscosity measurements in our study were performed for 77 polymer solutions pre-sheared at different energy input, the Ubbelohde viscometer gives us some flexibility compared to the Couette cell shear rheometer for which a large volume of polymer solution (approximately 12 mL) is needed and the measurement takes relatively much longer.

However, in order to confirm the validity of the measurements with the Ubbelohde viscometer, we measured the viscosities as a function of shear rate for 11 polymer solutions pre-sheared at different energy input with a commercial rheometer (MCR-302, Anton Paar GmbH) in a Couette cell (cup ID = 28.92 mm, bob OD = 26.66 mm, gap = 1.18 mm) and calculated the results with Ubbelohde viscosities. The shear rate of the Ubbelohde viscometer can be calculated using the Hagen-Poiseuille equation [132] given by:

$$\dot{\gamma} = \frac{4 \cdot u_D}{R} = \frac{4 \cdot V}{\pi \cdot R^3 \cdot t} \tag{B.11}$$

The calculated viscosity was according to the following equation:

$$\eta = K\rho t \tag{B.12}$$

where K is the Ubbelohde constant and is equal to 0.03 for the used Ubbelohde viscometer.

The viscosity of the un-sheared polymer solution determined with the Ubbelohde viscometer was found to be 12.5 ± 0.6 mPa s. The viscosity of the un-sheared polymer solution was also determined with the shear rheometer from low to high shear rates. The viscosity was measured at four intervals from low to high and then from high to low shear rate and again from low to high and from high to low. This was done to investigate the shape memory of the un-sheared polymer solution. As it is shown in Figure B.7 identical values of viscosity in the four intervals were measured. This means that shearing the polymer solution in the coquette geometry rheometer cell did not change the rheological behaviour. The viscosity curve indicated Newtonian behaviour at low shear rates; however, it was difficult to determine the viscosity data at shear rates smaller than 1 s^{-1} since it was within the range of sensitivity of the rheometer. The Newtonian behaviour was followed by shear-thinning behaviour. The viscosity measured by the Ubbelohde is also shown in Figure B.7, whereby the shear rate is calculated with the Hagen-Poiseuille equation. The slight discrepancy of < 5% between the viscosities measured by the Ubbelohde and the rheometer is within the experimental accuracy of the apparatuses.

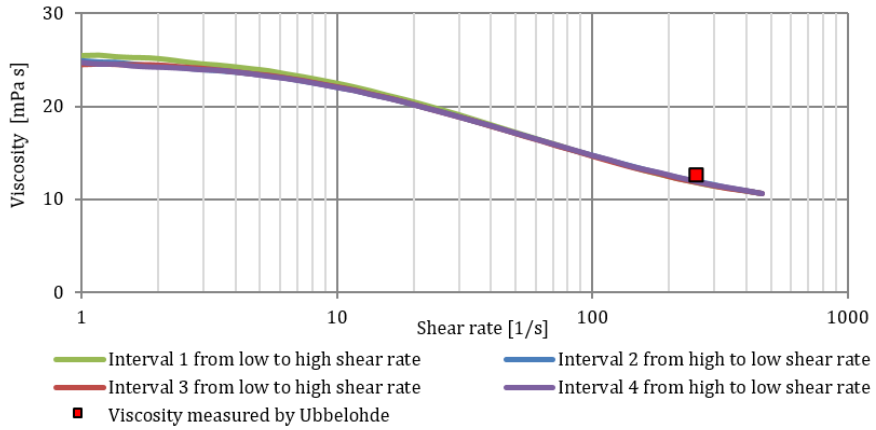

Figure B.7: Viscosity stability at changing shear rate of the un-sheared polymer solution, running the solution from low to high, high to low, low to high, high to low shear rate measured with the Anton Paar rheometer, and viscosity measured with the Ubbelohde viscometer

Figure B.8a shows the viscosity as a function of shear rate for the 11 polymer solutions pre-sheared at different energy input and Figure B.8b shows the correlation between the zero-shear viscosity obtained from the shear rheometer and Ubbelohde viscosity. As can be seen, the viscosity decreased by increasing the energy input regardless of the shearing device. On the other hand, the zero shear rate viscosity increased by a power-law function of Ubbelohde viscosity (see Figure B.8b). Considering the correlation indicated in Figure B.8b, all the viscosity values from the Ubbelohde can be converted to zero-shear rate viscosity.

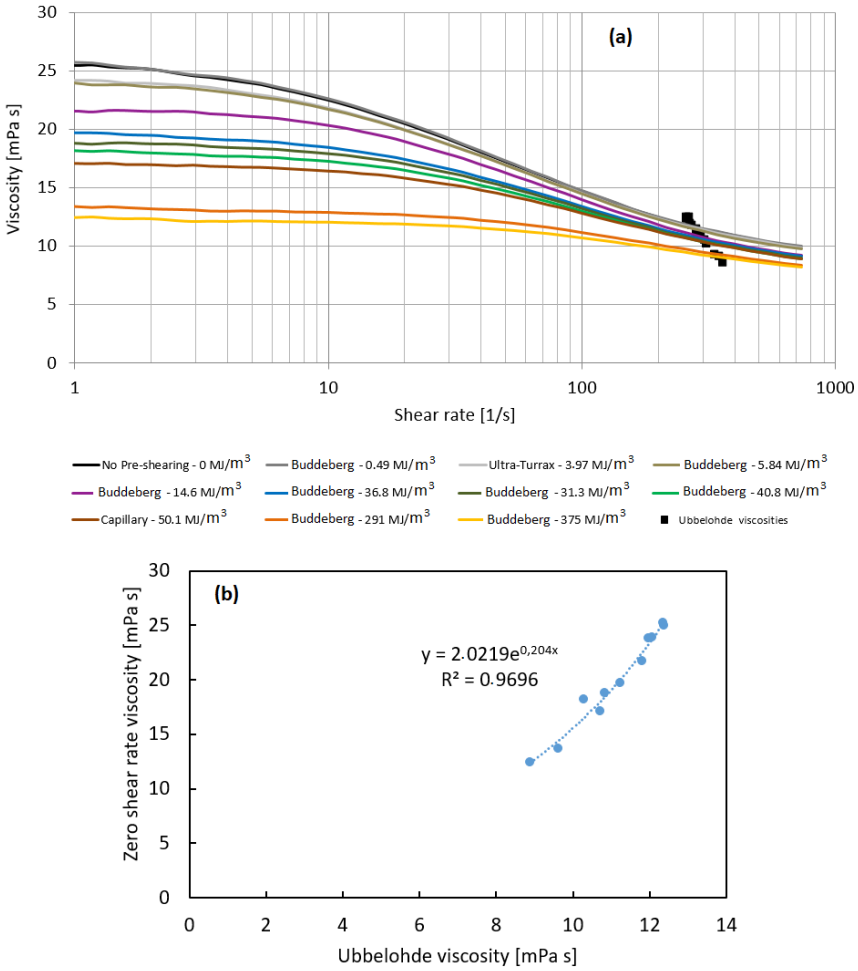

Figure B.8: (a) Viscosity as a function of shear rate measured by the shear rheometer. (b) Zero-shear rate viscosity obtained from the shear rheometer vs. the viscosity measured by the Ubbelohde viscometer

8 REFERENCES

1. Aruga, K.; Islam, M.M.; Jannat, A. Effects of COVID-19 on Indian Energy Consumption. *Sustainability* **2020**, *12*, 5616.
2. Grubler, A.; Johansson, T.; Mundaca, L.; Nakicenovic, N.; Pachauri, S.; Riahi, K.; Rogner, H.; Strupeit, L. Energy Primer. 2012; pp. 99-150.
3. Johnston, R.J., Blakemore, R., Bell, R. *The role of oil and gas companies in energy transition*; Atlantic Council: 2020.
4. Sandrea, I.; Sandrea, R. Global oil reserves - 1: Recovery factors leave vast target for EOR technologies. *OGJ* **2007**, *105*.
5. Muggeridge, A.; Cockin, A.; Webb, K.; Frampton, H.; Collins, I.; Moulds, T.; Salino, P. Recovery rates, enhanced oil recovery and technological limits. *Philos Trans A Math Phys Eng Sci* **2013**, *372*, 20120320-20120320, doi:10.1098/rsta.2012.0320.
6. Smalley, P.C.; Ross, A.W.; Brown, C.; Moulds, T.P.; Smith, M.J. Reservoir Technical Limits: A Framework for Maximizing Recovery From Oil Fields. *SPE-109555-PA* **2009**, *12*, 610-629, doi:10.2118/109555-PA.
7. Kantzas, A., Bryan, J., Taheri, S. *Fundamentals of Fluid Flow in Porous Media*; Perm Inc Tipm laboratory.
8. L.W. Lake, R.J., W. Rossen and G. Pope. *Fundamentals of enhanced oil recovery*; Society of Petroleum Engineers: 2014.
9. Seright, R.S.; Zhang, G.; Akanni, O.O.; Wang, D. A Comparison of Polymer Flooding With In-Depth Profile Modification. In Proceedings of Canadian Unconventional Resources Conference, Calgary, Alberta, Canada, 2011/1/1/; p. 13.
10. Sorbie, K.S. *Polymer-Improved Oil Recovery*; Springer Netherlands: 1991; 10.1007/978-94-011-3044-8.
11. Saleh, L.; Wei, M.; Bai, B. Data Analysis and Updated Screening Criteria for Polymer Flooding Based on Oilfield Data. *SPE-109555-PA* **2014**, *17*, 15-25, doi:10.2118/168220-PA.

12. Abidin, A.Z.; Puspasari, T.; Nugroho, W.A. Polymers for Enhanced Oil Recovery Technology. *Procedia Chemistry* **2012**, *4*, 11-16, doi:https://doi.org/10.1016/j.proche.2012.06.002.
13. Gbadamosi, A.O.; Junin, R.; Manan, M.A.; Agi, A.; Yusuff, A.S. An overview of chemical enhanced oil recovery: recent advances and prospects. *International Nano Letters* **2019**, *9*, 171-202, doi:10.1007/s40089-019-0272-8.
14. Dupuis, D.; Lewandowski, F.Y.; Steiert, P.; Wolff, C. Shear thickening and time-dependent phenomena: the case of polyacrylamide solutions. *Journal of Non-Newtonian Fluid Mechanics* **1994**, *54*, 11-32, doi:https://doi.org/10.1016/0377-0257(94)80013-8.
15. Peng, S.; Wu, C. Light Scattering Study of the Formation and Structure of Partially Hydrolyzed Poly(acrylamide)/Calcium(II) Complexes. *Macromolecules* **1999**, *32*, 585-589, doi:10.1021/ma9809031.
16. Ohmine, I.; Tanaka, T. Salt effects on the phase transition of ionic gels. **1982**, *77*, 5725-5729, doi:10.1063/1.443780.
17. Moradi-Araghi, A.; Doe, P.H. Hydrolysis and Precipitation of Polyacrylamides in Hard Brines at Elevated Temperatures. *SPE-14233-PA* **1987**, *2*, 189-198, doi:10.2118/13033-PA.
18. Campese, G.M.; Rodrigues, E.M.G.; Tambourgi, E.B.; Pessoa Jr, A. Determination of cloud-point temperatures for different copolymers. *Brazilian Journal of Chemical Engineering* **2003**, *20*, 335-337.
19. Al-Shakry, B.; Skauge, T.; Shaker Shiran, B.; Skauge, A. Polymer Injectivity: Investigation of Mechanical Degradation of Enhanced Oil Recovery Polymers Using In-Situ Rheology. *Energies* **2019**, *12*, doi:10.3390/en12010049.
20. Willhite, G.P.; Dominguez, J.G. MECHANISMS OF POLYMER RETENTION IN POROUS MEDIA. In *Improved Oil Recovery by Surfactant and Polymer Flooding*, Shah, D.O., Schechter, R.S., Eds. Academic Press: 1977; https://doi.org/10.1016/B978-0-12-641750-0.50021-9pp. 511-554.
21. Gogarty, W.B. Mobility Control With Polymer Solutions. *SPE-9297-PA* **1967**, *7*, 161-173, doi:10.2118/1566-B.
22. Szabo, M.T. Some Aspects of Polymer Retention in Porous Media Using a C14-Tagged Hydrolyzed Polyacrylamide. *Society of Petroleum Engineers Journal* **1975**, *15*, 323-337, doi:10.2118/4668-PA.

23. Jennings, R.R.; Rogers, J.H.; West, T.J. Factors Influencing Mobility Control By Polymer Solutions. *Journal of Petroleum Technology* **1971**, *23*, 391-401, doi:10.2118/2867-PA.

24. Pye, D.J. Improved Secondary Recovery by Control of Water Mobility. *Journal of Petroleum Technology* **1964**, *16*, 911-916, doi:10.2118/845-PA.

25. Sandiford, B.B. Laboratory and Field Studies of Water Floods Using Polymer Solutions to Increase Oil Recoveries. *Journal of Petroleum Technology* **1964**, *16*, 917-922, doi:10.2118/844-PA.

26. Chang, H.L. Polymer Flooding Technology Yesterday, Today, and Tomorrow. *Journal of Petroleum Technology* **1978**, *30*, 1113-1128, doi:10.2118/7043-PA.

27. Jewett, R.L.; Schurz, G.F. Polymer Flooding-A Current Appraisal. *Journal of Petroleum Technology* **1970**, *22*, 675-684, doi:10.2118/2545-PA.

28. Needham, R.B.; Doe, P.H. Polymer Flooding Review. *Journal of Petroleum Technology* **1987**, *39*, 1503-1507, doi:10.2118/17140-PA.

29. Du, Y.; Guan, L. Field-scale Polymer Flooding: Lessons Learnt and Experiences Gained During Past 40 Years. In Proceedings of SPE International Petroleum Conference in Mexico, Puebla Pue., Mexico, 2004/1/1/; p. 6.

30. Manrique, E.J.; Thomas, C.P.; Ravikiran, R.; Izadi Kamouei, M.; Lantz, M.; Romero, J.L.; Alvarado, V. EOR: Current Status and Opportunities. In Proceedings of SPE Improved Oil Recovery Symposium, Tulsa, Oklahoma, USA, 2010/1/1/; p. 21.

31. Corlay, P.; Lemouzy, P.; Eschard, R.; Zhang, L.R. Fully Integrated Reservoir Study and Numerical Forecast Simulations of Two-Polymer Pilots in Daqing Field. In Proceedings of International Meeting on Petroleum Engineering, Beijing, China, 1992/1/1/; p. 10.

32. Wang, D.; Cheng, J.; Wu, J.; Wang, Y. Producing by Polymer Flooding more than 300 Million Barrels of Oil, What Experiences Have Been Learnt? In Proceedings of SPE Asia Pacific Oil and Gas Conference and Exhibition, Melbourne, Australia, 2002/1/1/; p. 9.

33. Wang, D.; Wang, G.; Xia, H.; Yang, S.; Wu, W. Incremental Recoveries in the Field of Large Scale High Viscous-Elastic Fluid Flooding are Double that of Conventional Polymer Flooding. In Proceedings of SPE Annual Technical Conference and Exhibition, Denver, Colorado, USA, 2011/1/1/; p. 14.

34. Yang, F.; Wang, D.; Yang, X.; Sui, X.; Chen, Q.; Zhang, L. High Concentration Polymer Flooding is Successful. In Proceedings of SPE Asia Pacific Oil and Gas Conference and Exhibition, Perth, Australia, 2004/1/1/; p. 7.
35. Needham, R.B.; Threlkeld, C.B.; Gall, J.W. Control Of Water Mobility Using Polymers and Multivalent Cations. In Proceedings of SPE Improved Oil Recovery Symposium, Tulsa, Oklahoma, 1974/1/1/; p. 10.
36. Standnes, D.C.; Skjevrak, I. Literature review of implemented polymer field projects. *Journal of Petroleum Science and Engineering* **2014**, *122*, 761-775, doi:https://doi.org/10.1016/j.petrol.2014.08.024.
37. Mohsenatabar Firozjaii, A.; Saghafi, H.R. Review on chemical enhanced oil recovery using polymer flooding: Fundamentals, experimental and numerical simulation. *Petroleum* **2019**, https://doi.org/10.1016/j.petlm.2019.09.003, doi:https://doi.org/10.1016/j.petlm.2019.09.003.
38. Rellegadla, S.; Prajapat, G.; Agrawal, A. Polymers for enhanced oil recovery: fundamentals and selection criteria. *Applied Microbiology and Biotechnology* **2017**, *101*, 4387-4402, doi:10.1007/s00253-017-8307-4.
39. Wever, D.A.Z.; Picchioni, F.; Broekhuis, A.A. Polymers for enhanced oil recovery: A paradigm for structure–property relationship in aqueous solution. *Progress in Polymer Science* **2011**, *36*, 1558-1628, doi:https://doi.org/10.1016/j.progpolymsci.2011.05.006.
40. Kamal, M.S.; Sultan, A.S.; Al-Mubaiyedh, U.A.; Hussein, I.A. Review on Polymer Flooding: Rheology, Adsorption, Stability, and Field Applications of Various Polymer Systems. *Polymer Reviews* **2015**, *55*, 491-530, doi:10.1080/15583724.2014.982821.
41. Thomas, A.; Gaillard, N.; Favero, C.J.O.G.S.T.R.I.E.n. Some Key Features to Consider When Studying Acrylamide-Based Polymers for Chemical Enhanced Oil Recovery. **2012**, *67*, 887-902.
42. Scott, A.J.; Romero-Zerón, L.; Penlidis, A. Evaluation of Polymeric Materials for Chemical Enhanced Oil Recovery. **2020**, *8*, 361.
43. Al-Hajri, S.; Mahmood, S.M.; Abdulelah, H.; Akbari, S. An Overview on Polymer Retention in Porous Media. **2018**, *11*, 2751.
44. Scott, A.J.; Romero-Zerón, L.; Penlidis, A. Evaluation of Polymeric Materials for Chemical Enhanced Oil Recovery. *Processes* **2020**, *8*, 361.

45. Chauveteau, G. Fundamental Criteria in Polymer Flow Through Porous Media. In *Water-Soluble Polymers*, American Chemical Society: 1986; Vol. 213, pp. 227-267.

46. Moradi-Araghi, A.; Doe, P.H. Hydrolysis and precipitation of polyacrylamides in hard brines at elevated temperatures. **1987**, 10.2118/13033-PA, doi:10.2118/13033-PA.

47. Ash, S.G.; Clarke-Sturman, A.J.; Calvert, R.; Nisbet, T.M. Chemical Stability of Biopolymer Solutions. In Proceedings of SPE Annual Technical Conference and Exhibition, San Francisco, California, 1983/1/1/; p. 8.

48. Cadmus, M.C.; Jackson, L.K.; Burton, K.A.; Plattner, R.D.; Slodki, M.E. Biodegradation of Xanthan Gum by Bacillus sp. *Applied and environmental microbiology* **1982**, *44*, 5-11.

49. Schulz, D.N.; Kaladas, J.J.; Maurer, J.J.; Bock, J.; Pace, S.J.; Schulz, W.W. Copolymers of acrylamide and surfactant macromonomers: synthesis and solution properties. *Polymer* **1987**, *28*, 2110-2115, doi:https://doi.org/10.1016/0032-3861(87)90050-4.

50. Senan, C.; Meadows, J.; Shone, P.T.; Williams, P.A. Solution Behavior of Hydrophobically Modified Sodium Polyacrylate. *Langmuir* **1994**, *10*, 2471-2479, doi:10.1021/la00019a074.

51. Durand, A.; Hourdet, D. Synthesis and thermoassociative properties in aqueous solution of graft copolymers containing poly(N-isopropylacrylamide) side chains. *Polymer* **1999**, *40*, 4941-4951, doi:https://doi.org/10.1016/S0032-3861(98)00698-3.

52. Levitt, D.; Pope, G.A. Selection and Screening of Polymers for Enhanced-Oil Recovery. In Proceedings of SPE Symposium on Improved Oil Recovery, Tulsa, Oklahoma, USA, 2008/1/1/; p. 18.

53. Doe, P.H.; Moradi-Araghi, A.; Shaw, J.E.; Stahl, G.A. Development and Evaluation of EOR Polymers Suitable for Hostile Environments Part 1: Copolymers of Vinylpyrrolidone and Acrylamide. *SPE-14233-PA* **1987**, *2*, 461-467, doi:10.2118/14233-PA.

54. Klucker, R.; Candau, F.; Schosseler, F. Transient Behavior of Associating Copolymers in a Shear Flow. *Macromolecules* **1995**, *28*, 6416-6422, doi:10.1021/ma00123a005.

55. Soleimani, H.; Baig, M.K.; Yahya, N.; Khodapanah, L.; Sabet, M.; Demiral, B.M.R.; Burda, M. Synthesis of ZnO nanoparticles for oil–water interfacial tension reduction in enhanced oil recovery. *Applied Physics A* **2018**, *124*, 128, doi:10.1007/s00339-017-1510-4.

56. Arab, D.; Kantzas, A.; Bryant, S.L. Nanoparticle stabilized oil in water emulsions: A critical review. *Journal of Petroleum Science and Engineering* **2018**, *163*, 217-242, doi:https://doi.org/10.1016/j.petrol.2017.12.091.

57. Green, D.W.W., G.P. *Enhanced Oil Recovery*; Society of Petroleum Engineers: 1998.

58. Schneider, F.N.; Owens, W.W. Steady-State Measurements of Relative Permeability for Polymer/Oil Systems. *Society of Petroleum Engineers Journal* **1982**, *22*, 79-86, doi:10.2118/9408-PA.

59. Taber, J.J. Technical Screening Guides for the Enhanced Recovery of Oil. In Proceedings of SPE Annual Technical Conference and Exhibition, San Francisco, California, 1983/1/1/; p. 20.

60. Mennella, A.; Chiappa, L.; Bryant, S.L.; Burrafato, G. Pore-scale Mechanism for Selective Permeability Reduction by Polymer Injection. In Proceedings of SPE/DOE Improved Oil Recovery Symposium, Tulsa, Oklahoma, 1998/1/1/; p. 12.

61. Liang, J.-T.; Seright, R.S. Further Investigations of Why Gels Reduce Water Permeability More Than Oil Permeability. *SPE Production & Facilities* **1997**, *12*, 225-230, doi:10.2118/37249-PA.

62. Liang, B.; Jiang, H.; Li, J.; Chen, F.; Miao, W.; Yang, H.; Qiao, Y.; Chen, W. Mechanism Study of Disproportionate Permeability Reduction Using Nuclear Magnetic Resonance T2. *Energy & Fuels* **2018**, *32*, 4959-4968, doi:10.1021/acs.energyfuels.8b00420.

63. Ye, Z.; He, E.; Xie, S.; Han, L.; Chen, H.; Luo, P.; Shu, Z.; Shi, L.; Lai, N. The mechanism study of disproportionate permeability reduction by hydrophobically associating water-soluble polymer gel. *Journal of Petroleum Science and Engineering* **2010**, *72*, 64-66, doi:https://doi.org/10.1016/j.petrol.2010.03.004.

64. Barreau, P.; Bertin, H.; Lasseux, D.; Glénat, P.; Zaitoun, A. Water Control in Producing Wells: Influence of an Adsorbed-Polymer Layer on Relative Permeabilities and Capillary Pressure. *SPE-14233-PA* **1997**, *12*, 234-239, doi:10.2118/35447-PA.

65. Zaitoun, A.; Kohler, N. Two-Phase Flow Through Porous Media: Effect of an Adsorbed Polymer Layer. In Proceedings of SPE Annual Technical Conference and Exhibition, Houston, Texas, 1988/1/1/; p. 14.

66. Wang, D.; Cheng, J.; Yang, Q.; Wenchao, G.; Qun, L.; Chen, F. Viscous-Elastic Polymer Can Increase Microscale Displacement Efficiency in Cores. In Proceedings of SPE Annual Technical Conference and Exhibition, Dallas, Texas, 2000/1/1/; p. 10.

67. Emami Meybodi, H.; Kharrat, R.; Wang, X. Study of Microscopic and Macroscopic Displacement Behaviors of Polymer Solution in Water-Wet and Oil-Wet Media. *Transport in Porous Media* **2011**, *89*, 97-120, doi:10.1007/s11242-011-9754-5.

68. Hou, J.; Li, Z.; Zhang, S.; Cao, X.; Du, Q.; Song, X. Computerized Tomography Study of the Microscopic Flow Mechanism of Polymer Flooding. *Transport in Porous Media* **2009**, *79*, 407-418, doi:10.1007/s11242-008-9330-9.

69. Wei, B.; Romero-Zerón, L.; Rodrigue, D. Oil displacement mechanisms of viscoelastic polymers in enhanced oil recovery (EOR): a review. *Journal of Petroleum Exploration and Production Technology* **2014**, *4*, 113-121, doi:10.1007/s13202-013-0087-5.

70. Sheng, J. *Modern Chemical Enhanced Oil Recovery: Theory and Practice*; Gulf Professional Publishing: 2010.

71. Moan, M.; Chauveteau, G.; Ghoniem, S. Entrance effect in capillary flow of dilute and semi-dilute polymer solutions. *Journal of Non-Newtonian Fluid Mechanics* **1979**, *5*, 463-474, doi:https://doi.org/10.1016/0377-0257(79)85030-2.

72. Chauveteau, G.; Moan, M.; Magueur, A. Thickening behaviour of dilute polymer solutions in non-inertial elongational flows. *Journal of Non-Newtonian Fluid Mechanics* **1984**, *16*, 315-327, doi:https://doi.org/10.1016/0377-0257(84)85017-X.

73. Hoa, N.T.C., G.; Gaudu, R.; Anne-Archard, D. Relation entre le champ de vitesse d' elongation et l'apparition d'un comportement dilatant d'une solution de polymere diluee dans un ecoulement convergent non-inertiel. *C. R. Acad. Sci. Paris* **1982**, *294*.

74. Mirzaie Yegane, M.; Schmidt, J.; Dugonjic-Bilic, F.; Gerlach, B.; Boukany, P.E.; Zitha, P.L.J. Flow Enhancement of Water-Soluble Polymers through Porous

Media by Preshearing. *Industrial & Engineering Chemistry Research* **2021**, *60*, 3463-3473, doi:10.1021/acs.iecr.1c00099.

75. Delshad, M.; Kim, D.H.; Magbagbeola, O.A.; Huh, C.; Pope, G.A.; Tarahhom, F. Mechanistic Interpretation and Utilization of Viscoelastic Behavior of Polymer Solutions for Improved Polymer-Flood Efficiency. In Proceedings of SPE Symposium on Improved Oil Recovery, Tulsa, Oklahoma, USA, 2008/1/1/; p. 15.
76. Stavland, A.; Jonsbraten, H.; Lohne, A.; Moen, A.; Giske, N.H. Polymer Flooding - Flow Properties in Porous Media versus Rheological Parameters. In Proceedings of SPE EUROPEC/EAGE Annual Conference and Exhibition, Barcelona, Spain, 2010/1/1/; p. 15.
77. Kawale, D.; Bouwman, G.; Sachdev, S.; Zitha, P.L.J.; Kreutzer, M.T.; Rossen, W.R.; Boukany, P.E. Polymer conformation during flow in porous media. *Soft Matter* **2017**, *13*, 8745-8755, doi:10.1039/C7SM00817A.
78. Skauge, A.; Zamani, N.; Gausdal Jacobsen, J.; Shaker Shiran, B.; Al-Shakry, B.; Skauge, T. Polymer Flow in Porous Media: Relevance to Enhanced Oil Recovery. *Colloids and Interfaces* **2018**, *2*, 27.
79. Al-Shakry, B.; Skauge, T.; Shaker Shiran, B.; Skauge, A. Impact of Mechanical Degradation on Polymer Injectivity in Porous Media. *Polymers* **2018**, *10*, 742, doi:10.3390/polym10070742.
80. Browne, C.A.; Shih, A.; Datta, S.S. Pore-Scale Flow Characterization of Polymer Solutions in Microfluidic Porous Media. *Small* **2020**, *16*, 1903944, doi:10.1002/smll.201903944.
81. Chauveteau, G.; Moan, M. The onset of dilatant behaviour in non-inertial flow of dilute polymer solutions through channels with varying cross-sections. *J. Physique Lett.* **1981**, *42*, 201-204.
82. Flew, S.; Sellin, R.H.J. Non-Newtonian flow in porous media-a laboratory study of polyacrylamide solutions. *Journal of Non-Newtonian Fluid Mechanics* **1993**, *47*, 169-210, doi:https://doi.org/10.1016/0377-0257(93)80050-L.
83. Durst, F.; Haas, R.; Interthal, W. The nature of flows through porous media. *Journal of Non-Newtonian Fluid Mechanics* **1987**, *22*, 169-189, doi:https://doi.org/10.1016/0377-0257(87)80034-4.
84. Haas, R.; Durst, F. Viscoelastic flow of dilute polymer solutions in regularly packed beds. *Rheologica Acta* **1982**, *21*, 566-571, doi:10.1007/BF01534349.

85. Kawale, D.; Marques, E.; Zitha, P.L.J.; Kreutzer, M.T.; Rossen, W.R.; Boukany, P.E. Elastic instabilities during the flow of hydrolyzed polyacrylamide solution in porous media: effect of pore-shape and salt. *Soft Matter* **2017**, *13*, 765-775, doi:10.1039/C6SM02199A.

86. Gennes, P.G.D. Coil - stretch transition of dilute flexible polymers under ultrahigh velocity gradients. **1974**, *60*, 5030-5042, doi:10.1063/1.1681018.

87. Zimm, B.H. Dynamics of Polymer Molecules in Dilute Solution: Viscoelasticity, Flow Birefringence and Dielectric Loss. **1956**, *24*, 269-278, doi:10.1063/1.1742462.

88. Larson, R.G.; Magda, J.J. Coil-stretch transitions in mixed shear and extensional flows of dilute polymer solutions. *Macromolecules* **1989**, *22*, 3004-3010, doi:10.1021/ma00197a022.

89. Perkins, T.T.; Smith, D.E.; Chu, S. Single Polymer Dynamics in an Elongational Flow. *Science* **1997**, *276*, 2016, doi:10.1126/science.276.5321.2016.

90. Shaqfeh, E.S.G. The dynamics of single-molecule DNA in flow. *Journal of Non-Newtonian Fluid Mechanics* **2005**, *130*, 1-28, doi:https://doi.org/10.1016/j.jnnfm.2005.05.011.

91. Sachdev, S.; Muralidharan, A.; Boukany, P.E. Molecular Processes Leading to "Necking" in Extensional Flow of Polymer Solutions: Using Microfluidics and Single DNA Imaging. *Macromolecules* **2016**, *49*, 9578-9585, doi:10.1021/acs.macromol.6b01755.

92. Odell, J.; Müller, A.; Keller, A. Non-Newtonian Behaviour of Hydrolysed Polyacrylamide in Strong Elongational Flows: A Transient Network Approach. *Polymer* **1988**, *29*, 1179-1190, doi:10.1016/0032-3861(88)90042-0.

93. Wang, S.Q. Transient network theory for shear-thickening fluids and physically crosslinked networks. *Macromolecules* **1992**, *25*, 7003-7010, doi:10.1021/ma00051a043.

94. Galindo-Rosales, F.; Campo-Deaño, L.; Pinho, F.; van Bokhorst, E.; Hamersma, P.; Oliveira, M.; Alves, M. Microfluidic systems for the analysis of viscoelastic fluid flow phenomena in porous media. *Microfluidics and Nanofluidics* **2011**, *12*, 485-498, doi:10.1007/s10404-011-0890-6.

95. Howe, A.M.; Clarke, A.; Giernalczyk, D. Flow of concentrated viscoelastic polymer solutions in porous media: effect of MW and concentration on elastic

turbulence onset in various geometries. *Soft Matter* **2015**, *11*, 6419-6431, doi:10.1039/C5SM01042J.

96. Machado, A.; Bodiguel, H.; Beaumont, J.; Clisson, G.; Colin, A. Extra dissipation and flow uniformization due to elastic instabilities of shear-thinning polymer solutions in model porous media. **2016**, *10*, 043507, doi:10.1063/1.4954813.
97. Müller, A.; Sáez, A. The Rheology of Polymer Solutions in Porous Media. 1999; 10.1007/978-3-642-58252-3_11pp. 335-393.
98. Skauge, A.; Zamani, N.; Gausdal Jacobsen, J.; Shaker Shiran, B.; Al-Shakry, B.; Skauge, T. Polymer Flow in Porous Media: Relevance to Enhanced Oil Recovery. **2018**, *2*, 27.
99. Sadowski, T.J. Non - Newtonian Flow through Porous Media. II. Experimental. **1965**, *9*, 251-271, doi:10.1122/1.549023.
100. Sorbie, K.S.; Clifford, P.J.; Jones, E.R.W. The rheology of pseudoplastic fluids in porous media using network modeling. *Journal of Colloid and Interface Science* **1989**, *130*, 508-534, doi:https://doi.org/10.1016/0021-9797(89)90128-8.
101. Pearson, J.R.A.; Tardy, P.M.J. Models for flow of non-Newtonian and complex fluids through porous media. *Journal of Non-Newtonian Fluid Mechanics* **2002**, *102*, 447-473, doi:https://doi.org/10.1016/S0377-0257(01)00191-4.
102. Lopez, X.; Valvatne, P.H.; Blunt, M.J. Predictive network modeling of single-phase non-Newtonian flow in porous media. *Journal of Colloid and Interface Science* **2003**, *264*, 256-265, doi:https://doi.org/10.1016/S0021-9797(03)00310-2.
103. Savins, J.G. NON-NEWTONIAN FLOW THROUGH POROUS MEDIA. *Industrial & Engineering Chemistry* **1969**, *61*, 18-47, doi:10.1021/ie50718a005.
104. Sochi, T. Non-Newtonian flow in porous media. *Polymer* **2010**, *51*, 5007-5023, doi:https://doi.org/10.1016/j.polymer.2010.07.047.
105. Shenoy, A.V. Darcy-Forchheimer natural, forced and mixed convection heat transfer in non-Newtonian power-law fluid-saturated porous media. *Transport in Porous Media* **1993**, *11*, 219-241, doi:10.1007/BF00614813.
106. Schümmer, P. Mechanics of Non-Newtonian Fluids. Von W. R. Schowalter. Pergamon Press, Oxford–Frankfurt 1978. 1. Aufl., IX, 300 S., zahlr. Abb. u. Tab., geb., $ 35.00. **1979**, *51*, 766-766, doi:10.1002/cite.330510727.
107. McCabe, W.S., J; Harriott, P. *Unit Operations of Chemical Engineering (7th edition)*; McGraw-Hill Education: New York, 2004; pp. 1168 pages.

108. Scheidegger, A.E. Theoritical models of porous matter. *Producers Monthly, No. 10, 17* **1953**.

109. Sadowski, T.J.; Bird, R.B. Non - Newtonian Flow through Porous Media. I. Theoretical. **1965**, *9*, 243-250, doi:10.1122/1.549000.

110. Duda, J.L.; Hong, S.A.; Klaus, E.E. Flow of polymer solutions in porous media: inadequacy of the capillary model. *Industrial & Engineering Chemistry Fundamentals* **1983**, *22*, 299-305, doi:10.1021/i100011a005.

111. Dullien, F.A.L. 1 - Pore Structure. In *Porous Media (Second Edition)*, Dullien, F.A.L., Ed. Academic Press: San Diego, 1992; https://doi.org/10.1016/B978-0-12-223651-8.50007-9pp. 5-115.

112. Sorbie, K.S. Network Modeling of Xanthan Rheology in Porous Media in the Presence of Depleted Layer Effects. In Proceedings of SPE Annual Technical Conference and Exhibition, San Antonio, Texas, 1989/1/1/; p. 14.

113. Sochi, T. Pore-Scale Modeling of Non-Newtonian Flow in Porous Media. **2010**.

114. Marker, J.M. Dependence of Polymer Retention on Flow Rate. *Journal of Petroleum Technology* **1973**, *25*, 1307-1308, doi:10.2118/4423-PA.

115. Huh, C.; Lange, E.A.; Cannella, W.J. Polymer Retention in Porous Media. In Proceedings of SPE/DOE Enhanced Oil Recovery Symposium, Tulsa, Oklahoma, 1990/1/1/; p. 20.

116. Stutzmann, T.; Siffert, B. Contribution to the Adsorption Mechanism of Acetamide and Polyacrylamide on to Clays. *Clays and Clay Minerals* **1977**, *25*, 392-406, doi:10.1346/CCMN.1977.0250604.

117. Pefferkorn, E.; Nabzar, L.; Carroy, A. Adsorption of polyacrylamide to Na kaolinite: Correlation between clay structure and surface properties. *Journal of Colloid and Interface Science* **1985**, *106*, 94-103, doi:https://doi.org/10.1016/0021-9797(85)90384-4.

118. Shah, S.; Heinle, S.A.; Glass, J.E. Water-Soluble Polymer Adsorption From Saline Solutions. In Proceedings of SPE Oilfield and Geothermal Chemistry Symposium, Phoenix, Arizona, 1985/1/1/; p. 10.

119. Lee, J.-J.; Fuller, G.G. Adsorption and desorption of flexible polymer chains in flowing systems. *Journal of Colloid and Interface Science* **1985**, *103*, 569-577, doi:https://doi.org/10.1016/0021-9797(85)90132-8.

120. Zitha, P.L.J.; Chauveteau, G.; Léger, L. Unsteady-State Flow of Flexible Polymers in Porous Media. *Journal of Colloid and Interface Science* **2001**, *234*, 269-283, doi:https://doi.org/10.1006/jcis.2000.7306.

121. Cohen, Y.; Christ, F.R. Polymer Retention and Adsorption in the Flow of Polymer Solutions Through Porous Media. *SPE-14233-PA* **1986**, *1*, 113-118, doi:10.2118/12942-PA.

122. Dawson, R.; Lantz, R.B. Inaccessible Pore Volume in Polymer Flooding. *Society of Petroleum Engineers Journal* **1972**, *12*, 448-452, doi:10.2118/3522-PA.

123. Liauh, W.C.; Duda, J.L.; Klaus, E.E. An Investigation Of The Inaccessible Pore Volume Phenomena. Society of Petroleum Engineers: 1979; NAp 23.

124. DiMarzio, E.A.; Guttman, C.M. Separation by Flow. *Macromolecules* **1970**, *3*, 131-146, doi:10.1021/ma60014a005.

125. Chauveteau, G.; Kohler, N. Influence of Microgels in Polysaccharide Solutions on Their Flow Behavior Through Porous Media. *Society of Petroleum Engineers Journal* **1984**, *24*, 361-368, doi:10.2118/9295-PA.

126. Kolodziej, E.J. Mechanism of Microgel Formation in Xanthan Biopolymer Solutions. In Proceedings of SPE Annual Technical Conference and Exhibition, Dallas, Texas, 1987/1/1/; p. 16.

127. van Domselaar, H.R.; Fortmuller, C. On the Transport Properties of a Rod-Type Polymer in Sand Packs. In Proceedings of European Petroleum Conference, Cannes, France, 1992/1/1/; p. 9.

128. Lotsch, T.; Muller, T.; Pusch, G. The Effect of Inaccessible Pore Volume on Polymer Coreflood Experiments. In Proceedings of SPE Oilfield and Geothermal Chemistry Symposium, Phoenix, Arizona, 1985/1/1/; p. 10.

129. Hughes, D.S.; Teeuw, D.; Cottrell, C.W.; Tollas, J.M. Appraisal of the Use of Polymer Injection To Suppress Aquifer Influx and To Improve Volumetric Sweep in a Viscous Oil Reservoir. *SPE-14233-PA* **1990**, *5*, 33-40, doi:10.2118/17400-PA.

130. Osterloh, W.T.; Law, E.J. Polymer Transport and Rheological Properties for Polymer Flooding in the North Sea. In Proceedings of SPE/DOE Improved Oil Recovery Symposium, Tulsa, Oklahoma, 1998/1/1/; p. 12.

131. Documentation., U.T. Volume II Documentation for UTCHEM 2017_3: A Three-Dimensional Chemical Flood Simulator. **2017**.

132. Seright, R.S. The Effects of Mechanical Degradation and Viscoelastic Behavior on Injectivity of Polyacrylamide Solutions. *Society of Petroleum Engineers Journal* **1983**, *23*, 475-485, doi:10.2118/9297-PA.

133. Wei, B.; Romero-Zerón, L.; Rodrigue, D. Mechanical Properties and Flow Behavior of Polymers for Enhanced Oil Recovery. *Journal of Macromolecular Science, Part B* **2014**, *53*, 625-644, doi:10.1080/00222348.2013.857546.

134. Liang, K.; Han, P.; Chen, Q.; Su, X.; Feng, Y. Comparative Study on Enhancing Oil Recovery under High Temperature and High Salinity: Polysaccharides Versus Synthetic Polymer. *ACS omega* **2019**, *4*, 10620-10628, doi:10.1021/acsomega.9b00717.

135. Lakatos, I.; Lakatos-Szabó, J.; Tóth, J. Factors Influencing Polyacrylamide Adsorption in Porous Media and Their Effect on Flow Behavior. In *Surface Phenomena in Enhanced Oil Recovery*, Shah, D.O., Ed. Springer US: Boston, MA, 1981; 10.1007/978-1-4757-0337-5_37pp. 821-842.

136. Lecourtier, J.; Lee, L.T.; Chauveteau, G. Adsorption of polyacrylamides on siliceous minerals. *Colloids and Surfaces* **1990**, *47*, 219-231, doi:https://doi.org/10.1016/0166-6622(90)80074-E.

137. Szabo, M.T. An Evaluation of Water-Soluble Polymers For Secondary Oil Recovery - Parts 1 and 2. *Journal of Petroleum Technology* **1979**, *31*, 553-570, doi:10.2118/6601-PA.

138. Vermolen, E.C.M.; Van Haasterecht, M.J.T.; Masalmeh, S.K.; Faber, M.J.; Boersma, D.M.; Gruenenfelder, M.A. Pushing the envelope for polymer flooding towards high-temperature and high-salinity reservoirs with polyacrylamide based ter-polymers. In Proceedings of SPE Middle East Oil and Gas Show and Conference, Manama, Bahrain, 2011/1/1/; p. 9.

139. Dong, H.; Fang, S.; Wang, D.; Wang, J.; Liu, Z.L.; Hou, W. Review of Practical Experience & Management by Polymer Flooding at Daqing. In Proceedings of SPE Symposium on Improved Oil Recovery, Tulsa, Oklahoma, USA, 2008/1/1/; p. 18.

140. Zhang, X.; Pan, F.; Guan, W.; Li, D.; Li, X.; Guo, S. A Novel Method of Optimizing the Moelcular Weight of Polymer Flooding. In Proceedings of SPE Enhanced Oil Recovery Conference, Kuala Lumpur, Malaysia, 2011/1/1/; p. 4.

141. Odell, J.A.; Muller, A.J.; Narh, K.A.; Keller, A. Degradation of polymer solutions in extensional flows. *Macromolecules* **1990**, *23*, 3092-3103, doi:10.1021/ma00214a011.

142. Nguyen, T.Q.; Kausch, H.H. Effects of solvent viscosity on polystyrene degradation in transient elongational flow. *Macromolecules* **1990**, *23*, 5137-5145, doi:10.1021/ma00226a017.

143. Buchholz, B.A.; Zahn, J.M.; Kenward, M.; Slater, G.W.; Barron, A.E. Flow-induced chain scission as a physical route to narrowly distributed, high molar mass polymers. *Polymer* **2004**, *45*, 1223-1234, doi:https://doi.org/10.1016/j.polymer.2003.11.051.

144. Kuijpers, M.W.A.; Iedema, P.D.; Kemmere, M.F.; Keurentjes, J.T.F. The mechanism of cavitation-induced polymer scission; experimental and computational verification. *Polymer* **2004**, *45*, 6461-6467, doi:https://doi.org/10.1016/j.polymer.2004.06.051.

145. Sivalingam, G.; Agarwal, N.; Madras, G. Distributed midpoint chain scission in ultrasonic degradation of polymers. *AIChE Journal* **2004**, *50*, 2258-2265, doi:10.1002/aic.10185.

146. Dang, T.Q.C.; Chen, Z.; Nguyen, T.B.N.; Bae, W. Investigation of Isotherm Polymer Adsorption in Porous Media. *Petroleum Science and Technology* **2014**, *32*, 1626-1640, doi:10.1080/10916466.2010.547910.

147. Yang, C.Z.Y., H.K.; Li, G.Z.; Cui, G.Z.; Yuan, H. Adsorption mechanisms and chromatographic separation. In *Yu, J.Y.; Song, W.C.; Li, Z.P. et al. (Eds.), Fundamentals and Advances in Combined Chemical Flooding*, China Petrochemical Press.: 2002.

148. Lipatov, Y.S.S., L.M. *Adsorption of Polymers*; Wiley: 1974.

149. Gramain, P.; Myard, P. Adsorption studies of polyacrylamides in porous media. *Journal of Colloid and Interface Science* **1981**, *84*, 114-126, doi:https://doi.org/10.1016/0021-9797(81)90265-4.

150. Zhang, G.; Seright, R. Effect of Concentration on HPAM Retention in Porous Media. *SPE Journal* **2014**, *19*, 373-380, doi:10.2118/166265-PA.

151. Deng, Y.; Dixon, J.B.; White, G.N. Adsorption of Polyacrylamide on Smectite, Illite, and Kaolinite. *Soil Science Society of America Journal* **2006**, *70*, 297-304, doi:https://doi.org/10.2136/sssaj2005.0200.

152. Zheng, C.G.; Gall, B.L.; Gao, H.W.; Miller, A.E.; Bryant, R.S. Effects of Polymer Adsorption and Flow Behavior on Two-Phase Flow in Porous Media. *SPE-109555-PA* **2000**, *3*, 216-223, doi:10.2118/64270-PA.

153. Müller, A.J.; Odell, J.A.; Carrington, S. Degradation of semidilute polymer solutions in elongational flows. *Polymer* **1992**, *33*, 2598-2604, doi:https://doi.org/10.1016/0032-3861(92)91143-P.

154. Smith, F.W. The Behavior of Partially Hydrolyzed Polyacrylamide Solutions in Porous Media. *Journal of Petroleum Technology* **1970**, *22*, 148-156, doi:10.2118/2422-PA.

155. Vela, S.; Peaceman, D.W.; Sandvik, E.I. Evaluation of Polymer Flooding in a Layered Reservoir With Crossflow, Retention, and Degradation. *Society of Petroleum Engineers Journal* **1976**, *16*, 82-96, doi:10.2118/5102-PA.

156. Seright, R.S. Impact of Permeability and Lithology on Gel Performance. In Proceedings of SPE/DOE Enhanced Oil Recovery Symposium, Tulsa, Oklahoma, 1992/1/1/; p. 11.

157. Seright, R.S.; Martin, F.D. Impact of Gelation pH, Rock Permeability, and Lithology on the Performance of a Monomer-Based Gel. *SPE-14233-PA* **1993**, *8*, 43-50, doi:10.2118/20999-PA.

158. Broseta, D.; Medjahed, F.; Lecourtier, J.; Robin, M. Polymer Adsorption/Retention in Porous Media: Effects of Core Wettability and Residual Oil. *SPE Advanced Technology Series* **1995**, *3*, 103-112, doi:10.2118/24149-PA.

159. Kolodziej, E.J. Transport Mechanisms of Xanthan Biopolymer Solutions in Porous Media. In Proceedings of SPE Annual Technical Conference and Exhibition, Houston, Texas, 1988/1/1/; p. 16.

160. Sulpizi, M.; Gaigeot, M.-P.; Sprik, M. The Silica–Water Interface: How the Silanols Determine the Surface Acidity and Modulate the Water Properties. *Journal of Chemical Theory and Computation* **2012**, *8*, 1037-1047, doi:10.1021/ct2007154.

161. Tschapek, M. The Point of Zero Charge (pzc) of Kaolinite and SiO2 + Al2O3 Mixtures. *Clay Minerals* **1974**, *10*, 219-229, doi:10.1180/claymin.1974.010.4.01.

162. Farooq, U.; Tweheyo, M.T.; Sjöblom, J.; Øye, G. Surface Characterization of Model, Outcrop, and Reservoir Samples in Low Salinity Aqueous Solutions. *Journal of Dispersion Science and Technology* **2011**, *32*, 519-531, doi:10.1080/01932691003756936.

163. Peksa, A.E.; Wolf, K.-H.A.A.; Zitha, P.L.J. Bentheimer sandstone revisited for experimental purposes. *Marine and Petroleum Geology* **2015**, *67*, 701-719, doi:https://doi.org/10.1016/j.marpetgeo.2015.06.001.

164. Gkay, D.H.; Rex, R.W. FORMATION DAMAGE IN SANDSTONES CAUSED BY CLAY DISPERSION AND MIGRATION. In *Clays and Clay Minerals*, Bailey, S.W., Ed. Pergamon: 1966; https://doi.org/10.1016/B978-0-08-011908-3.50033-5pp. 355-366.

165. Simon, D.E.; McDaniel, B.W.; Coon, R.M. Evaluation of Fluid pH Effects on Low Permeability Sandstones. In Proceedings of SPE Annual Fall Technical Conference and Exhibition, New Orleans, Louisiana, 1976/1/1/; p. 12.

166. Appel, C.; Ma, L.Q.; Dean Rhue, R.; Kennelley, E. Point of zero charge determination in soils and minerals via traditional methods and detection of electroacoustic mobility. *Geoderma* **2003**, *113*, 77-93, doi:https://doi.org/10.1016/S0016-7061(02)00316-6.

167. Morris, E.R.; Rees, D.A.; Young, G.; Walkinshaw, M.D.; Darke, A. Order-disorder transition for a bacterial polysaccharide in solution. A role for polysaccharide conformation in recognition between Xanthomonas pathogen and its plant host. *Journal of Molecular Biology* **1977**, *110*, 1-16, doi:https://doi.org/10.1016/S0022-2836(77)80095-8.

168. Dentini, M.; Crescenzi, V.; Blasi, D. Conformational properties of xanthan derivatives in dilute aqueous solution. *International Journal of Biological Macromolecules* **1984**, *6*, 93-98, doi:https://doi.org/10.1016/0141-8130(84)90070-9.

169. Holzwarth, G. Conformation of the extracellular polysaccharide of Xanthomonas campestris. *Biochemistry* **1976**, *15*, 4333-4339, doi:10.1021/bi00664a030.

170. Kierulf, C.; Sutherland, I.W. Thermal stability of xanthan preparations. *Carbohydrate Polymers* **1988**, *9*, 185–194, doi:10.1016/0144-8617(88)90024-0.

171. Sabhapondit, A.; Borthakur, A.; Haque, I. Characterization of acrylamide polymers for enhanced oil recovery. *Journal of Applied Polymer Science* **2003**, *87*, 1869-1878, doi:10.1002/app.11491.

172. Zhong, C.; Luo, P.; Ye, Z.; Chen, H. Characterization and Solution Properties of a Novel Water-soluble Terpolymer For Enhanced Oil Recovery. *Polymer Bulletin* **2009**, *62*, 79-89, doi:10.1007/s00289-008-1007-6.

173. Wu, G.; Yu, L.; Jiang, X. Synthesis and properties of an acrylamide-based polymer for enhanced oil recovery: A preliminary study. *Advances in Polymer Technology* **2018**, *37*, 2763-2773, doi:10.1002/adv.21949.

174. Gao, C.; Shi, J.; Zhao, F. Successful polymer flooding and surfactant-polymer flooding projects at Shengli Oilfield from 1992 to 2012. *Journal of Petroleum Exploration and Production Technology* **2014**, *4*, 1-8, doi:10.1007/s13202-013-0069-7.

175. Saleh, L.; Wei, M.; Bai, B. Data Analysis and Novel Screening Criteria for Polymer Flooding Based on a Comprehensive Database. In Proceedings of SPE Improved Oil Recovery Symposium, Tulsa, Oklahoma, USA, 2014/4/12/; p. 18.

176. Morel, D.C.; Vert, M.; Jouenne, S.; Gauchet, R.; Bouger, Y. First Polymer Injection in Deep Offshore Field Angola: Recent Advances in the Dalia/Camelia Field Case. *Oil and Gas Facilities* **2012**, *1*, 43-52, doi:10.2118/135735-PA.

177. Morel, D.C.; Jouenne, S.; Vert, M.; Nahas, E. Polymer Injection in Deep Offshore Field: The Dalia Angola Case. In Proceedings of SPE Annual Technical Conference and Exhibition, Denver, Colorado, USA, 2008/1/1/; p. 12.

178. Leonhardt, B.; Santa, M.; Steigerwald, A.; Kaeppler, T. Polymer Flooding with the Polysaccharide Schizophyllan - First Field Trial Results. **2013**, 10.3997/2214-4609.20142599, doi:10.3997/2214-4609.20142599.

179. Prasad, D.; Ernst, B.; Incera, G.; Leonhardt, B.; Reimann, S.; Mahler, E.; Zarfl, M. Field Testing the Polysaccharide Schizophyllan - Single Well Test Design and Current Results.

180. Wassmuth, F.R.; Green, K.; Arnold, W.; Cameron, N. Polymer Flood Application to Improve Heavy Oil Recovery at East Bodo. *Journal of Canadian Petroleum Technology* **2009**, *48*, 55-61, doi:10.2118/09-02-55.

181. Delamaide, E.; Zaitoun, A.; Renard, G.; Tabary, R. Pelican Lake Field: First Successful Application of Polymer Flooding In a Heavy-Oil Reservoir. *SPE-109555-PA* **2014**, *17*, 340-354, doi:10.2118/165234-PA.

182. Zhou, W.; Zhang, J.; Han, M.; Xiang, W.; Feng, G.; Jiang, W. Application of Hydrophobically Associating Water-soluble Polymer for Polymer Flooding in China Offshore Heavy Oilfield. In Proceedings of International Petroleum Technology Conference, Dubai, U.A.E., 2007/1/1/; p. 5.

183. Demin, W.; Zhang, Z.; Chun, L.; Cheng, J.; Du, X.; Li, Q. A Pilot for Polymer Flooding of Saertu Formation S II 10-16 in the North of Daqing Oil Field. In

Proceedings of SPE Asia Pacific Oil and Gas Conference, Adelaide, Australia, 1996/1/1/; p. 11.

184. Liu, B.; Sun, X.S.; Wang, K.; Xu, H.; Liu, Q.; Liu, X.; Song, S. Flooded by High Concentration Polymer Doubled Oil Recovery of Common Polymer on Field Test with 20% Closed to the Result of Lab Test in Daqing. In Proceedings of International Oil Conference and Exhibition in Mexico, Veracruz, Mexico, 2007/1/1/; p. 9.
185. Kang, X.; Zhang, J.; Sun, F.; Zhang, F.; Feng, G.; Yang, J.; Zhang, X.; Xiang, W. A Review of Polymer EOR on Offshore Heavy Oil Field in Bohai Bay, China. **2011**, 10.2118/144932-MS, doi:10.2118/144932-MS.
186. He, J.; Song, Z.; Qiu, L.; Xie, F.; Tan, Z.; Yue, Q.; Li, X. High Temperature Polymer Flooding in Thick Reservoir in ShuangHe Oilfield. In Proceedings of SPE International Oil and Gas Conference and Exhibition in China, Beijing, China, 1998/1/1/; p. 11.
187. de Melo, M.A.; Holleben, C.R.; Silva, I.G.; de Barros Correia, A.; Silva, G.A.; Rosa, A.J.; Lins, A.G., Jr.; de Lima, J.C. Evaluation of Polymer-Injection Projects in Brazil. In Proceedings of SPE Latin American and Caribbean Petroleum Engineering Conference, Rio de Janeiro, Brazil, 2005/1/1/; p. 17.
188. de Melo, M.A.; da Silva, I.P.G.; de Godoy, G.M.R.; Sanmartim, A.N. Polymer Injection Projects in Brazil: Dimensioning, Field Application and Evaluation. In Proceedings of SPE/DOE Improved Oil Recovery Symposium, Tulsa, Oklahoma, 2002/1/1/; p. 11.
189. Al-saadi, F.S.; Al-amri, B.A.; Al Nofli, S.M.; Van Wunnik, J.N.M.; Jaspers, H.F.; Al Harthi, S.; Shuaili, K.; Cherukupalli, P.K.; Chakravarthi, R. Polymer Flooding in a Large Field in South Oman - Initial Results and Future Plans. In Proceedings of SPE EOR Conference at Oil and Gas West Asia, Muscat, Oman, 2012/1/1/; p. 7.
190. Koning, E.J.L.; Mentzer, E.; Heemskerk, J. Evaluation of a Pilot Polymer Flood in the Marmul Field, Oman. In Proceedings of SPE Annual Technical Conference and Exhibition, Houston, Texas, 1988/1/1/; p. 9.
191. Moe Soe Let, K.P.; Manichand, R.N.; Seright, R.S. Polymer Flooding a ~500-cp Oil. In Proceedings of SPE Improved Oil Recovery Symposium, Tulsa, Oklahoma, USA, 2012/1/1/; p. 13.

192. Kumar, P.; Raj, R.; Koduru, N.; Kumar, S.; Pandey, A. Field Implementation of Mangala Polymer Flood: Initial Challenges, Mitigation and Management. In Proceedings of SPE EOR Conference at Oil and Gas West Asia, Muscat, Oman, 2016/3/21/; p. 20.

193. Mehta, N.; Kapadia, G.; Selvam, V. *Challenges in Full Field Polymer Injection Mangala in Field*; 2016; 10.2118/179807-MS.

194. Peiffer, D.G. Hydrophobically associating polymers and their interactions with rod-like micelles. *Polymer* **1990**, *31*, 2353-2360, doi:https://doi.org/10.1016/0032-3861(90)90324-R.

195. Zhuang, D.-q.; Ai-hua Da, J.C.; Zhang, Y.-x.; Dieing, R.; Ma, L.; Haeussling, L. Hydrophobically modified polyelectrolytes II: synthesis and characterization of poly(acrylic acid-co-alkyl acrylate). **2001**, *12*, 616-625, doi:10.1002/pat.79.

196. Zhou, H.; Song, G.-Q.; Zhang, Y.-X.; Chen, J.; Jiang, M.; Hogen-Esch, T.E.; Dieing, R.; Ma, L.; Haeussling, L. Hydrophobically Modified Polyelectrolytes, 4. Synthesis and Solution Properties of Fluorocarbon-Containing Poly(acrylic acid). **2001**, *202*, 3057-3064, doi:10.1002/1521-3935(20011001)202:15<3057::Aid-macp3057>3.0.Co;2-5.

197. Abu-Sharkh, B.F.; Yahaya, G.O.; Ali, S.A.; Kazi, I.W. Solution and interfacial behavior of hydrophobically modified water-soluble block copolymers of acrylamide and N-phenethylacrylamide. **2001**, *82*, 467-476, doi:10.1002/app.1873.

198. McCormick, C.L.; Johnson, C.B. Water-Soluble Polymers. XXXIV. Ampholyte Terpolymers of Sodium 3-Acrylamido-3-Methylbutanoatewith 2-Acrylamido-2-Methylpropane-Dimethylammonium Chloride and Acrylamide: Synthesis and Absorbency Behavior. *Journal of Macromolecular Science: Part A - Chemistry* **1990**, *27*, 539-547, doi:10.1080/00222339009349641.

199. Shedge, A.S.; Lele, A.K.; Wadgaonkar, P.P.; Hourdet, D.; Perrin, P.; Chassenieux, C.; Badiger, M.V. Hydrophobically Modified Poly(acrylic acid) Using 3-Pentadecylcyclohexylamine: Synthesis and Rheology. **2005**, *206*, 464-472, doi:10.1002/macp.200400392.

200. McCormick, C.L.S., L. C. Water-Soluble Copolymers .46. Hydrophilic Sulfobetaine Copolymers of Acrylamide and 3-(2-Acrylamido-2-Methylpropanedimethyl-Ammonio)-1-Propanesulphonate. *Polymer* **1992**, *33*, 4617-4624.

201. Xie, X.; Hogen-Esch, T.E. Copolymers of N,N-Dimethylacrylamide and 2-(N-ethylperfluorooctanesulfonamido)ethyl Acrylate in Aqueous Media and in Bulk. Synthesis and Properties. *Macromolecules* **1996**, *29*, 1734-1745, doi:10.1021/ma950687l.

202. Wang, Y.; Lu, Z.; Han, Y.; Feng, Y.; Tang, C. A Novel Thermoviscosifying Water-Soluble Polymer for Enhancing Oil Recovery from High-Temperature and High-Salinity Oil Reservoirs. *Advanced Materials Research* **2011**, *306-307*, 654-657, doi:10.4028/www.scientific.net/AMR.306-307.654.

203. Rashidi, M. Physico-Chemistry Characterization of Sulfonated Polyacrylamide Polymers for Use in Polymer Flooding. The University of Bergen, Bergen, 2010.

204. Gaillard, N.; Giovannetti, B.; Leblanc, T.; Thomas, A.; Braun, O.; Favero, C. Selection of Customized Polymers to Enhance Oil Recovery from High Temperature Reservoirs. In Proceedings of SPE Latin American and Caribbean Petroleum Engineering Conference, Quito, Ecuador, 2015/11/18/; p. 15.

205. Bataweel, M.A.; Yadhalli Shivaprasad, A.; Nasr-El-Din, H.A. Low-Tension Polymer Flooding Using Amphoteric surfactant in High Salinity/High Hardness and High Temperature Conditions in Sandstone Cores. In Proceedings of SPE EOR Conference at Oil and Gas West Asia, Muscat, Oman, 2012/1/1/; p. 23.

206. Wu, Y.; Mahmoudkhani, A.; Watson, P.; Fenderson, T.R.; Nair, M. Development of New Polymers with Better Performance under Conditions of High Temperature and High Salinity. In Proceedings of SPE EOR Conference at Oil and Gas West Asia, Muscat, Oman, 2012/1/1/; p. 11.

207. Leblanc, T.; Braun, O.; Thomas, A.; Divers, T.; Gaillard, N.; Favero, C. Rheological Properties of Stimuli-Responsive Polymers in Solution to Improve the Salinity and Temperature Performances of Polymer-Based Chemical Enhanced Oil Recovery Technologies. In Proceedings of SPE Asia Pacific Enhanced Oil Recovery Conference, Kuala Lumpur, Malaysia, 2015/8/11/; p. 17.

208. Zhu, Y.Y.; Luo, W.L.; Jian, G.Q.; Wang, C.A.; Hou, Q.F.; Niu, J.L. Development and Performance of Water Soluble Salt-Resistant Polymers for Chemical Flooding. *Advanced Materials Research* **2012**, *476-478*, 227-235, doi:10.4028/www.scientific.net/AMR.476-478.227.

209. Sabhapondit, A.; Borthakur, A.; Haque, I. Water Soluble Acrylamidomethyl Propane Sulfonate (AMPS) Copolymer as an Enhanced Oil Recovery Chemical. *Energy & Fuels* **2003**, *17*, 683-688, doi:10.1021/ef010253t.

210. Mothé, C.G.; Correia, D.Z.; de França, F.P.; Riga, A.T. Thermaland rheological study of polysaccharides for enhanced oil recovery. *Journal of Thermal Analysis and Calorimetry* **2006**, *85*, 31-36, doi:10.1007/s10973-005-7339-7.

211. Ryles, R.G. Chemical Stability Limits of Water-Soluble Polymers Used in Oil Recovery Processes. *SPE-14233-PA* **1988**, *3*, 23-34, doi:10.2118/13585-PA.

212. Bridgewater, J.; Pace, S.; Gardner, G.; Schulz, D. Enhanced oil recovery with hydrophobically associating polymers containing n-vinyl-pyrrolidone functionality. **1987**.

213. McCormick, C.L.; Nonaka, T.; Johnson, C.B. Water-soluble copolymers: 27. Synthesis and aqueous solution behaviour of associative acrylamideN-alkylacrylamide copolymers. *Polymer* **1988**, *29*, 731-739, doi:https://doi.org/10.1016/0032-3861(88)90092-4.

214. McCormick, C.L.; Middleton, J.C.; Cummins, D.F. Water-soluble copolymers. 37. Synthesis and characterization of responsive hydrophobically modified polyelectrolytes. *Macromolecules* **1992**, *25*, 1201-1206, doi:10.1021/ma00030a001.

215. Hill, A.; Candau, F.; Selb, J. Properties of hydrophobically associating polyacrylamides: influence of the method of synthesis. *Macromolecules* **1993**, *26*, 4521-4532, doi:10.1021/ma00069a017.

216. Dowling, K.C.; Thomas, J.K. A novel micellar synthesis and photophysical characterization of water-soluble acrylamide-styrene block copolymers. *Macromolecules* **1990**, *23*, 1059-1064, doi:10.1021/ma00206a025.

217. Candau, F.; Selb, J. Hydrophobically-modified polyacrylamides prepared by micellar polymerization1Part of this paper was presented at the conference on `Associating Polymer', Fontevraud, France, November 1997.1. *Advances in Colloid and Interface Science* **1999**, *79*, 149-172, doi:https://doi.org/10.1016/S0001-8686(98)00077-3.

218. English, R.J.; Laurer, J.H.; Spontak, R.J.; Khan, S.A. Hydrophobically Modified Associative Polymer Solutions: Rheology and Microstructure in the Presence of Nonionic Surfactants. *Industrial & Engineering Chemistry Research* **2002**, *41*, 6425-6435, doi:10.1021/ie020409s.

219. Feng, Y.; Billon, L.; Grassl, B.; Khoukh, A.; François, J. Hydrophobically associating polyacrylamides and their partially hydrolyzed derivatives prepared

by post-modification. 1. Synthesis and characterization. *Polymer* **2002**, *43*, 2055-2064, doi:https://doi.org/10.1016/S0032-3861(01)00774-1.

220. Volpert, E.; Selb, J.; Candau, F. Influence of the Hydrophobe Structure on Composition, Microstructure, and Rheology in Associating Polyacrylamides Prepared by Micellar Copolymerization. *Macromolecules* **1996**, *29*, 1452-1463, doi:10.1021/ma951178m.
221. Lara-Ceniceros, A.C.; Rivera-Vallejo, C.; Jiménez-Regalado, E.J. Synthesis, characterization and rheological properties of three different associative polymers obtained by micellar polymerization. *Polymer Bulletin* **2007**, *58*, 425-433, doi:10.1007/s00289-006-0675-3.
222. Maia, A.M.S.; Costa, M.; Borsali, R.; Garcia, R.B. Rheological Behavior and Scattering Studies of Acrylamide-Based Copolymer Solutions. **2005**, *229*, 217-227, doi:10.1002/masy.200551127.
223. Xu, B.; Li, L.; Zhang, K.; Macdonald, P.M.; Winnik, M.A.; Jenkins, R.; Bassett, D.; Wolf, D.; Nuyken, O. Synthesis and Characterization of Comb Associative Polymers Based on Poly(ethylene oxide). *Langmuir* **1997**, *13*, 6896-6902, doi:10.1021/la960612q.
224. Alami, E.; Almgren, M.; Brown, W. Interaction of Hydrophobically End-Capped Poly(ethylene oxide) with Nonionic Surfactants in Aqueous Solution. Fluorescence and Light Scattering Studies. *Macromolecules* **1996**, *29*, 5026-5035, doi:10.1021/ma9518161.
225. Yekta, A.; Duhamel, J.; Brochard, P.; Adiwidjaja, H.; Winnik, M.A. A fluorescent probe study of micelle-like cluster formation in aqueous solutions of hydrophobically modified poly(ethylene oxide). *Macromolecules* **1993**, *26*, 1829-1836, doi:10.1021/ma00060a006.
226. Maechling-Strasser, C.; François, J.; Clouet, F.; Tripette, C. Hydrophobically end-capped poly (ethylene oxide) urethanes: 1. Characterization and experimental study of their association in aqueous solution. *Polymer* **1992**, *33*, 627-636, doi:https://doi.org/10.1016/0032-3861(92)90742-F.
227. Yang, X.; Liu, J.; Li, P.; Liu, C. Self-assembly properties of hydrophobically associating perfluorinated polyacrylamide in dilute and semi-dilute solutions. *Journal of Polymer Research* **2015**, *22*, doi:10.1007/s10965-015-0750-2.
228. Huang, Z.; Lu, H.; He, Y. Amphoteric hydrophobic associative polymer: I synthesis, solution properties and effect on solution properties of surfactant.

Colloid and Polymer Science **2006**, *285*, 365-370, doi:10.1007/s00396-006-1570-z.

229. Gou, S.; Luo, S.; Liu, T.; Zhao, P.; He, Y.; Pan, Q.; Guo, Q. A novel water-soluble hydrophobically associating polyacrylamide based on oleic imidazoline and sulfonate for enhanced oil recovery. *New Journal of Chemistry* **2015**, *39*, 7805-7814, doi:10.1039/C5NJ01153A.
230. Shashkina, Y.A.; Zaroslov, Y.D.; Smirnov, V.A.; Philippova, O.E.; Khokhlov, A.R.; Pryakhina, T.A.; Churochkina, N.A. Hydrophobic aggregation in aqueous solutions of hydrophobically modified polyacrylamide in the vicinity of overlap concentration. *Polymer* **2003**, *44*, 2289-2293, doi:https://doi.org/10.1016/S0032-3861(03)00043-0.
231. Quan, H.; Li, Z.; Huang, Z. Self-assembly properties of a temperature- and salt-tolerant amphoteric hydrophobically associating polyacrylamide. *RSC Advances* **2016**, *6*, 49281-49288, doi:10.1039/C6RA05779A.
232. Argillier, J.F.; Audibert, A.; Lecourtier, J.; Moan, M.; Rousseau, L. Solution and adsorption properties of hydrophobically associating water-soluble polyacrylamides. *Colloids and Surfaces A: Physicochemical and Engineering Aspects* **1996**, *113*, 247-257, doi:https://doi.org/10.1016/0927-7757(96)03575-3.
233. Grassl, B.; Francois, J.; Billon, L. Associating behaviour of polyacrylamide modified with a new hydrophobic zwitterionic monomer. **2001**, *50*, 1162-1169, doi:10.1002/pi.751.
234. Zhong, C.; Huang, R.; Zhang, X.; Dai, H. Synthesis, characterization, and solution properties of an acrylamide-based terpolymer with butyl styrene. **2007**, *103*, 4027-4038, doi:10.1002/app.25546.
235. Al-Sabagh, A.M.; Kandile, N.G.; El-Ghazawy, R.A.; Noor El-Din, M.R.; El-Sharaky, E.A. Solution properties of hydrophobically modified polyacrylamides and their potential use for polymer flooding application. *Egyptian Journal of Petroleum* **2016**, *25*, 433-444, doi:https://doi.org/10.1016/j.ejpe.2015.03.014.
236. Al-Sabagh, A.M.; Kandile, N.G.; El-Ghazawy, R.A.; Noor El-Din, M.R.; El-Sharaky, E.A. Novel Polymerizable Nonionic Surfactants (Surfmers) Corporate with Alkenylsuccinic Anhydride: Synthesis, Surface, and Thermodynamic Properties. *Journal of Dispersion Science and Technology* **2012**, *33*, 1458-1469, doi:10.1080/01932691.2011.620830.

237. Zhong, C.; Jiang, L.; Peng, X. Synthesis and solution behavior of comb-like terpolymers with poly(ethylene oxide) macromonomer. **2010**, *48*, 1241-1250, doi:10.1002/pola.23888.

238. Mirzaie Yegane, M.; Hashemi, F.; Vercauteren, F.; Meulendijks, N.; Gharbi, R.; Boukany, P.E.; Zitha, P. Rheological response of a modified polyacrylamide–silica nanoparticles hybrid at high salinity and temperature. *Soft Matter* **2020**, 10.1039/D0SM01254H, doi:10.1039/D0SM01254H.

239. Hourdet, D.; Gadgil, J.; Podhajecka, K.; Badiger, M.V.; Brûlet, A.; Wadgaonkar, P.P. Thermoreversible Behavior of Associating Polymer Solutions: Thermothinning versus Thermothickening. *Macromolecules* **2005**, *38*, 8512-8521, doi:10.1021/ma050786r.

240. Bokias, G.; Hourdet, D.; Iliopoulos, I.; Staikos, G.; Audebert, R. Hydrophobic Interactions of Poly(N-isopropylacrylamide) with Hydrophobically Modified Poly(sodium acrylate) in Aqueous Solution. *Macromolecules* **1997**, *30*, 8293-8297, doi:10.1021/ma970884f.

241. Hourdet, D.; L'Alloret, F.; Audebert, R. Synthesis of thermoassociative copolymers. *Polymer* **1997**, *38*, 2535-2547, doi:https://doi.org/10.1016/S0032-3861(96)00808-7.

242. Bastiat, G.; Grassl, B.; François, J. Study of sodium dodecyl sulfate/poly(propylene oxide) methacrylate mixed micelles for the synthesis of thermo-associative polymers by micellar polymerization. **2002**, *51*, 958-965, doi:10.1002/pi.1049.

243. Stahl, G.A.; Moradi-Araghi, A.; Doe, P.H. High Temperature and Hardness Stable Copolymers of Vinylpyrrolidone and Acrylamide. In *Water-Soluble Polymers for Petroleum Recovery*, Stahl, G.A., Schulz, D.N., Eds. Springer US: Boston, MA, 1988; 10.1007/978-1-4757-1985-7_6pp. 121-130.

244. The Advanced Energy Consortium Availabe online: (accessed on

245. Michel, V.; Yoshiharu, D.; Karl-Heinz, H.; Michael, H.; Philip, H.; Przemyslaw, K.; Marguerite, R.; François, S. Terminology for biorelated polymers and applications (IUPAC Recommendations 2012). *Pure and Applied Chemistry* **2012**, *84*, 377-410, doi:https://doi.org/10.1351/PAC-REC-10-12-04.

246. Ogolo, N.A.; Olafuyi, O.A.; Onyekonwu, M.O. Enhanced Oil Recovery Using Nanoparticles. In Proceedings of SPE Saudi Arabia Section Technical Symposium and Exhibition, Al-Khobar, Saudi Arabia, 2012/1/1/; p. 9.

247. Zhao, M.; Zhang, Y.; Chenwei, Z.; Dai, C.; Gao, M.; Li, Y.; Lv, W.; Jiang, J.; Wu, Y. Can More Nanoparticles Induce Larger Viscosities of Nanoparticle-Enhanced Wormlike Micellar System (NEWMS)? *Materials (Basel, Switzerland)* **2017**, *10*, doi:10.3390/ma10091096.

248. Miranda, C.R.; Lara, L.S.d.; Tonetto, B.C. Stability and Mobility of Functionalized Silica Nanoparticles for Enhanced Oil Recovery Applications. In Proceedings of SPE International Oilfield Nanotechnology Conference and Exhibition, Noordwijk, The Netherlands, 2012/1/1/; p. 11.

249. Wang, L.; Wang, Z.; Yang, H.; Yang, G. The study of thermal stability of the SiO2 powders with high specific surface area. *Materials Chemistry and Physics* **1999**, *57*, 260-263, doi:https://doi.org/10.1016/S0254-0584(98)00226-0.

250. Ding, H.; Zhang, N.; Zhang, Y.; Wei, M.; Bai, B. Experimental Data Analysis of Nanoparticles for Enhanced Oil Recovery. *Industrial & Engineering Chemistry Research* **2019**, *58*, 12438-12450, doi:10.1021/acs.iecr.9b02132.

251. Li, K.; Wang, D.; Jiang, S. Review on enhanced oil recovery by nanofluids. *Oil & Gas Science and Technology* **2018**, *73*, 37, doi:10.2516/ogst/2018025.

252. Rezk, M.Y.; Allam, N.K. Impact of Nanotechnology on Enhanced Oil Recovery: A Mini-Review. *Industrial & Engineering Chemistry Research* **2019**, *58*, 16287-16295, doi:10.1021/acs.iecr.9b03693.

253. Kazemzadeh, Y.; Shojaei, S.; Riazi, M.; Sharifi, M. Review on application of nanoparticles for EOR purposes: A critical review of the opportunities and challenges. *Chinese Journal of Chemical Engineering* **2019**, *27*, 237-246, doi:https://doi.org/10.1016/j.cjche.2018.05.022.

254. Kamal, M.S.; Adewunmi, A.A.; Sultan, A.S.; Al-Hamad, M.F.; Mehmood, U. Recent Advances in Nanoparticles Enhanced Oil Recovery: Rheology, Interfacial Tension, Oil Recovery, and Wettability Alteration. *Journal of Nanomaterials* **2017**, *2017*, 2473175, doi:10.1155/2017/2473175.

255. Sun, X.; Zhang, Y.; Chen, G.; Gai, Z. Application of Nanoparticles in Enhanced Oil Recovery: A Critical Review of Recent Progress. *Energies* **2017**, *10*, 345.

256. ShamsiJazeyi, H.; Miller, C.A.; Wong, M.S.; Tour, J.M.; Verduzco, R. Polymer-coated nanoparticles for enhanced oil recovery. *Journal of Applied Polymer Science* **2014**, *131*, doi:10.1002/app.40576.

257. Bera, A.; Belhaj, H. Application of nanotechnology by means of nanoparticles and nanodispersions in oil recovery - A comprehensive review. *Journal of Natural*

Gas Science and Engineering **2016**, *34*, 1284-1309, doi:https://doi.org/10.1016/j.jngse.2016.08.023.

258. Negin, C.; Ali, S.; Xie, Q. Application of nanotechnology for enhancing oil recovery – A review. *Petroleum* **2016**, *2*, 324-333, doi:https://doi.org/10.1016/j.petlm.2016.10.002.
259. Schmidt, D.P.; Soo, H.; Radke, C.J. Linear Oil Displacement by the Emulsion Entrapment Process. *Society of Petroleum Engineers Journal* **1984**, *24*, 351-360, doi:10.2118/11333-PA.
260. Khambharatana, F.; Thomas, S.; Ali, S.M.F. Macroemulsion Rheology and Drop Capture Mechanism During Flow in Porous Media. In Proceedings of SPE International Oil and Gas Conference and Exhibition in China, Beijing, China, 1998/1/1/; p. 9.
261. Schramm, L. *Emulsions : fundamentals and applications in the petroleum industry / Laurier L. Schramm, editor*; 1992.
262. Kumar, G.; Kakati, A.; Mani, E.; Sangwai, J.S. Stability of nanoparticle stabilized oil-in-water Pickering emulsion under high pressure and high temperature conditions: comparison with surfactant stabilized oil-in-water emulsion. *Journal of Dispersion Science and Technology* **2020**, 10.1080/01932691.2020.1730888, 1-14, doi:10.1080/01932691.2020.1730888.
263. Zhang, T.; Roberts, M.; Bryant, S.L.; Huh, C. Foams and Emulsions Stabilized With Nanoparticles for Potential Conformance Control Applications. In Proceedings of SPE International Symposium on Oilfield Chemistry, The Woodlands. Texas, 2009/1/1/; p. 17.
264. Pei, H.H.; Zhang, G.C.; Ge, J.J.; Zhang, J.; Zhang, Q.; Fu, L.P. Investigation of Nanoparticle and Surfactant Stabilized Emulsion to Enhance Oil Recovery in Waterflooded Heavy Oil Reservoirs. In Proceedings of SPE Canada Heavy Oil Technical Conference, Calgary, Alberta, Canada, 2015/6/9/; p. 11.
265. Kim, I.; Worthen, A.J.; Lotfollahi, M.; Johnston, K.P.; DiCarlo, D.A.; Huh, C. Nanoparticle-Stabilized Emulsions for Improved Mobility Control for Adverse-mobility Waterflooding. In Proceedings of SPE Improved Oil Recovery Conference, Tulsa, Oklahoma, USA, 2016/4/11/; p. 10.
266. Munshi, M.; Singh, V.N.; Kumar, M.; Singh, J. Effect of nanoparticle size on sessile droplet contact angle. *Journal of Applied Physics* **2008**, *103*, doi:10.1063/1.2912464.

267. Ravera, F.; Santini, E.; Loglio, G.; Ferrari, M.; Liggieri, L. Effect of Nanoparticles on the Interfacial Properties of Liquid/Liquid and Liquid/Air Surface Layers. *The Journal of Physical Chemistry B* **2006**, *110*, 19543-19551, doi:10.1021/jp0636468.

268. Suleimanov, B.A.; Ismailov, F.S.; Veliyev, E.F. Nanofluid for enhanced oil recovery. *Journal of Petroleum Science and Engineering* **2011**, *78*, 431-437, doi:https://doi.org/10.1016/j.petrol.2011.06.014.

269. Hendraningrat, L.; Li, S.; Torsæter, O. A coreflood investigation of nanofluid enhanced oil recovery. *Journal of Petroleum Science and Engineering* **2013**, *111*, 128-138, doi:https://doi.org/10.1016/j.petrol.2013.07.003.

270. Zargartalebi, M.; Barati, N.; Kharrat, R. Influences of hydrophilic and hydrophobic silica nanoparticles on anionic surfactant properties: Interfacial and adsorption behaviors. *Journal of Petroleum Science and Engineering* **2014**, *119*, 36-43, doi:https://doi.org/10.1016/j.petrol.2014.04.010.

271. Wasan, D.T.; Nikolov, A.D. Spreading of nanofluids on solids. *Nature* **2003**, *423*, 156-159, doi:10.1038/nature01591.

272. Das, S.K.C., S.U.S.; Yu,W.; Pradeep,T. *Nanofluids ScienceandTechnology*; John Wiley & Sons, Inc Publishing: Hoboken, NJ, 2008.

273. Wasan, D.; Nikolov, A.; Kondiparty, K. The wetting and spreading of nanofluids on solids: Role of the structural disjoining pressure. *Current Opinion in Colloid & Interface Science* **2011**, *16*, 344-349, doi:https://doi.org/10.1016/j.cocis.2011.02.001.

274. Liu, K.-L.; Kondiparty, K.; Nikolov, A.D.; Wasan, D. Dynamic Spreading of Nanofluids on Solids Part II: Modeling. *Langmuir* **2012**, *28*, 16274-16284, doi:10.1021/la302702g.

275. Karimi, A.; Fakhroueian, Z.; Bahramian, A.; Pour Khiabani, N.; Darabad, J.B.; Azin, R.; Arya, S. Wettability Alteration in Carbonates using Zirconium Oxide Nanofluids: EOR Implications. *Energy & Fuels* **2012**, *26*, 1028-1036, doi:10.1021/ef201475u.

276. Ju, B.; Fan, T. Experimental study and mathematical model of nanoparticle transport in porous media. *Powder Technology* **2009**, *192*, 195-202, doi:https://doi.org/10.1016/j.powtec.2008.12.017.

277. Hendraningrat, L.; Li, S.; Torsater, O. Effect of Some Parameters Influencing Enhanced Oil Recovery Process using Silica Nanoparticles: An Experimental

Investigation. In Proceedings of SPE Reservoir Characterization and Simulation Conference and Exhibition, Abu Dhabi, UAE, 2013/9/16/; p. 10.

278. Chow, T.S. Viscosities of concentrated dispersions. *Physical Review E* **1993**, *48*, 1977-1983, doi:10.1103/PhysRevE.48.1977.
279. Eastman, J.A.; Phillpot, S.R.; Choi, S.U.S.; Keblinski, P. Thermal transport in nanofluids. In *Annual Review of Materials Research*, 2004; Vol. 34, pp 219-246.
280. Hughes, A.J. The Einstein Relation between Relative Viscosity and Volume Concentration of Suspensions of Spheres. *Nature* **1954**, *173*, 1089-1090, doi:10.1038/1731089a0.
281. Sandhu, A. *Nature Nanotechnology* **2007**, 445.
282. Chevalier, J.; Tillement, O.; Ayela, F. Rheological properties of nanofluids flowing through microchannels. **2007**, *91*, 233103, doi:10.1063/1.2821117.
283. Chevalier, J.; Tillement, O.; Ayela, F. Structure and rheology of ${\text{SiO}}_{2}$ nanoparticle suspensions under very high shear rates. *Physical Review E* **2009**, *80*, 051403, doi:10.1103/PhysRevE.80.051403.
284. Namburu, P.K.; Kulkarni, D.P.; Dandekar, A.; Das, D.K. Experimental investigation of viscosity and specific heat of silicon dioxide nanofluids. *Micro and Nano Letters* **2007**, *2*, 67-71, doi:10.1049/mnl:20070037.
285. Venerus, D.C.; Buongiorno, J. Viscosity measurement of colloidal dispersion (nanofluids) for heat transfer applications. *Appl. Rheol.* **2010**, *20*.
286. Wang, X.T. Numerical solution of time-varying systems with a stretch by general Legendre wavelets. *Applied Mathematics and Computation* **2008**, *198*, 613-620, doi:10.1016/j.amc.2007.08.058.
287. Masoumi, N.; Sohrabi, N.; Behzadmehr, A. A new model for calculating the effective viscosity of nanofluids. *Journal of Physics D: Applied Physics* **2009**, *42*, 055501, doi:10.1088/0022-3727/42/5/055501.
288. Keblinski, P.; Phillpot, S.R.; Choi, S.U.S.; Eastman, J.A. Mechanisms of heat flow in suspensions of nano-sized particles (nanofluids). *International Journal of Heat and Mass Transfer* **2001**, *45*, 855-863, doi:10.1016/S0017-9310(01)00175-2.
289. Wang, B.X.; Zhou, L.P.; Peng, X.F. A fractal model for predicting the effective thermal conductivity of liquid with suspension of nanoparticles. *International Journal of Heat and Mass Transfer* **2003**, *46*, 2665-2672, doi:10.1016/S0017-9310(03)00016-4.

290. Evans, W.; Prasher, R.; Fish, J.; Meakin, P.; Phelan, P.; Keblinski, P. Effect of aggregation and interfacial thermal resistance on thermal conductivity of nanocomposites and colloidal nanofluids. *International Journal of Heat and Mass Transfer* **2008**, *51*, 1431-1438, doi:https://doi.org/10.1016/j.ijheatmasstransfer.2007.10.017.

291. Einstein, A.; Fürth, R. *Investigations on the theory of Brownian movement*; Dover Publications: New York, N.Y., 1956.

292. Balasubramanian, G.; Sen, S.; Puri, I.K. Shear viscosity enhancement in water–nanoparticle suspensions. *Physics Letters A* **2012**, *376*, 860-863, doi:https://doi.org/10.1016/j.physleta.2011.12.041.

293. Aladag, B.; Halelfadl, S.; Doner, N.; Maré, T.; Duret, S.; Estellé, P. Experimental investigations of the viscosity of nanofluids at low temperatures. *Applied Energy* **2012**, *97*, 876-880, doi:https://doi.org/10.1016/j.apenergy.2011.12.101.

294. Maghzi, A.; Kharrat, R.; Mohebbi, A.; Ghazanfari, M.H. The impact of silica nanoparticles on the performance of polymer solution in presence of salts in polymer flooding for heavy oil recovery. *Fuel* **2014**, *123*, 123-132, doi:https://doi.org/10.1016/j.fuel.2014.01.017.

295. Cao, J.; Song, T.; Zhu, Y.; Wang, X.; Wang, S.; Yu, J.; Ba, Y.; Zhang, J. Aqueous hybrids of amino-functionalized nanosilica and acrylamide-based polymer for enhanced oil recovery. *RSC Advances* **2018**, *8*, 38056-38064, doi:10.1039/C8RA07076H.

296. Zhan, J.; Zheng, T.; Piringer, G.; Day, C.; McPherson, G.L.; Lu, Y.; Papadopoulos, K.; John, V.T. Transport Characteristics of Nanoscale Functional Zerovalent Iron/Silica Composites for in Situ Remediation of Trichloroethylene. *Environmental Science & Technology* **2008**, *42*, 8871-8876, doi:10.1021/es800387p.

297. Liu, Y.; Majetich, S.A.; Tilton, R.D.; Sholl, D.S.; Lowry, G.V. TCE Dechlorination Rates, Pathways, and Efficiency of Nanoscale Iron Particles with Different Properties. *Environmental Science & Technology* **2005**, *39*, 1338-1345, doi:10.1021/es049195r.

298. Phenrat, T.; Saleh, N.; Sirk, K.; Kim, H.-J.; Tilton, R.D.; Lowry, G.V. Stabilization of aqueous nanoscale zerovalent iron dispersions by anionic polyelectrolytes: adsorbed anionic polyelectrolyte layer properties and their effect

on aggregation and sedimentation. *Journal of Nanoparticle Research* **2008**, *10*, 795-814, doi:10.1007/s11051-007-9315-6.

299. Yang, G.C.C.; Tu, H.-C.; Hung, C.-H. Stability of nanoiron slurries and their transport in the subsurface environment. *Separation and Purification Technology* **2007**, *58*, 166-172, doi:https://doi.org/10.1016/j.seppur.2007.07.018.
300. Schrick, B.; Hydutsky, B.W.; Blough, J.L.; Mallouk, T.E. Delivery Vehicles for Zerovalent Metal Nanoparticles in Soil and Groundwater. *Chemistry of Materials* **2004**, *16*, 2187-2193, doi:10.1021/cm0218108.
301. Caldelas, F.M.; Murphy, M.; Huh, C.; Bryant, S.L. Factors Governing Distance of Nanoparticle Propagation in Porous Media. In Proceedings of SPE Production and Operations Symposium, Oklahoma City, Oklahoma, USA, 2011/1/1/; p. 16.
302. Skauge, T.; Spildo, K.; Skauge, A. Nano-sized Particles For EOR. In Proceedings of SPE Improved Oil Recovery Symposium, Tulsa, Oklahoma, USA, 2010/1/1/; p. 10.
303. El-Diasty, A.I.; Aly, A.M. Understanding the Mechanism of Nanoparticles Applications in Enhanced Oil Recovery. In Proceedings of SPE North Africa Technical Conference and Exhibition, Cairo, Egypt, 2015/9/14/; p. 19.
304. Zhang, T.; Murphy, M.J.; Yu, H.; Bagaria, H.G.; Yoon, K.Y.; Nielson, B.M.; Bielawski, C.W.; Johnston, K.P.; Huh, C.; Bryant, S.L. Investigation of Nanoparticle Adsorption During Transport in Porous Media. *SPE Journal* **2015**, *20*, 667-677, doi:10.2118/166346-PA.
305. Eduok, U.; Suleiman, R.; Khaled, M.; Akid, R. Enhancing water repellency and anticorrosion properties of a hybrid silica coating on mild steel. *Progress in Organic Coatings* **2016**, *93*, 97-108, doi:https://doi.org/10.1016/j.porgcoat.2016.01.006.
306. Fadil, M.; Chauhan, D.S.; Quraishi, M.A. Smart Coating Based on Urea-Formaldehyde Microcapsules Loaded with Benzotriazole for Corrosion Protection of Mild Steel in 3.5 % NaCl. *Russian Journal of Applied Chemistry* **2018**, *91*, 1721-1728, doi:10.1134/S107042721810021X.
307. Suleiman, R.; Dafalla, H.; El Ali, B. Novel hybrid epoxy silicone materials as efficient anticorrosive coatings for mild steel. *RSC Advances* **2015**, *5*, 39155-39167, doi:10.1039/C5RA04500B.
308. Keller, A.A.; Wang, H.; Zhou, D.; Lenihan, H.S.; Cherr, G.; Cardinale, B.J.; Miller, R.; Ji, Z. Stability and Aggregation of Metal Oxide Nanoparticles in

Natural Aqueous Matrices. *Environmental Science & Technology* **2010**, *44*, 1962-1967, doi:10.1021/es902987d.

309. Saleh, N.; Phenrat, T.; Sirk, K.; Dufour, B.; Ok, J.; Sarbu, T.; Matyjaszewski, K.; Tilton, R.D.; Lowry, G.V. Adsorbed Triblock Copolymers Deliver Reactive Iron Nanoparticles to the Oil/Water Interface. *Nano Letters* **2005**, *5*, 2489-2494, doi:10.1021/nl0518268.
310. Sharma, V.K.; Siskova, K.M.; Zboril, R.; Gardea-Torresdey, J.L. Organic-coated silver nanoparticles in biological and environmental conditions: Fate, stability and toxicity. *Advances in Colloid and Interface Science* **2014**, *204*, 15-34, doi:https://doi.org/10.1016/j.cis.2013.12.002.
311. Akbari, S.; Mahmood, S.M.; Tan, I.M.; Ghaedi, H.; Ling, O.L. Assessment of Polyacrylamide Based Co-Polymers Enhanced by Functional Group Modifications with Regards to Salinity and Hardness. **2017**, *9*, 647.
312. Algharaib, M.; Alajmi, A.; Gharbi, R. Improving polymer flood performance in high salinity reservoirs. *Journal of Petroleum Science and Engineering* **2014**, *115*, 17-23, doi:https://doi.org/10.1016/j.petrol.2014.02.003.
313. Yuan, T.; Liu, Z.; Gao, R.; Hu, G.; Zhang, G.; Zhao, J. Enhanced oil recovery from high-salinity reservoirs by cationic gemini surfactants. *Journal of Applied Polymer Science* **2018**, *135*, 46086, doi:10.1002/app.46086.
314. Mayne, J.E.O. The problem of painting rusty steel. *Journal of Applied Chemistry* **1959**, *9*, 673-680, doi:10.1002/jctb.5010091208.
315. Mirzaie Yegane, M.; Battistutta, E.; Zitha, P. Mechanistic Simulation and History Matching of Alkaline-Surfactant-Polymer ASP Core Flooding Experiment at Optimum vs. Under-Optimum Salinity Conditions. In Proceedings of SPE Europec featured at 81st EAGE Conference and Exhibition, London, England, UK, 2019/6/3/; p. 22.
316. Al-Shakry, B.; Skauge, T.; Shaker Shiran, B.; Skauge, A. Polymer Injectivity: Investigation of Mechanical Degradation of Enhanced Oil Recovery Polymers Using In-Situ Rheology. **2018**, *12*, 49.
317. Tessarolli, F.G.C.; Souza, S.T.S.; Gomes, A.S.; Mansur, C.R.E. Gelation Kinetics of Hydrogels Based on Acrylamide⁻AMPS⁻NVP Terpolymer, Bentonite, and Polyethylenimine for Conformance Control of Oil Reservoirs. *Gels* **2019**, *5*, 7, doi:10.3390/gels5010007.

318. Petit, L.; Bouteiller, L.; Brûlet, A.; Lafuma, F.; Hourdet, D. Responsive Hybrid Self-Assemblies in Aqueous Media. *Langmuir* **2007**, *23*, 147-158, doi:10.1021/la061466j.

319. Portehault, D.; Petit, L.; Pantoustier, N.; Ducouret, G.; Lafuma, F.; Hourdet, D. Hybrid thickeners in aqueous media. *Colloids and Surfaces A: Physicochemical and Engineering Aspects* **2006**, *278*, 26-32, doi:https://doi.org/10.1016/j.colsurfa.2005.11.089.

320. Hourdet, D.; Petit, L. Hybrid Hydrogels: Macromolecular Assemblies through Inorganic Cross-Linkers. *Macromolecular Symposia* **2010**, *291-292*, 144-158, doi:10.1002/masy.201050518.

321. Lin, W.-C.; Fan, W.; Marcellan, A.; Hourdet, D.; Creton, C. Large Strain and Fracture Properties of Poly(dimethylacrylamide)/Silica Hybrid Hydrogels. *Macromolecules* **2010**, *43*, 2554-2563, doi:10.1021/ma901937r.

322. Portehault, D.; Petit, L.; Hourdet, D. Synthesis and self assembly processes of aqueous thermoresponsive hybrid formulations. *Soft Matter* **2010**, *6*, 2178-2186, doi:10.1039/B926052H.

323. Bhardwaj, P.; Singh, S.; Singh, V.; Aggarwal, S.; Mandal, U.K. Nanosize Polyacrylamide/SiO2 Composites by Inverse Microemulsion Polymerization. *International Journal of Polymeric Materials and Polymeric Biomaterials* **2008**, *57*, 404-416, doi:10.1080/00914030701729156.

324. Hu, Z.; Haruna, M.; Gao, H.; Nourafkan, E.; Wen, D. Rheological Properties of Partially Hydrolyzed Polyacrylamide Seeded by Nanoparticles. *Industrial & Engineering Chemistry Research* **2017**, *56*, 3456-3463, doi:10.1021/acs.iecr.6b05036.

325. Zhu, D.; Wei, L.; Wang, B.; Feng, Y. Aqueous Hybrids of Silica Nanoparticles and Hydrophobically Associating Hydrolyzed Polyacrylamide Used for EOR in High-Temperature and High-Salinity Reservoirs. *Energies* **2014**, *7*, 3858-3871, doi:10.3390/en7063858.

326. Greenwood, P. Aqueous silane modified silica sols: theory and preparation. *Pigment & Resin Technology* **2011**, *40*, 275-284, doi:10.1108/03699421111176171.

327. Saunders, S.R.; Eden, M.R.; Roberts, C.B. Modeling the Precipitation of Polydisperse Nanoparticles Using a Total Interaction Energy Model. *The Journal of Physical Chemistry C* **2011**, *115*, 4603-4610, doi:10.1021/jp200116a.

328. Skoglund, S.; Lowe, T.A.; Hedberg, J.; Blomberg, E.; Wallinder, I.O.; Wold, S.; Lundin, M. Effect of Laundry Surfactants on Surface Charge and Colloidal Stability of Silver Nanoparticles. *Langmuir* **2013**, *29*, 8882-8891, doi:10.1021/la4012873.

329. Wu, X.Y.; Hunkeler, D.; Hamielec, A.E.; Pelton, R.H.; Woods, D.R. Molecular weight characterization of poly(acrylamide-co-sodium acrylate). I. Viscometry. **1991**, *42*, 2081-2093, doi:10.1002/app.1991.070420736.

330. Blute, I.; Pugh, R.J.; van de Pas, J.; Callaghan, I. Silica nanoparticle sols: 1. Surface chemical characterization and evaluation of the foam generation (foamability). *Journal of Colloid and Interface Science* **2007**, *313*, 645-655, doi:https://doi.org/10.1016/j.jcis.2007.05.013.

331. Book, F.; Ekvall, M.T.; Persson, M.; Lönnerud, S.; Lammel, T.; Sturve, J.; Backhaus, T. Ecotoxicity screening of seven different types of commercial silica nanoparticles using cellular and organismic assays: Importance of surface and size. *NanoImpact* **2019**, *13*, 100-111, doi:https://doi.org/10.1016/j.impact.2019.01.001.

332. Aveyard, R.; Binks, B.P.; Clint, J.H. Emulsions stabilised solely by colloidal particles. *Advances in Colloid and Interface Science* **2003**, *100-102*, 503-546, doi:https://doi.org/10.1016/S0001-8686(02)00069-6.

333. Benoit, D.N.; Zhu, H.; Lilierose, M.H.; Verm, R.A.; Ali, N.; Morrison, A.N.; Fortner, J.D.; Avendano, C.; Colvin, V.L. Measuring the Grafting Density of Nanoparticles in Solution by Analytical Ultracentrifugation and Total Organic Carbon Analysis. *Analytical Chemistry* **2012**, *84*, 9238-9245, doi:10.1021/ac301980a.

334. Andrade, L.C.F.; Petronílio, J.A.; Maneschy, C.E.d.A.; Cruz, D.O.d.A. The carreau-yasuda fluids: a skin friction equation for turbulent flow in pipes and kolmogorov dissipative scales %J Journal of the Brazilian Society of Mechanical Sciences and Engineering. **2007**, *29*, 162-167.

335. Hotze, E.M.; Phenrat, T.; Lowry, G.V. Nanoparticle aggregation: challenges to understanding transport and reactivity in the environment. *Journal of environmental quality* **2010**, *39*, 1909-1924.

336. Israelachvili, J. *Intermolecular and Surface Forces 3rd Edition*; Academic Press: 2011.

337. Raghavan, S.R.; Hou, J.; Baker, G.L.; Khan, S.A. Colloidal Interactions between Particles with Tethered Nonpolar Chains Dispersed in Polar Media: Direct Correlation between Dynamic Rheology and Interaction Parameters. *Langmuir* **2000**, *16*, 1066-1077, doi:10.1021/la9815953.

338. Ohshima, H. Effective Surface Potential and Double-Layer Interaction of Colloidal Particles. *Journal of Colloid and Interface Science* **1995**, *174*, 45-52, doi:https://doi.org/10.1006/jcis.1995.1362.

339. Tadros, T. General Principles of Colloid Stability and the Role of Surface Forces. 2014; 10.1002/9783527631193.ch1pp. 1-22.

340. Vincent, B.; Edwards, J.; Emmett, S.; Jones, A. Depletion flocculation in dispersions of sterically-stabilised particles ("soft spheres"). *Colloids and Surfaces* **1986**, *18*, 261-281, doi:https://doi.org/10.1016/0166-6622(86)80317-1.

341. Jones, A.; Vincent, B. Depletion flocculation in dispersions of sterically-stabilised particles 2. Modifications to theory and further studies. *Colloids and Surfaces* **1989**, *42*, 113-138, doi:https://doi.org/10.1016/0166-6622(89)80081-2.

342. Moskovits, M.; Vlčková, B. Adsorbate-Induced Silver Nanoparticle Aggregation Kinetics. *The Journal of Physical Chemistry B* **2005**, *109*, 14755-14758, doi:10.1021/jp051177o.

343. Berg, J.C. *An Introduction to Interfaces & Colloids ← the Bridge to Nanoscience;*; World Scientific Publishing Co. Pte. Ltd: Singapore, 2010.

344. Metin, C.O.; Bonnecaze, R.T.; Lake, L.W.; Miranda, C.R.; Nguyen, Q.P. Aggregation kinetics and shear rheology of aqueous silica suspensions. *Applied Nanoscience* **2014**, *4*, 169-178, doi:10.1007/s13204-012-0185-6.

345. Omurlu, C.; Lake, L.; Miranda, C.; P. Nguyen, Q. Stability of aqueous silica nanoparticle dispersions. *Journal of Nanoparticle Research* **2011**, *13*, 839-850, doi:10.1007/s11051-010-0085-1.

346. Worthen, A.J.; Tran, V.; Cornell, K.A.; Truskett, T.M.; Johnston, K.P. Steric stabilization of nanoparticles with grafted low molecular weight ligands in highly concentrated brines including divalent ions. *Soft Matter* **2016**, *12*, 2025-2039, doi:10.1039/C5SM02787J.

347. Silvera Batista, C.A.; Larson, R.G.; Kotov, N.A. Nonadditivity of nanoparticle interactions. **2015**, *350*, 1242477, doi:10.1126/science.1242477 %J Science.

348. Mahdavian, A.-R.; Abdollahi, M.; Bijanzadeh, H.R. Kinetic study of radical polymerization. III. Solution polymerization of acrylamide by 1H-NMR. *Journal of Applied Polymer Science* **2004**, *93*, 2007-2013, doi:10.1002/app.20649.

349. Al-Shammari, B.; Al-Fariss, T.; Al-Sewailm, F.; Elleithy, R. The effect of polymer concentration and temperature on the rheological behavior of metallocene linear low density polyethylene (mLLDPE) solutions. *Journal of King Saud University - Engineering Sciences* **2011**, *23*, 9-14, doi:https://doi.org/10.1016/j.jksues.2010.07.001.

350. Ait - Kadi, A.; Carreau, P.J.; Chauveteau, G. Rheological Properties of Partially Hydrolyzed Polyacrylamide Solutions. **1987**, *31*, 537-561, doi:10.1122/1.549959.

351. Berg, S.; van Wunnik, J. Shear Rate Determination from Pore-Scale Flow Fields. *Transport in Porous Media* **2017**, *117*, 229-246, doi:10.1007/s11242-017-0830-3.

352. Battistutta, E.; van Kuijk, S.R.; Groen, K.V.; Zitha, P.L.J. Alkaline-Surfactant-Polymer (ASP) Flooding of Crude Oil at Under-Optimum Salinity Conditions. In Proceedings of SPE Asia Pacific Enhanced Oil Recovery Conference, Kuala Lumpur, Malaysia, 2015/8/11/; p. 20.

353. Cannella, W.J.; Huh, C.; Seright, R.S. Prediction of Xanthan Rheology in Porous Media. In Proceedings of SPE Annual Technical Conference and Exhibition, Houston, Texas, 1988/1/1/; p. 16.

354. Paterson, R.W.; Abernathy, F.H. Turbulent flow drag reduction and degradation with dilute polymer solutions. *Journal of Fluid Mechanics* **1970**, *43*, 689-710, doi:10.1017/S0022112070002677.

355. Kang, K.; Lee, L.J.; Koelling, K.W. High shear microfluidics and its application in rheological measurement. *Experiments in Fluids* **2005**, *38*, 222-232, doi:10.1007/s00348-004-0901-4.

356. Hu, X.; Boukany, P.; Hemminger, O.; Lee, L. The Use of Microfluidics in Rheology. *Macromolecular Materials and Engineering* **2011**, *296*, 308-320, doi:10.1002/mame.201000246.

357. Rems, L.; Kawale, D.; Lee, L.J.; Boukany, P.E. Flow of DNA in micro/nanofluidics: From fundamentals to applications. *Biomicrofluidics* **2016**, *10*, 043403-043403, doi:10.1063/1.4958719.

358. Banik, B.L.; Fattahi, P.; Brown, J.L. Polymeric nanoparticles: the future of nanomedicine. *Wiley Interdiscip Rev Nanomed Nanobiotechnol* **2016**, *8*, 271-299, doi:10.1002/wnan.1364.

359. El-Say, K.M.; El-Sawy, H.S. Polymeric nanoparticles: Promising platform for drug delivery. *Int J Pharm* **2017**, *528*, 675-691, doi:10.1016/j.ijpharm.2017.06.052.

360. Nakamura, K. *Photopolymers: Photoresist materials, processes, and applications*; 2014; pp. 1-176.

361. Chen, Y. Nanofabrication by electron beam lithography and its applications: A review. *Microelectronic Engineering* **2015**, *135*, 57-72, doi:https://doi.org/10.1016/j.mee.2015.02.042.

362. Seright RS, M.J., Holzwarth G. Mechanical degradation of polyacrylamides induced by flow through porous-media. *ACS Polym. Prepr.* **1981**, *22*, 30-33.

363. Beyer, M.K.; Clausen-Schaumann, H. Mechanochemistry: The Mechanical Activation of Covalent Bonds. *Chemical Reviews* **2005**, *105*, 2921-2948, doi:10.1021/cr030697h.

364. Giudice, F.D.; Haward, S.J.; Shen, A.Q. Relaxation time of dilute polymer solutions: A microfluidic approach. *Journal of Rheology* **2017**, *61*, 327-337, doi:10.1122/1.4975933.

365. Jouenne, S.; Chakibi, H.; Levitt, D. Polymer Stability After Successive Mechanical-Degradation Events. *SPE Journal* **2018**, *23*, 18-33, doi:10.2118/186103-PA.

366. Garrepally, S.; Jouenne, S.; Olmsted, P.; Lequeux, F. *Scission of flexible polymers in contraction flow: predicting the effects of multiple passages*; 2019.

367. Armanet, L.; Hunkeler, D. Phase inversion of polyacrylamide-based inverse-emulsions: Influence of inverting-surfactant type and concentration. *Journal of Applied Polymer Science* **2007**, *103*, 3567-3584, doi:10.1002/app.25062.

368. González Rivera, J.; Hernández Barajas, J.; Gutiérrez Carrillo, A.; Aguilera Alvarado, A.F. Preparation of highly concentrated inverse emulsions of acrylamide-based anionic copolymers as efficient water rheological modifiers. *Journal of Applied Polymer Science* **2016**, *133*, doi:10.1002/app.43502.

369. Sorbie, K.S.; Roberts, L.J. A Model for Calculating Polymer Injectivity Including the Effects of Shear Degradation. In Proceedings of SPE Enhanced Oil Recovery Symposium, Tulsa, Oklahoma, 1984/1/1/; p. 18.

370. Lim, T.; Uhl, J.T.; Prud'homme, R.K. The Interpretation of Screen-Factor Measurements. *SPE Reservoir Engineering* **1986**, *1*, 272-276, doi:10.2118/12285-pa.

371. Yerramilli, S.S.; Zitha, P.L.J.; Yerramilli, R.C. Novel Insight into Polymer Injectivity for Polymer Flooding. In Proceedings of SPE European Formation Damage Conference & Exhibition, Noordwijk, The Netherlands, 2013/6/5/; p. 23.

372. Hunkeler, D.; Nguyen, T.Q.; Kausch, H.H. Polymer solutions under elongational flow: 2. An evaluation of models of polymer dynamics for transient and stagnation point flows. *Polymer* **1996**, *37*, 4271-4281, doi:https://doi.org/10.1016/0032-3861(96)00187-5.

373. Vanapalli, S.A.; Islam, M.T.; Solomon, M.J. Scission-induced bounds on maximum polymer drag reduction in turbulent flow. **2005**, *17*, 095108, doi:10.1063/1.2042489.

374. Odell, J.A.; Keller, A. Flow-induced chain fracture of isolated linear macromolecules in solution. **1986**, *24*, 1889-1916, doi:10.1002/polb.1986.090240901.

375. Rems, L.; Kawale, D.; Lee, L.J.; Boukany, P.E. Flow of DNA in micro/nanofluidics: From fundamentals to applications. *Biomicrofluidics* **2016**, *10*, 043403, doi:10.1063/1.4958719.

376. Kamerkar, P.A.; Edwards, B.J. An experimental study of slip flow in capillaries and semihyperbolically converging dies. *Polymer Engineering & Science* **2007**, *47*, 159-167, doi:https://doi.org/10.1002/pen.20692.

377. Hudson, N.E.; Jones, T.E.R. The Al project—an overview. *Journal of Non-Newtonian Fluid Mechanics* **1993**, *46*, 69-88, doi:https://doi.org/10.1016/0377-0257(93)80004-U.

378. Walters, K. RECENT DEVELOPMENTS IN RHEOMETRY. In *Theoretical and Applied Rheology*, Moldenaers, P., Keunings, R., Eds. Elsevier: Amsterdam, 1992; https://doi.org/10.1016/B978-0-444-89007-8.50010-1pp. 16-23.

379. Henaut, I.; Glenat, P.; Cassar, C.; Gainville, M.; Hamdi, K.; Pagnier, P. Mechanical Degradation Kinetics of Polymeric DRAs. In Proceedings of 8th North American Conference on Multiphase Technology, Banff, Alberta, Canada, 2012/6/20/; p. 14.

380. Sánchez Pérez, J.A.; Rodríguez Porcel, E.M.; Casas López, J.L.; Fernández Sevilla, J.M.; Chisti, Y. Shear rate in stirred tank and bubble column bioreactors.

Chemical Engineering Journal **2006**, *124*, 1-5, doi:https://doi.org/10.1016/j.cej.2006.07.002.

381. Sanchez Perez, J.A.; Rodriguez Procel, E.M.; Casas Lopez, J.L. Shear rate in stirred tank and bubble column bioreactors. *Chemical Engineering Journal 124* **2006**, 1-5.
382. Dupas, A.; Henaut, I.; Rousseau, D.; Poulain, P.; Tabary, R.; Argillier, J.-F.; Aubry, T. Impact of Polymer Mechanical Degradation on Shear and Extensional Viscosities: Toward Better Injectivity Forecasts in Polymer Flooding Operations. In Proceedings of SPE International Symposium on Oilfield Chemistry, The Woodlands, Texas, USA, 2013/4/8/; p. 11.
383. Díaz, F.A.; Torné, J.P.; Prada, A.; Perez, G. Shear degradation model of HPAM solutions for the design of regulator valves in polymer flooding EOR. *Journal of Petroleum Exploration and Production Technology* **2020**, *10*, 2587-2599, doi:10.1007/s13202-020-00905-5.
384. Seright, R.S.; Seheult, J.M.; Talashek, T. Injectivity Characteristics of EOR Polymers. *SPE Reservoir Evaluation & Engineering* **2009**, *12*, 783-792, doi:10.2118/115142-pa.
385. Driver, J.W.; Britton, C.; Hernandez, R.; Glushko, D.; Pope, G.A.; Delshad, M. Conditioning Polymer Solutions for Injection into Tight Reservoir Rocks. In Proceedings of SPE Improved Oil Recovery Conference, Tulsa, Oklahoma, USA, 2018/4/14/; p. 10.
386. Al-Shakry, B.; Shiran, B.S.; Skauge, T.; Skauge, A. Enhanced Oil Recovery by Polymer Flooding: Optimizing Polymer Injectivity. In Proceedings of SPE Kingdom of Saudi Arabia Annual Technical Symposium and Exhibition, Dammam, Saudi Arabia, 2018/8/16/; p. 22.
387. Ivanov, M.R.; Haes, A.J. Anionic Functionalized Gold Nanoparticle Continuous Full Filling Separations: Importance of Sample Concentration. *Analytical Chemistry* **2012**, *84*, 1320-1326, doi:10.1021/ac2022376.
388. Ait-Kadi, A. Rheological Properties of Partially Hydrolyzed Polyacrylamide Solutions. *Journal of Rheology - J RHEOL* **1987**, *31*, doi:10.1122/1.549959.
389. Walldal, C.; Åkerman, B. Effect of Ionic Strength on the Dynamic Mobility of Polyelectrolytes. *Langmuir* **1999**, *15*, 5237-5243, doi:10.1021/la981475v.
390. Bruns, D.; de Oliveira, T.E.; Rottler, J.; Mukherji, D. Tuning Morphology and Thermal Transport of Asymmetric Smart Polymer Blends by Macromolecular

Engineering. *Macromolecules* **2019**, *52*, 5510-5517, doi:10.1021/acs.macromol.9b00806.

391. Metzner, A.B.; Otto, R.E. Agitation of non-Newtonian fluids. **1957**, *3*, 3-10, doi:10.1002/aic.690030103.
392. Nienow, A.W. Hydrodynamics of Stirred Bioreactors. *Applied Mechanics Reviews* **1998**, *51*, 3-32, doi:10.1115/1.3098990 %J Applied Mechanics Reviews.
393. Ducla, J.M.; Desplanches, H.; Chevalier, J.L. EFFECTIVE VISCOSITY OF NON-NEWTONIAN FLUIDS IN A MECHANICALLY STIRRED TANK. *Chemical Engineering Communications* **1983**, *21*, 29-36, doi:10.1080/00986448308940273.
394. Posarac, D.; Watkinson, P. Mixing of lignin-based slurry fuel. *The Canadian Journal of Chemical Engineering* **2000**, *78*, 265-270, doi:10.1002/cjce.5450780134.
395. Nouri, J.; Hockey, R. Power Number Correlation between Newtonian and Non-Newtonian Fluids in a Mixing Vessel. *Journal of Chemical Engineering of Japan - J CHEM ENG JPN* **1998**, *31*, 848-852, doi:10.1252/jcej.31.848.
396. Torrez, C.; André, C. Power Consumption of a Rushton Turbine Mixing Viscous Newtonian and Shear-thinning Fluids: Comparison between Experimental and Numerical Results. **1998**, *21*, 599-604, doi:10.1002/(sici)1521-4125(199807)21:7<599::Aid-ceat599>3.0.Co;2-6.
397. Wu, J.; Graham, L.J.; Noui Mehidi, N. Estimation of agitator flow shear rate. **2006**, *52*, 2323-2332, doi:10.1002/aic.10857.
398. Toledo, R.T. *Fundamentals of Food Process Engineering*; Springer; Softcover reprint of hardcover 3rd ed. 2007 edition: 2007.
399. Rushton, J.H.C., E. W.; Everett, H. J. Power characteristics of mixing impellers Part 1. *Chem. Eng. Progress* **1950**, *46*.
400. Bates, R.L.; Fondy, P.L.; Corpstein, R.R. Examination of Some Geometric Parameters of Impeller Power. *Industrial & Engineering Chemistry Process Design and Development* **1963**, *2*, 310-314, doi:10.1021/i260008a011.
401. Hershey HC, B.R. *Transport Phenomena: A Unified Approach, vol 1*; Brodkey Publishing: Columbus, Ohio, USA, 1988.
402. Furukawa, H.; Kamiya, T.; Kato, Y. Correlation of Power Consumption of Double Impeller Based on Impeller Spacing in Laminar Region. *International Journal of Chemical Engineering* **2019**, *2019*, 1-7, doi:10.1155/2019/4564589.

403. Kamerkar, P.A.; Edwards, B. An experimental study of slip flow in capillaries and semihyperbolically converging dies. *Polymer Engineering & Science* **2007**, *47*, 159-167, doi:10.1002/pen.20692.

404. Feigl, K.; Tanner, F.X.; Edwards, B.J.; Collier, J.R. A numerical study of the measurement of elongational viscosity of polymeric fluids in a semihyperbolically converging die. *Journal of Non-Newtonian Fluid Mechanics* **2003**, *115*, 191-215, doi:https://doi.org/10.1016/j.jnnfm.2003.08.002.

405. Graillat, C.; Pichot, C.; Guyot, A.; El Aasser, M.S. Inverse emulsion polymerization of acrylamide. I. Contribution to the study of some mechanistic aspects. **1986**, *24*, 427-449, doi:10.1002/pola.1986.080240304.

406. Gooch, J.W. Ubbelohde Viscometer. In *Encyclopedic Dictionary of Polymers*, Gooch, J.W., Ed. Springer New York: New York, NY, 2011; 10.1007/978-1-4419-6247-8_12276pp. 777-777.

9 SCIENTIFIC CONTRIBUTION

Journal papers

- **Mirzaie Yegane, M**., Hashemi F., Vercauteren, F., Meulendijks, N., Gharbi, R., Boukany, P.E., Zitha, P.L.J. Rheological response of a modified polyacrylamide–silica nanoparticles hybrid at high salinity and temperature. Soft Matter, 2020, 16, 10198-10210 (doi: 10.1039/D0SM01254H), **featured on the cover of the journal**
- **Mirzaie Yegane, M**., Schmidt J., Dugonjic-Bilic, F., Gerlach, B., Boukany, P.E., Zitha, P.L.J. Flow enhancement of water-soluble polymers through porous media by pre-shearing. Industrial & Engineering Chemistry Research, 2021, 60, 8, 3463–3473 (doi: 10.1021/acs.iecr.1c00099)
- Kottsova, A.K., **Mirzaie Yegane, M**., Tchistiakov A.A., Zitha, P.L.J. Effect of electrostatic interaction on the retention and remobilization of colloidal particles in porous media. Colloids and Surfaces A: Physicochemical and Engineering Aspects, 2021, 617 (13), 126371 - (doi: 10.1016/j.colsurfa.2021.126371)
- **Mirzaie Yegane, M**., Boukany, P.E., Zitha, P.L.J. Fundamentals of water-soluble polymers and nanoparticles flow in porous media for enhanced oil recovery. Manuscript in preparation
- **Mirzaie Yegane, M**., Battistutta, E., Zitha, P.L.J. Mechanistic simulation of alkaline-surfactant-polymer core flooding experiment. SPE Journal - Under review
- **Mirzaie Yegane, M**., Boukany, P.E., Zitha, P.L.J. Transport of a polymer - nanoparticles hybrid in porous media. Manuscript in preparation

Conference papers

- **Mirzaie Yegane, M**., Ayatollahi, S., Bashtani, F., Romero, C. Solar generated steam injection in Hamca, Venezuelan extra Heavy oil reservoir; simulation study for oil recovery performance, economical and environmental feasibilities. SPE EUROPEC 2015 (doi: 10.2118/174305-MS)
- **Mirzaie Yegane, M**., Bashtani, F., Tahmasbi, A., Ayatollahi, S., Al-Wahabi, Y.M. Comparing different scenarios for thermal enhanced oil recovery in fractured

reservoirs using hybrid (Solar-Gas) steam generators, a simulation study. SPE EUROPEC 2016 (doi: 10.2118/180101-MS)

- **Mirzaie Yegane, M**., Battistutta, E., Zitha, P.L.J. Mechanistic simulation and history matching of alkaline-surfactant-polymer ASP core flooding experiment at optimum vs. under-optimum salinity conditions. SPE EUROPEC 2019 (doi: 10.2118/195564-MS)
- Schmidt J., **Mirzaie Yegane, M**., Dugonjic-Bilic, F., Gerlach, B., Zitha, P.L.J. Novel method for mitigating injectivity issues during polymer flooding at high salinity conditions. SPE EUROPEC 2019 (doi: 10.2118/195454-MS)

Conference talks and posters

- **Mirzaie Yegane, M**., Schmidt J., Dugonjic-Bilic, F., Gerlach, B., Boukany, P.E., Zitha, P.L.J. Flow enhancement of water-soluble polymers through porous media by pre-shearing. Oral presentation at the annual conference of international society of porous media (Interpore). August 2020, **Qingdao, China** (held online due to COVID-19)
- **Mirzaie Yegane, M**., Battistutta, E., Zitha, P.L.J. Mechanistic simulation and history matching of alkaline-surfactant-polymer ASP core flooding experiment at optimum vs. under-optimum salinity conditions. Oral presentation at SPE EUROPEC. June 2019, **London, United Kingdom**
- **Mirzaie Yegane, M**., Battistutta, E., Zitha, P.L.J. Numerical modelling of chemical enhanced hydrocarbon recovery processes. Poster presentation at the first workshop of CO_2 management and utilization in Brazilian pre-salt oilfields. June 2018, **Rio de Janeiro, Brazil**
- **Mirzaie Yegane, M**., Battistutta, E., Zitha. Alkaline-surfactant-polymer at optimum vs. under-optimum salinity conditions. Oral presentation at international conference on integrated petroleum engineering and geosciences (ICIPEG). August 2016, **Kuala Lumpur, Malaysia**
- **Mirzaie Yegane, M**., Bashtani, F., Tahmasbi, A., Ayatollahi, S., Al-Wahabi, Y.M. Comparing different scenarios for thermal enhanced oil recovery in fractured reservoirs using hybrid (Solar-Gas) steam generators, a simulation study. Oral presentation at SPE EUROPEC. June 2016, **Vienna, Austria**

- **Mirzaie Yegane, M**., Ayatollahi, S., Bashtani, F., Romero, C. Solar generated steam injection in Hamca, Venezuelan extra Heavy oil reservoir; simulation study for oil recovery performance, economical and environmental feasibilities. Oral presentation at SPE EUROPEC. June 2015, **Madrid, Spain**

10 ACKNOWLEDGEMENTS

Undertaking this PhD has been a truly life-changing experience for me and it would not have been possible without the support, guidance, belief, encouragement, and friendship that I received from many people.

Firstly, I would like to thank my promotor Prof. **Pacelli Zitha** for giving me this unique opportunity to pursue a PhD under his guidance. The past four years have been an incredibly rewarding part of my life and I could not wish for a better supervisor. Pacelli, I am grateful to you for valuable lessons in research and academic life that have helped me grow both professionally and personally. I would like to thank you for our frequent meetings and spontaneous discussions that have had a monumental contribution towards the end-result of this thesis. You guided me through my PhD journey but at the same time, you also gave me the freedom to explore my own ideas. Pacelli, thank you for the trust and faith that you had in me, so I can be involved in diverse and often multidisciplinary projects, teaching, supervision of several students, and organisation of scientific workshops. This trust has given me a great deal of confidence. I very much enjoyed the trips that we had together to Iran and Brazil. Thank you for creating a warm and friendly atmosphere in our group. I always felt welcome to come and talk to you about various subjects from science to politics and life in general. Thank you for participating in the clip that I made for Martijn's graduation as the supporting actor. Working with you in the past years has been one of the privileges of my life. There is no way I can ever thank you enough for all you have done for me.

In my second year, Dr. **Pouyan Boukany** joined the supervisory team of my PhD research as my second promotor and I could not be happier for that. Pouyan, I am incredibly privileged and blessed to have had your support and encouragement over the past years. Thank you for all the valuable discussions, meetings, and brainstorming sessions. Conducting fundamental research on the rheology and physical-chemical properties of polymers was quite far from my background but you made it much easier for me by providing intelligent guidance and target-oriented supervision. Thank you for challenging me and encouraging me to expand my comfort zone. Thank you for your thorough review of my manuscripts and for teaching me that every word matters. I appreciate your

suggestion to attend the rheology conference in Slovenia. This was a highly rewarding experience for me and helped me learn many things in the field of polymer rheology. Your persistent dedication and enthusiasm have helped me to grow as a scientist and to develop my personality.

My PhD project was a collaboration between Delft University of Technology, TNO, and Kuwait Oil Company. I am grateful to them for funding this project. I would like to sincerely thank my colleagues at TNO materials solutions group in Eindhoven and TNO applied geosciences group in Utrecht. Dr. **Filip Neele**, **Frank Vercauteren**, **Nicole Meulendijks**, **Jacco Eversdijk**, **Jelle Rohlfs**, Dr. **Bas van Ravensteijn**, Dr. **Maurice Mourad**, and **Daniel Turkenburg** are gratefully acknowledged for their help, support, and useful advice throughout this project. I closely worked with this wonderful group of people in the first two and half years of my PhD and I have learned a lot from them, particularly in the field of chemistry. I very much enjoyed the dynamics and interactions that I experienced within an industrial project. Thanks to all of you for the weekly meetings, joint effort to perform some of the experiments, and preparing the presentations and reports for the progress meetings with our industrial partner. This has truly been an educational experience for me and I have enjoyed working with you. I am grateful to Prof. **Ridha Gharbi** from Kuwait Oil Company for his fruitful comments and valuable discussions during quarterly progress meetings. They have been crucial for shaping the project, and I have always learned many things at these meetings. Ridha, thank you also for being part of my doctoral defence committee.

I am grateful to the rest of my doctoral defence committee, Prof. **William Rossen**, Dr. **Julia Gebert**, Prof. **Stephen Picken**, and Prof. **Yujun Feng** for taking the time to review my dissertation and provide valuable comments. Bill, thank you for all the wonderful discussions in the past four years. You have always inspired me as a true scientist.

A special thanks to Prof. **Mojdeh Delshad** and Prof. **Kami Sepehrnoori** for the invitation to a research visit at the University of Texas and Austin and their support to make it possible. It was unfortunate that it did not happen due to the circumstances.

I am thankful to Prof. **Shahab Ayatollahi**, the supervisor of my BSc project at Sharif University of Technology. He was the first one to believe in me as someone who can conduct high-quality research. Thanks to his guidance and encouragement, I published two conference papers from my BSc project which helped me pursue other research opportunities.

I performed many experiments during my PhD in the different laboratories in the geosciences and engineering department, chemical engineering department, mechanical engineering department, and water management department. The help of many technical experts at these labs has been vital for my experiments. My work was productive and efficient due to the help of **Michiel Slob**, **Marc Friebel**, **Jolanda van Haagen**, **Ellen Meijvogel-de Koning**, **Karel Heller**, **Wim Verwaal**, **Jens van den Berg**, **Joost van Meel**, **Paul Vermeulen**, **Armand Middeldorp**, **Ron Penners**, **Ben Norder**, Dr. **Stephen Eustace**, **Mohammed Jafar**, **Richard Huizenga**, and **Henk van Asten**. Special thanks to **Michiel** for helping with the core-flood experiments and for providing me with technical advice and support, **Marc** for assisting with the microfluidic experiments, and **Jolanda** for her support in analytical chemistry. I want to also thank Dr. **Karl-Heinz Wolf** for the fruitful discussions. Dr. **Fatemeh Hashemi** is greatly acknowledged for performing delicate experiments with the TEM machine.

I would like to take the chance to thank the academic staff of the reservoir engineering group at TU Delft, Prof. **William Rossen**, Dr. **Hadi Hajibeygi**, Dr. **Rouhi Farajzadeh**, Dr. **Denis Voskov**, Prof. **Hans Bruining**, Prof. **Jan-Dirk Jansen**, Prof. **David Bruhn**, Dr. **Phil Vardon**, Dr. **Femke Vossepoel** and Dr. **Maren Brehme**, for creating a friendly atmosphere within the group and always being available for scientific discussions. Your feedback in RE seminars has certainly helped to improve the quality of my research. **Margot Bosselaar-Perk**, **Ralf Haak**, **Lydia Broekhuijsen-Bentvelzen**, **Marlijn Ammerlaan**, **Marja Roep-Van der Klis**, **Nancy van Veen**, and **Marijke Schillemans-Van Tuijl**, **Regina Hoffmann**, and **Hannie Zwiers**, thanks to all of you for your assistance with the administrative work. You have always helped me quickly with a smile on your face and I appreciate that.

Over the past years, I had the opportunity and privilege to supervise and mentor four MSc students, **Julia Schmidt**, **Abdulaziz Fattah**, **Alaa Said**, and **Anna Kottsova**, and four BSc students, **Dieuwe Boelens**, **Frederik van Ballaer**, **Khalid Rovio**, and **Rens van der Vleuten**. I feel proud that you chose to work with me. Without your significant contribution, this thesis would not have been in its current shape. Through Julia's and Anna's works I had the privilege to collaborate with TouGas Oilfield Solutions from Germany and Skolkovo Institute of Science and Technology from Russia, respectively. I am thankful to them for the permission to publish the articles.

I would like to express my gratitude to all of my friends and colleagues within the department: Dr. **Siavash Kahrobaei**, Dr. **Jiakun Gong**, **Xiaocong Lyu**, Dr. **Mark Khait**, Dr. **Anna Peksa**, Dr. **Bander Alquaimi**, **Siamak Abolhassani**, Dr. **Mojtaba Talebian**, Dr. **Chris Boeije**, **Kai Li**, Dr. **Durgesh Kawale**, Dr. **Eduardo Barros**, **Muhammad Mohsan**, Dr. **Elisa Battistutta**, Dr. **Ahmed Hussain**, Dr. **Sanaz Saeid**, **Wesam Al Muttawa**, **Hamad Al Kharra'a**, Dr. **Alexander Wilsdorf**, Dr. **Faisal Al Saadi**, Dr. **Jakolien van der Meer**, **Amin Fatemi**, Dr. **Jinyu Tang**, **Kishan Ramesh**, **Sara Shokrollahzadeh Behbahani**, Dr. **Matteo Cusini**, **Nakul Mahalle**, Dr. **Mojtaba Hosseini-Nasab**, Dr. **Nikita Lenchenkov**, Dr. **Rafael de Moraes**, Dr. **Rodrigo Salazar**, Dr. **Longlong Li**, Dr. **Yuhang Wang**, **Xiaoming Tian,** and Dr. **Yang Wang**.

I want to thank my colleague and friend Dr. **Martijn Janssen** with whom I co-organised a workshop on "CO_2 Management and Utilization in Brazilian Pre-Salt Oilfields" held in Rio de Janeiro, Brazil, 2018. Martijn, it has been an absolute pleasure to work with you and I am grateful for all the fun and amazing times that we have spent together. I had so much fun during the trips that we went together to Brazil and the United Kingdom. Thank you also for checking the Dutch summary of my thesis. I am thankful to Dr. **Sian Jones** for always being available when I needed her. Sian, you are a true expert when it comes to working with different experimental setups in the lab. Thank you for giving useful advice to me and my students. The yummy Monday cakes and yearly potluck dinners have been a lot of fun. I also appreciate that you took the time to proofread my thesis. **Guanqun (Brandon) Yu**, Dr. **Swej Shah**, Dr. **Martijn Janssen**, and **Kiarash Mansour Pour**, thank you for being such fun colleagues and maintaining an amusing atmosphere in the office. We have had a lot of fun and many relaxing evenings together. In particular, I will always remember the Christmas drinks. It has been truly joyful to hang out with you guys.

During my time in Delft, I was lucky enough to meet some wonderful people who became good friends of mine. I want to thank the members of "The Gang", **Fardin Azimi**, **Alina Colling**, **Mousa Hosseinimehr**, Dr. **Matei Tene**, **Leonoor Tideman** and **Cantika Felita**. We have had so many fun activities together such as dinner nights, BBQs, golfing, cycling, movie nights, festivals, and trips, only to mention a few. Fardin, I absolutely enjoyed our hiking trip to Austria. Alina and Mousa, the trip to Germany was really fun. Thanks to all of you for the amazing times and for many more to come.

During my time at Sharif University of technology, I was fortunate to be friends with many talented individuals who have now landed in the finest institutions around the world. I am incredibly proud to have kept my close friendship with some of them for more than 12 years. **Hassan Andolhosseini**, **Ali Meschi Amoli**, **Reza Alibakhshi**, you are true friends and you have always been there for me both in the happiest and most difficult days of my life. You have filled my life with pleasure and amusement and had spread so many colours around it. I am grateful for all the memories that we have together. Dr. **Mohammadhossein Dabaghi**, we have been friends since high school and have kept a close friendship for almost 18 years. I could not ask for a better friend. Thank you for everything that you have done for me. Dr. **Behzad Nobakht**, I met you during my time in Turin. Your energy and positivity kept me going during some of my difficult days in Italy. Without your valuable advice, I might not have been where I am today.

Finally, my deepest gratitude goes to my parents, **Ahmadali** and **Shahnaz**. I cannot even begin to imagine what you have been through to have your only child so far away from you for many years. Everything I am today, and everything I may become tomorrow, is all for the sacrifices that you have made for me. You two are the most valuable possessions in my life. Thank you for sticking with me throughout life and for giving me everything you could. To you, I dedicate this thesis.

11 ABOUT THE AUTHOR

Mohsen Mirzaie Yegane was born on August 20th, 1989 in Borojerd, Iran. He has obtained his BSc. and MSc. in petroleum engineering from Sharif University of Technology (Iran) and Politecnico di Torino (Italy), respectively. He joined the department of geoscience and engineering at Delft University of Technology in 2015 as a guest researcher where he worked on the numerical modelling of chemical enhanced oil recovery methods. In 2016, he joined Binga Energy as a reservoir engineer and worked on the development of gas fields in The Netherlands using reservoir simulation. He then returned to Delft University of Technology and started his PhD studies in 2017 under the supervision of Prof. dr. Pacelli Zitha and Dr. Pouyan Boukany. During his tenure as a PhD candidate, he worked on multiple projects with a focus on flow in porous media. He had several collaborations namely with TNO from The Netherlands, Kuwait Oil Company from Kuwait, TouGas Oilfield Solutions from Germany, and Skolkovo Institute of Science and Technology from Russia. In particular, he worked very closely with TNO materials solutions group in Eindhoven and visited there frequently. As a volunteer activity, he was part of the organizing committee of the 1st workshop on "CO_2 Management and Utilization in Brazilian Pre-Salt Oilfields" held in 2018 in Rio de Janeiro, Brazil, and served as a board member for the society of petroleum engineers student chapter at Delft.

Besides conducting research, Mohsen has a strong passion for cinema. He has made two short films so far. He is also a big football enthusiast and has participated in several competitions. Mohsen also enjoys traveling and spending time with his family and friends.

"Nano" comes from the Greek word "dwarf". Nanoparticles, or ultrafine particles, are defined as a particle of matter ranging in size from 1 to 100 nm, which is 1 million times smaller than the size of a football. Alternatively, the difference in size between a nanoparticle and a football is the same difference in size between the football and the earth.

The small size of the nanoparticles results in many interesting characteristics such as high specific surface area, high surface energy, and active chemical responses which provide a platform to easily modify their surface. The aim of using nanoparticles for chemical enhanced oil recovery is to improve on the existing conventional methods, by co-injection of nanoparticles with other chemical agents such as polymers and surfactants. The nanoparticles can penetrate into small pore spaces that are not accessible to conventional chemical agents. Moreover, because of the ease of surface modification of nanoparticles, they can easily be tailored to adjust the rock and fluid properties including wettability, interfacial tension, and mobility ratio in order to improve the oil recovery.